2013-060

Summary report of the 2013 Geophysical Work and Mineralogical Study on the Charlotte Property

Final report for 2013 YMIP Funding under the Target Evaluation Module

Whitehorse Mining District

NTS 115 I/03

387428mE, 6883427mN (NAD83, Zone 8N)

DD1-2 (YA59596-YA59597)
DOME 6-7 (73542-73543)
DOME 16-20(73702-73706
DOME 49-58(77770-77779)
DOME 78-84 (81842-81848)
EEK 14-18 (YA87223-YA87227)
HIW 9 -17 (YA23835-YA23843)
ONT 40 (YA87206)
TBR 1-8 (YA86690-YA86697)
WAR EAGLE (4279)
ARLEP (4368)
PUB (55663)
JAM (55890)
DD15-28 (YA59610 – YA59623)
DOME 8(73694)
DOME 25-28(77746-77749)
DOME 60-61 (77781-77782)
DOME 86 (81850)
HIW 1-2 (YA24813-YA24814)
JOANNE 1-6 (74283-74288)
ONT 42 (YA87208)
ROSE (4241)
SHAMROCK (4354)
PHYLLIS (4369)
SUN DOG (55665)
PAM (55892)
DOME 1-4 (73537-73540)
DOME 14 (73700)
DOME 33-43(77754-77764)
DOME 63-66 (77784-77787)
EEK 1-9 (YA87210-YA87218)
HIW 7 (YA24819)
ONT 38 (YA87204)
ONT 44-47 (YA92665-658)
GOLDEN EAGLE (4278)
SPOT (4361)
RUB (55633)
CUB (55666)

Prepared by:
Bev Quist
Ansell Capital Corp
3rd Floor - Bellevue Centre
235 - 15th Street
West Vancouver, BC Canada
V7T 2X1
January 2014

Contents

1 Introduction 4

2 Project Area Location and Access 4

3 Climate, physiography and infrastructure 12

4 Terms of Reference and Source Material 12

5 Historical work 12

6 Project Rationale 16

7 Geology 16

7.1 Regional Geological Setting 16

7.2 Property Geology 23

8 2013 Work 32

8.1 IP survey details 32

8.2 Mineralogical work 35

8.2.1 Mineralogical Methods 35

9 Sample collection, ground mag and radiometrics 35

10 Data interpretation 37

10.1 Ground Geophysics 37

10.1.1 FLEX Zone Interpretation (taken directly from Fage (2014) unless otherwise stated). 37

10.1.2 OK Zone Interpretation (taken directly from Fage, 2014) 43

10.2 Mineralogical Interpretation (Taken directly from Dalsin and Groat (2014)- see complete report in appendix) 45

11 Conclusions and Recommendations 55

12 Statement of Expenditures 56

13 Statement of qualifications 57

14 References 58

Figure 1. Territorial location of the Charlotte Property (Dadson & Struyk, 2012). 4
Figure 2. Location of Charlotte claims (Dadson & Struyk, 2012). 6
Figure 3. Claim names and 2011 Work Locations (Struyk & Dadson, 2011) 7
Figure 4. Surficial geology underlying Charlotte Property 18
Figure 5. First Vertical Derivative geophysics (100 m spacing), Yukon Plateau, publically available dataset. 19
Figure 6. Underlying bedrock geology of the Charlotte Property. Geology courtesy of the Yukon Geological Survey 20
Figure 7. Zones of mineralization on the Charlotte property. Courtesy of Guinness Exploration (2010) 22
Figure 8. Geology of Charlotte property. Geology from Coast Mountain (2013). 26
Figure 9. Total magnetic intensity from 2009 airborne VTEM survey 27
Figure 10. B field (EM) from 2009 airborne VTEM survey 28
Figure 11. MINFILE locations on and surrounding the Charlotte property 31
Figure 12. Location of the 2013 FLEX and Orloff-King (OK) IP and Resistivity surveys. 33
Figure 13. FLEX zone IP lines and locations of DDH and IP sections with DDH 34
Figure 14. Resistivity, Chargeability, and drill holes with Au over the FLEX zone, along line L050N 38
Figure 15. Resistivity, Chargeability, and drill holes with Au over the FLEX zone, along line L200N 39
Figure 16. Level plan of surface resistivity over the FLEX zone (Fage, 2014) 40
Figure 17. Screenshot of 3D resistivity in the FLEX zone. Black lines represent historical drill holes. View is looking roughly northeast. 41
Figure 18. 2013 IP/RES survey on the FLEX zone and 2012 Coast Mountain Geological geology 42
Figure 19. 2013 IP/RES survey on the FLEX zone and 2012 Coast Mountain Geological geology 44
Figure 20. Locations of veins (Hangingwall vein (HW), Footwall vein (FW), and Main) in the FLEX zone. The East vein (EW) is approximately 20-30 meters east of FW 47
Figure 21. Gold and silver plot for the Main, HW, FW and East vein (Dalsin and Groat, 2014). All veins show a positive correlation between gold and silver; the HW has strong correlation. 53
Figure 22. Gold and silver plotted for sulphide, oxide and transitional minerals (Dalsin and Groat, 2014); all mineral types show a positive correlation. 54

1 Introduction

This report covers work performed on the Charlotte Property under the 2013 Yukon Mining Incentive Program "Target Evaluation" Module.

2 Project Area Location and Access

The Charlotte property is located on NTS mapsheet 115I03 in the Mount Nansen area of the west-central Yukon Territory, Canada (Figure 1). The property is road accessible and is approximately 60 km west of the town of Carmacks (Figure 2), which can supply lodging, fuel and groceries. It is located 180 km northwest of Whitehorse, which has all the amenities required to service an advanced stage exploration or mining project and contains an international airport with daily service to Calgary, Edmonton and Vancouver. The property contains 128 full and fractional contiguous quartz mining claims and leases and covers an area of 2332 hectares. It is located within the Whitehorse Mining district. Central coordinates are 387400mE, 6883427mN, NAD83, zone 8N. The claims are held by 101073531 Saskatchewan Ltd.

The Mt. Nansen area is part of the traditional territory of the Little Salmon/Carmacks First Nation; much of the property lies on crown land and management is the responsibility of the Yukon Territorial

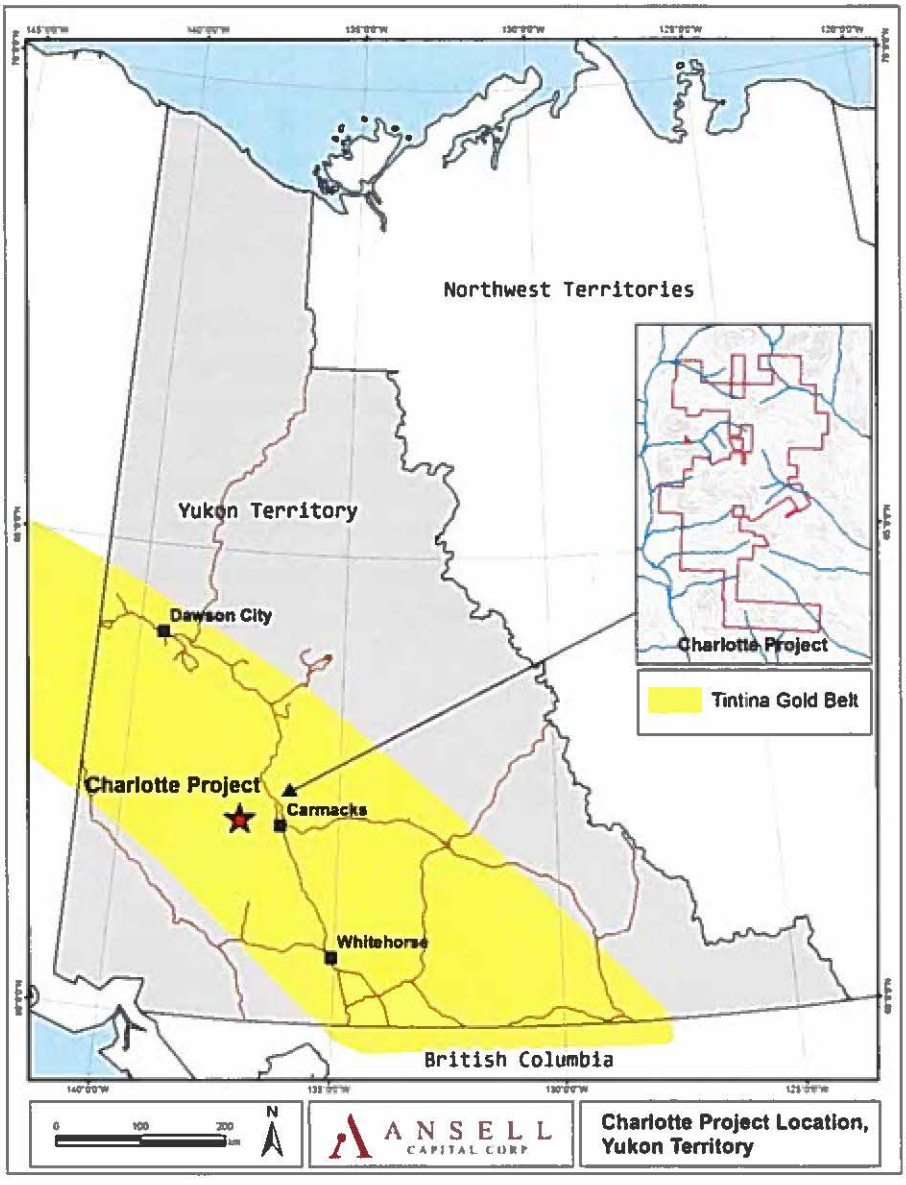


Figure 1. Territorial location of the Charlotte Property (Dadson & Struyk, 2012).

Government. However, part of the property lies on settlement land and is subject to the terms and conditions of the 1998 final negotiated agreement between the governments of Canada, the Yukon and the Little Salmon/Carmacks First Nation. The legal mineral claim owner retains the right to work on claims held in good standing that overlie settlement lands. However, if the mineral claims are allowed to lapse, the area under expired tenure will revert to the First Nation.

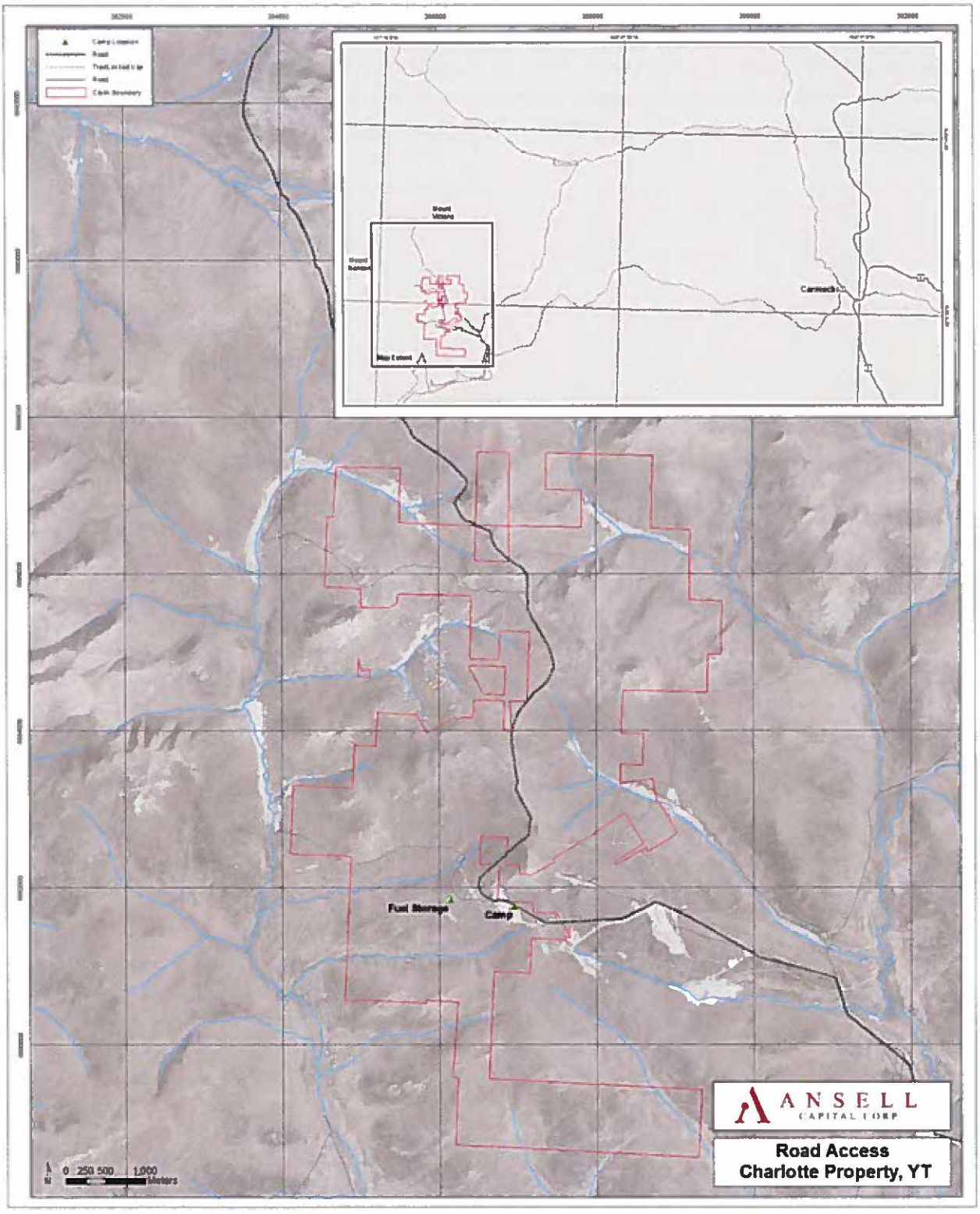


Figure 2. Location of Charlotte claims (Dadson & Struyk, 2012).

.

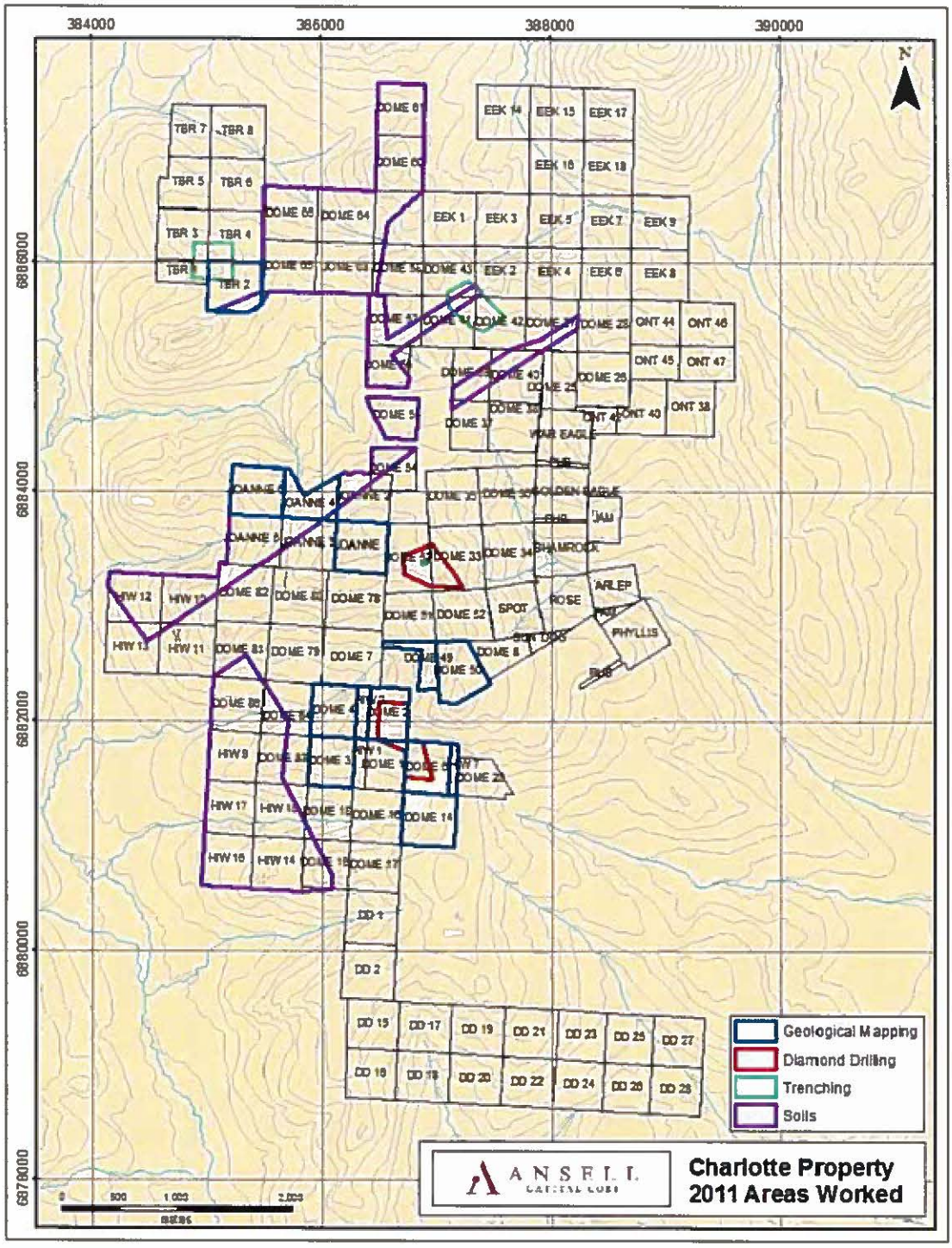


Figure 3. Claim names and 2011 Work Locations (Struyk & Dadson, 2011)

Table 1. Summary of Charlotte claims and leases

Grant Number	LEASE_NUMB	Claim type	Tenure Status	Claim Name	Owner Name	Expiry Date	District	Area (Ha)
77759		Quartz	Active	DOME 38	101073531 Saskatchewan Ltd. - 100%	2/6/2026 0:00	Whitehorse	18.4751097
YA59623		Quartz	Active	DD 28	101073531 Saskatchewan Ltd. - 100%	2/6/2026 0:00	Whitehorse	18.7058444
YA59616		Quartz	Active	DD 21	101073531 Saskatchewan Ltd. - 100%	2/6/2026 0:00	Whitehorse	19.6396029
YA24813		Quartz	Active	HIW 1	101073531 Saskatchewan Ltd. - 100%	2/6/2026 0:00	Whitehorse	4.73693227
YA92657		Quartz	Active	ONT 46	101073531 Saskatchewan Ltd. - 100%	2/6/2026 0:00	Whitehorse	18.4796314
YA92658		Quartz	Active	ONT 47	101073531 Saskatchewan Ltd. - 100%	2/6/2026 0:00	Whitehorse	14.4079598
74284		Quartz	Active	JOANNE 2	101073531 Saskatchewan Ltd. - 100%	2/6/2026 0:00	Whitehorse	19.5132191
YA86697		Quartz	Active	TBR 8	101073531 Saskatchewan Ltd. - 100%	2/6/2026 0:00	Whitehorse	21.7926123
YA86692		Quartz	Active	TBR 3	101073531 Saskatchewan Ltd. - 100%	2/6/2027 0:00	Whitehorse	20.0313331
YA59615		Quartz	Active	DD 20	101073531 Saskatchewan Ltd. - 100%	2/6/2026 0:00	Whitehorse	19.8958243
81846		Quartz	Active	DOME 82	101073531 Saskatchewan Ltd. - 100%	2/6/2026 0:00	Whitehorse	23.2627546
4278	OW00045	Quartz	Active	GOLDEN EAGLE	101073531 Saskatchewan Ltd. - 100%	10/9/2019 0:00	Whitehorse	20.9632294
73706		Quartz	Active	DOME 20	101073531 Saskatchewan Ltd. - 100%	2/6/2026 0:00	Whitehorse	13.4170429
YA86691		Quartz	Active	TBR 2	101073531 Saskatchewan Ltd. - 100%	2/6/2027 0:00	Whitehorse	20.1593817
YA87225		Quartz	Active	EEK 16	101073531 Saskatchewan Ltd. - 100%	2/6/2026 0:00	Whitehorse	21.7634759
4354	OW00047	Quartz	Active	SHAMROCK	101073531 Saskatchewan Ltd. - 100%	10/9/2019 0:00	Whitehorse	20.7338593
77762		Quartz	Active	DOME 41	101073531 Saskatchewan Ltd. - 100%	2/6/2026 0:00	Whitehorse	20.7565466
YA23839		Quartz	Active	HIW 13	101073531 Saskatchewan Ltd. - 100%	2/6/2026 0:00	Whitehorse	20.7234232
YA87204		Quartz	Active	ONT 38	101073531 Saskatchewan Ltd. - 100%	2/6/2026 0:00	Whitehorse	20.2571983
74286		Quartz	Active	JOANNE 4	101073531 Saskatchewan Ltd. - 100%	2/6/2026 0:00	Whitehorse	14.7783017
77770		Quartz	Active	DOME 49	101073531 Saskatchewan Ltd. - 100%	2/6/2026 0:00	Whitehorse	8.17949345
73703		Quartz	Active	DOME 17	101073531 Saskatchewan Ltd. - 100%	2/6/2026 0:00	Whitehorse	18.4123222
55666	OW00058	Quartz	Active	CUB	101073531 Saskatchewan Ltd. - 100%	10/9/2019 0:00	Whitehorse	1.2889379
YA87206		Quartz	Active	ONT 40	101073531 Saskatchewan Ltd. - 100%	2/6/2026 0:00	Whitehorse	18.3435009
77773		Quartz	Active	DOME 52	101073531 Saskatchewan Ltd. - 100%	2/6/2026 0:00	Whitehorse	21.8452231
YA24819		Quartz	Active	HIW 7	101073531 Saskatchewan Ltd. - 100%	2/6/2026 0:00	Whitehorse	3.01098552
YA59613		Quartz	Active	DD 18	101073531 Saskatchewan Ltd. - 100%	2/6/2026 0:00	Whitehorse	19.8545026
YA59610		Quartz	Active	DD 15	101073531 Saskatchewan Ltd. - 100%	2/6/2026 0:00	Whitehorse	19.1974691
YA59618		Quartz	Active	DD 23	101073531 Saskatchewan Ltd. - 100%	2/6/2026 0:00	Whitehorse	18.6932444
77787		Quartz	Active	DOME 66	101073531 Saskatchewan Ltd. - 100%	2/6/2026 0:00	Whitehorse	21.2558004
YA59597		Quartz	Active	DD 2	101073531 Saskatchewan Ltd. - 100%	2/6/2026 0:00	Whitehorse	22.3495533
77781		Quartz	Active	DOME 60	101073531 Saskatchewan Ltd. - 100%	2/6/2026 0:00	Whitehorse	20.0622107
77761		Quartz	Active	DOME 40	101073531 Saskatchewan Ltd. - 100%	2/6/2026 0:00	Whitehorse	20.5111252

Grant Number	LEASE_NUMB	Claim type	Tenure Status	Claim Name	Owner Name	Expiry Date	District	Area (Ha)
YA87216		Quartz	Active	EEK 7	101073531 Saskatchewan Ltd. - 100%	2/6/2026 0:00	Whitehorse	19.9720284
73540		Quartz	Active	DOME 4	101073531 Saskatchewan Ltd. - 100%	2/6/2026 0:00	Whitehorse	17.9757418
74287		Quartz	Active	JOANNE 5	101073531 Saskatchewan Ltd. - 100%	2/6/2026 0:00	Whitehorse	19.8257387
81847		Quartz	Active	DOME 83	101073531 Saskatchewan Ltd. - 100%	2/6/2026 0:00	Whitehorse	18.7154029
73542		Quartz	Active	DOME 6	101073531 Saskatchewan Ltd. - 100%	2/6/2026 0:00	Whitehorse	17.322637
YA87217		Quartz	Active	EEK 8	101073531 Saskatchewan Ltd. - 100%	2/6/2026 0:00	Whitehorse	21.9087647
77776		Quartz	Active	DOME 55	101073531 Saskatchewan Ltd. - 100%	2/6/2026 0:00	Whitehorse	13.0922484
YA87212		Quartz	Active	EEK 3	101073531 Saskatchewan Ltd. - 100%	2/6/2026 0:00	Whitehorse	20.6953953
77758		Quartz	Active	DOME 37	101073531 Saskatchewan Ltd. - 100%	2/6/2026 0:00	Whitehorse	14.2344752
YA86690		Quartz	Active	TBR 1	101073531 Saskatchewan Ltd. - 100%	2/6/2027 0:00	Whitehorse	8.92257136
YA23836		Quartz	Active	HIW 10	101073531 Saskatchewan Ltd. - 100%	2/6/2026 0:00	Whitehorse	20.8280769
YA23838		Quartz	Active	HIW 12	101073531 Saskatchewan Ltd. - 100%	2/6/2026 0:00	Whitehorse	19.9265471
YA59596		Quartz	Active	DD 1	101073531 Saskatchewan Ltd. - 100%	2/6/2026 0:00	Whitehorse	20.6164881
YA59620		Quartz	Active	DD 25	101073531 Saskatchewan Ltd. - 100%	2/6/2026 0:00	Whitehorse	18.1769692
81844		Quartz	Active	DOME 80	101073531 Saskatchewan Ltd. - 100%	2/6/2026 0:00	Whitehorse	24.1992926
YA87214		Quartz	Active	EEK 5	101073531 Saskatchewan Ltd. - 100%	2/6/2026 0:00	Whitehorse	20.8046291
YA59612		Quartz	Active	DD 17	101073531 Saskatchewan Ltd. - 100%	2/6/2026 0:00	Whitehorse	19.3749233
YA87223		Quartz	Active	EEK 14	101073531 Saskatchewan Ltd. - 100%	2/6/2026 0:00	Whitehorse	21.3552824
55633	OW00054	Quartz	Active	RUB	101073531 Saskatchewan Ltd. - 100%	10/9/2019 0:00	Whitehorse	1.83779452
77785		Quartz	Active	DOME 64	101073531 Saskatchewan Ltd. - 100%	2/6/2026 0:00	Whitehorse	23.0213855
YA23842		Quartz	Active	HIW 16	101073531 Saskatchewan Ltd. - 100%	2/6/2026 0:00	Whitehorse	19.8565465
YA59622		Quartz	Active	DD 27	101073531 Saskatchewan Ltd. - 100%	2/6/2026 0:00	Whitehorse	19.4924957
4369	OW00052	Quartz	Active	PHYLLIS	101073531 Saskatchewan Ltd. - 100%	10/9/2019 0:00	Whitehorse	20.2561632
YA87211		Quartz	Active	EEK 2	101073531 Saskatchewan Ltd. - 100%	2/6/2026 0:00	Whitehorse	20.0798123
73543		Quartz	Active	DOME 7	101073531 Saskatchewan Ltd. - 100%	2/6/2026 0:00	Whitehorse	25.3413872
YA23837		Quartz	Active	HIW 11	101073531 Saskatchewan Ltd. - 100%	2/6/2026 0:00	Whitehorse	21.5503897
YA23840		Quartz	Active	HIW 14	101073531 Saskatchewan Ltd. - 100%	2/6/2026 0:00	Whitehorse	19.5526841
4241	OW00044	Quartz	Active	ROSE	101073531 Saskatchewan Ltd. - 100%	10/9/2019 0:00	Whitehorse	20.4164708
YA87227		Quartz	Active	EEK 18	101073531 Saskatchewan Ltd. - 100%	2/6/2026 0:00	Whitehorse	20.7447107
55665	OW00057	Quartz	Active	SUN DOG	101073531 Saskatchewan Ltd. - 100%	10/9/2019 0:00	Whitehorse	3.19918938
YA87226		Quartz	Active	EEK 17	101073531 Saskatchewan Ltd. - 100%	2/6/2026 0:00	Whitehorse	20.013193
77771		Quartz	Active	DOME 50	101073531 Saskatchewan Ltd. - 100%	2/6/2026 0:00	Whitehorse	18.8333669
73539		Quartz	Active	DOME 3	101073531 Saskatchewan Ltd. - 100%	2/6/2026 0:00	Whitehorse	17.2884798

Grant Number	LEASE_NUMB	Claim type	Tenure Status	Claim Name	Owner Name	Expiry Date	District	Area (Ha)
55892	OW00060	Quartz	Active	PAM	101073531 Saskatchewan Ltd. - 100%	10/9/2019 0:00	Whitehorse	2.63889099
77747		Quartz	Active	DOME 26	101073531 Saskatchewan Ltd. - 100%	2/6/2026 0:00	Whitehorse	22.5392691
81850		Quartz	Active	DOME 86	101073531 Saskatchewan Ltd. - 100%	2/6/2026 0:00	Whitehorse	20.758657
YA23843		Quartz	Active	HIW 17	101073531 Saskatchewan Ltd. - 100%	2/6/2026 0:00	Whitehorse	19.9192605
77760		Quartz	Active	DOME 39	101073531 Saskatchewan Ltd. - 100%	2/6/2026 0:00	Whitehorse	14.9548847
YA59614		Quartz	Active	DD 19	101073531 Saskatchewan Ltd. - 100%	2/6/2026 0:00	Whitehorse	20.1658115
77784		Quartz	Active	DOME 63	101073531 Saskatchewan Ltd. - 100%	2/6/2026 0:00	Whitehorse	22.5043274
77774		Quartz	Active	DOME 53	101073531 Saskatchewan Ltd. - 100%	2/6/2026 0:00	Whitehorse	22.7986562
73694		Quartz	Active	DOME 8	101073531 Saskatchewan Ltd. - 100%	2/6/2026 0:00	Whitehorse	12.4709645
81848		Quartz	Active	DOME 84	101073531 Saskatchewan Ltd. - 100%	2/6/2026 0:00	Whitehorse	19.3692777
YA23835		Quartz	Active	HIW 9	101073531 Saskatchewan Ltd. - 100%	2/6/2026 0:00	Whitehorse	19.4431693
YA87213		Quartz	Active	EEK 4	101073531 Saskatchewan Ltd. - 100%	2/6/2026 0:00	Whitehorse	20.6837248
YA24814		Quartz	Active	HIW 2	101073531 Saskatchewan Ltd. - 100%	2/6/2026 0:00	Whitehorse	5.15222209
73538		Quartz	Active	DOME 2	101073531 Saskatchewan Ltd. - 100%	2/6/2026 0:00	Whitehorse	15.5124522
YA92656		Quartz	Active	ONT 45	101073531 Saskatchewan Ltd. - 100%	2/6/2026 0:00	Whitehorse	12.9076287
77748		Quartz	Active	DOME 27	101073531 Saskatchewan Ltd. - 100%	2/6/2026 0:00	Whitehorse	20.3188518
55663	OW00056	Quartz	Active	PUB	101073531 Saskatchewan Ltd. - 100%	10/9/2019 0:00	Whitehorse	1.93481351
74285		Quartz	Active	JOANNE 3	101073531 Saskatchewan Ltd. - 100%	2/6/2026 0:00	Whitehorse	20.3640373
YA86693		Quartz	Active	TBR 4	101073531 Saskatchewan Ltd. - 100%	2/6/2027 0:00	Whitehorse	20.8361231
4279	OW00046	Quartz	Active	WAR EAGLE	101073531 Saskatchewan Ltd. - 100%	10/9/2019 0:00	Whitehorse	20.7743982
YA87224		Quartz	Active	EEK 15	101073531 Saskatchewan Ltd. - 100%	2/6/2026 0:00	Whitehorse	21.2153392
77763		Quartz	Active	DOME 42	101073531 Saskatchewan Ltd. - 100%	2/6/2026 0:00	Whitehorse	19.933087
77778		Quartz	Active	DOME 57	101073531 Saskatchewan Ltd. - 100%	2/6/2026 0:00	Whitehorse	20.4689804
77777		Quartz	Active	DOME 56	101073531 Saskatchewan Ltd. - 100%	2/6/2026 0:00	Whitehorse	13.3533722
73704		Quartz	Active	DOME 18	101073531 Saskatchewan Ltd. - 100%	2/6/2026 0:00	Whitehorse	18.560826
YA59611		Quartz	Active	DD 16	101073531 Saskatchewan Ltd. - 100%	2/6/2026 0:00	Whitehorse	19.209568
YA87215		Quartz	Active	EEK 6	101073531 Saskatchewan Ltd. - 100%	2/6/2026 0:00	Whitehorse	19.5779596
4361	OW00049	Quartz	Active	SPOT	101073531 Saskatchewan Ltd. - 100%	10/9/2019 0:00	Whitehorse	19.9176328
YA86695		Quartz	Active	TBR 6	101073531 Saskatchewan Ltd. - 100%	2/6/2027 0:00	Whitehorse	20.9176714
77756		Quartz	Active	DOME 35	101073531 Saskatchewan Ltd. - 100%	2/6/2026 0:00	Whitehorse	22.3908842
YA92655		Quartz	Active	ONT 44	101073531 Saskatchewan Ltd. - 100%	2/6/2026 0:00	Whitehorse	16.7960542
YA87208		Quartz	Active	ONT 42	101073531 Saskatchewan Ltd. - 100%	2/6/2026 0:00	Whitehorse	5.73371459
73537		Quartz	Active	DOME 1	101073531 Saskatchewan Ltd. - 100%	2/6/2026 0:00	Whitehorse	15.0980049

Grant Number	LEASE_NUMB	Claim type	Tenure Status	Claim Name	Owner Name	Expiry Date	District	Area (Ha)
77757		Quartz	Active	DOME 36	101073531 Saskatchewan Ltd. - 100%	2/6/2026 0:00	Whitehorse	23.9664541
77772		Quartz	Active	DOME 51	101073531 Saskatchewan Ltd. - 100%	2/6/2026 0:00	Whitehorse	19.04514
81842		Quartz	Active	DOME 78	101073531 Saskatchewan Ltd. - 100%	2/6/2026 0:00	Whitehorse	25.4135815
YA87210		Quartz	Active	EEK 1	101073531 Saskatchewan Ltd. - 100%	2/6/2026 0:00	Whitehorse	21.0665289
77755		Quartz	Active	DOME 34	101073531 Saskatchewan Ltd. - 100%	2/6/2026 0:00	Whitehorse	23.2886438
74288		Quartz	Active	JOANNE 6	101073531 Saskatchewan Ltd. - 100%	2/6/2026 0:00	Whitehorse	19.6946591
YA59617		Quartz	Active	DD 22	101073531 Saskatchewan Ltd. - 100%	2/6/2026 0:00	Whitehorse	19.1711517
73705		Quartz	Active	DOME 19	101073531 Saskatchewan Ltd. - 100%	2/6/2026 0:00	Whitehorse	16.7342674
77749		Quartz	Active	DOME 28	101073531 Saskatchewan Ltd. - 100%	2/6/2026 0:00	Whitehorse	21.7413011
81845		Quartz	Active	DOME 81	101073531 Saskatchewan Ltd. - 100%	2/6/2026 0:00	Whitehorse	22.5157163
77786		Quartz	Active	DOME 65	101073531 Saskatchewan Ltd. - 100%	2/6/2026 0:00	Whitehorse	20.6599348
YA86696		Quartz	Active	TBR 7	101073531 Saskatchewan Ltd. - 100%	2/6/2026 0:00	Whitehorse	15.9601893
YA87218		Quartz	Active	EEK 9	101073531 Saskatchewan Ltd. - 100%	2/6/2026 0:00	Whitehorse	22.6364217
73702		Quartz	Active	DOME 16	101073531 Saskatchewan Ltd. - 100%	2/6/2026 0:00	Whitehorse	20.6067157
YA86694		Quartz	Active	TBR 5	101073531 Saskatchewan Ltd. - 100%	2/6/2027 0:00	Whitehorse	18.3404274
81843		Quartz	Active	DOME 79	101073531 Saskatchewan Ltd. - 100%	2/6/2026 0:00	Whitehorse	24.1011397
4368	OW00051	Quartz	Active	ARLEP	101073531 Saskatchewan Ltd. - 100%	10/9/2019 0:00	Whitehorse	14.4781567
77775		Quartz	Active	DOME 54	101073531 Saskatchewan Ltd. - 100%	2/6/2026 0:00	Whitehorse	14.687693
77746		Quartz	Active	DOME 25	101073531 Saskatchewan Ltd. - 100%	2/6/2026 0:00	Whitehorse	15.1949114
55890	OW00059	Quartz	Active	JAM	101073531 Saskatchewan Ltd. - 100%	10/9/2019 0:00	Whitehorse	11.6417234
YA59621		Quartz	Active	DD 26	101073531 Saskatchewan Ltd. - 100%	2/6/2026 0:00	Whitehorse	17.6519428
YA59619		Quartz	Active	DD 24	101073531 Saskatchewan Ltd. - 100%	2/6/2026 0:00	Whitehorse	18.3024042
73700		Quartz	Active	DOME 14	101073531 Saskatchewan Ltd. - 100%	2/6/2026 0:00	Whitehorse	21.0720875
77779		Quartz	Active	DOME 58	101073531 Saskatchewan Ltd. - 100%	2/6/2026 0:00	Whitehorse	15.0905024
77764		Quartz	Active	DOME 43	101073531 Saskatchewan Ltd. - 100%	2/6/2026 0:00	Whitehorse	20.4720472
74283		Quartz	Active	JOANNE 1	101073531 Saskatchewan Ltd. - 100%	2/6/2026 0:00	Whitehorse	19.7878907
YA23841		Quartz	Active	HIW 15	101073531 Saskatchewan Ltd. - 100%	2/6/2026 0:00	Whitehorse	20.1473406
77782		Quartz	Active	DOME 61	101073531 Saskatchewan Ltd. - 100%	2/6/2026 0:00	Whitehorse	18.9107473
77754		Quartz	Active	DOME 33	101073531 Saskatchewan Ltd. - 100%	2/6/2026 0:00	Whitehorse	25.5014237

3 Climate, physiography and infrastructure

The property lies in a temperate continental climate with warm summers and cold winters; the average season temperature varies from -25°C to 15°C. Average precipitation is 250 mm. Permafrost is pervasive; north-facing slopes rarely have an active layer and south facing slopes typically have an active layer of 1-2 m.

4 Terms of Reference and Source Material

All coordinates and maps utilize NAD83 datum and are projected to UTM zone 8. Distances are reported in metric, directions in true north, and funds in Canadian dollars.

5 Historical work

The following is a brief outline of the history of exploration in the area taken directly from Dadson and Struyk (2012):

1899: Captain Henry Seymour discovered placer gold in Nansen Creek. Other placer discoveries were made in the early 1900s, but none were large enough or rich enough for sustained development (Lecuyer, 1997).

1930: Gold was discovered in the Mt. Freegold area to the north and after considerable work the La Forma Mine was brought into production (Saunders, 1980).

1937: Silver and lead was discovered by K. Paulson on what is now the Klaza Property immediately north of the Charlotte property (Saunders, 1980).

1943: Prospectors A. Brown and G. McDade discovered the first lode gold deposit, now known as the Brown-McDade Deposit, located immediately to the east of the Charlotte Property.

1946: Brown-McDade Mines Ltd. formed and began an extensive program of underground drilling and development. Concurrently, Conwest Explorations Ltd. discovered and explored the Webber Zone while the Huestis Syndicate identified and delineated the Huestis Zone, both currently on the Charlotte Property.

1958: Interest in the Mt. Nansen area was revived.

1962: The Mt. Nansen Exploration Syndicate optioned properties that overlap with the Charlotte claim block. This group explored the Webber and Huestis Zones with geochemical surveys, bulldozer trenching and one diamond drill hole in the Webber.

1963: Mt. Nansen Mines was formed by the syndicate. The Webber Zone was further explored with bulldozer trenching and three diamond drill holes

1964: Peso Silver Mines Limited acquires control of Mt. Nansen Mines Ltd. and continued exploration on the Brown-McDade, Webber and Huestis Zones with underground development and diamond drilling between 1964 and 1967 (Walls and Eaton, 1987).

1965: Peso Silver trenched on the Discovery property located to the west of the Charlotte claims (Ellemers and Stroshein, 2005).

1967: A production decision was made and construction of a 200 ton/day mill was started at the Brown-McDade property.

1968: On the same ground as Peso Silver's work Associated Geological Services undertook a soil sampling survey (Ellemers and Stroshien, 2005).

1969: Copper porphyry deposit known as Cyprus was discovered on the NW corner of the property.

1968 and 1969: Esanser Explorations Ltd. conducted exploration on the neighboring Klaza Property which included geochemical and geophysical surveys, geological mapping, rock sampling, some trenching and also the construction of 14 km of road from the Mount Nansen Mines campsite (Saunders, 1980).

1970: Cyprus showing worked by Area Exploration Company a subsidiary of Cyprus Exploration Corporation. They undertook soil geochemistry and airborne geophysics.

1971: Mount Nansen Mines undertook reconnaissance geological mapping and silt sampling on the adjacent Etzel Property (McClintock, 1986)

1973: Detailed exploration continued on the Cyprus showing with ground geochemical and geophysical surveys, 3463 m of diamond drilling and 951 m of percussion drilling (Franzen, 1986)

1975: Production ceased until 1975 when the Brown-McDade Mine was reopened.

1978: Asbestos Corp. completed trenching and drilled 8 holes for 122 m on what will become the Aurchem Exploration Ltd's Discovery Creek Project immediately west of the Charlotte claims. This drilling was following up anomalous gold values in trenches located north of the Etzel (Ellemers and Stroshein, 2005).

1980: BRX Mining and Petroleum Ltd. completed three short bulldozer trenches, seven drill holes for 447.3 m and a geochemical soil survey on the Tawa, now the Klaza Property (Saunders, 1980).

1984: Due to unfavourable results, the Brown-McDade property remains inactive until it was acquired by BYG Resources Inc. ("BYG") (Stroshein, 2007b). The nearby Etzel Property was staked by Mr. Gordon Dickson.

1985: Chevron Minerals optioned the claims that now comprise the current Charlotte Property, as well as those that cover the Brown-McDade mine and mill site.

1985 and 1987: Archer, Cathro & Associates was contracted by Chevron to oversee and execute an intensive exploration program (Eaton and Archer, 1988). By the end of the 1987 field season, Archer-Cathro had completed or overseen geological mapping over various parts of the property, test geophysical surveys, a 6300 soil geochemical survey, aerial photography, baseline and claim surveys, rehabilitation of the Brown-McDade adit portal, 24,121 m of excavator trenching, 1283.5 m of percussion drilling in 17 holes, 2605 m of diamond drilling in 41 holes, and metallurgical, geotechnical and environmental studies (Eaton and Walls, 1988). Exploration focused mainly on delineation of oxide mineralization near surface that would be amenable to open-pit mining. However drilling also expanded the underground sulphide occurrence at the Webber and Huestis Zones (Eaton and Archer, 1989). The previously unrecognized Flex Zone was discovered during this time.

1985: Mr. Gordon Dickson undertakes bulldozer trenching on the Etzel Property.

Pre-1986 and 1986: Kerr Addison optioned the Discovery Project claims and undertakes geological mapping, sampling as well as magnetometer, VLF-EM, SP and resistivity surveys, trenching and the drilling of 19 holes for 1594 m (Ellemers and Stroshein, 2005).

Pearl Resources options the Etzel and Wedge claims from Mr. Gordon Dickson and undertook geological mapping.

1987 -1988: Chesbar Resources Inc. drilled 2372 m in 21 holes on the Discovery Project claims (Ellemers and Stroshein, 2005).

1988: BYG took on sole proprietorship of the Mt. Nansen Project with exploration conducted by Archer-Cathro which consisted of 1473 m of trenching on the Dickson, Huestis and Brown-McDade Zones and 5397 m of diamond drilling primarily on the Brown-McDade Zone and substantially less on the Orloff-King and Dickson Zones (Eaton and Archer,1989). Exploration was put on hiatus between 1989 and 1994.

1989 to 1994: BYG undertook metallurgical testing, mill flow sheet designs, tailings disposal assessments, and baseline environmental and assessment studies during the exploration hiatus between 1989 and 1994.

1994 to 1996: BYG's exploration on the property consisted of:

- Diamond drilling on the Brown-McDade and Flex in 1994 (990 m in 12 holes).
- Diamond drilling on the Flex and Huestis in 1995 (1,490 m in 21 holes).
- Diamond drilling programs in 1996 consisted of 7 holes (400 m) on the Webber and Huestis/Flex junction and 10 holes (700 m) on the BMD hanging wall zone (Vince Vein).

1996 to 1997: Mining and milling of oxide ore from the Brown-McDade pit commenced November 1996 and ran until November 1997 with commercial gold production achieved on January 1, 1997.

1998: BYG's diamond drilling in 1998 included 30 holes (2,229 m) on the Flex Zone, 10 holes (762 m) on the BMD, 12 holes (1,009 m) on the BMD trend, 4 holes (402 m) on the Breccia Zone (approximately 1 km north of the Brown-McDade Zone), and 1 hole (123 m) on the Orloff King (Middleton, 2009).

Late 1997 to 1999: The mill was forced to close when unseasonably heavy rainfall runoff coupled with mill effluent caused a water imbalance that the tailings impoundment could not adequately contain. Water treatment facilities were installed to meet water quality discharge objectives and the mine restarts in January 1998. The mill was forced to work at less than full mill capacity until new pumping equipment could be installed which overcame circuit problems and finally allowed the mill to operate at full capacity. The mine ceased production in February 1999 (Denholm et al., 2000).

1999: BYG was ordered to terminate operations in 1999 due to non-compliance with the terms of the water license set forth by the Yukon Water Board. BYG entered into bankruptcy shortly after termination and the property came under the control of the Department of Indian and Northern Affairs ("DIAND"). D. Manning and Associates of Vancouver, BC was appointed by DIAND as receiver the same year, but soon resigned.

2001: Aurchem Exploration Ltd. performed prospecting and geological mapping on the Discovery Project claims.

2002 to 2003: Aurchem Exploration Ltd. followed this work up with trenching.

2004: Aurchem Exploration Ltd. completed 8 diamond drill holes for 695 m on the Discovery Project (Ellemers and Stroshein, 2005).

2004: PriceWaterhouseCoopers ("PWC") was appointed receiver of the former BYG property and subsequently divided the property into a core claim block and a peripheral claim block. The core claim block was withdrawn from staking for environmental remediation. The peripheral claim block was opened up to tender (Denholm et al., 2000).

2007 to 2008: 101073531 Saskatchewan Ltd (Sask Co) purchased the peripheral claim block, which includes the Charlotte claim block, from PWC in two transactions for a total of $3.2 million. In addition, Sask Co entered into an option with PWC to acquire the Dome 12 claim in consideration of the sum of $25,000 expiring 2018 (Middelton, 2009).

Sask Co undertakes an airborne VTEM-Magnetic survey. A total of 638 line kms were flown (Middelton, 2009).

2009: Airborne VTEM was flown of the property

2010: Guinness Exploration Inc. commenced work on the Charlotte Property in 2010 which saw the completion of 14 drill holes for 1442.82 m, as well as excavator trenching and limited reconnaissance mapping and rock sampling. Later that year Ansell Capital Corp. options the Charlotte Property from Guinness Exploration.

2011: Ansell Capital Corp. optioned the Discovery Creek Property from Aurchem Exploration. Ansell undertook diamond drilling (3607.93 m in 22 holes), soil sampling (1107 samples), geological mapping, excavator trenching (591.71 m) and claim staking on both the Charlotte and Discovery Creek properties. Results detailed several Au in soil anomalies and the continuation of the known grade and tenor of the Flex Zone veins.

Great Bear Resources optioned the Etzel claims from Ansell Corp. drilled three holes for 696.17 m, collected 478 soil samples to trace the extensive gold in soil anomalies on the adjacent Klaza Property and completed 255.7 m of excavator trenching.

Rockhaven Resources Ltd. diamond drills intersect significant mineralization along an 850 m strike length within the Klaza Zone. The zone remains open for expansion along strike in both directions and at depth. Mineralization exhibited exceptional continuity with 36 of 40 diamond drill holes testing the Klaza zone in 2010 and 2011 intersecting at least 1.0 gram gold equivalent/tonne over widths ranging between 3.04 and 36.50 m (average 13.04 m). This zone was open to extension down-dip and along strike in both directions.

2012: Ansell completes six diamond drill holes on the Flex Zone for 1883.46 m and two mapped/sampled trenches (373.71 m) in the Eliza Creek Extension area on porphyry targets.

6 Project Rationale

The Charlotte property is located in the Tintina Gold Belt, a known gold belt, and is in an area with a history of gold production. The property is located directly adjacent to the Mount Nansen gold –silver mine, a past producer which is currently under the jurisdiction of the abandoned mines department of Yukon Government and funded by the federal government. The Charlotte property shares some of the same geology as the Mount Nansen Mine.

Although sufficient funding was not available for a large drill program in 2013, forward momentum was maintained by conducting a detailed mineralogical study and a ground geophysical study. These two studies provide valuable information to the project and will allow for more informed decision making when it comes to sighting additional drill holes for future drill programs and expanding on the geological story.

7 Geology

7.1 Regional Geological Setting

The Charlotte property is located in the Tintina Gold Belt, a 200 kilometer wide by 1200 kilometer long series of Late Cretaceous granitoid intrusions which extend from central Alaska, across central Yukon to the Yukon-British Columbia border. Significant gold deposits in the Tintina gold belt include: Pogo, Fort Knox, True North, Donlin Creek and Shotgun (Figure 1) (Dadson & Struyk, 2012). The property occurs in

the Yukon-Tanana Terrane, an accreted conglomerate of terranes bounded by the Denali Fault to the southwest and by the Tintina Fault to the Northeast. The area is northwest of the maximum extent of the Wisconsin continental glaciation; the lack of glaciation on the property has resulted in deep weathering of up to 70 meters.

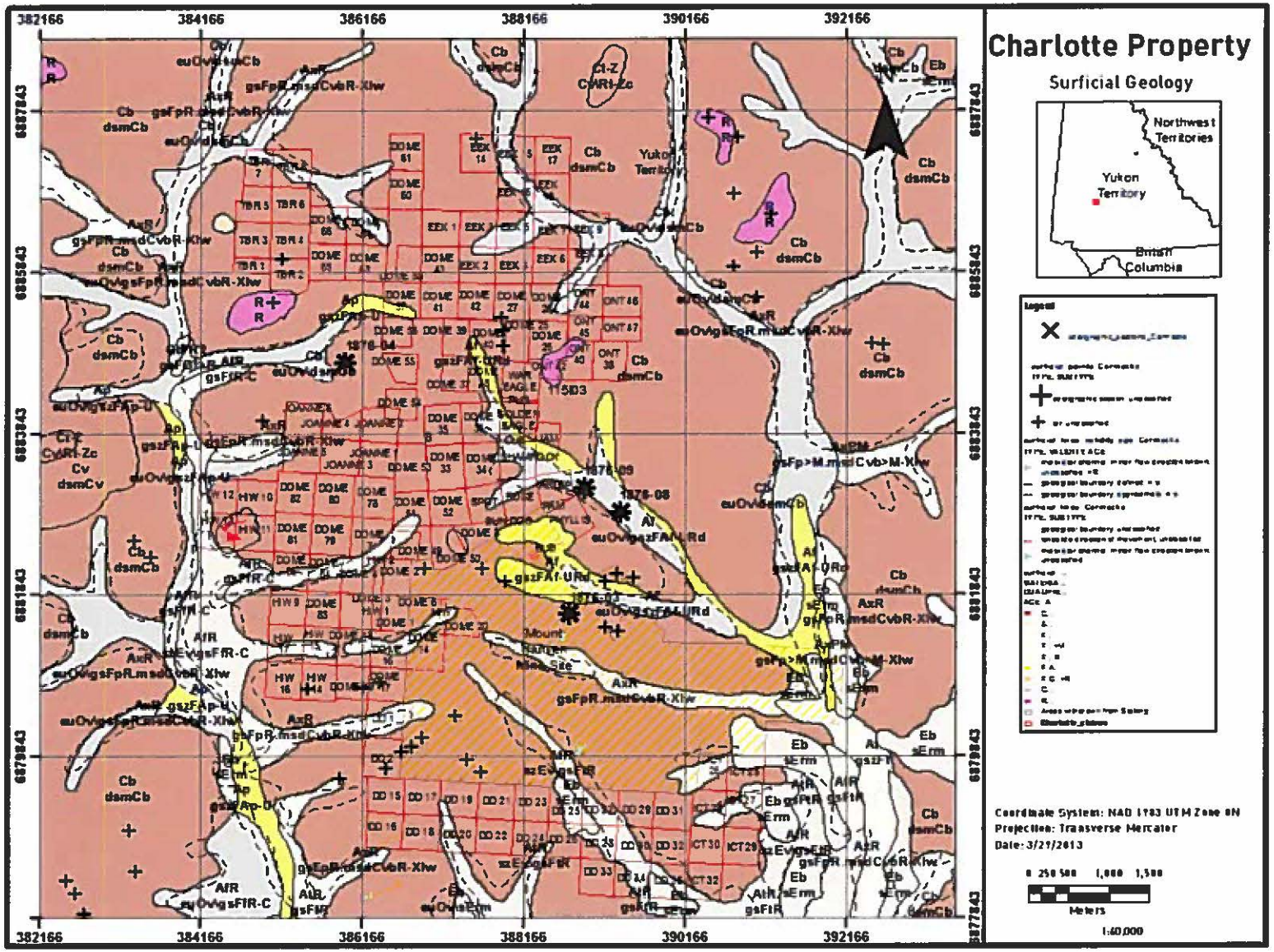


Figure 4. Surficial geology underlying Charlotte Property

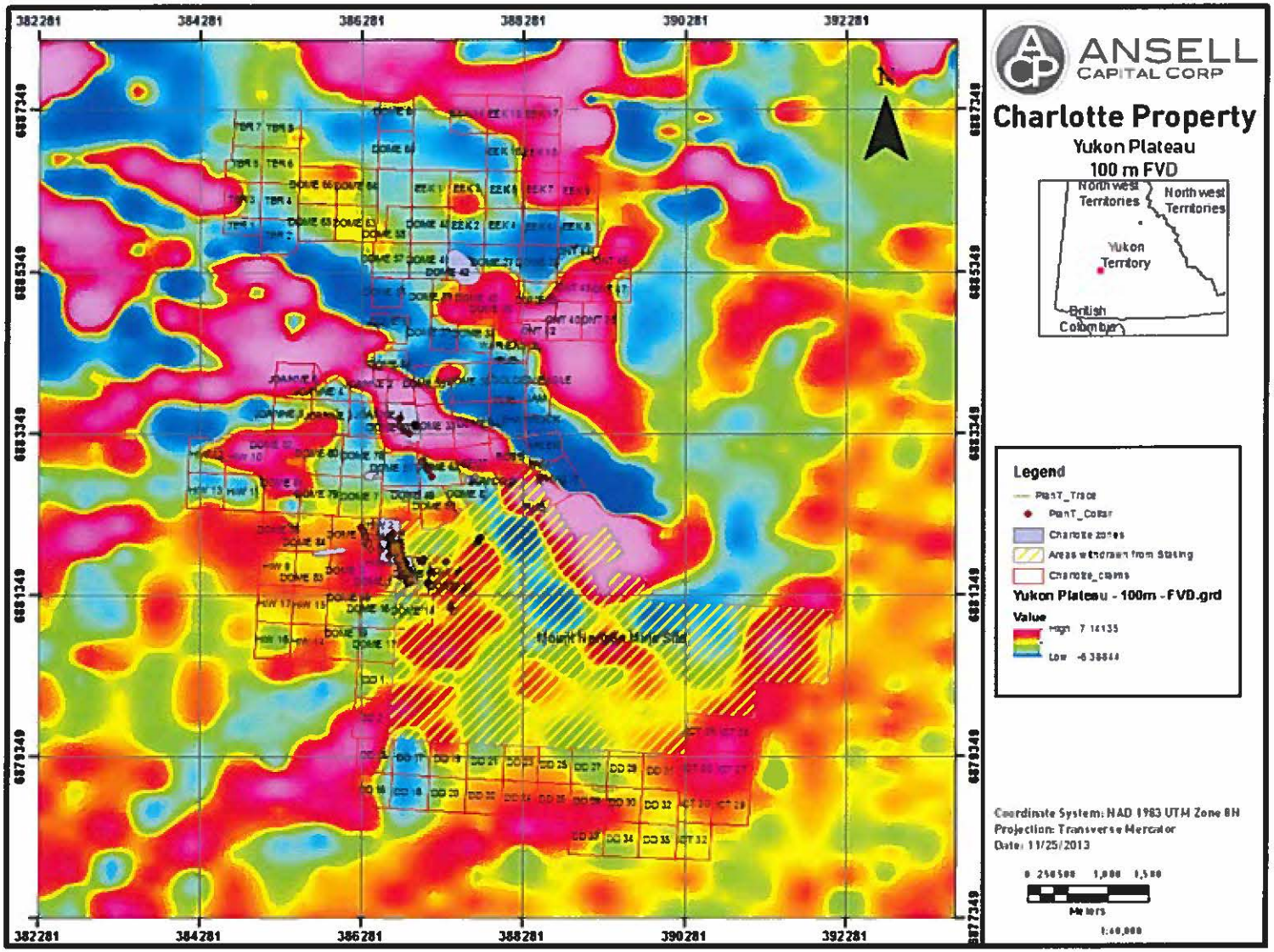


Figure 5. First Vertical Derivative geophysics (100 m spacing), Yukon Plateau, publically available dataset.

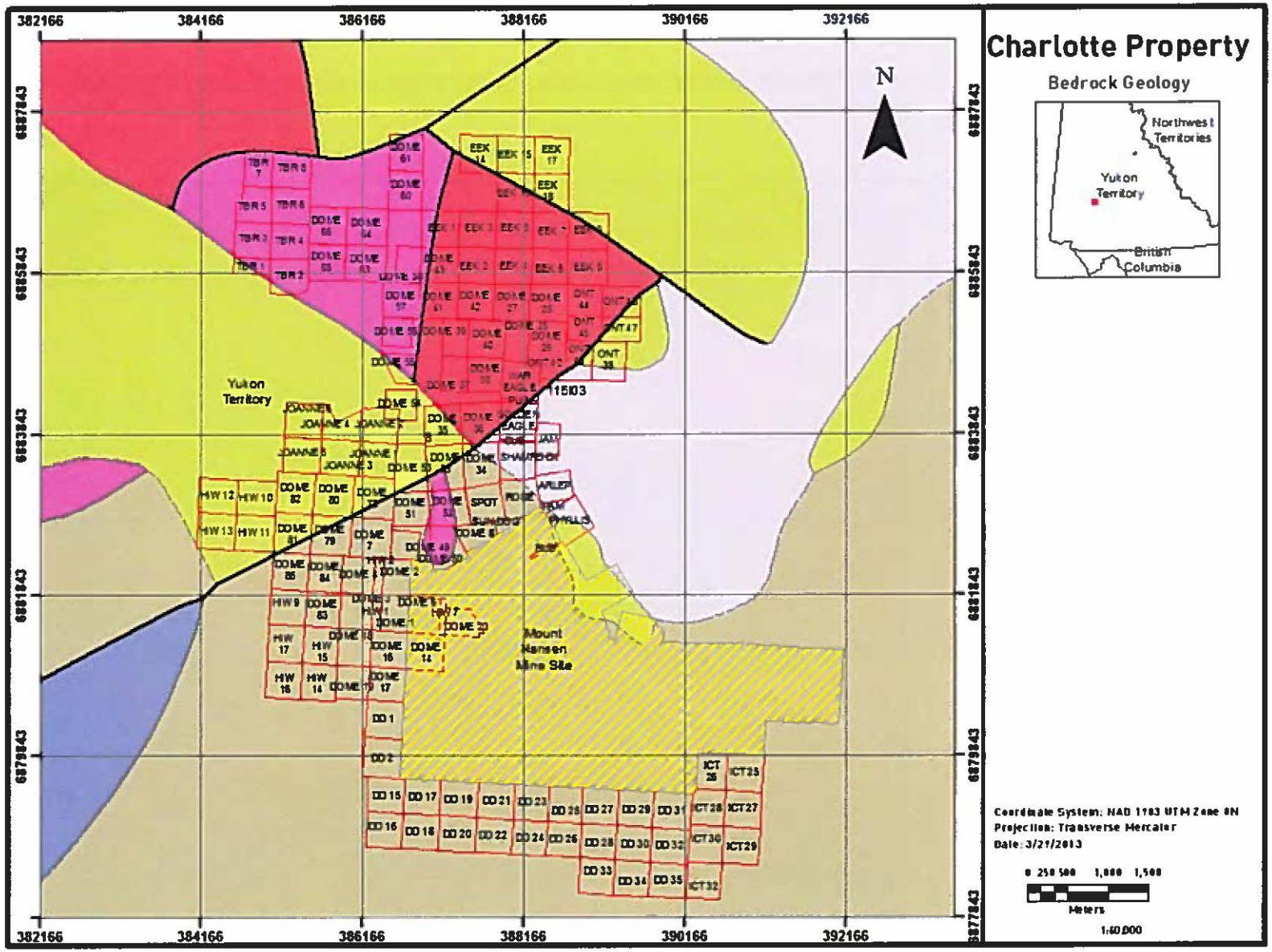
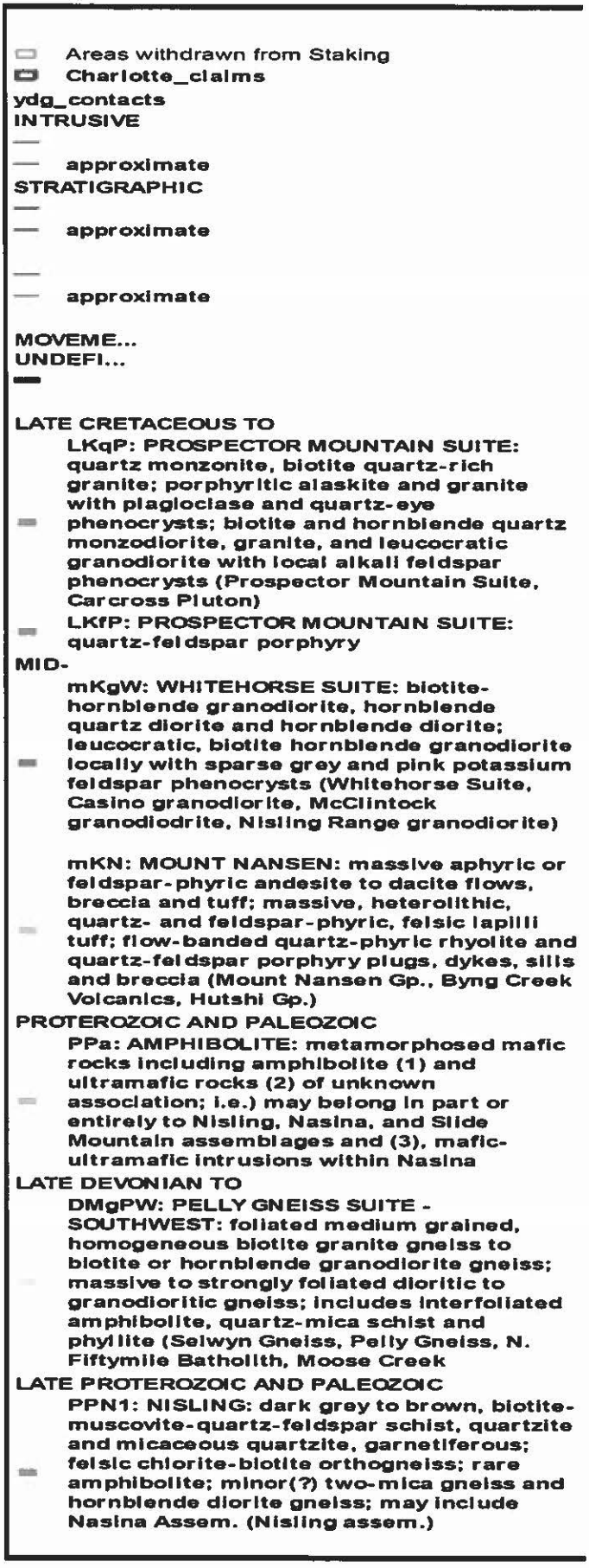


Figure 6. Underlying bedrock geology of the Charlotte Property. Geology courtesy of the Yukon Geological Survey.


Areas withdrawn from Staking
Charlotte_claims
ydg_contacts
INTRUSIVE
approximate
STRATIGRAPHIC
approximate
approximate
MOVEME...
UNDEFI...
LATE CRETACEOUS TO
LKqP: PROSPECTOR MOUNTAIN SUITE: quartz monzonite, biotite quartz-rich granite; porphyritic alaskite and granite with plagioclase and quartz-eye phenocrysts; biotite and hornblende quartz monzodiorite, granite, and leucocratic granodiorite with local alkali feldspar phenocrysts (Prospector Mountain Suite, Carcross Pluton)
LKfP: PROSPECTOR MOUNTAIN SUITE: quartz-feldspar porphyry
MID-
mKgW: WHITEHORSE SUITE: biotite-hornblende granodiorite, hornblende quartz diorite and hornblende diorite; leucocratic, biotite hornblende granodiorite locally with sparse grey and pink potassium feldspar phenocrysts (Whitehorse Suite, Casino granodiorite, McClintock granodiodrite, Nisling Range granodiorite)
mKN: MOUNT NANSEN: massive aphyric or feldspar-phyric andesite to dacite flows, breccia and tuff; massive, heterolithic, quartz- and feldspar-phyric, felsic lapilli tuff; flow-banded quartz-phyric rhyolite and quartz-feldspar porphyry plugs, dykes, sills and breccia (Mount Nansen Gp., Byng Creek Volcanics, Hutshi Gp.)
PROTEROZOIC AND PALEOZOIC
PPa: AMPHIBOLITE: metamorphosed mafic rocks including amphibolite (1) and ultramafic rocks (2) of unknown association; i.e.) may belong in part or entirely to Nisling, Nasina, and Slide Mountain assemblages and (3), mafic-ultramafic intrusions within Nasina
LATE DEVONIAN TO
DMgPW: PELLY GNEISS SUITE - SOUTHWEST: foliated medium grained, homogeneous biotite granite gneiss to biotite or hornblende granodiorite gneiss; massive to strongly foliated dioritic to granodioritic gneiss; includes interfoliated amphibolite, quartz-mica schist and phyllite (Selwyn Gneiss, Pelly Gneiss, N. Fiftymile Batholith, Moose Creek
LATE PROTEROZOIC AND PALEOZOIC
PPN1: NISLING: dark grey to brown, biotite-muscovite-quartz-feldspar schist, quartzite and micaceous quartzite, garnetiferous; felsic chlorite-biotite orthogneiss; rare amphibolite; minor(?) two-mica gneiss and hornblende diorite gneiss; may include Nasina Assem. (Nisling assem.)

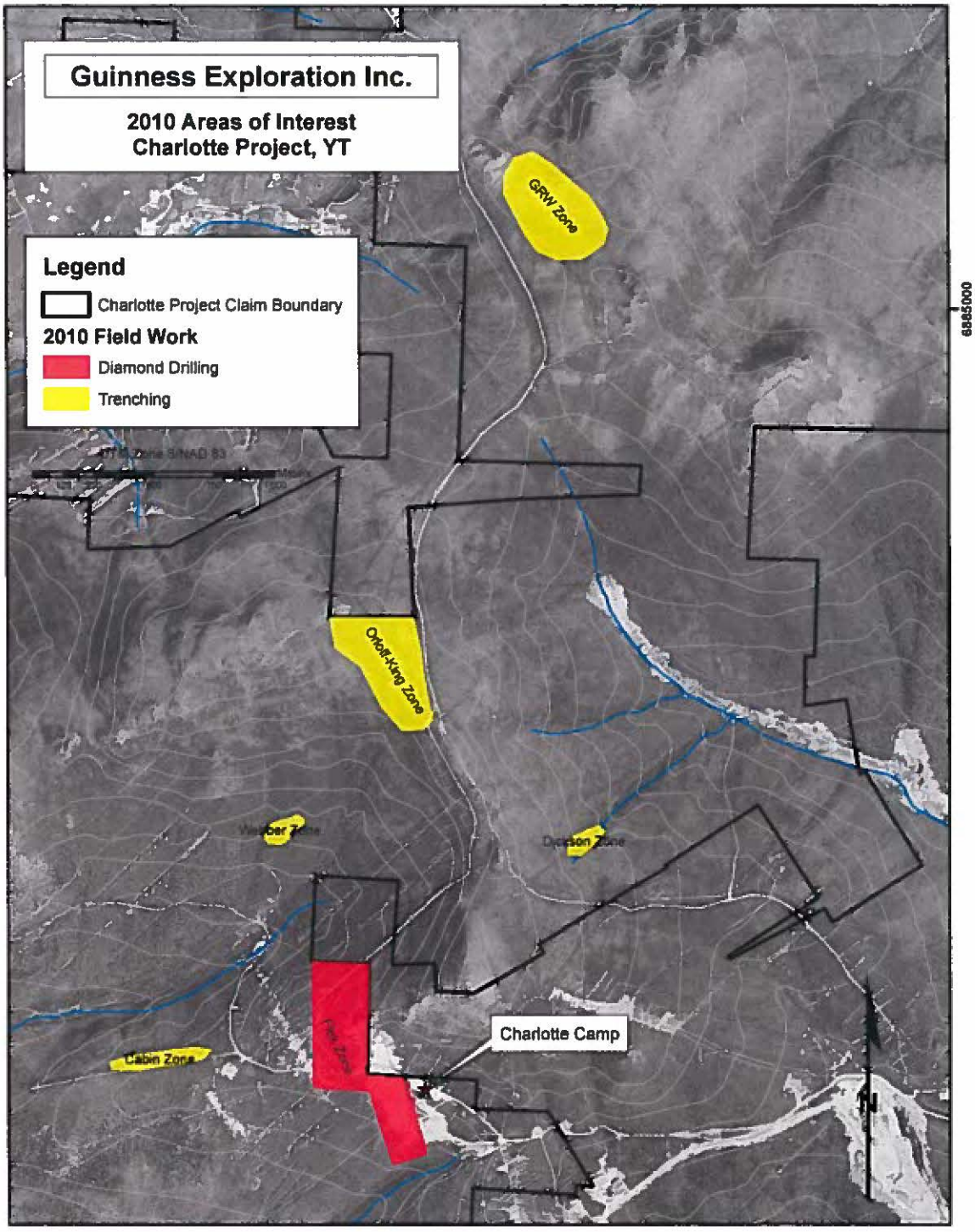


Figure 7. Zones of mineralization on the Charlotte property. Courtesy of Guinness Exploration (2010)

7.2 Property Geology

Near Mount Nansen, the Yukon-Tanana Terrane is composed of Devonian and older meta-igneous and meta-sedimentary rocks dominated by chlorite schist and felsic ortho-gneiss (Hart and Langdon, 1997). Early Jurassic alkali-feldspar-rich plutonic suites intrude the metamorphic rocks and the mid-Cretaceous Dawson Range batholiths, a granodiorite sill, is the most prominent intrusive in the area.

The property is underlain predominantly by Proterozoic and Paleozoic amphibolites (Nasina Assemblage), mid Cretaceous andsite-dacite flows (Mount Nansen group), mid Cretaceous biotite-hornblende grandiorites & hornblende quartz diorites (Whitehorse suite, Dawson Range Batholith), and late Cretaceous quartz monzonite (Prospector Mountain Suite) (Figure 8). Minor carbonates occur near the property

Dadson & Struyk (2012) mapped the property most recently and provide a summary of the geology:

> Four rock types dominate the immediate geology of the Charlotte Property (Figure 8). These are the Paleozoic metamorphic Nasina Assemblage to the south, the mid-Cretaceous granodiorite of the Dawson Range batholiths in the centre, the mid-Cretaceous, quartz-feldspar porphyry of the Coffee Creek plutonic suite to the north and the mid-Cretaceous andesite of the Mt. Nansen Group volcanic suite, coeval to the Coffee Creek plutonic suite, surrounding the claim block (Walls and Eaton, 1987).
>
> The oldest rocks underlying the claim block are metamorphosed rocks of the Paleozoic Nasina Assemblage. These occur in the southern portion of the property and include strongly foliated, intercalated quartz-feldspar-chlorite gneiss, quartzite, amphibolite and augen gneiss. Foliation generally strikes northeast and dips steeply to the northwest. The main mineralized zones including the Webber, Flex and Huestis Zones (Melling, 1995) are hosted by these rocks.
>
> A mid-Cretaceous Dawson Range batholith of medium to coarse-grained and locally foliated biotite-hornblende granodiorite intrudes the Nasina Assemblage in the northern third of the property. At the very north end of the property, this granodiorite has in turn been intruded by a large mid- Cretaceous pluton of the Mount Nansen (quartz-feldspar) Porphyry Intrusive complex which is related to the Coffee Creek Plutonic Suite (Melling, 1995).
>
> Both the metamorphic and intrusive rocks are unconformably overlain by the andesite of the Mt. Nansen Volcanic Suite, which dominates the central portion of the property and is typified by fragmental and flow units. Small plugs, dykes and sills of quartz-feldspar porphyry are observed to intrude this andesite (Melling, 1995). The main quartz-feldspar porphyry intrusive complex hosts the porphyry style mineralization known on the property (Sawyer and Dickinson, 1975).
>
> Five hydrothermal alteration facies have been documented and include propylitic, phyllic, silicic, argillic and potassic. Of these the propylitic is most widespread and is commonly associated with plutonic rocks adjacent to the Mount Nansen Porphyry system.

The property and area have undergone a complex structural history of folding and faulting/shearing. Complex fault intersections in igneous host rock such as quartz-feldspar porphyry can produce steeply plunging breccia pipes. A number of these occurrences have been documented across the property and include those within the Mount Nansen Porphyry complex (Eaton and Archer, 1989).

The structural setting has had a dramatic effect on the morphology of the vein systems which vary from planar and consolidated, such as the Huestis and Webber Zones, to complex and anatomising, like the Flex Zone. Vein systems are continuous up to 550 m in length and from 2 m to as much as 8 m wide (Denholm et al., 2000). Faulting and shearing are the two main structural features of the property.

Two mineralization styles occur on the Charlotte Property: precious metal vein and porphyry style. Both conform generally to accepted deposit models. Further, they fit into an encompassing model for transition from porphyry to epithermal style mineralization (Hart and Langdon, 1997).

The main mineralized zones consist of a series of anastomosing, sulphide-quartz veins that are preferentially hosted in northwesterly trending fault/shear structures. These structures appear to cut foliated Early Mississippian gneissic rocks and are spatially related to the mid-Cretaceous intrusive suite. A secondary northeasterly-trending set of fault structures is known from detailed mapping at several mineralized zones. The northeasterly structures appear to cross-cut and offset the main fault structures, creating structurally-suitable areas for the localization of mineralization at the intersection with northwesterly faults.

Typical vein gangue mineralogy consists of quartz $\pm$ carbonate. Sulphides tend to occur in semi-massive to massive rods, or as smaller masses, blebs and disseminations throughout the vein system. Sulphide mineralogy tends to be dominated by pyrite with lesser galena, sphalerite, chalcopyrite, arsenopyrite and stibnite (Denholm et al., 2000). Gold mineralization occurs as fine-grained inclusions (5-40 microns) within or at the interstices between sulphide crystals (Lecuyer, 1997). Silver mineralization typically occurs as inclusions within galena and sphalerite crystals. High cadmium values are also associated with gold and silver mineralization. Estimates for a silver to gold ratio vary according to the worker and their set of parameters. Denholm et al (2000) reported silver to gold ratio of 7:1 in vein style mineralization and 3:1 in breccia-pipe style mineralization. BYG reported an average ratio of 50:1 (Stroshein, 1998).

The second mineralized style occurs as a low grade porphyry copper-molybdenum zone associated with a quartz feldspar porphyry intrusion in the northeastern end of the property. The Cu-Mo mineralization is typically found as both stockworks and disseminations. Copper mineralization is widespread and has a typical grade of <0.12% Cu. Molybdenum mineralization, on the other hand, is associated with localized silicification and breccia zones. Molybdenum values on the property are generally low with an average grade of approximately <0.01% Mo. Local higher grade Cu – Mo zones are noted from fracture systems and also associated with rare

precious metal values. Lead, zinc, silver and gold values are also associated with porphyry-mineralization, but have not been systematically explored (Sawyer and Dickinson, 1975).

Some zones have a well-developed leach cap overtop of a supergene enrichment, which gives way at depth to hypogene sulphide mineralization. Surficial weathering can vary in depth from 5 m to 150 m, depending on location and slope aspect. It does not occur in every deposit and prospect, but notably in the BMD, Flex and Porphyry zones (Stroshein, 1998; Walls and Eaton, 1987). Substantial enrichment and alteration can occur to 150 m depth, but seems to wane after 75 m. In the vein zones, such as the BMD, the ore mineralogy has not been studied in detail but supergene enrichment does not seem to significantly affect gold or silver grades. However, in the Porphyry zone, supergene enrichment has locally doubled grades. The highest copper grades there range from 0.5-0.6% Cu (Walls and Eaton, 1987).

There are numerous historically described mineralized zones located on and adjacent to the Charlotte Property. The mineralized structures, which occur in a 2.5 km wide, 15 km long trend known as the Mount Nansen Trend, exhibit differential and variable intensities of regional metasomatism and hydrothermal alteration, typified by strong bleaching and intensive clay development.

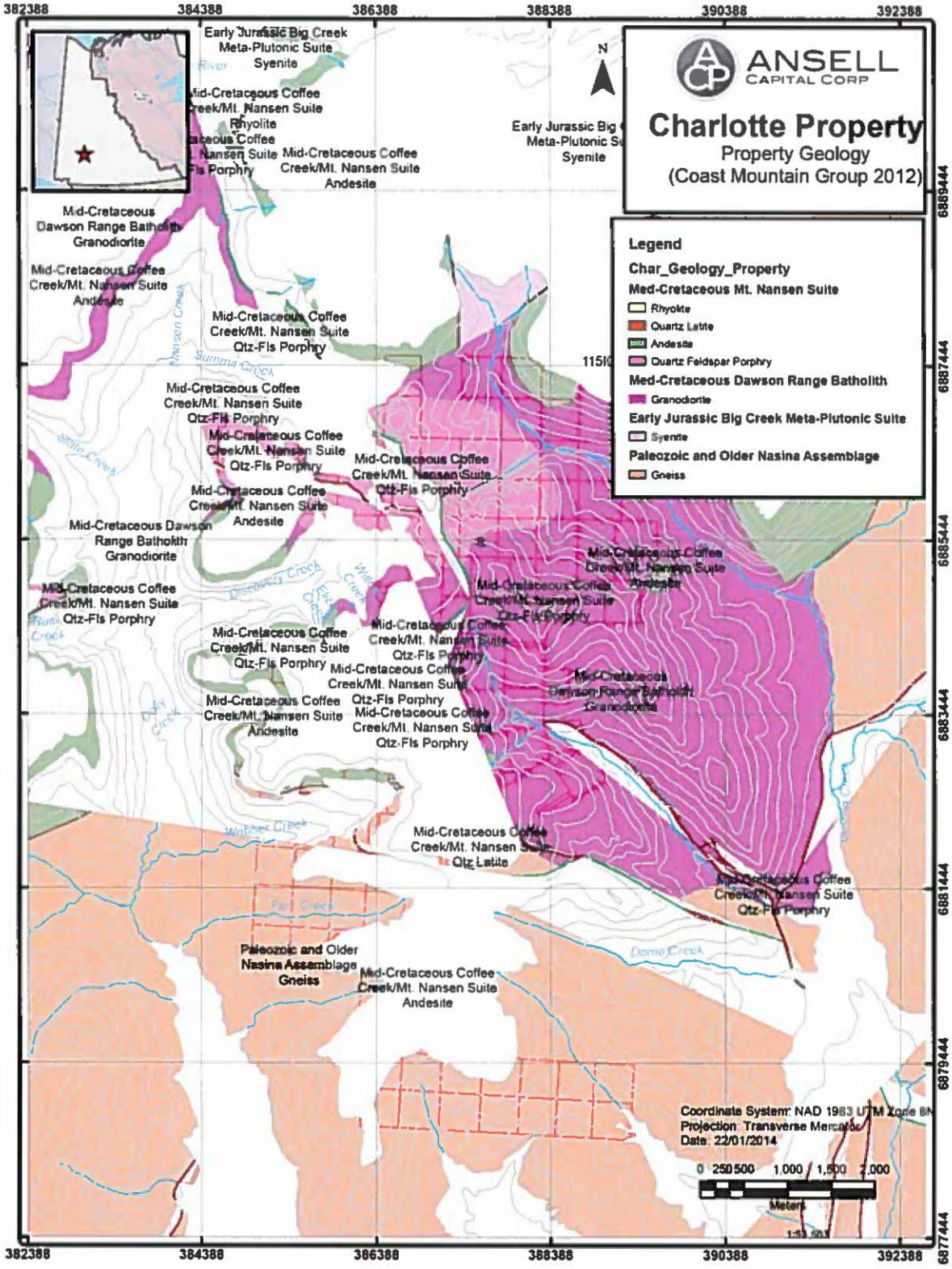


Figure 8. Geology of Charlotte property. Geology from Coast Mountain (2013).

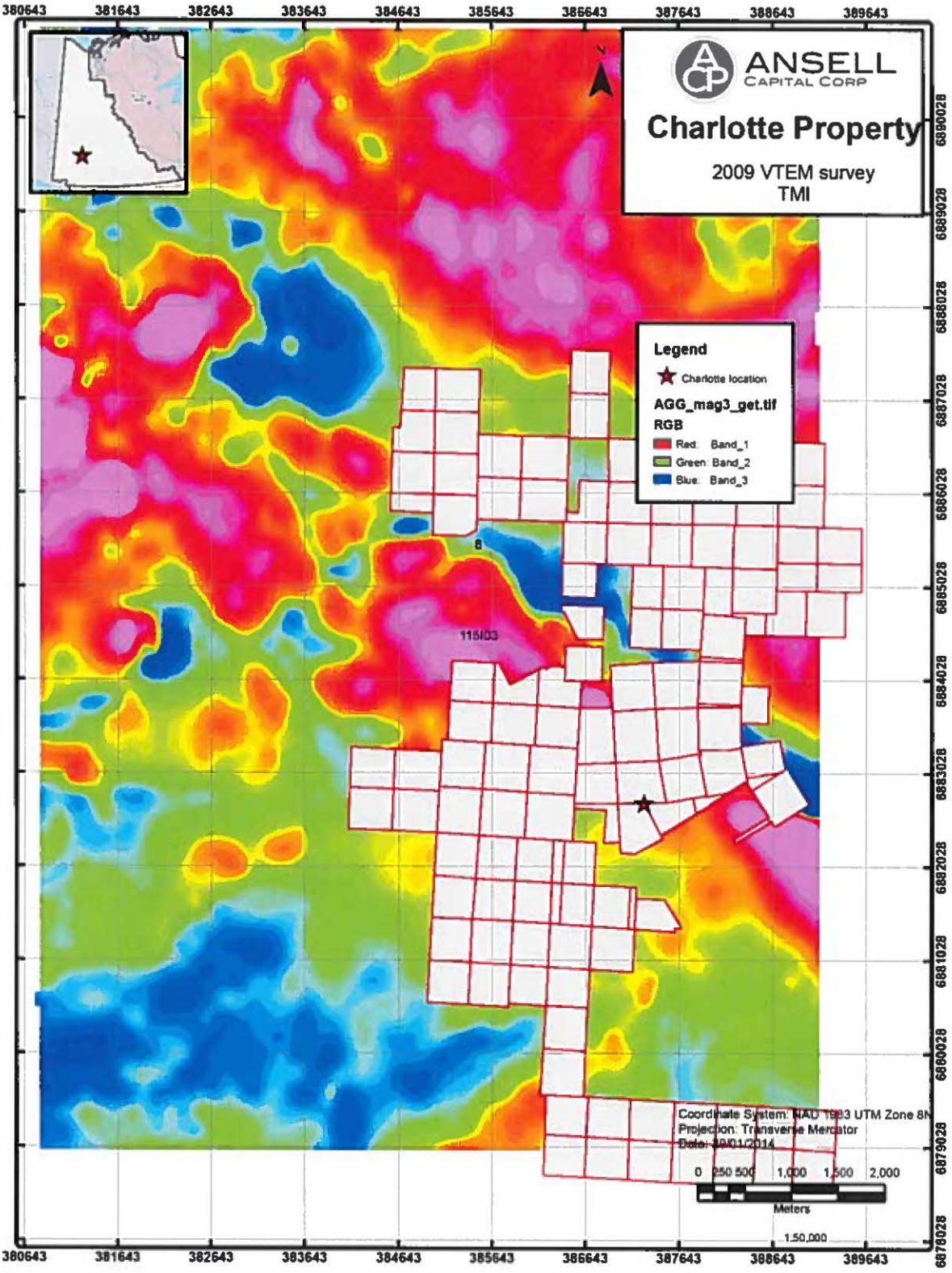


Figure 9. Total magnetic intensity from 2009 airborne VTEM survey

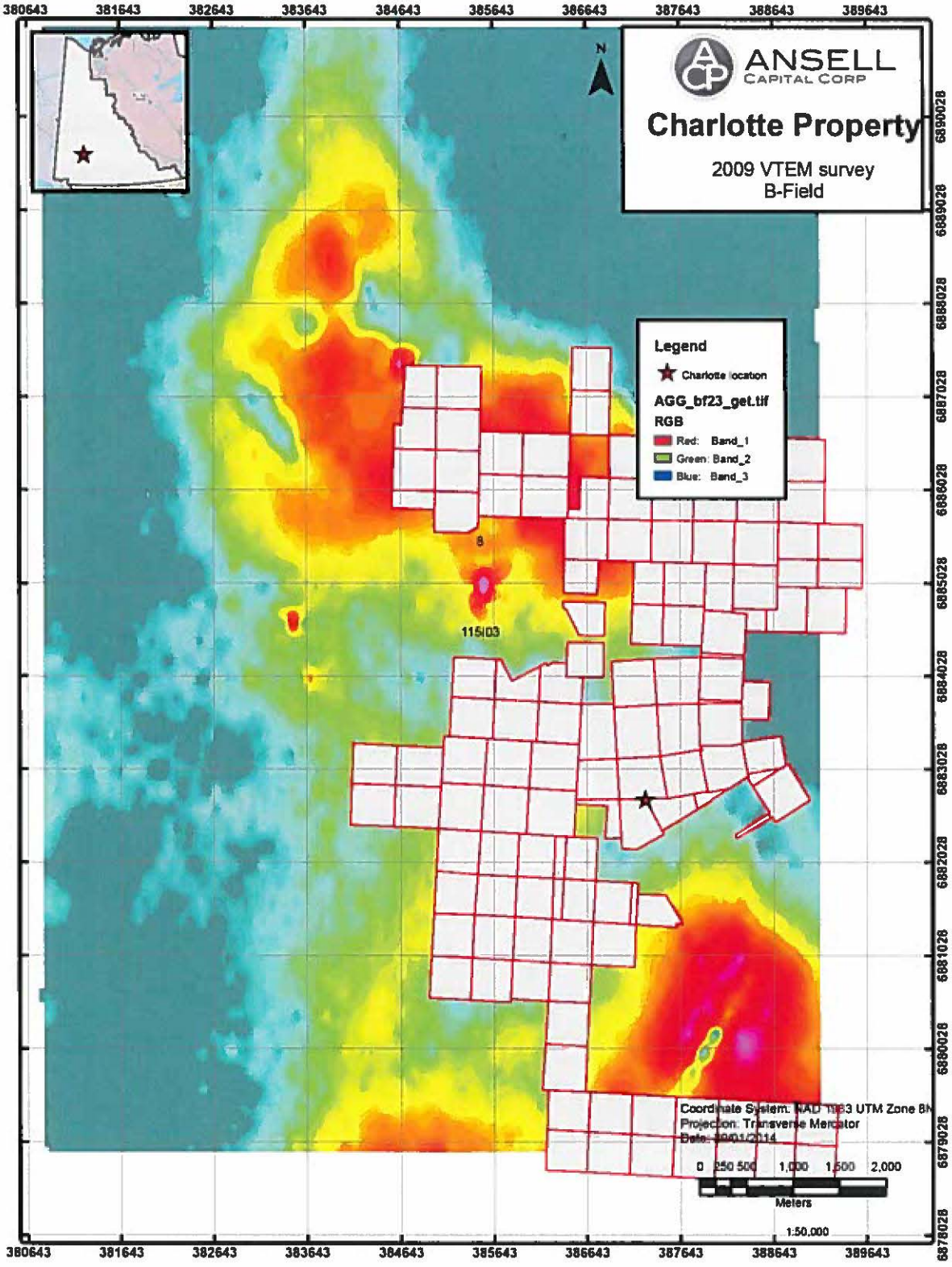


Figure 10. B field (EM) from 2009 airborne VTEM survey

The following is a description of the mineralized zones on the property, taken from Dadson and Struyk (2012) (Figure 7).

Flex Zone

The Flex Zone, which is presumed to be a well and complexly developed fault structure, lies between the Webber and Huestis Zones. It was discovered in 1985 and has been since defined by stripping, surface trenching and diamond drilling. It is comprised of a complex series of anastomosing narrow quartz veins that in fill fractures in the Paleozoic aged metamorphic basement rocks (Denholm et al, 2000). The veins, including the Main Vein, the Footwall Vein, the East and Hanging Wall Veins, are sub-parallel and dip steeply to the west (Anderson and Stroshein, 1998). The veins are offset by unmineralized east to northeast trending faults. The Flex Zone has been delineated over a strike length of 550 m and is open at depth (Struyk and Dadson, 2012; Denholm et al, 2000; Melling, 1995). The top 15-40 m of the Flex Zone has undergone significant supergene alteration and therefore the sulphide minerals within the veins are mostly altered to limonite or other oxides (Denholm et al, 2000; Melling, 1995). Structural control on the individual veins is complex which makes for difficult correlation between surface showings and drill hole intercepts (Denholm et al, 2000). Further compounding the problem, is the historical stripping of the Main zone which made re-establishment of hole locations drilled prior to 1998 difficult. The veins range from 5 to 110 cm thick but extensive silicification of the wall rock extends ore grade widths up to 7 m (Stroshein, 2007b).

Orloff-King Zone

The historical work on the Orloff-King Zone, located 1400 m N of the Flex Zone focused on the low grade oxide mineralization exposed in trenches and intersected in shallow drill holes. In 2010, however, exploration focused on unfinished trenches located to the northwest of known mineralization. Here discontinuous mineralization has been outlined through extensive trenching over a strike length of approximately 1 km. This zone is open to the north, has a northwest extension, and has peak grades of 7.05 g/t Au and 34.7 g/t Ag over 0.7 m. In 2011 saw the completion of mapping 1 trench left open from 2010 for 49.30 m and 4 drill holes for a total of 607.46 m. Work confirmed the presence of several narrow Au+/-Ag sulphide breccia zones with alteration halos that are narrower than those seen in the Flex zone but parallel to the regional mineralizing trend. The zone is open to the NW, SE and at depth.

Webber Zone

The Webber Zone consists of a NW striking and SW dipping quartz vein system hosted by the metamorphic assemblage and an extensive northeast striking porphyry body. The system is comprised of two veins, the No. 1 and No. 2, which occur respectively along a fault's foot and hanging walls. These veins which vary in width from 0.3 m to 2.0 m have been explored over a strike length of 500 m through a combination of surface stripping, trenching and underground development. From the underground work the gold mineralization associated with arsenopyrite and lesser stibnite occurs in shoots or rods which are typically 25 m in horizontal strike length and 100 m along plunge. Sampling has defined seventeen ore shoots which on average grade

14.06 2012 Assessment Report on the Charlotte Property November 1, 2012 Coast Mountain Geological Ltd. 24 gpt Au and 917 gpt Ag. Transitions between mineralized and unmineralized sections of vein tend to be very sharp and shoots tend to correlate well with surface mineralization. Historic diamond drilling has tested vein continuity above and below the adit, as well as along strike. This work indicates that the Webber zone is truncated to the northwest by the Webber Creek Fault.

Cabin, GRW, Dickson Zones

Other mineralized zones of the Charlotte Property include the Cabin, GRW, and Dickson. All are vein targets but have received significantly less development than the major zones. These targets have been explored with soil geochemistry and follow-up trenching. None, to date, have been diamond drilled.

There are a variety of MINFILE localities located on or near the property (Figure 11 and Table 2).

Table 2. Summary of MINFILE localities near the Charlotte property

MINFILE name and number	TYPE	STATUS	COMMODITY	HYPERLINK
115I 093 GOULTER (Au, Ag - porphyry)	Porphyry	Drilled Prospect	Au, Ag	http://www.geology.gov.yk.ca/publications/minfile/text_files/115I/115I093.pdf
115I 064 BROWN-MCDADE (Au, Ag - vein)	Vein	Deposit	Au, Ag	http://www.geology.gov.yk.ca/publications/minfile/text_files/115I/115I064.pdf
115I 065 MOUNT NANSEN (Au, Ag - vein)	Vein	Deposit	Au, Ag	http://www.geology.gov.yk.ca/publications/minfile/text_files/115I/115I065.pdf
115I 066 CYPRUS (Cu, Mo - porphyry)	Porphyry	Drilled Prospect	Cu, Mo	http://www.geology.gov.yk.ca/publications/minfile/text_files/115I/115I066.pdf
115I 067 ESANSEE (Ag, Au, Pb - vein)	Vein	Drilled Prospect	Ag, Au, Pb	http://www.geology.gov.yk.ca/publications/minfile/text_files/115I/115I067.pdf
115I 065 MOUNT NANSEN (Au, Ag - vein)	Vein	Deposit	Au, Ag	http://www.geology.gov.yk.ca/publications/minfile/text_files/115I/115I065.pdf
115I 123 ANG (vein)	Vein	Showing		http://www.geology.gov.yk.ca/publications/minfile/text_files/115I/115I123.pdf

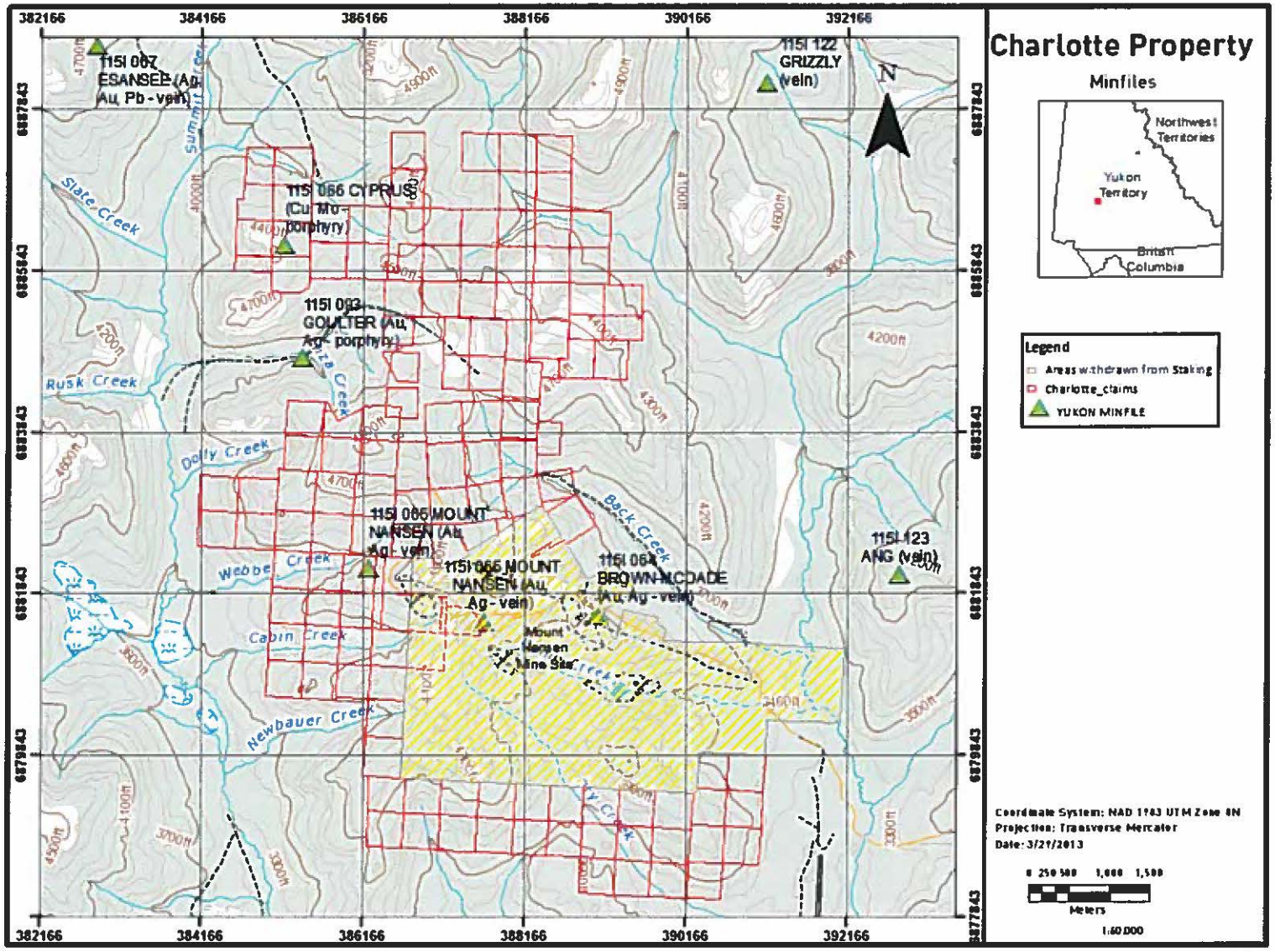


Figure 11. MINFILE locations on and surrounding the Charlotte property

8 2013 Work

Completed work on the Charlotte in 2013 differed slightly from the work proposed in the original YMIP application. Mapping and structural interpretation did not take place, but 4.565 line km of ground was covered by a ground IP survey and 29 rocks were collected and sent for thin section and detailed mineralogical work. A small ground mag and radiometric survey was conducted, but the data was not useable.

The primary exploration target for 2013 was the Flex zone (Figure 7). This area was selected because it had the most amount of work (drilling) completed on it and thus is the best understood out of all the zones.

8.1 IP survey details

Ansell Capital Corporation commissioned GroundTruth Exploration Inc of Dawson City to conduct a high resolution DC Resististivity/IP (HRRIP) geophysical survey on the Charlotte property. 9 profiles on the FLEX and 2 profiles on the OK (Orloff-King) were conducted and read for resistivity and chargeability using multiple arrays. All of the lines were 415 m in horizontal length, resulting in a total survey length of 4.565 line km. Two of the lines on the Flex are part of a 2013 case study in partnership with the Yukon Geological Survey. Figure 12 shows the location of the 2013 ground geophysics survey and Figure 13 shows the FLEX survey lines and historical drill hole collar locations.

The bulk of the work was completed from September 7-14th 2013; technical difficulties with an IP receiver on the FLEX survey resulted in a return trip on October 2nd 2013 to complete the work.

Field operating procedures, data processing techniques and a detailed report can be found in the complete Geophyiscal Survey Report (Fage, 2014), located in the appendix.

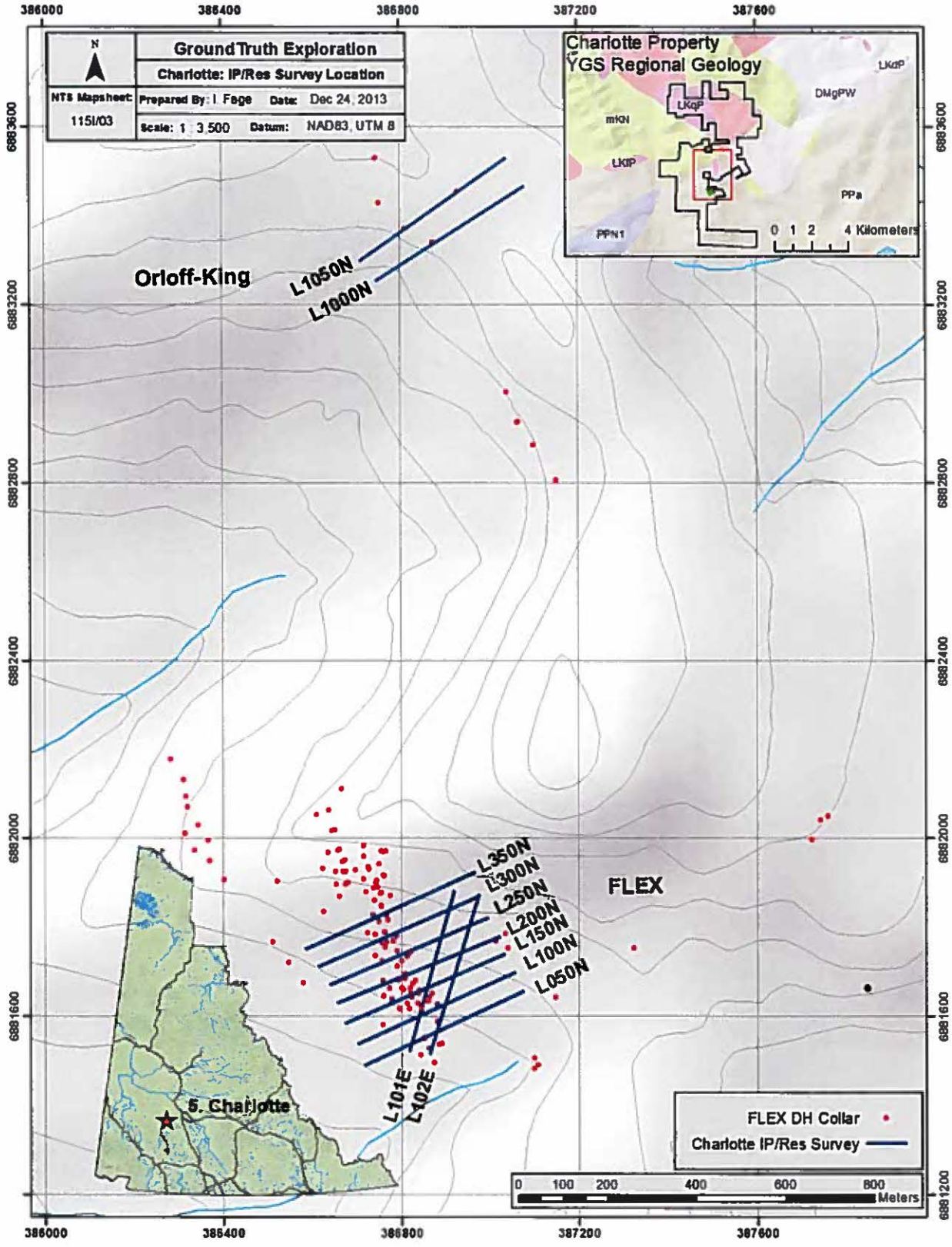


Figure 12. Location of the 2013 FLEX and Orloff-King (OK) IP and Resistivity surveys.

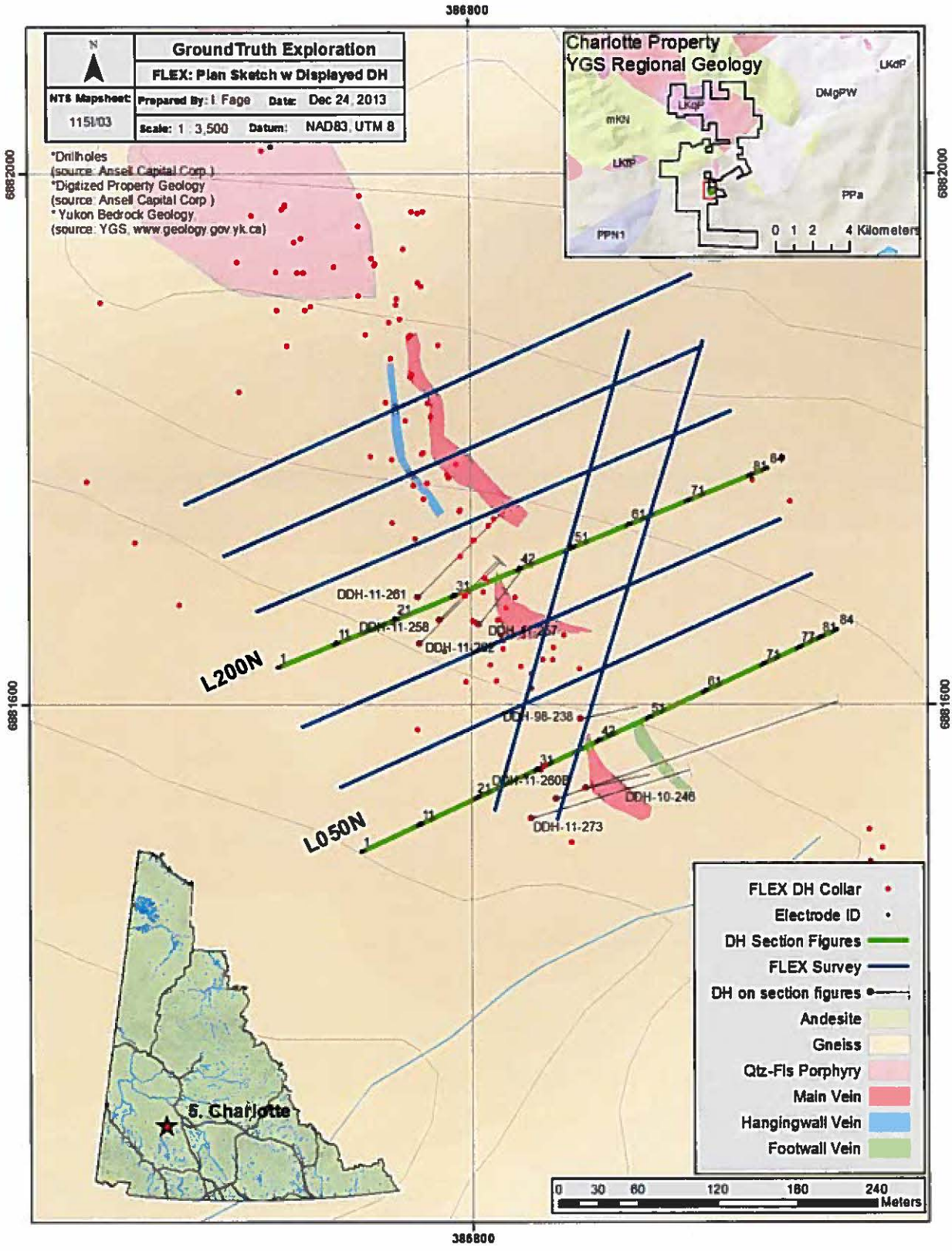


Figure 13. FLEX zone IP lines and locations of DDH and IP sections with DDH.

8.2 Mineralogical work

A detailed report on the mineralogy from samples collected this summer can be found in the appendix. The objective of the mineralogical report was to identify which mineral phases host high contents of Au, Ag, Cu and Sb, as well as examine the paragenetic relationships of those phases. 29 rock samples were collected by Ansell Capital Corp and 34 thin sections were created by Vancouver Petroprahics.

Mineralogical report was conducted because historical "historical mineral processing and metallurgical testing encountered major problems relating to: (1) different extraction methods required by the sulfide and oxide ores; (2) complex silver-lead-antimony sulfosalts and arsenic minerals; (3) the refractory nature of the sulfide ore; and (4) the high clay content of the oxide ore. The objectives of the [mineralogical] study were to: (1) identify the gold-, silver-, copper-, antimony-, and arsenic-containing mineralogical phases; and (2) characterize the abundance, texture, and paragenetic relationships of each of these phases" (Dalsin and Groat, 2014).

8.2.1 Mineralogical Methods

Taken from Dalsin and Groat (2014) (see appendix for complete report).

> Twenty-nine rock samples were obtained from Ansell Capital, and 34 areas for polished sections were picked by the authors [Dalsin and Groat (2014)]. The samples were sent to Vancouver Petrographics to be prepared for polished section. The polished sections were then scanned using a Nikon slide scanner, and high resolution images in plane-polarized and cross-polarized light were obtained. These scans were used as navigational maps when utilizing the microscopes. Optical petrography was conducted using the authors Olympus CX-31P petrographic microscope (transmitted and reflected light with camera capability). The Phillips XL30 scanning electron microscope (SEM) at the University of British Columbia, equipped with an energy-dispersion X-ray spectrometer, was utilized for more detailed mineralogical investigation on selected polished section. The 18 selected polished sections were carbon coated prior to observation with the SEM. Detailed investigation consisted of backscattered electron (BSE) images and energy-dispersive X-ray spectra (EDX). During SEM analysis, a beam spot size of 6 μm was used with an excitation

9 Sample collection, ground mag and radiometrics

29 rock samples were collected on the property this summer for the mineralogical study. A couple lines of groundmag and radiometrics

The magnetometer unit used was a GSM-19 (Overhauser) magnetometer designed by GEMsys with the following specifications:

Sensitivity: 0.022 nT @ 1 Hz, (0.015 nT option)
Resolution: 0.01 nT

Absolute Accuracy: +/- 0.1 nT
Dynamic Range: 20,000 to 120,000 nT
Gradient Tolerance: Over 10,000 nT/m
Sampling Intervals: 60+, 5, 3, 2, 1, 0.5, 0.2 sec
Operating Temperature: -55°C to +50°C

The spectrometer was a Radiation Solutions RS-125 = 2x2" (6.3cu ins) Sodium-Iodide detector with an energy response from 30 keV-3000keV.

Unfortunately the amount of data collected was too small for the author to plot on a map or to make any meaningful conclusions about.

10 Data interpretation

10.1 Ground Geophysics

10.1.1 FLEX Zone Interpretation (taken directly from Fage (2014) unless otherwise stated).

The FLEX survey examined from South to North shows a resistivity low at mid traverse (200m) that dips steeply to the East at depth or is vertically oriented at depth in most traverses. This feature is prominent in traverses: L050N ,L150N,L200N,L250N,350N.(Figures 2,4,5,6,8). When this resistivity feature is plotted with FLEX drillhole data on Sections 050N and 200N, (Figures 13, 14) we see that mineralization is related to the resistivity low (050N) or possibly the Western contact of resistivity low feature (200N).

The plan map of inverted resistivity at the 1270m level (Figure 16)shows a prominent North-South resistivity low lineament running through the survey area (Figure 16) with a shorter NE oriented Res low feature also crossing on the west side of lines 250N and 300N. The major N-S Res low feature bisects the survey area into a highly resistive (low conductivity) body on the West and a less resistive body (moderate-high conductivity) on the East. When mineralization projected to surface (digitized from Ansell figure) is overlaid on the resistivity plan map (Figure 17) we see a correlation between the main vein mineralization and the west contact of the main N-S resistivity low feature.

A preliminary interpretation is that the main N-S res low feature is mapping out the faulted and clay altered zone of the deposit which would likely be of relatively higher conductivity than surrounding host rock.

There is a strong correlation between chargeability high features that are coincident with the above discussed resistivity lows and drillhole mineralization. These target chargeability highs are also showing to be oriented as steeply dipping to the east. Chargeable oxide mineralization, clays and high sulphide content is expected to be the reason for the coincident chargeability high with resistivity low and denotes ore zone potential.

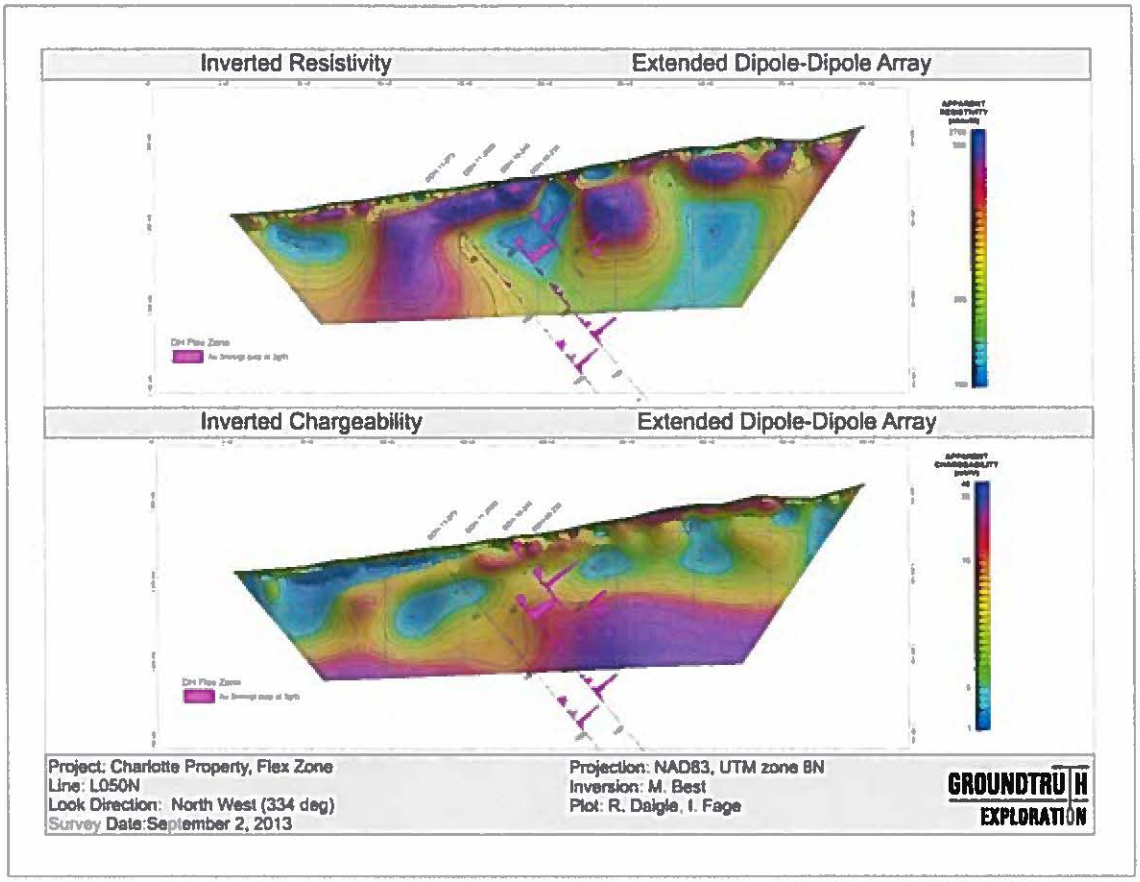


Figure 14. Resistivity, Chargeability, and drill holes with Au over the FLEX zone, along line L050N.

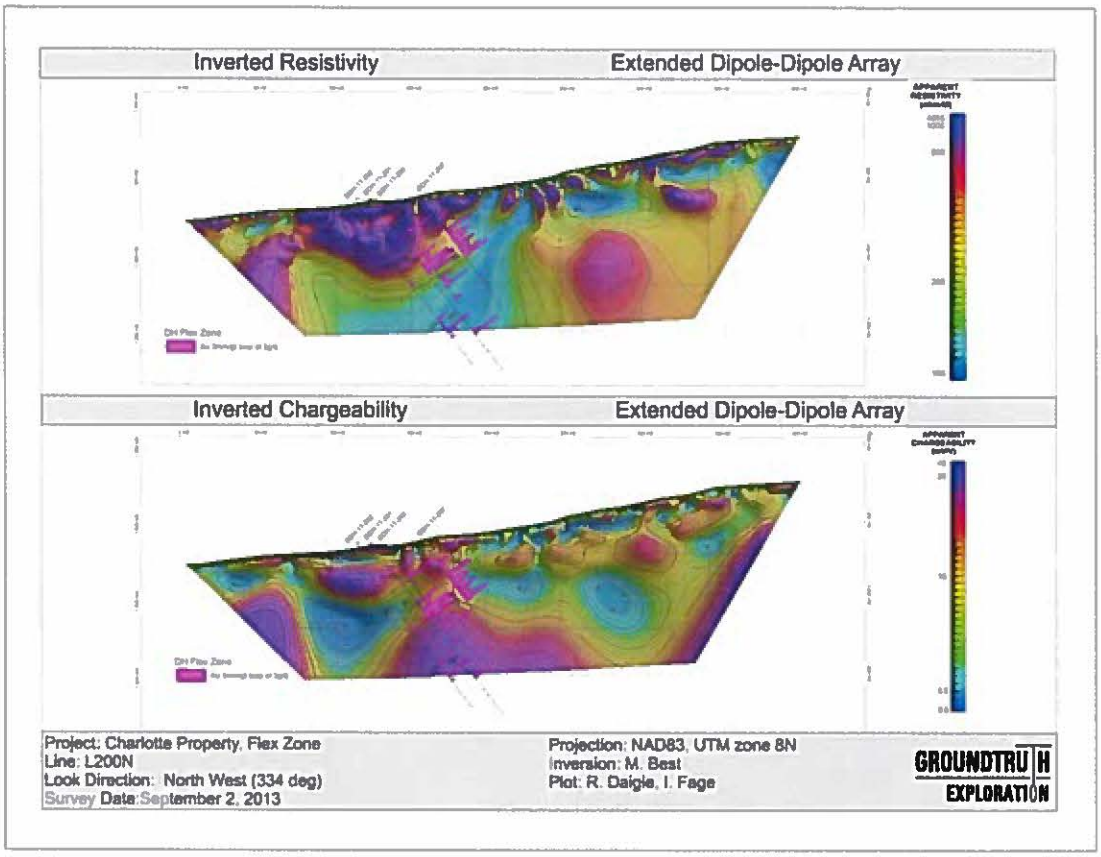


Figure 15. Resistivity, Chargeability, and drill holes with Au over the FLEX zone, along line L200N

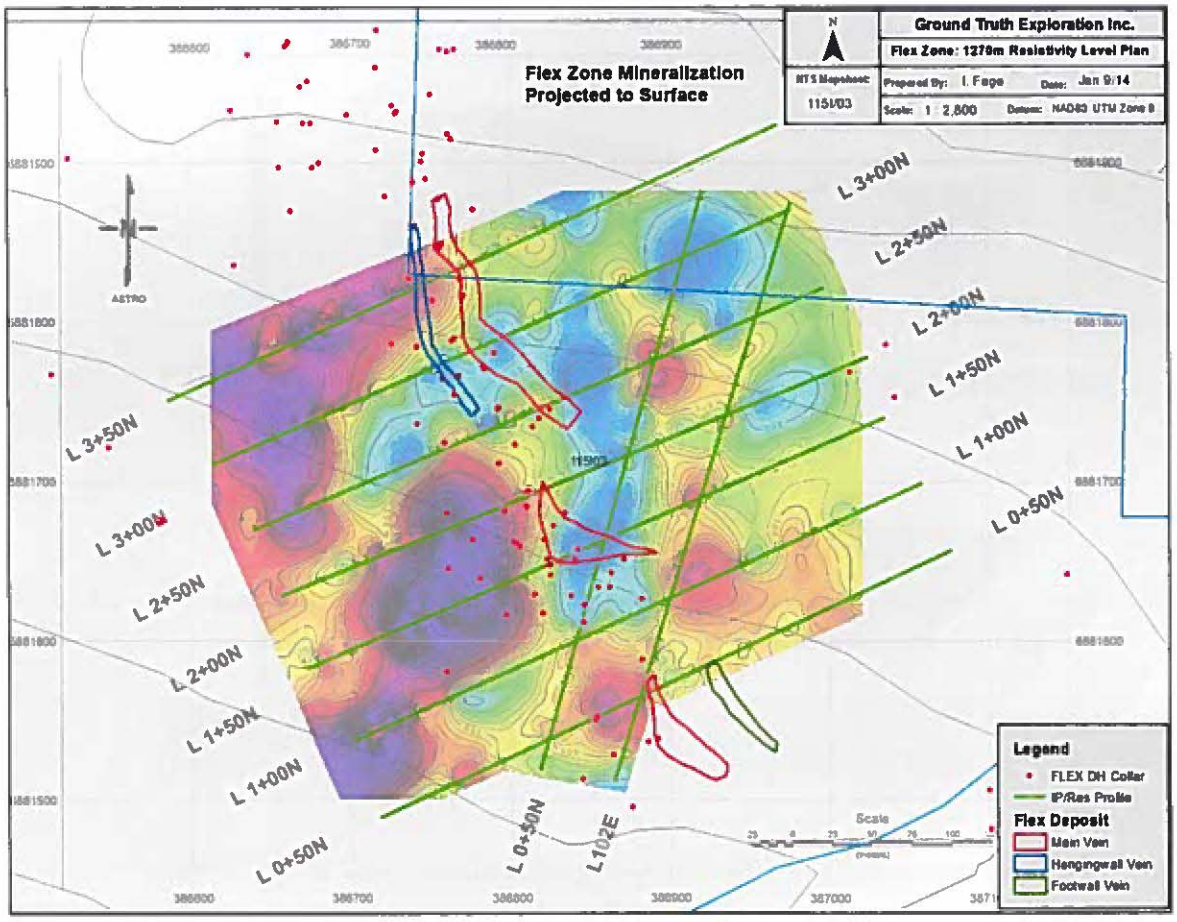


Figure 16. Level plan of surface resistivity over the FLEX zone (Fage, 2014).

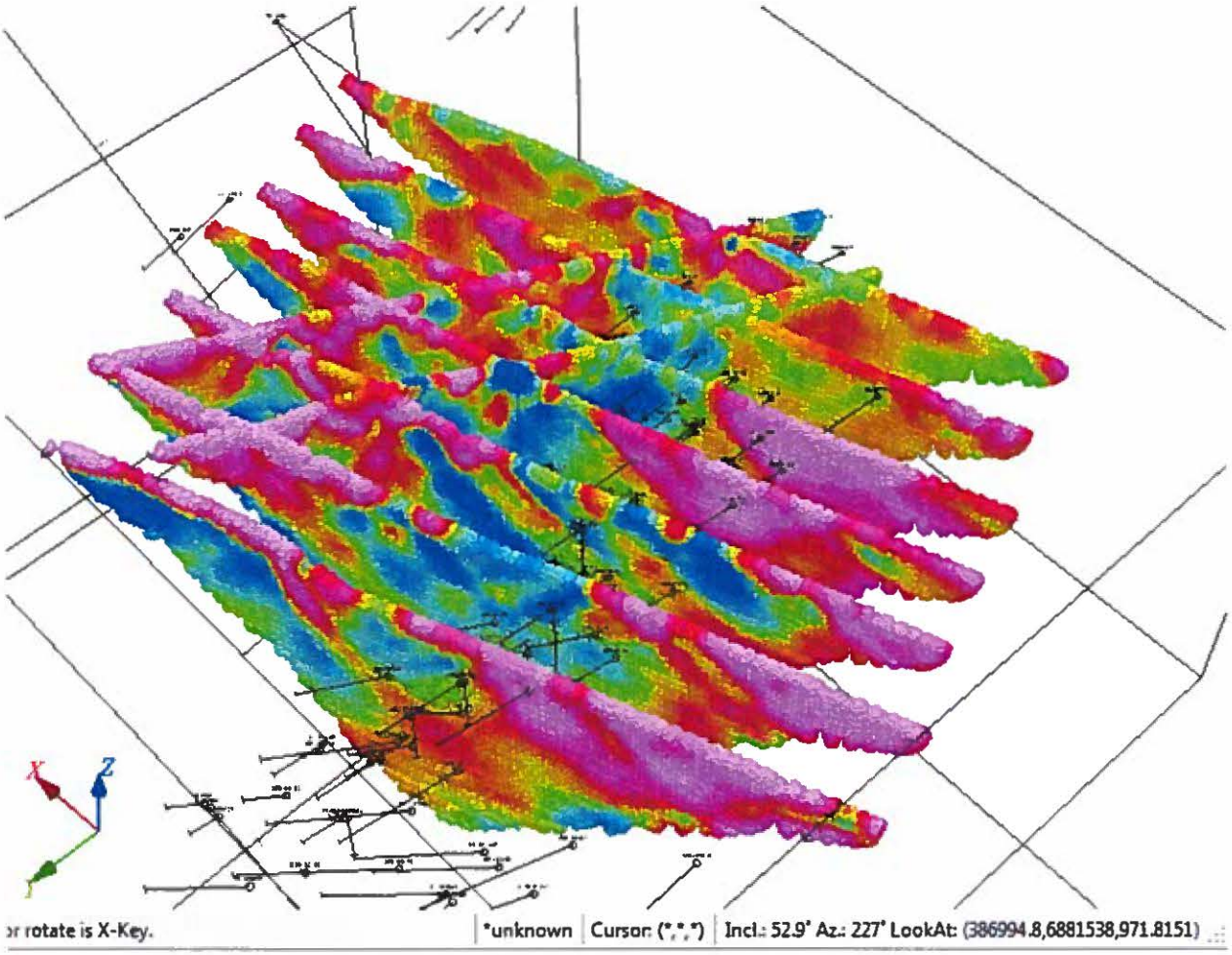


Figure 17. Screenshot of 3D resistivity in the FLEX zone. Black lines represent historical drill holes. View is looking roughly northeast.

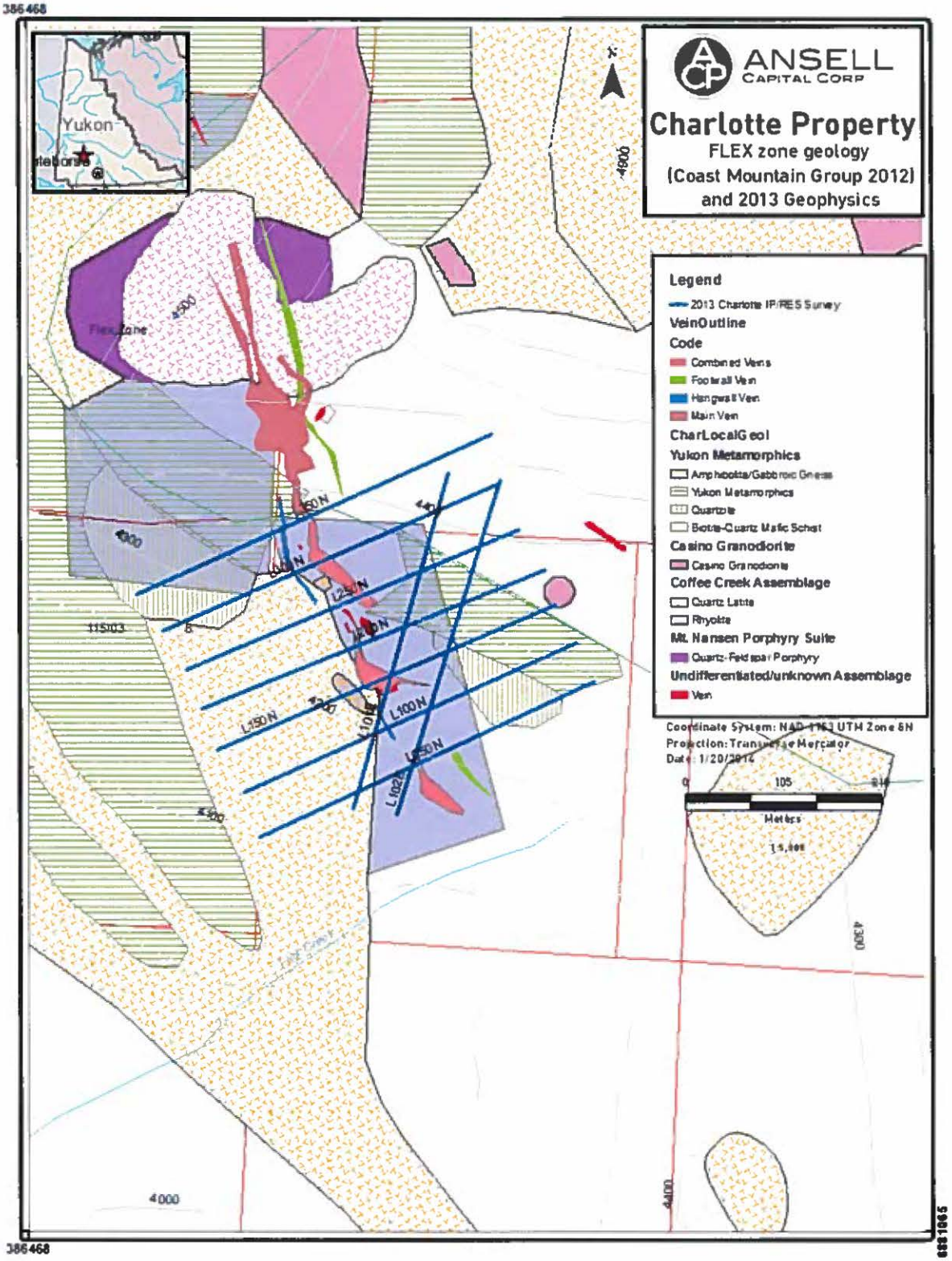


Figure 18. 2013 IP/RES survey on the FLEX zone and 2012 Coast Mountain Geological geology

10.1.2 OK Zone Interpretation (taken directly from Fage, 2014)

Both traverses on the OK target show significant near surface chargeability high anomalies (> 30mv/v). The southern traverse (1000N, fig 11) indicates this chargeability feature is possibly dipping to the SW while the northern traverse (1050N, fig 12) shows the IP high to be vertically oriented. There is a coincident inverted resistivity low feature at depth on 1050N traverse at centre of profile line. The near surface chargeability high on 1000N traverse (210-250m) also shows a coincident strong resistivity low (fig 11). Both of these targets are of interest for mineral potential.

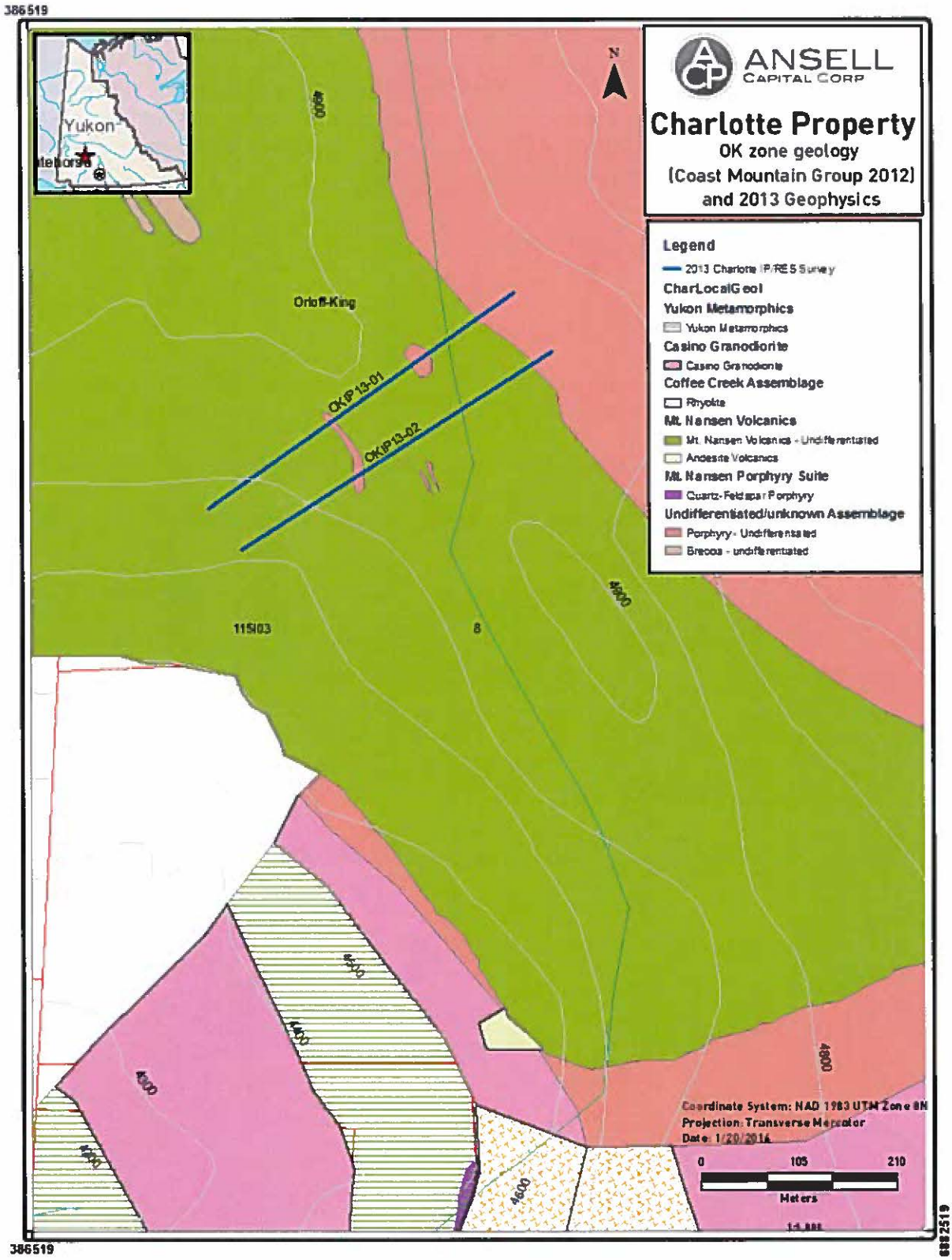


Figure 19. 2013 IP/RES survey on the FLEX zone and 2012 Coast Mountain Geological geology

10.2 Mineralogical Interpretation (Taken directly from Dalsin and Groat (2014)- see complete report in appendix)

The mineralization of the polished thin sections was carefully examined with a focus on identifying the phases that host Au and Ag. Interpretation is based solely on the observed sections. The mineralogy of the sections is summarized in Table 3.

In general, it appears that the mineralization is hosted in quartz veins that were emplaced into a hydrothermally altered, quartz-rich host rock. The alteration consisted of muscovite, or similar K-rich mica; field observations would commonly refer to this as sericite. The host rock commonly contains disseminated pyrite as discrete crystals. In some sections the host rock is altered to Fe-oxide and/or As-Fe-oxide. In section MIN-21 one group of crystals was large enough to be identified as the As-Fe-oxide symplesite; in other occurrences the grains were too fine-grained to identify the mineral optically.

The quartz-sulfide veins consist of varying amounts of arsenopyrite, pyrite, sphalerite, galena, Sb-sulfosalts (freibergite, boulangerite, bournonite), and various sulfate and oxide accessory minerals. Arsenopyrite is the dominant mineral observed within the quartz-sulfide veins. Pyrite and sphalerite appear to form coevally with the arsenopyrite. The galena and Sb-sulfosalts are commonly observed in-filling around the other sulfides and quartz grains; this is evidence that they formed later than the arsenopyrite, pyrite and sphalerite. The sulfate and oxide minerals appear to form as a result of oxidation and alteration of pre-existing primary mineralization (discussed in further detail below).

Freibergite, boulangerite and bournonite, and to some extent galena, were difficult to distinguish in reflected light. Galena commonly has a higher bireflectance; the surface appears more pristine, and locally cleavage and triangular pits are observed. In contrast, the Sb-sulfosalts commonly show small round pits due to the very fine-grained nature of the crystals. The larger crystals of boulangerite illustrate the acicular nature of the crystals better than the smaller grains, and demonstrate a higher bireflectance relative to the other Sb-sulfosalt minerals. Bournonite and freibergite have little to no bireflectance under reflected light, making them especially difficult to distinguish from each other, as shown in section MIN-1B.

Silver is also hosted within the minerals freibergite, pyrargite, acanthite, and an unknown sulfate mineral (Fe-As-Ag-Sb-Au-Pb). Freibergite is the most common Ag-bearing mineral observed. Pyrargite, acanthite and the unknown sulfate were observed rarely and are commonly very fine-grained.

Gold is predominately hosted in a variety of unidentified sulfates (containing Fe-As-Sb-Au-Pb, Fe-As-Au-Pb, and Fe-As-Ag-Sb-Au-Pb), and within S-Si-O (Ca-Fe-Cu-As-Au) minerals, as illustrated in sections MIN-15 and MIN-21. Small Au peaks in SEM-EDX spectra were observed in As-Fe-oxide minerals. Small peaks in the EDX spectra show that Au may also exist locally within the arsenopyrite and the Sb-sulfosalt minerals. The Fe-As-Au-Pb-sulfate may be a form of beudantite [$PbFe_3(AsO_4)(SO_4)(OH)_6$], in which the Au has substituted for another element, likely As. This mineral is commonly found in the oxidized zones of polymetallic deposits. The Ca-Fe-Cu-As-Au-S-Si-O mineral may be a sulfate or silicate; further analysis

is required. Both the sulfate and S-Si-O minerals that host the Au likely formed from the breakdown of the Sb-sulfosalt minerals, arsenopyrite, and quartz. Sections MIN-15 and MIN-21 come from core intersections with the highest Au concentrations and appear to host areas of sulfide mineralization that have undergone a partial degree of oxidation and alteration. This enabled the breakdown of Au-bearing primary minerals, allowing the Au and other elements to mobilize into the secondary sulfate and S-Si-O minerals. It is possible that, as alteration increased, these elements were remobilized and leached away; this would explain why sections that come from highly oxidized intersections have little Au or Ag.

Further work could be done to better characterize some of the more unusual mineralogy, but for the purposes of basic metallurgy this report is likely sufficient. Electron probe microanalysis (EPMA) could be completed on arsenopyrite, freibergite, boulangerite, bournonite, and the unknown Au- and Ag-bearing minerals. This technique may also assist with determining how much Au is in the arsenopyrite. Analysis of freibergite, boulangerite and bournonite would confirm the optical identification of these minerals, as there are other minerals with the same or similar chemistry and mineralogical properties that are not as common. EPMA of Au- and Ag-bearing minerals is unlikely to result in a firm identification, given that BSE imaging from the SEM shows a fairly uniform texture, but it would show the amount of Au and/or Ag within the crystal structure. Since these unknown minerals are also opaque and/or very fine-grained it is unlikely that they could be extracted from the polished sections for use in single-crystal X-ray diffraction.

In summary, the mineralization appears to be hosted in quartz-sulfide veins that were emplaced into a quartz-rich rock. The host rock has subsequently been altered to varying degrees to muscovite, and hosts pyrite. Sphalerite, pyrite, and arsenopyrite are among the first sulfide minerals to form, followed by galena and Sb-sulfosalt minerals that infilled around the quartz and sulfides. The latter stage probably included the formation of the first Ag phases. Subsequently, the quartz-sulfide veins were weakly to moderately oxidized, and the sulfide and sulfosalt minerals broke down into sulfate and S-Si-O phases. This breakdown enabled the concentration of Au and Ag. Finally, further oxidation and alteration leached Au and Ag out of the rock, suggesting a late stage metasomatic overprinting.

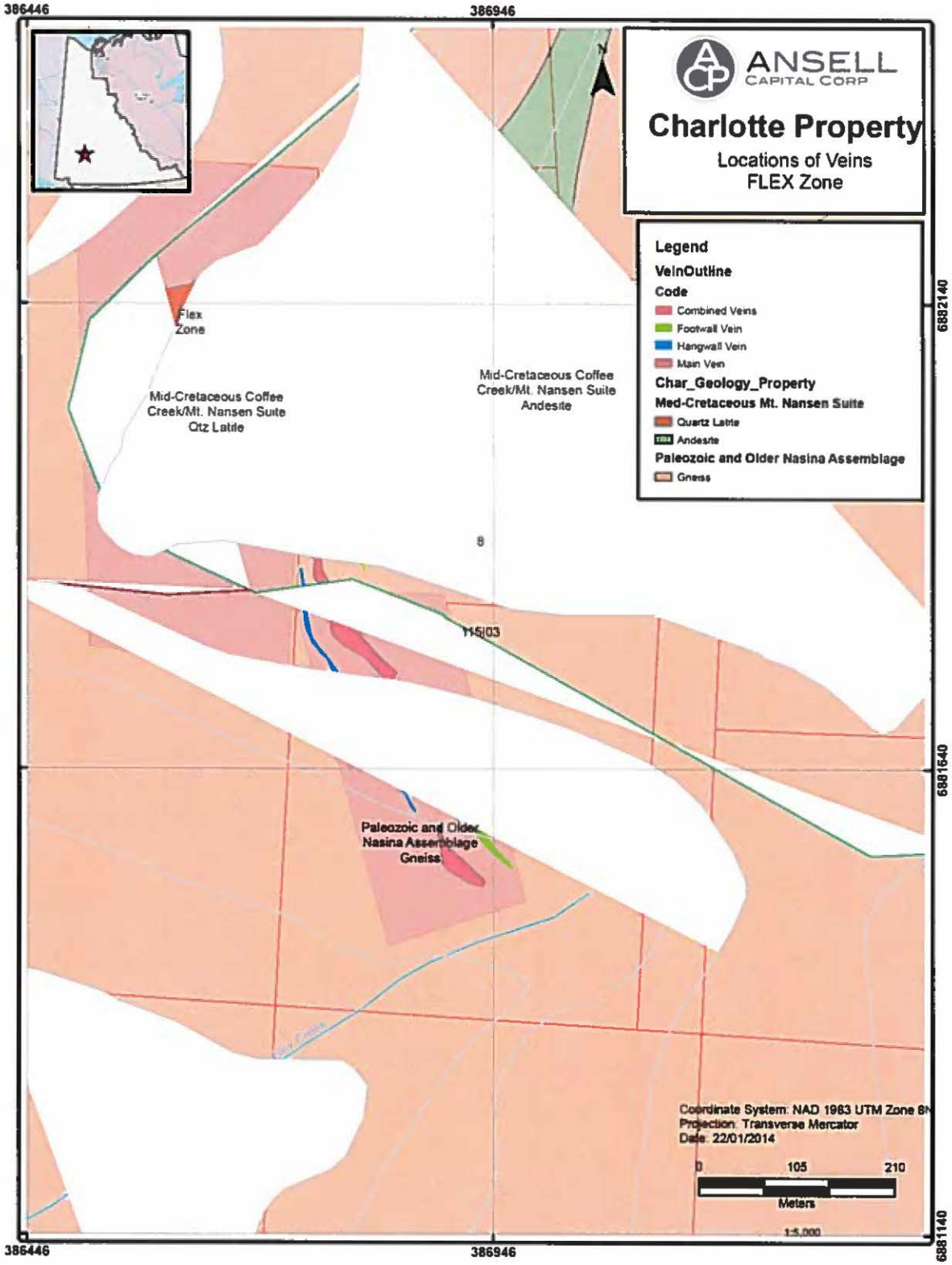


Figure 20. Locations of veins (Hangingwall vein (HW), Footwall vein (FW), and Main) in the FLEX zone. The East vein (EW) is approximately 20-30 meters east of FW

	Mineral Name	Abbreviation	Formula
Rock Forming Minerals	quartz	qtz	SiO_2
	calcite	cal	$CaCO_3$
	ankerite	ank	$Ca(Fe, Mg, Mn)(CO_3)_2$
	dolomite	dol	$CaMg(CO_3)_2$
	muscovite	ms	$KAl_2(AlSi_3O_{10})(OH)_2$
Sulphide and Sulphosalt Minerals	acanthite	acan	Ag_2S
	arsenopyrite	apy	FeAsS
	boulangerite	boul	$Pb_5Sb_4S_{11}$
	bournonite	bour	$CuPbSbS_3$
	chalcopyrite	ccp	$CuFeS_2$
	freibergite	frei	$Ag_6(Cu_4Fe_2)Sb_4S_{13-x}$
	galena	gn	PbS
	pyrargyrite	pyra	Ag3SbS3
	pyrite	py	FeS_2
	sphalerite	sp	ZnS
	stibnite	stib	Sb_2S_3

Table 3. Summary of mineral compositions of samples (Dalsin and Groat, 2014).

Sample #	Sulfides and sulfosalts								Unknown†	Rock forming minerals					
	acan	apy	ccp	gn	py	sp	stib	Sb-sulfosalt		qtz	cal	ank	dol	carb	alt+qtz
MIN-001A		1		2	35	7				x		x	x		
MIN-001B		tr		1	23	2		4		x					
MIN-002		25	tr	7	tr	3		5		x					
MIN-003A					1.5	0.5				x			x		
MIN-003B		tr		tr	1	tr				x				x	x
MIN-004		69		1	3	2				x	x	x	x		
MIN-005A					tr					x					x
MIN-005B					1					x					x
MIN-006		35		6	40	9				x					
MIN-007		45		8	tr	7				x		x			
MIN-008A		5		2	13	10				x					x
MIN-008B		15		1	4	15				x					x
MIN-009		10		1	12	7				x					x
MIN-010		tr		tr	2			tr		x					x
MIN-011		tr			1	tr				x					x
MIN-012		1			1					x					x
MIN-013										x					x
MIN-014										x					x
MIN-015		68		1	1	12		3	tr	x					
MIN-016		5								x					
MIN-017		10		2	8	5				x					x
MIN-018		1			5	1		tr		x					x
MIN-019		3		1	6					x					x
MIN-020		19		1	10	5		tr		x					
MIN-021	tr	2			1				tr	x					x
MIN-022		9		2	7	15				x					x
MIN-023		15			8	2				x		x			x

Sample #	Sulfides and sulfosalts								Unknown†	Rock forming minerals					
	acan	apy	ccp	gn	py	sp	stib	Sb-sulfosalt		qtz	cal	ank	dol	carb	alt+qtz
MIN-001A		1		2	35	7				x		x	x		
MIN-001B		tr		1	23	2		4		x					
MIN-002		25	tr	7	tr	3		5		x					
MIN-003A					1.5	0.5				x			x		
MIN-003B		tr		tr	1	tr				x				x	x
MIN-004		69		1	3	2				x	x	x	x		
MIN-005A					tr					x					x
MIN-005B					1					x					x
MIN-006		35		6	40	9				x					
MIN-007		45		8	tr	7				x		x			
MIN-008A		5		2	13	10				x					x
MIN-008B		15		1	4	15				x					x
MIN-009		10		1	12	7				x					x
MIN-010		tr		tr	2			tr		x					x
MIN-011		tr			1	tr				x					x
MIN-012		1			1					x					x
MIN-013										x					x
MIN-014										x					x
MIN-024A		6		0.5	3	0.5				x					x
MIN-024B		35		tr	8	2		5		x					x
MIN-025		3			12					x					x
MIN-026		4			6					x					x
MIN-027		28		3	tr	3		1		x					
MIN-028		tr		3	22	35				x					
MIN-029		3		1	21	50				x					

†Unknown Au and/or Ag bearing oxides and sulfates

Table 4. Summary of mineralogical thin sections, including: drillhole number, depth, assay value, assay number, zone, field category etc

Sample #	Drill hole #	Depth	Assay #	Assay Value		Zone	Field category	Sulphides and Sulphosalts								Unknown Au and/or Ag bearing oxides and sulphates	Rock Forming Minerals					
				Au g/t	Ag g/t			acan	apy	ccp	gn	py	sp	stib	Sb-sulphosalt		qtz	cal	ank	dol	carb	alt+qtz
MIN-001A	12-280	195.25	17503 11	27.3	129 7	Main	SU		1		2	35	7				x		x	x		
MIN-001B	12-280	195.25	17503 11	27.3	129 7	Main	SU		tra ce		1	23	2		4		x					
MIN-002	12-280	145.50	17502 54	73.3	152 7	HW	SU		25	tra ce	7	tra ce	3		5		x					
MIN-003A	12-278	185.30	17489 27	9.83	93	?Main	SU					1.5	0.5				x			x		
MIN-003B	12-278	185.30	17489 27	9.83	93	?Main	SU		tra ce		tra ce	1	tra ce				x				x	x
MIN-004	12-277	297.00	17488 53	27.4	76	Main	SU		69		1	3	2				x	x	x	x		
MIN-005A	12-276	112.50	17486 56	0.39 4	<2	HW	OX					tra ce					x					x
MIN-005B	12-276	113.00	17486 57	1.16	54	HW	OX					1					x					x
MIN-006	12-276	204.00	17486 87	60.7	106 9	FW	SU		35		6	40	9				x					
MIN-007	12-275	292.00	17486 17	12.2	217	FW	SU		45		8	tra ce	7				x		x			
MIN-008A	11-254	97.40	10646 91	28.4	674	HW	Transition		5		2	13	10				x					x
MIN-008B	11-254	97.40	10646 91	28.4	674	HW	Transition		15		1	4	15				x					x
MIN-009	11-254	152.80	10647 42	9.9	279	FW	SU/Trans?		10		1	12	7				x					x
MIN-010	11-255	118.20	10648 46	1.41	135	HW	Transition		tra ce		tra ce	2			trace		x					x
MIN-011	11-255	132.00	10648 62	26.7	721	HW/Main?	SU/Trans?		tra ce			1	tra ce				x					x
MIN-012	11-256	26.00	10649 98	0.52	1.3	HW stringer	OX		1			1					x					x
MIN-	11-256	81.5	10650	19.8	77.1	HW	OX/Trans										x					x

013		0	47															
MIN-014	11-256	93.2 5	10650 57	9.64	28.5	Main	SU/Trans?								x			x
MIN-015	11-257	51.4 0	10649 47	151. 1	255 0	Main	Transition		68	1	1	12	3	trace	x			
MIN-016	11-258	31.9 5	10651 19	8.26	11.3	HW stringer	OX		5						x			
MIN-017	11-258	61.8 5	10651 47	16	256	HW	Transition		10	2	8	5			x			x
MIN-018	11-259	59.1 5	10652 27	38.6	225 9	Main	Transition		1		5	1	trace		x			x
MIN-019	11-259	90.0 0	10652 57	18.6	117	FW	Transition		3	1	6				x			x
MIN-020	11-262	108. 00	10658 30	62.8	771	HW	SU/Trans?		19	1	10	5	trace		x			
MIN-021	11-271	37.4 5	10671 28	83.4	885	Main	OX	trace	2		1			trace	x			x
MIN-022	11-271	104. 80	10671 87	31.7	626	FW	SU		9	2	7	15			x			x
MIN-023	11-271	142. 00	10672 21	7.6	92	East Vein	SU		15		8	2			x	x		x
MIN-024A	11-272	100. 00	10673 33	53.5	184 6	Main	SU/Trans?		6	0.5	3	0.5			x			x
MIN-024B	11-272	100. 00	10673 33	53.5	184 6	Main	SU/Trans?		35	trace	8	2	5		x			x
MIN-025	11-272	175. 90	10674 00	2.39	224 5	FW	SU		3		12				x			x
MIN-026	11-273	182. 50	10669 31	7.85	4	East Vein	SU		4		6				x			x
MIN-027	11-274	81.5 0	10674 74	29.9	894	HW	SU/Trans?		28	3	trace	3	1		x			
MIN-028	11-274	127. 00	10675 20	19.6	166 5	Main	SU/Trans?		trace	3	22	35			x			
MIN-029	11-274	180. 50	10675 64	9.6	508	FW	SU		3	1	21	50			x			

.

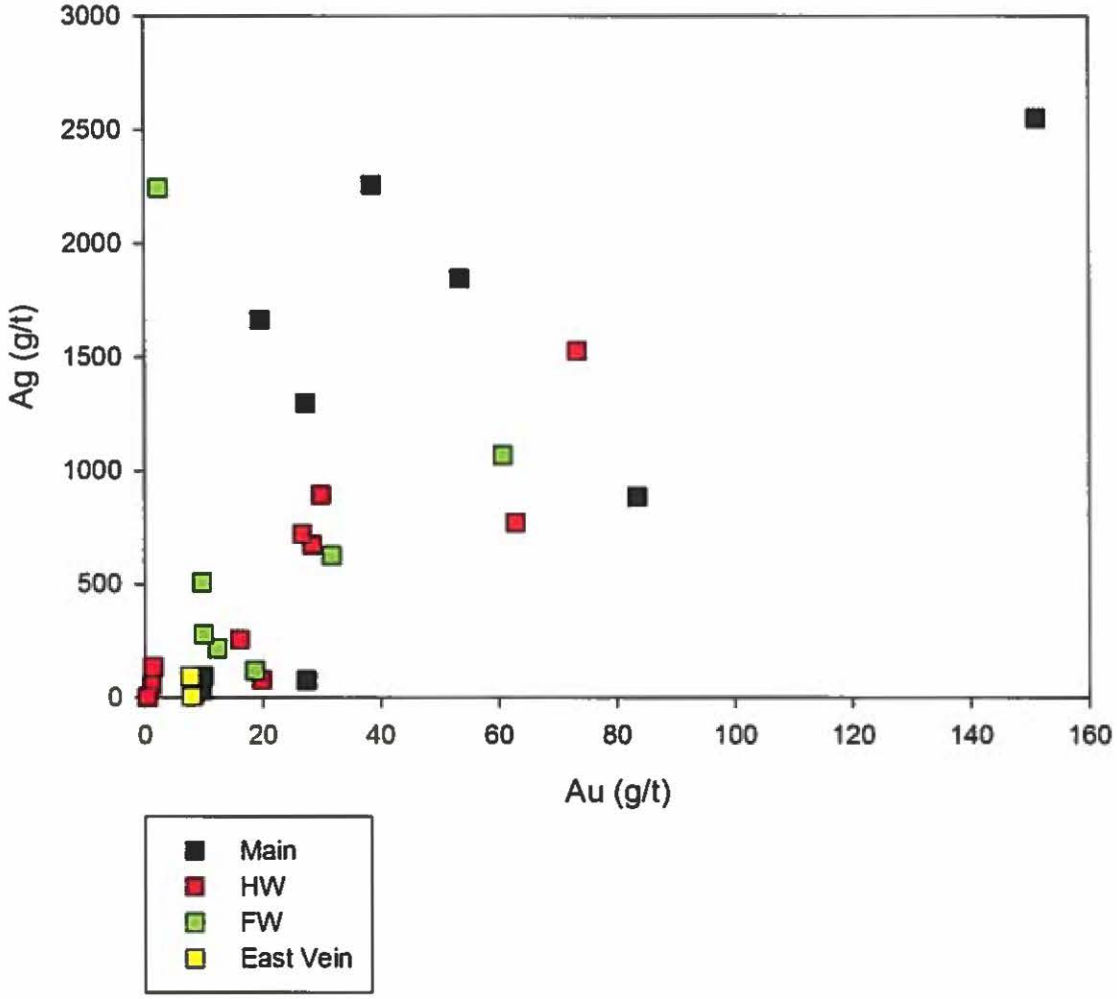


Figure 21. Gold and silver plot for the Main, HW, FW and East vein (Dalsin and Groat, 2014). All veins show a positive correlation between gold and silver; the HW has strong correlation.

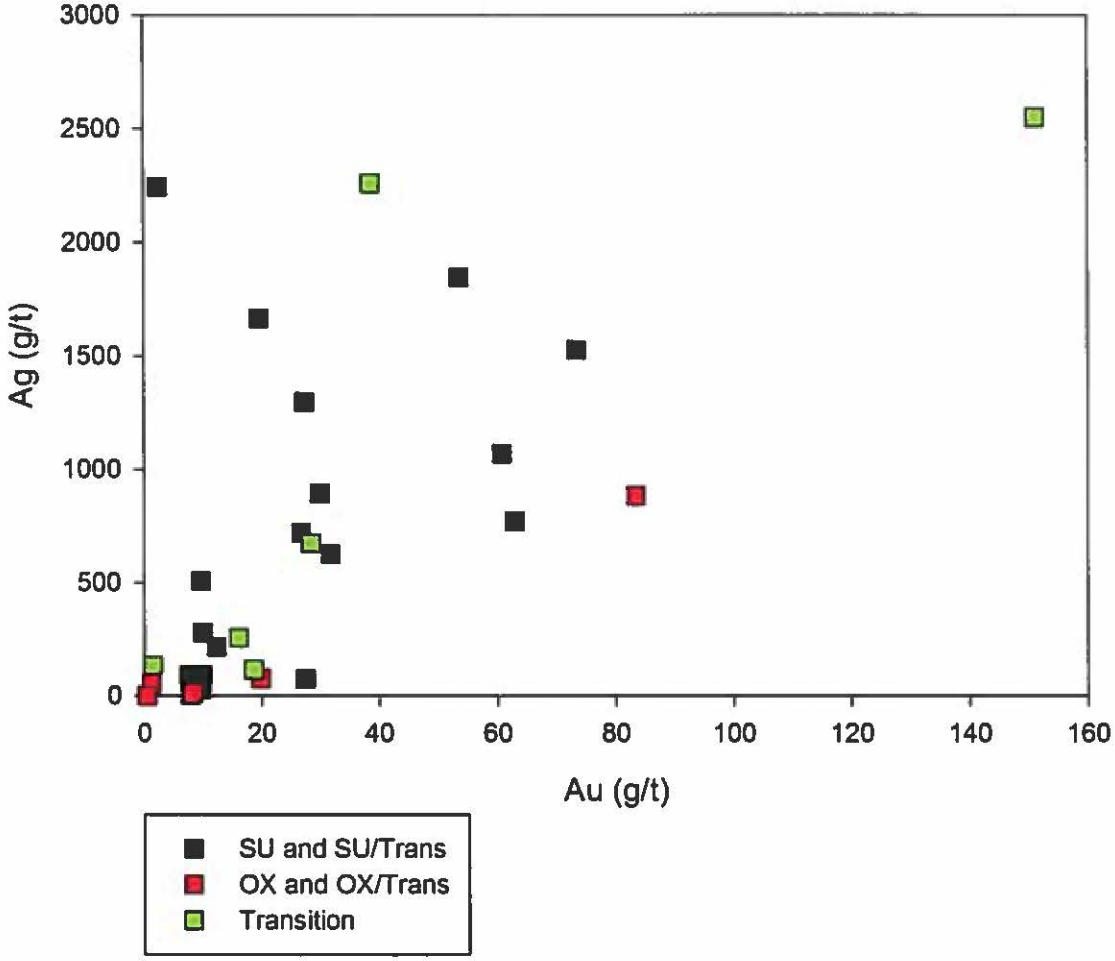


Figure 22. Gold and silver plotted for sulphide, oxide and transitional minerals (Dalsin and Groat, 2014); all mineral types show a positive correlation.

11 Conclusions and Recommendations

The mineralogical study revealed some refractory minerals that may be difficult to process; sulfates will be the easiest to process and sulfides and sulfosalts will be more difficult due to their refractory nature and arsenic. More work should be done to narrow down which zones have more sulfates and thus will be easier to process. In the future, more mineralogical or metallurgical studies may be needed if the property reaches production stage. Mineral assemblages described in the 2014 mineralogy report should be added to the drill hole database in progress to determine which areas contain the highest level of gold- and silver-bearing minerals which are favourable for extraction.

The resistivity and IP survey revealed several anomalies on the OK zone which should be investigated by diamond drilling. Geophysics on the FLEX zone revealed that areas of low resistivity (high conductivity) corresponded reasonably well known mineralized zones, possibly because the mineralized zones may be structurally controlled and areas of structural weakness tend to be associated with increased clay and water content or because of the presence of oxide mineralization and high sulphide. The survey conducted in 2013 should be expanded to include the Webber and maybe Cabin, GRW, and Dickson Zones.

The airborne survey conducted in 2009 should be inverted into a 3D model (Figure 9, Figure 10)

A trip to the Mount Nansen mine, pending permission, should be conducted in 2014. Infill-mapping of government and Coast Mountain maps with an emphasis on structure should also take place on the property.

The database created by Coast Mountain Geological, which contains assays, maps, papers etc, should be investigated further and added to. Work should continue on the 3D drill hole database and 2D cross sections of historical drill holes and 2013 geophysics should be plotted to determine patterns, anomalies and develop new targets. Historical soil results should be leveled for year, surficial geology and bedrock geology where applicable.

The property has promising mineralogy and further drill holes appear to be warranted. Research will be conducted as to how many more holes and their spacing are needed to produce an inferred resource. Examination, compilation and synthesis of historical data, coupled with a site visit to the property to conduct surface geological mapping will result in the property being ready for additional drilling in 2014, with the aim of producing a resource, pending funds.

12 Statement of Expenditures

Payee	Total	GST	Expense											
			IP/Res Survey	*Mag rental*	*Spectrometer*	*Labour*	*Air Fare*	*Hotel*	*Truck rental*	*Auto*	*Meals*	*Office*	*Report*	*Mineralology*
Ground Truth Exploration	$ 29,966.21	$ 1,426.96	$ 28,539.25											
JCMP Management	$ 4,037.25	$ 192.25		$ 200.00	$ 70.00	$ 3,575.00								
Jeff Poloni-expense	$ 3,756.48	$ 129.32					$ 1,875.26	$ 355.00	$ 687.95	$ 249.31	$ 459.64			
Jeff Delany	$ 1,800.00					$ 1,800.00								
Chris Healey-expense	$ 2,210.61	$ 72.63					$ 602.95	$ 546.25	$ 708.54	$ 28.55	$ 231.69	$ 20.00		
Healex Consulting	$ 3,150.00	$ 150.00				$ 3,000.00								
Kingston Geosciences	$ 7,296.97	$ 295.09												$ 7,001.88
Jeff Poloni-expense	$ 339.13	$ 14.51						$ 7.50		$ 168.28	$ 148.84			
Walla Geosciences	$ 1,496.25	$ 71.25											$ 1,425.00	
Totals	$ 54,052.90	$ 2,352.01	$ 28,539.25	$ 200.00	$ 70.00	$ 8,375.00	$ 2,478.21	$ 908.75	$ 1,396.49	$ 446.14	$ 840.17	$ 20.00	$ 1,425.00	$ 7,001.88

13 Statement of qualifications

I, Bev Quist, of 963 Gleneagles Dr, Kamloops British Columbia, hereby certify that:

1. I am a graduate from the University of Victoria with a B.Sc. (2009) and from Queen's University (2011) with a M.Sc. I
2. I am a self-employed geologist retained by Ansell Capital Corp
3. I am a member in good standing with the Society of Economic Geologists.
4. I have worked in the Yukon since 2008 on generative projects, grassroots projects and properties. I've explored in the Yukon for tungsten, gold, rare earth elements, vanadium and Ni-Cu PGEs References
5. I am the author of "Summary report of the 2013 Geophysical Work and Mineralogical Study on the Charlotte Property"



Bev Quist, M.Sc.

14 References

Dadson, P., Struyk, N.M., 2012, Assessment Report on the 2012 Trenching and Diamond Drill Program, Charlotte Property, Whitehorse Mining District, Yukon Territory.

Dalsin, M., and Groat, L.A., 2014, Charlotte Property Au-Ag Polished Sections: Mineralogical Report, November 2013, Completed for Ansell Capital Corp.

Denholm, E., Dumka, D. and Farquharson, G., 2000. A Review of the Mount Nansen Property, Yukon Territory. Unpublished report for Department of Indian Affairs and Northern Development.

Eaton, W.D., and Archer, A.R., 1989. Report on the Geology and Mineral Inventory of the Mount Nansen and Tawa Properties, Yukon Territory with Assessment of the Economical Potential for Open Pit Mining of Oxidized Mineralization in the Brown-McDade Zone. Report for BYG Natural Resources Inc and Chevron Minerals Ltd.

Fage, I., 2014, Geophysical Survey Report: High Resolution Resistivity and Induced Polarization, Charlotte Project, Groundtruth Exploration Inc.

Guinness Exploration, 2010, unpublished maps.

Lecuyer, N.L., 1997. Mount Nansen Property Huestis and Webber Zones Feasibility Study. Report for BYG Natural Resources Inc.

Middelton, R.S., 2009. National Instrument 43-101 Report on the Mount Nansen Property and the Tawa Property, Whitehorse Mining District, Yukon Territory for 101073531 Saskatchewan Ltd.

Nelson, J.L. and Colpron, M., 2007. Tectonics and metallogeny of the Canadian and Alaskan Cordillera, 1.8 Ga to present. In: Mineral Deposits of Canada: A Synthesis of Major Deposit Types, District Metallogeny, the Evolution of Geological Provinces, and Exploration Methods, W.D. Goodfellow (ed.), Mineral Deposit Division, Geological Association of Canada, Special Publication 5, p. 755-791

Stroshein, R.W., 2007b. Geological Exploration Summary Mount Nansen Project Brown McDade Deposit (Peripheral Claims), Yukon Territory. Report for Department of Energy, Mines and Resources, Assessment and Abandoned Mines Branch and PriceWatershouseCoopers Inc.

Struyk, N. M., and Dadson, P., 2011, Assessment Report on the 2011 Trenching and Diamond Drilling Program, Charlotte Property, Whitehorse Mining District, Yukon Territory.

Walls, M.J. and Eaton, W.D., 1987. Nansen Project Final Report. Yukon Mineral Assessment Report. Document No: 092122.

15 Appendix 1- IP report

Geophysical Survey Report:

High Resolution Resistivity and Induced Polarization

Charlotte Project

Whitehorse Mining District

NTS Sheets 115 I/03

62°03'N. Lat., 137°10'W. Long.

for

Ansell Capital Corp.

Prepared by: I. Fage
Date of Survey: September 7-14, 2013
Date of Report: January 5, 2014

Table of Contents

Table of Contents

Table of Figures

1 Introduction 4

2 Survey 4

2.1 Personnel 4

2.2 Survey Summary and Arrays 4

2.3 Field Survey Operating Procedures 6

2.4 Data Processing 6

3 Survey Results and Interpretation 6

3.1 Results 6

3.2 Interpretation 7

Appendix A – Arrays surveyed, data deliverables

Appendix B - Survey Theory

Appendix C- Equipment Specifications

Table of Figures

Figure 1 - Survey Location 5

Figure 2 - Section 050N Inversion (extended Dipole-Dipole Array) 8

Figure 3 – Section 100N Inversion (extended Dipole-Dipole Array) 9

Figure 4 – Section 150N Inversion (extended Dipole-Dipole Array) 10

Figure 5 – Section 200N Inversion (extended Dipole-Dipole Array) 11

Figure 6 – Section 250N Inversion (extended Dipole-Dipole Array) 12

Figure 7 – Section 300N Inversion (extended Dipole-Dipole Array) 13

Figure 8 – Section 350N Inversion (extended Dipole-Dipole Array) 14

Figure 9 – Section 101E Inversion (extended Dipole-Dipole Array) 15

Figure 10 – Section102E Inversion (extended Dipole-Dipole Array) 16

Figure 11 – Section 1000N Inversion (extended Dipole-Dipole Array) 17

Figure 12 – Section 1050N Inversion (extended Dipole-Dipole Array) 18

Figure 13 – Section 050N Inversion w DH overlay (extended Dipole-Dipole Array) 19

Figure 14 – Section 200N Inversion w DH overlay (extended Dipole-Dipole Array) 20

Figure 15 – FLEX survey Level Plan Inverted Resistivity (extended Dipole-Dipole Array) 21

Figure 16 – FLEX survey Level Plan Inverted Chargeability (extended Dipole-Dipole Array) 22

Figure 17 – FLEX survey Level Plan Inverted Resistivity w Mineralization overlay 23

1 Introduction

Groundtruth Exploration Inc. of Dawson City, YT was commissioned to conduct a High Resolution DC Resistivity/IP (HRRIP) geophysical survey for Ansell Capital Corporation on the Charlotte Project in the Mt. Nansen area, in Yukon Territory (NTS mapsheet 115I/03). The HRRIP survey was conducted from September 7th-14th, 2013 to and October 2nd, 2013.

A total of 9 profiles on the FLEX and 2 profiles on the OK were read for both resistivity and chargeability using multiple arrays. Two of the lines read on the Flex make part of a 2013 Case Study in partnership with the Yukon Geological Survey (YGS), and approved by Ansell Capital Corp.

The Flex Survey was conducted over near surface mineralized structures that have been confirmed with significant drilling. The FLEX Survey is comprised of nine traverses of 415m in horizontal length (see figure 2). The OK survey is located on a drill confirmed mineralized structure and is located 1.5km North of the Flex zone. Two traverses of 415m horizontal length were surveyed across the OK target (see figure 14). Several arrays were used on all profiles to best evaluate the optimal array for mapping the mineralized system. Results of these surveys form the basis of this report. Additional work and interpretation has been left to the client's discretion.

2 Survey

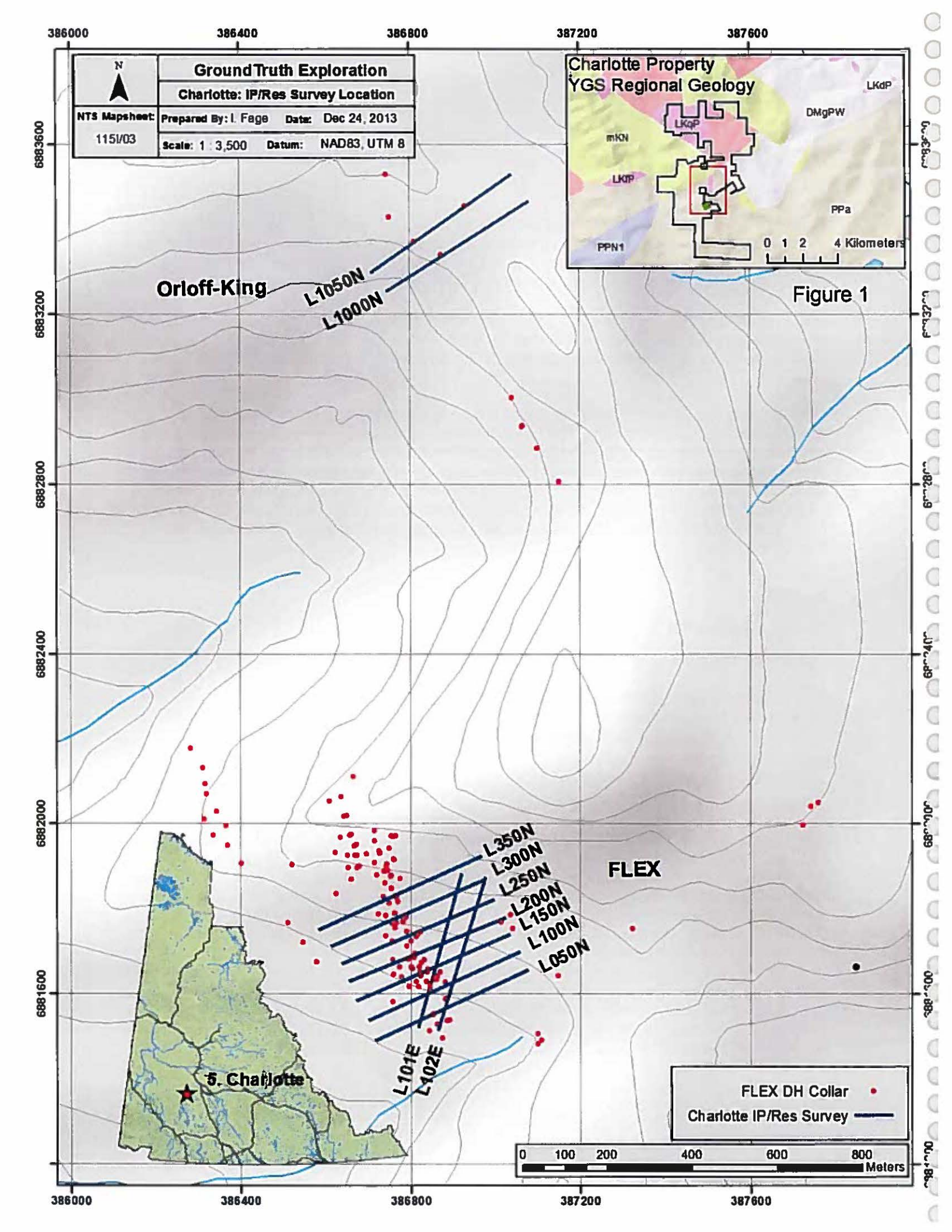
2.1 Personnel

The survey was conducted by the following Ground Truth Exploration personnel:

- Richard Daigle, Lead Geophysical Operator and Crew Chief
- David Cox, Secondary Lead and GPS Technician
- Hector Barrientos, Geo Technician
- Kyle Boggild, Geo Technician
- Janna Stecyk, Geo Technician

2.2 Survey Summary and Arrays

The line-cutting and high definition DC ("HRDC") Resistivity ("Res") and induced polarization ("IP") surveys were conducted from September 7 to 14, and Oct 2nd,2013. The survey consisted nine traverses on the FLEX zone and two traverses on the Orloff-King (OK) zone. On the FLEX zone, seven parallel traverses each of 415m horizontal length, oriented at 243° azimuth were surveyed and crosscut by an additional two traverses a of 415m length oriented at 195° azimuth (total 9 traverses). On the OK zone, two parallel traverses each of 415m horizontal length, oriented at 235° azimuth were surveyed.
Multiple arrays were used to maximize qualitative data on the ground that, at the time, had unknown properties. The survey started on the line furthest to the South and the crew worked lines successively to the North. Crew had planned to survey FLEX and OK in one survey, but encountered technical issue with IP receiver after completion of the FLEX survey and returned to complete OK survey on Oct 2nd, 2013.


386000
386400
386800
387200
387600
6883600
6883200
6882800
6882400
6882000
6881600
N
Ground Truth Exploration
Charlotte: IP/Res Survey Location
NTS Mapsheet: 115I/03
Prepared By: I. Fage
Date: Dec 24, 2013
Scale: 1 : 3,500
Datum: NAD83, UTM 8
Charlotte Property
YGS Regional Geology
LKdP
DMgPW
LKqP
mKN
LKdP
PPa
PPN1
0 1 2 4 Kilometers
Figure 1
Orloff-King
L1050N
L1000N
L350N
L300N
L250N
L200N
L150N
L100N
L050N
FLEX
L101E
L102E
5. Charlotte
FLEX DH Collar
Charlotte IP/Res Survey
0 100 200 400 600 800
Meters

The FLEX and OK surveys lines were oriented perpendicular to know mineralized structures. Electrode spacing was set at 5m and all lines were surveyed with a spread of 84 electrodes covering a total horizontal length of 415m per profile.

2.3 Field Survey Operating Procedures

The survey is completed in the filed according to the following steps:

- A crew of five is utilized to run the survey
- Midpoint of traverse line is located using differential GPS and line is sighted and established in both directions using compass and pickets
- Minimal brush is cut along line to sight pickets and lay cables
- Crew measures electrode positions at 5m spacing with measuring tape
- Electrodes placed and hammered to depth of 50cm (15% of electrode spacing)
- Cables are laid and attached to electrodes
- Contact resistance test ("CRT") is conducted
- Calcium chloride added to all electrodes >2k ohms and CRT redone
- Extra electrodes added to electrodes with high contact resistance and CRT redone
- Survey is done once satisfactory contact resistance is achieved
- Operator does survey while Assistant operator establishes differential GPS line and the rest of the crew moves to prepare next line

2.4 Data Processing

The collected data is downloaded in the field after every array and checked for integrity. This allows any field errors to be identified and corrected before moving the equipment. The RES/IP data is processed every evening by the lead operator in the field using EarthImager2D software provided by Advanced Geosciences Inc. Resistivity data misfits are removed and the cleaned data-set is inverted. The same process is done with the IP data. Terrain corrections collected using the differential GPS are applied to the inversions. The GPS data is processed using GNSS Solutions software. All unedited data is archived along with the command files for later verification if required. A *.csv is created containing the collected GPS traverse points. A *.shp file is created containing the collected GPS traverse points. A table of surveyed electrode XYZ locations is provided. Files containing inverted IP & RES data are provided.

3 Survey Results and Interpretation

3.1 Results

The FLEX IP/Res survey covers known mineralization of the Flex zone with a total of 9 traverses spaced at 50m line spacing. It covers the target with an area of approximately 400m by 300m. The Orloff-King Survey was covered by 2 traverses spaced at 50m. The Extended Dipole-Dipole array (xDD) was determined by survey lead, R. Daigle to provide the best overall signal to noise ratio and is the method of map and section presentation in this report. Section figures showing inverted resistivity and chargeability are shown for all traverses (figures 2-12).

Drillhole data overlays are shown for sections L050N and L200N on FLEX (figures 13-14). Level Plan maps of inverted resistivity and chargeability at the 1270m-1280m level are shown (figures 15-16) and projected veins are overlaid on resistivity plan map (figure 17).

3.2 Interpretation

FLEX

The FLEX survey examined from South to North shows a resistivity low at mid traverse (200m) that dips steeply to the East at depth or is vertically oriented at depth in most traverses. This feature is prominent in traverses: L050N ,L150N,L200N,L250N,350N.(Figures 2,4,5,6,8). When this resistivity feature is plotted with Flex drillhole data on Sections 050N and 200N, (Figures 13, 14) we see that mineralization is related to the resistivity low (050N) or possibly the Western contact of resistivity low feature (200N).

The plan map of inverted resistivity at the 1270m level shows a prominent North-South resistivity low lineament running through the survey area (Figure 16) with a shorter NE oriented Res low feature also crossing on the west side of lines 250N and 300N. The major N-S Res low feature bisects the survey area into a highly resistive (low conductivity) body on the West and a less resistive body (moderate-high conductivity) on the East. When mineralization projected to surface (digitized from Ansell figure) is overlaid on the resistivity plan map (Figure 17) we see a correlation between the main vein mineralization and the west contact of the main N-S resistivity low feature.

A preliminary interpretation is that the main N-S res low feature is mapping out the faulted and clay altered zone of the deposit which would likely be of relatively higher conductivity than surrounding host rock.

There is a strong correlation between chargeability high features that are coincident with the above discussed resistivity lows and drillhole mineralization. These target chargeability highs are also showing to be oriented as steeply dipping to the east. Chargeable oxide mineralization, clays and high sulphide content is expected to be the reason for the coincident chargeability high with resistivity low and denotes ore zone potential.

ORLOFF-KING

Both traverses on the OK target show significant near surface chargeability high anomalies (> 30mv/v). The southern traverse (1000N, fig 11) indicates this chargeability feature is possibly dipping to the SW while the northern traverse (1050N, fig 12) shows the IP high to be vertically oriented. There is a coincident inverted resistivity low feature at depth on 1050N traverse at centre of profile line. The near surface chargeability high on 1000N traverse (210-250m) also shows a coincident strong resistivity low (fig 11). Both of these targets are of interest for mineral potential.

Ansell Capital Corporation

FLEX

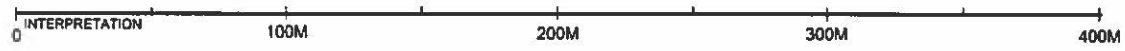
Charlotte Project

Nansen Mountain Area, NTS: 115-I/03.
Whitehorse Mining District, Yukon Territories.

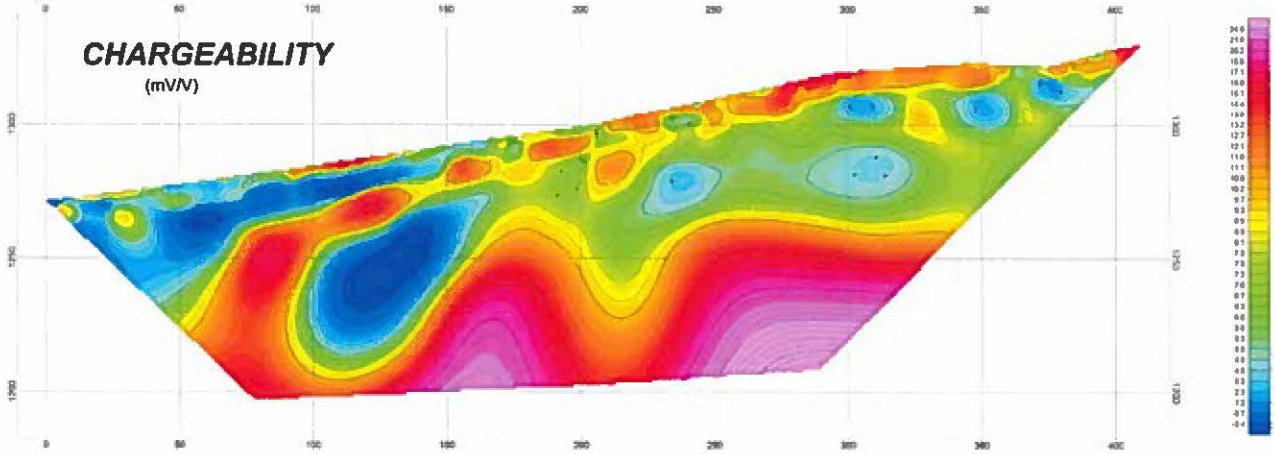
Section 50N

INVERSION
High Resolution Resistivity/IP Survey

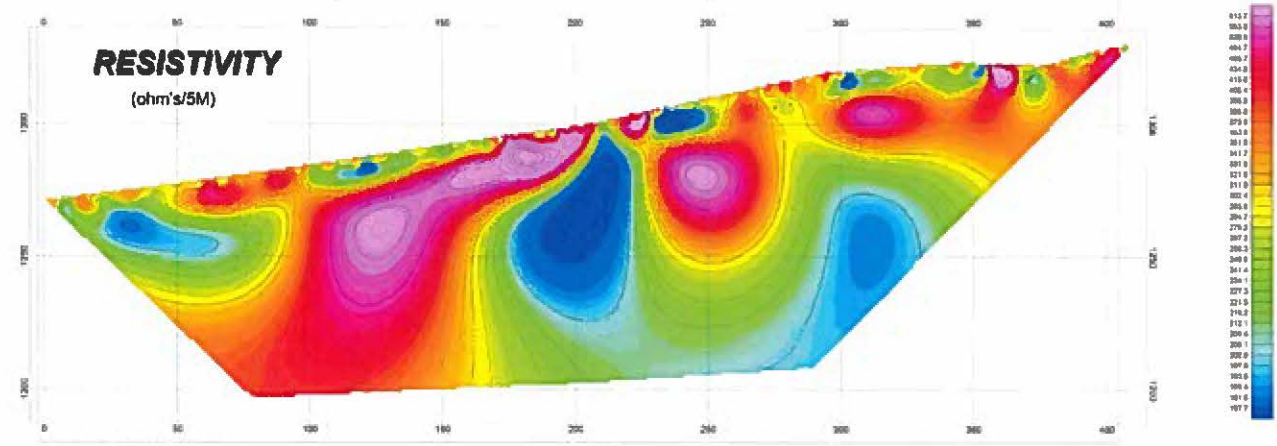
Figure 2



LOOKING NORTH

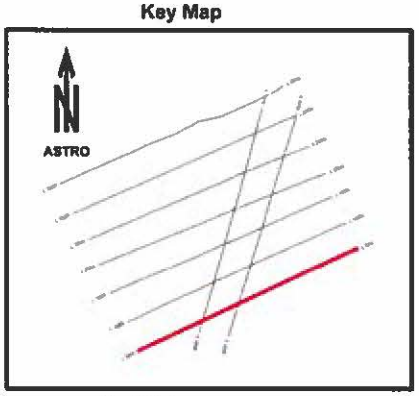


4598 pts. read, 0.06 to 11.99 mV/ V Range, 2.96 mV/ V Mean.

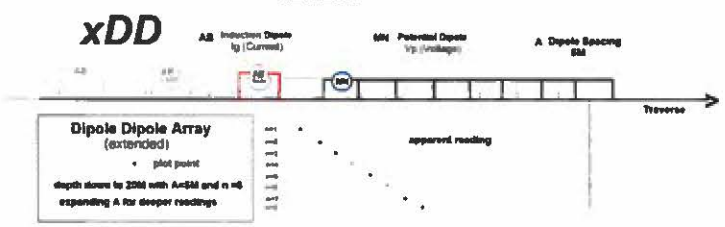


4707 pts. read, 50.7 to 1301 ohm's/ 5M Range, 313 ohm's/ 5M Mean.

Key Map



LEGEND



Supersting by AGI (Advanced Geoscience Inc.)
Time Domain Equipment
84 Electrode System
A (spacing) = 5M, 415M Traverse

Ansell Capital Corporation

FLEX

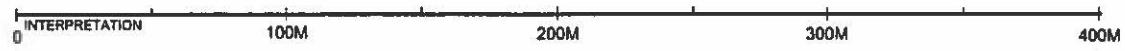
Charlotte Project

Nansen Mountain Area, NTS: 115-I/03.
Whitehorse Mining District, Yukon Territories.

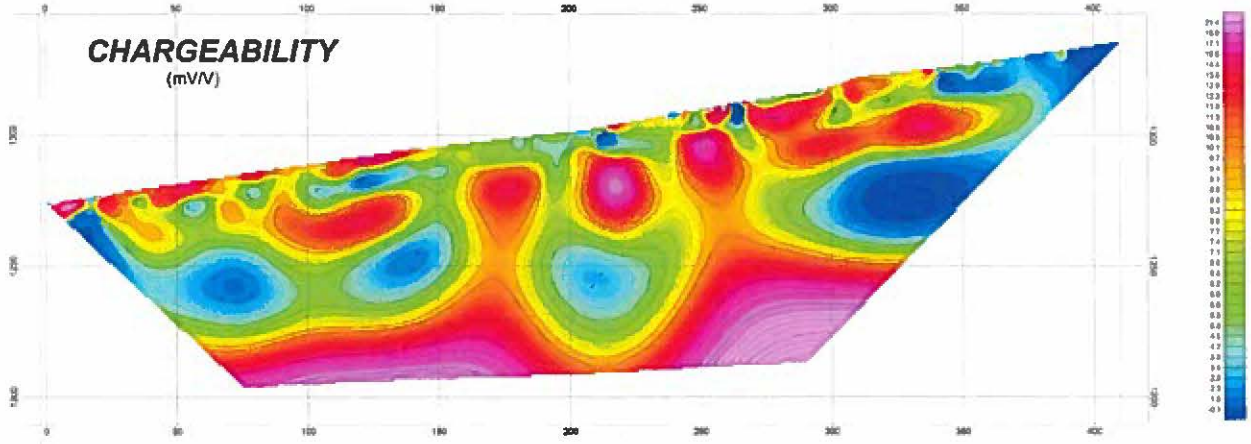
Section 100N

INVERSION
High Resolution Resistivity/IP Survey

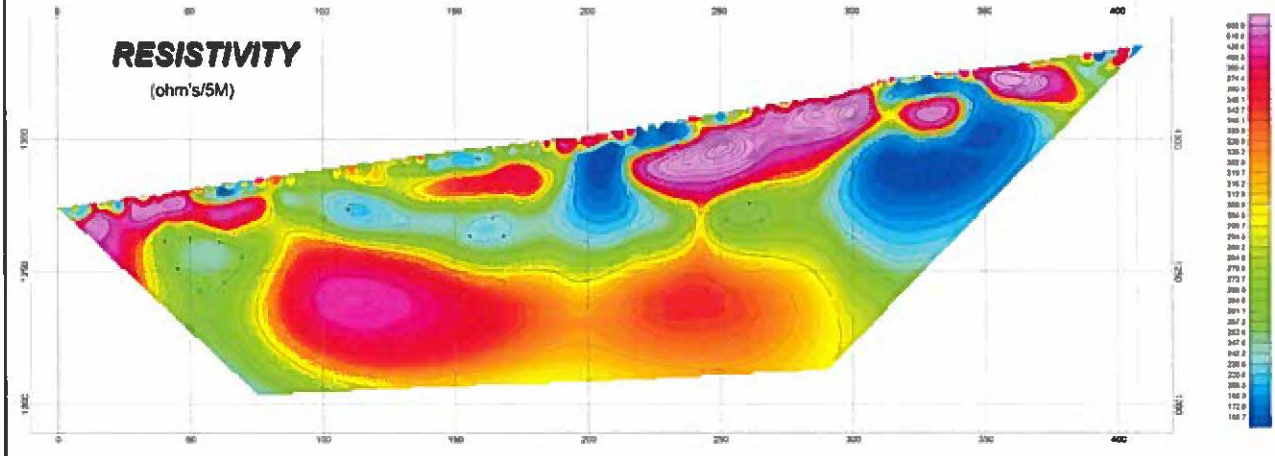
Figure 3



LOOKING NORTH

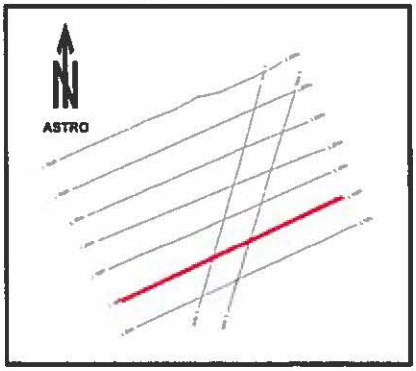


4598 pts. read, 0.06 to 11.99 mV/ V Range, 2.96 mV/ V Mean.

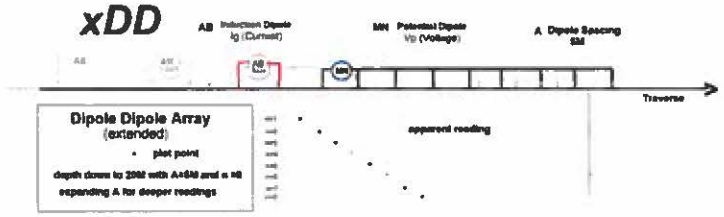


4707 pts. read, 50.7 to 1301 ohm's/ 5M Range, 313 ohm's/ 5M Mean.

Key Map



LEGEND



Supersting by AGI (Advanced Geoscience Inc.)
Time Domain Equipment
84 Electrode System
A (spacing) = 5M, 415M Traverse

Ansell Capital Corporation

FLEX

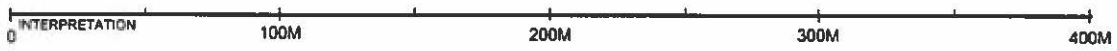
Charlotte Project

Nansen Mountain Area, NTS: 115-I/03.
Whitehorse Mining District, Yukon Territories.

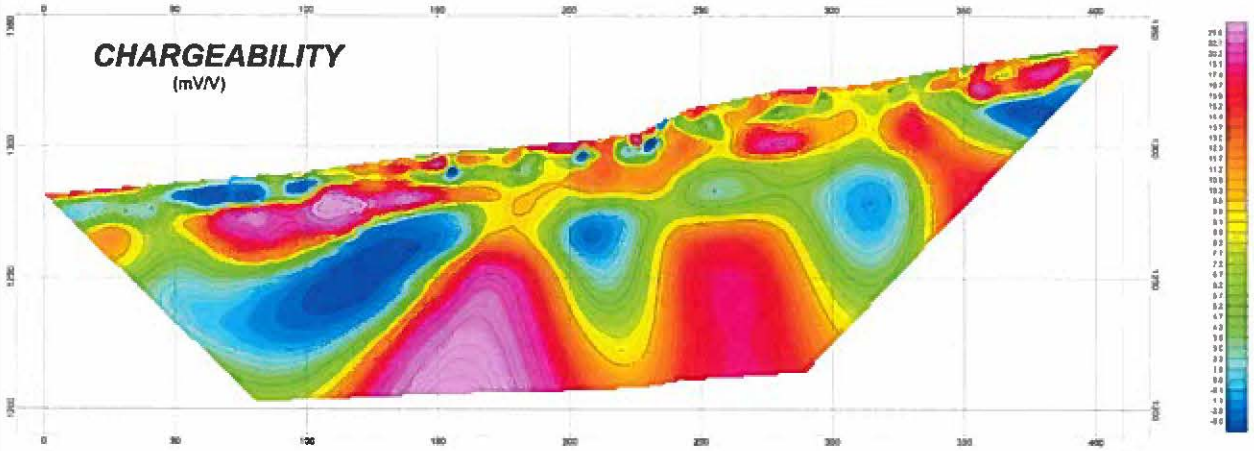
Section 150N

INVERSION
High Resolution Resistivity/IP Survey

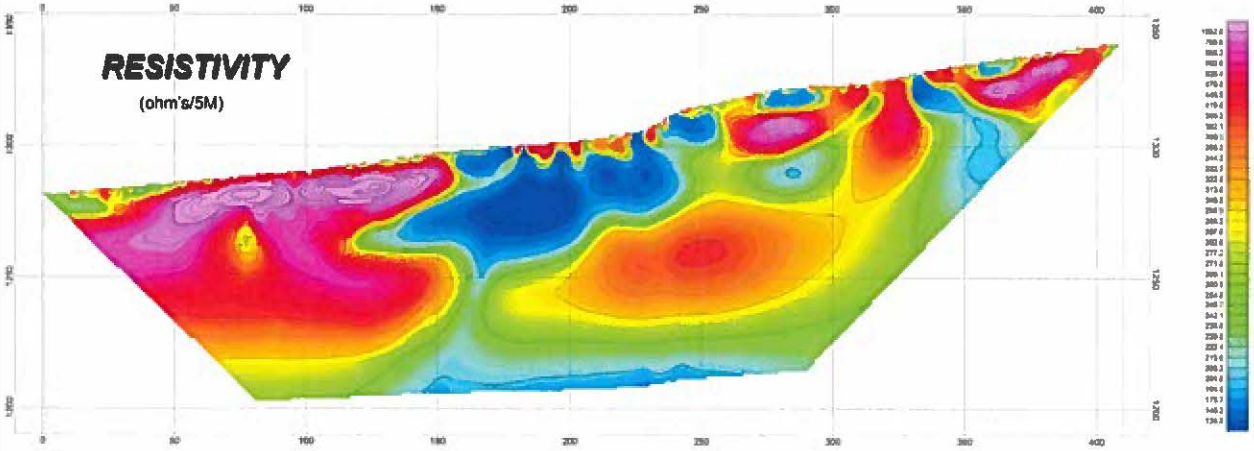
Figure 4



LOOKING NORTH

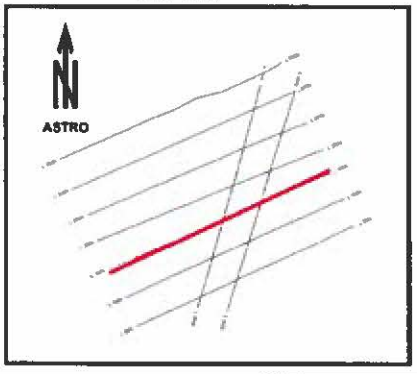


4598 pts. read, 0.06 to 11.99 mV/ V Range, 2.96 mV/ V Mean.

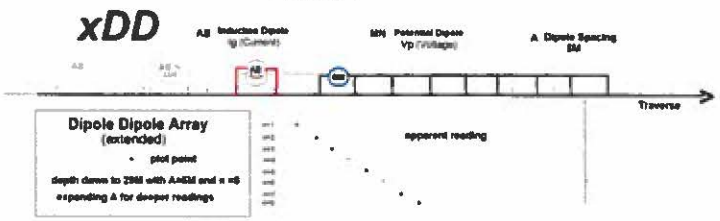


4707 pts. read, 50.7 to 1301 ohm's/ 5M Range, 313 ohm's/ 5M Mean.

Key Map



LEGEND



Supersting by AGI (Advanced Geoscience Inc.)
Time Domain Equipment
84 Electrode System
A (spacing) = 5M, 415M Traverse

Ansell Capital Corporation

FLEX

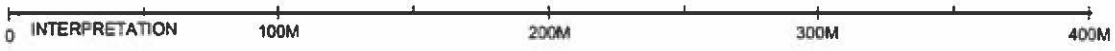
Charlotte Project

Nansen Mountain Area, NTS: 115-I/03.
Whitehorse Mining District, Yukon Territories.

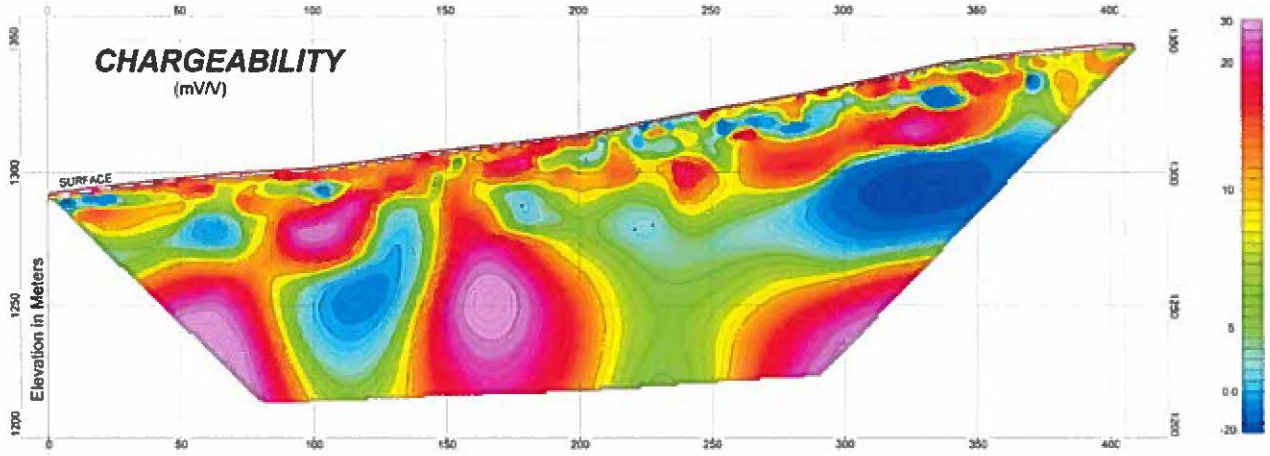
Section 200N

INVERSION
High Resolution Resistivity/IP Survey

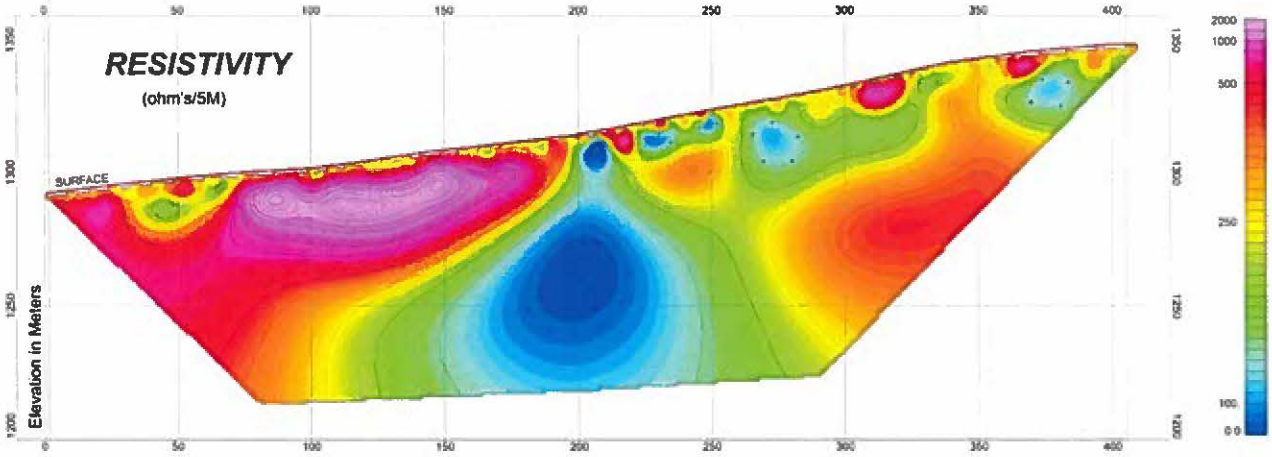
Figure 5



LOOKING NORTH

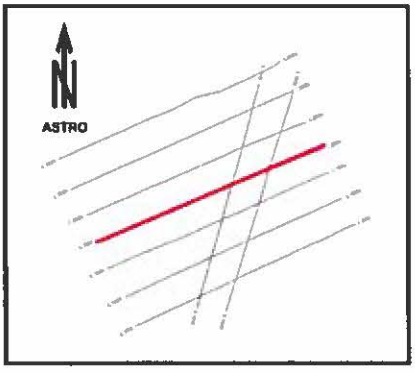


4602 pts. read, 0.02 to 10.6 mV/ V Range, 3.47 mV/ V Mean

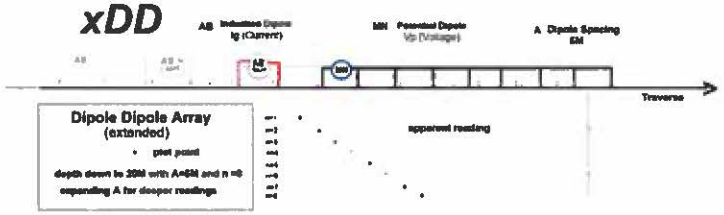


4697 Data pts. read, 35.8 to 1494 ohm's/ 5M Range, 316 ohm's/ 5M Mean.

Key Map



LEGEND



Supersting by AGI (Advanced Geoscience Inc.)
Time Domain Equipment
84 Electrode System
A (spacing) = 5M, 415M Traverse

Ansell Capital Corporation

FLEX

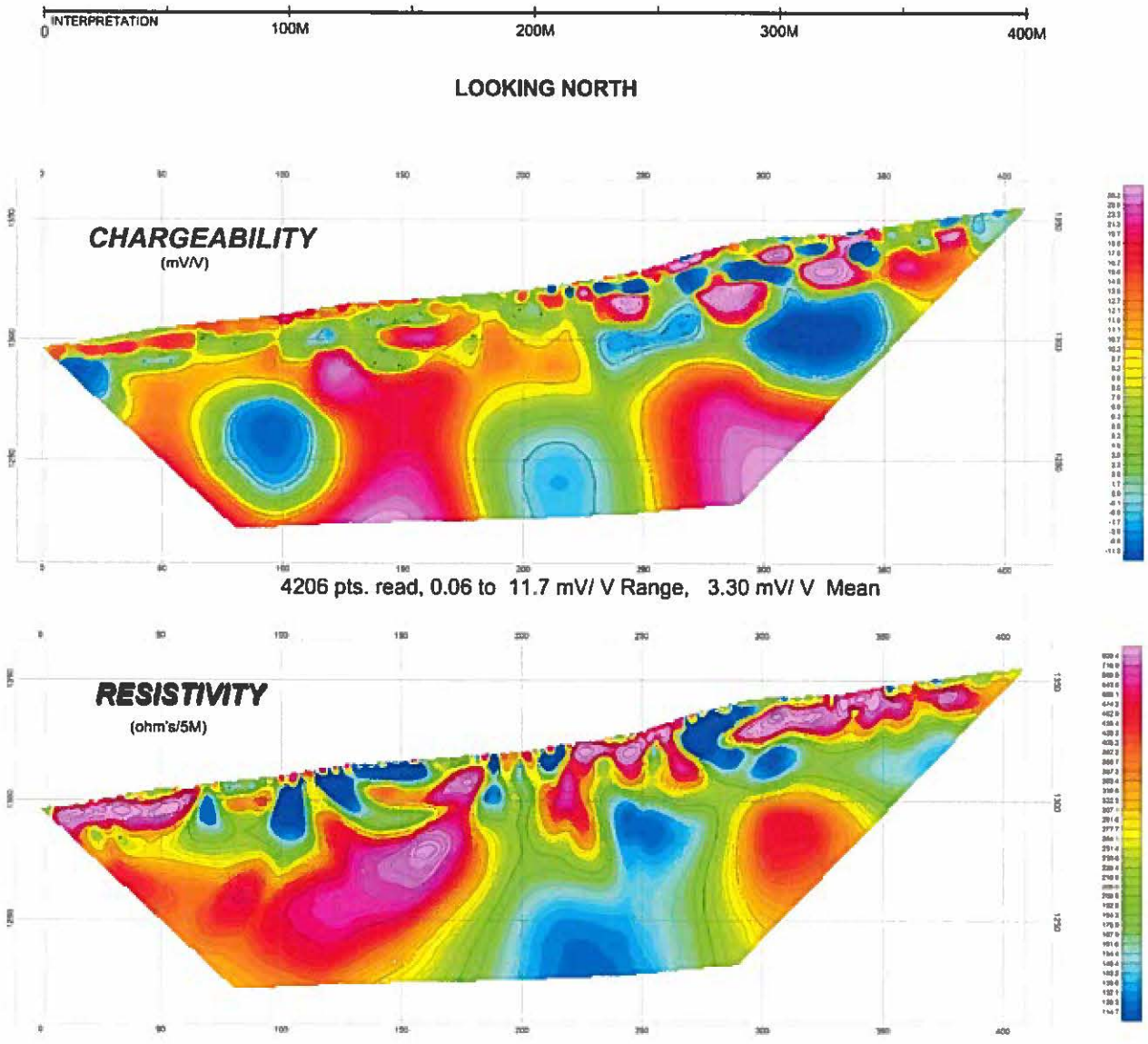
Charlotte Project

Nansen Mountain Area, NTS: 115-I/03.
Whitehorse Mining District, Yukon Territories.

Section 250N

INVERSION
High Resolution Resistivity/IP Survey

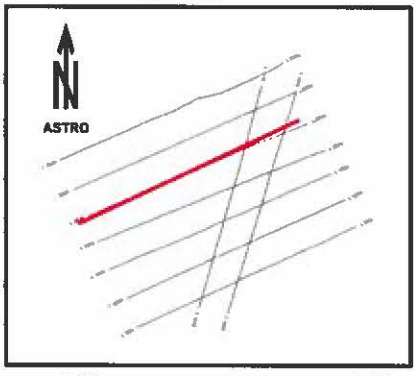
Figure 6



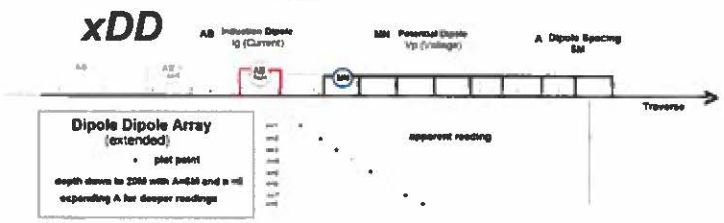
4206 pts. read, 0.06 to 11.7 mV/ V Range, 3.30 mV/ V Mean

4608 Data pts. read, 8.33 to 4958 ohm's/ 5M Range, 290 ohm's/ 5M Mean.

Key Map



LEGEND



Supersting by AGI (Advanced Geoscience Inc.)
Time Domain Equipment
84 Electrode System
A (spacing) = 5M, 415M Traverse

Ansell Capital Corporation

FLEX

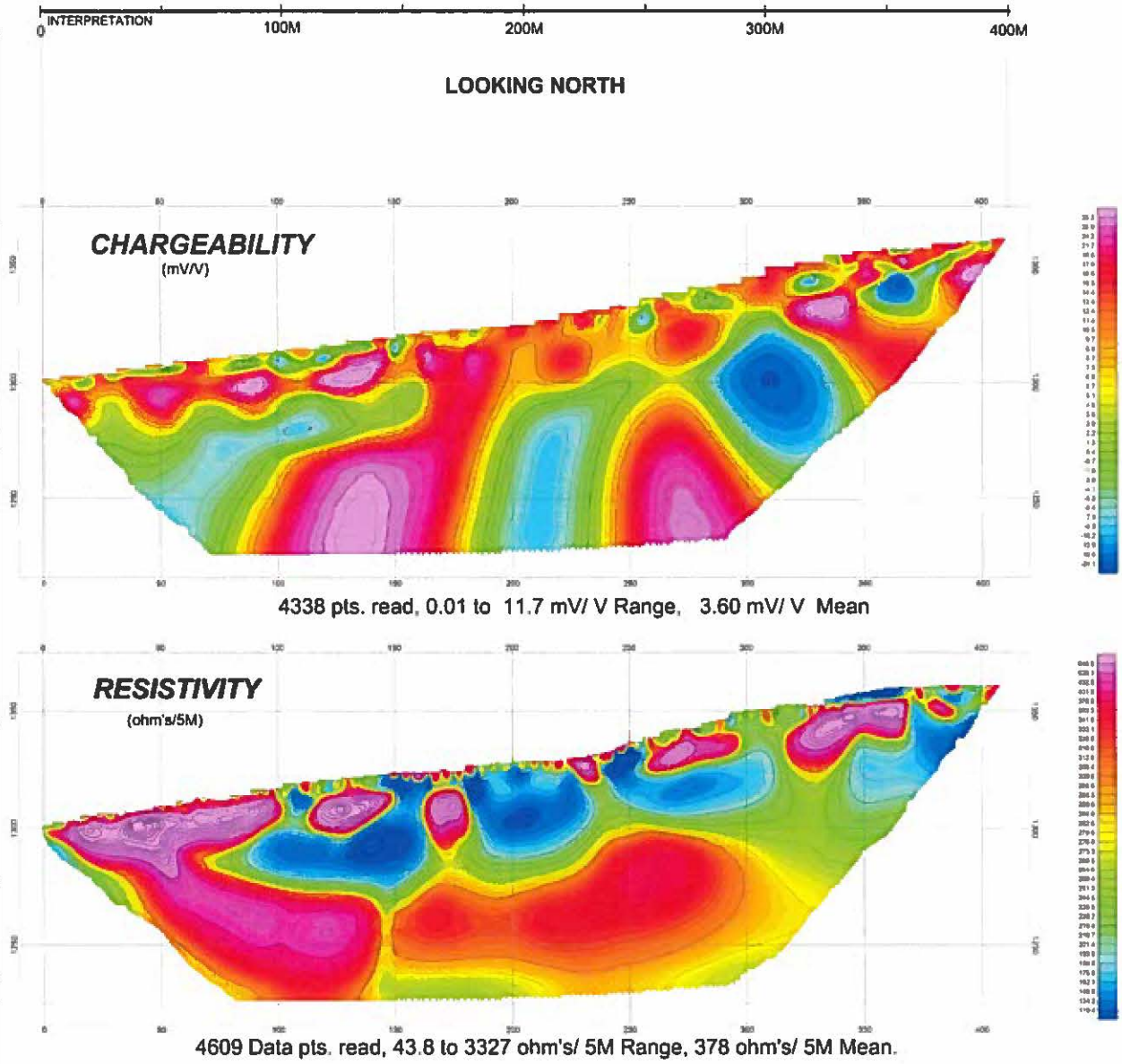
Charlotte Project

Nansen Mountain Area, NTS: 115-I/03.
Whitehorse Mining District, Yukon Territories.

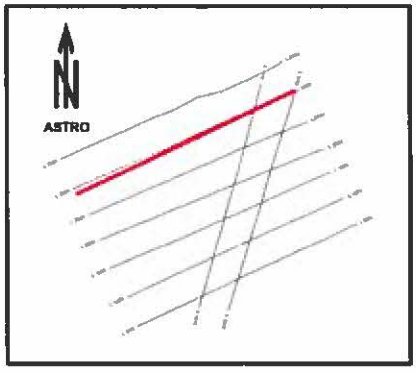
Section 300N

INVERSION
High Resolution Resistivity/IP Survey

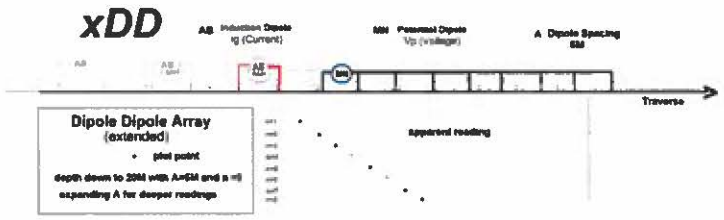
Figure 7



Key Map



LEGEND



Supersting by AGI (Advanced Geoscience Inc.)
Time Domain Equipment
84 Electrode System
A (spacing) = 5M, 415M Traverse

Ansell Capital Corporation

FLEX

Charlotte Project

Nansen Mountain Area, NTS: 115-I/03.

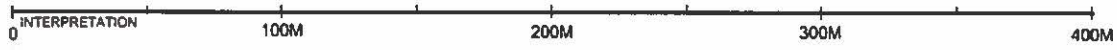
Whitehorse Mining District, Yukon Territories.

Section 350N

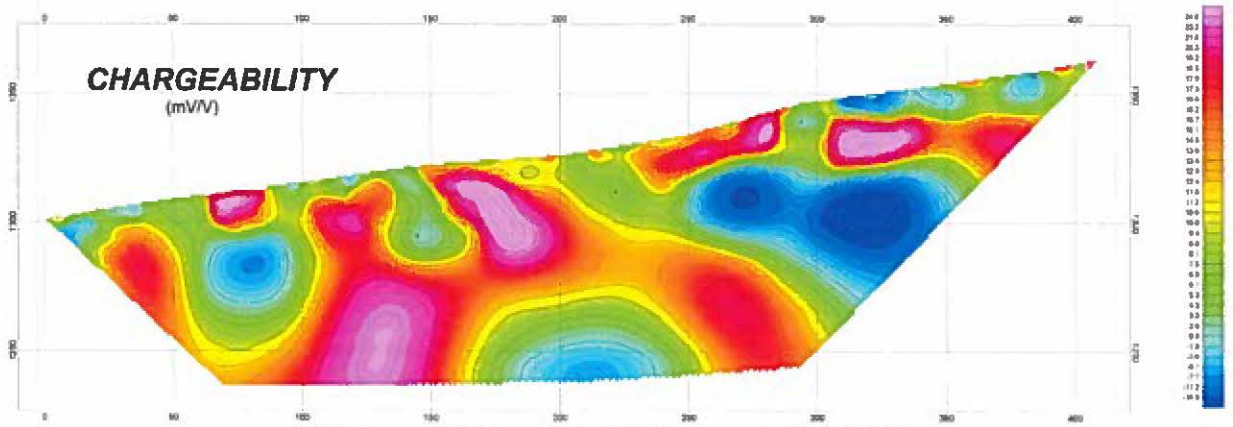
INVERSION

High Resolution Resistivity/IP Survey

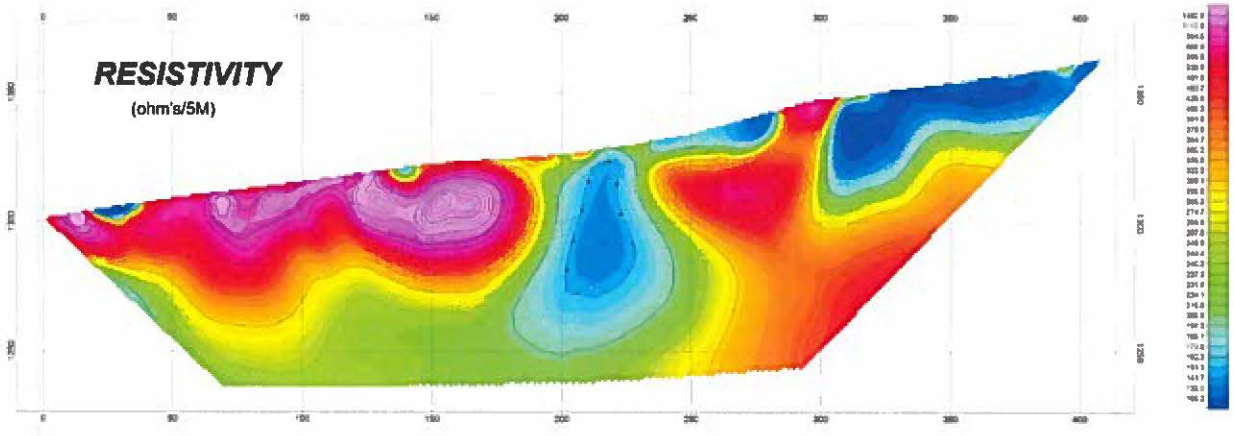
Figure 8



LOOKING NORTH

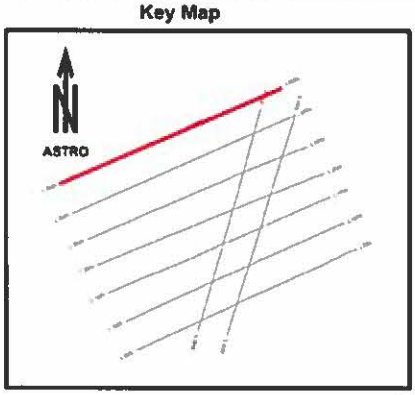


4336 pts. read, 0.01 to 11.8 mV/ V Range, 3.69mV/ V Mean

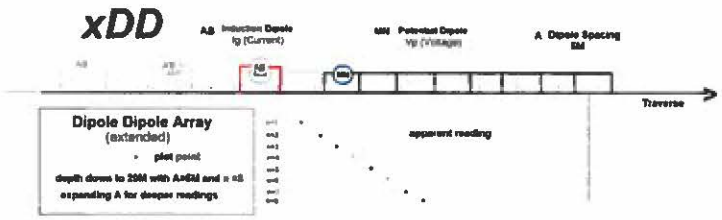


4698 Data pts. read, 43.8 to 3327 ohm's/ 5M Range, 378 ohm's/ 5M Mean.

Key Map



LEGEND



Supersting by AGI (Advanced Geoscience Inc.)
Time Domain Equipment
84 Electrode System
A (spacing) = 5M, 415M Traverse

Ansell Capital Corporation

FLEX

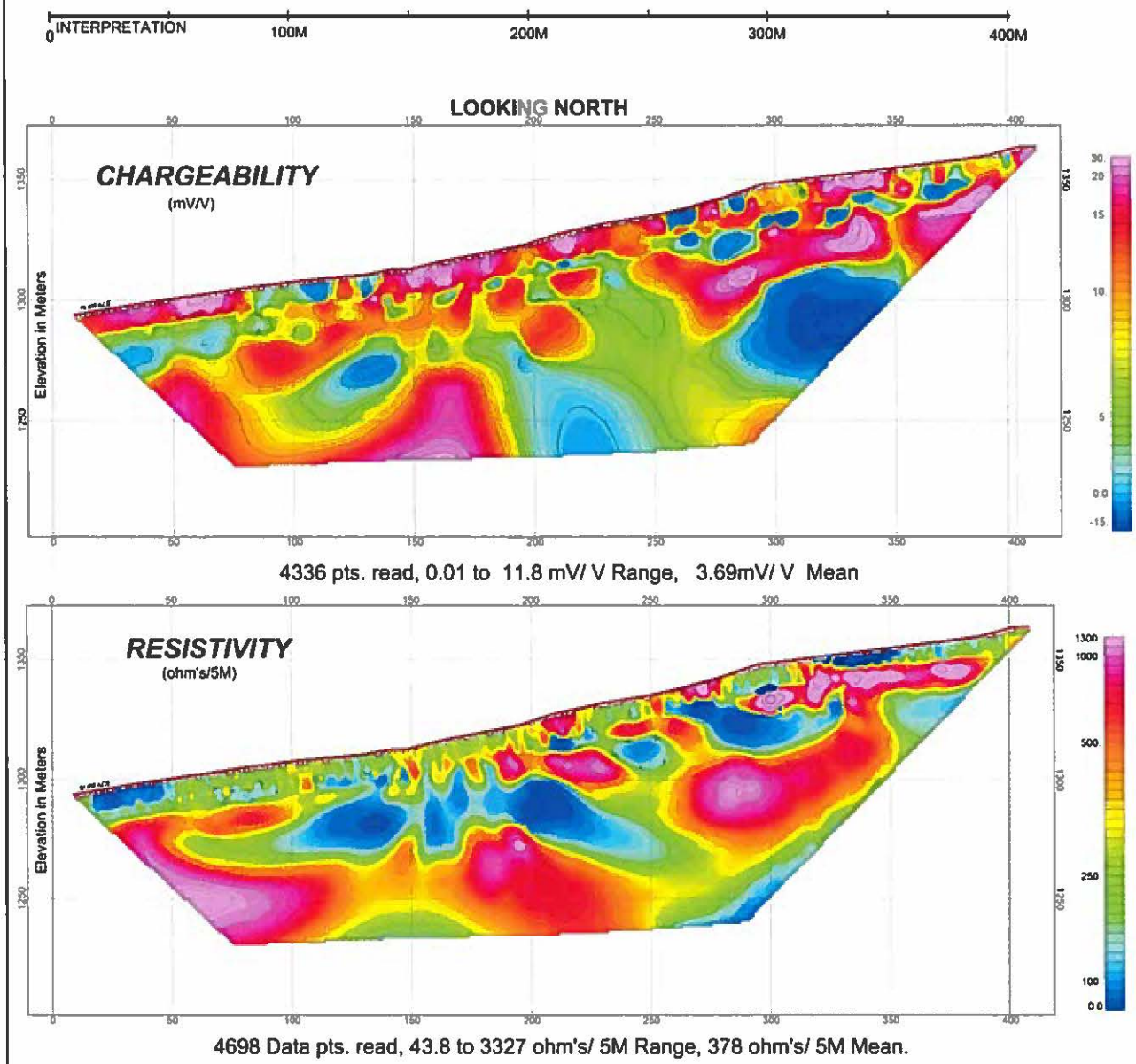
Charlotte Project

Nansen Mountain Area, NTS: 115-I/03.
Whitehorse Mining District, Yukon Territories.

Section 101E

INVERSION
High Resolution Resistivity/IP Survey

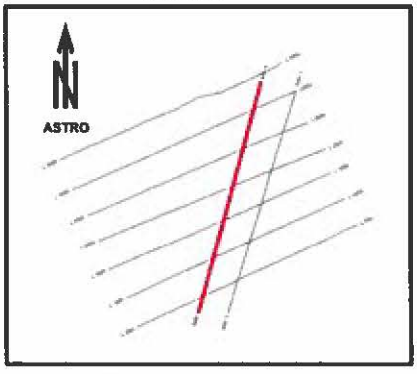
Figure 9



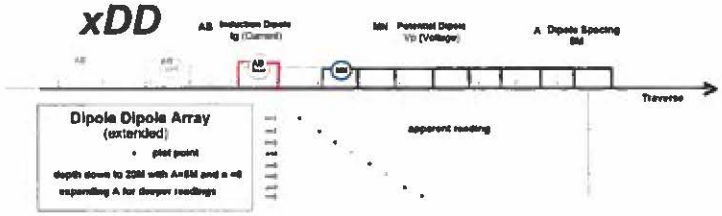
4336 pts. read, 0.01 to 11.8 mV/ V Range, 3.69mV/ V Mean

4698 Data pts. read, 43.8 to 3327 ohm's/ 5M Range, 378 ohm's/ 5M Mean.

Key Map



LEGEND



Supersting by AGI (Advanced Geoscience Inc.)
Time Domain Equipment
84 Electrode System
A (spacing) = 5M, 415M Traverse

Ansell Capital Corporation

FLEX

Charlotte Project

Nansen Mountain Area, NTS: 115-I/03.

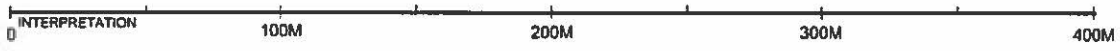
Whitehorse Mining District, Yukon Territories.

Section 102E

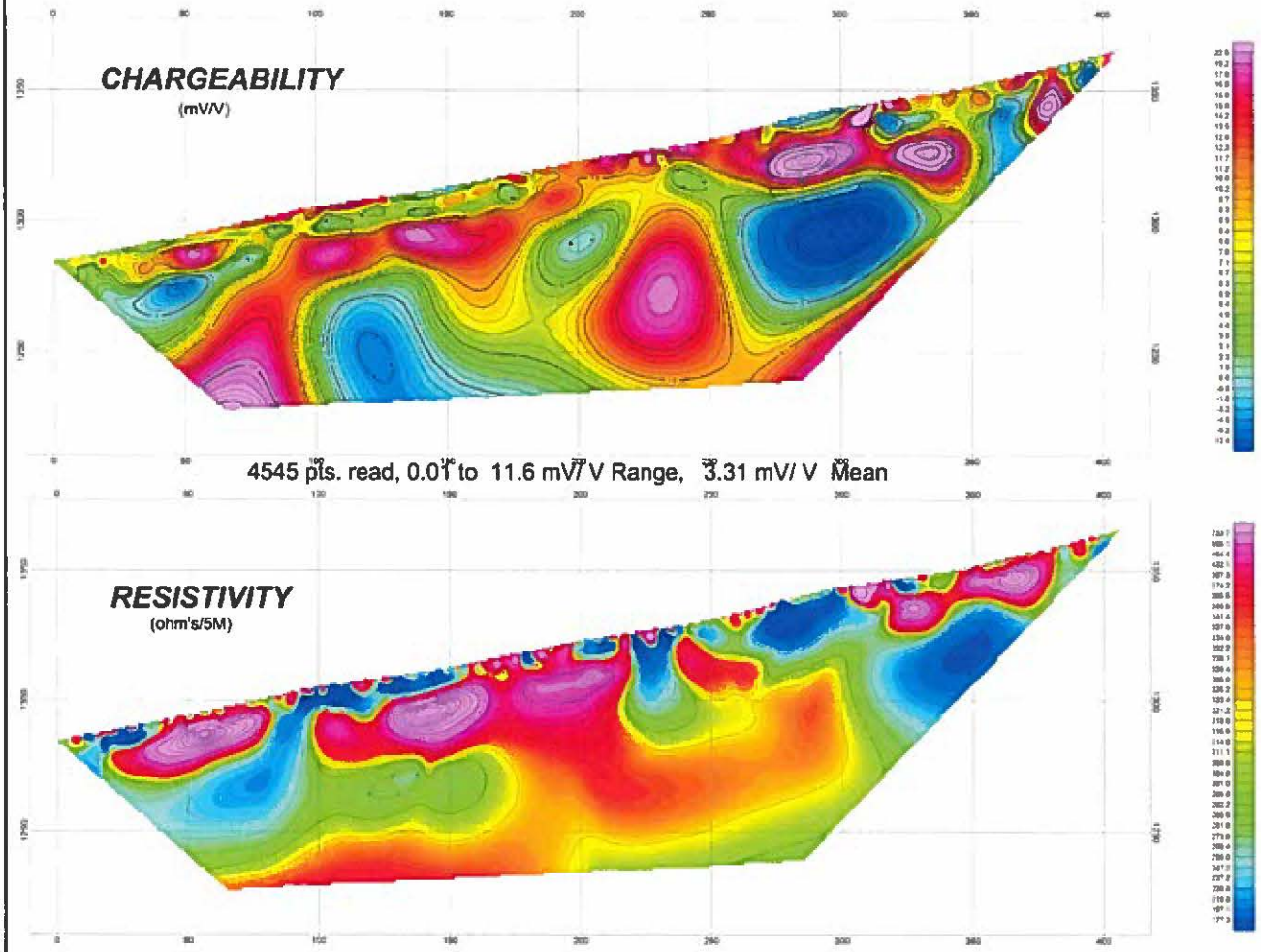
INVERSION

High Resolution Resistivity/IP Survey

Figure 10



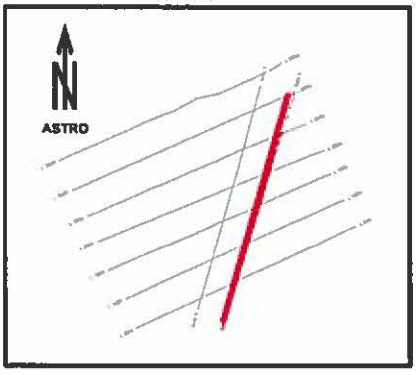
LOOKING NORTH



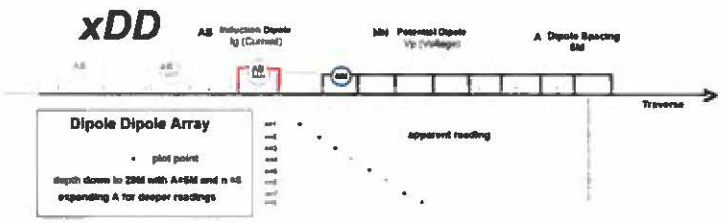
4545 pts. read, 0.01 to 11.6 mV/V Range, 3.31 mV/ V Mean

4708 Data pts. read, 73.3 to 4216 ohm's/ 5M Range, 335 ohm's/ 5M Mean.

Key Map



LEGEND



Supersting by AGI (Advanced Geoscience Inc.)
Time Domain Equipment
84 Electrode System
A (spacing) = 5M, 415M Traverse

Ansell Capital Corporation

OK

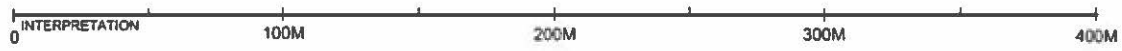
Charlotte Project

Nansen Mountain Area, NTS: 115-I/03.
Whitehorse Mining District, Yukon Territories.

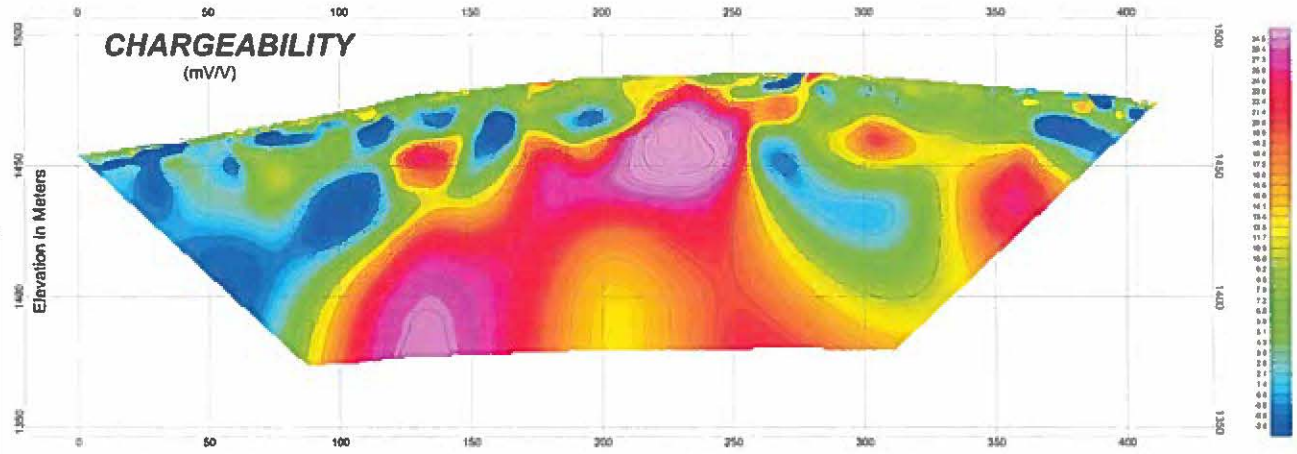
Section 1000N

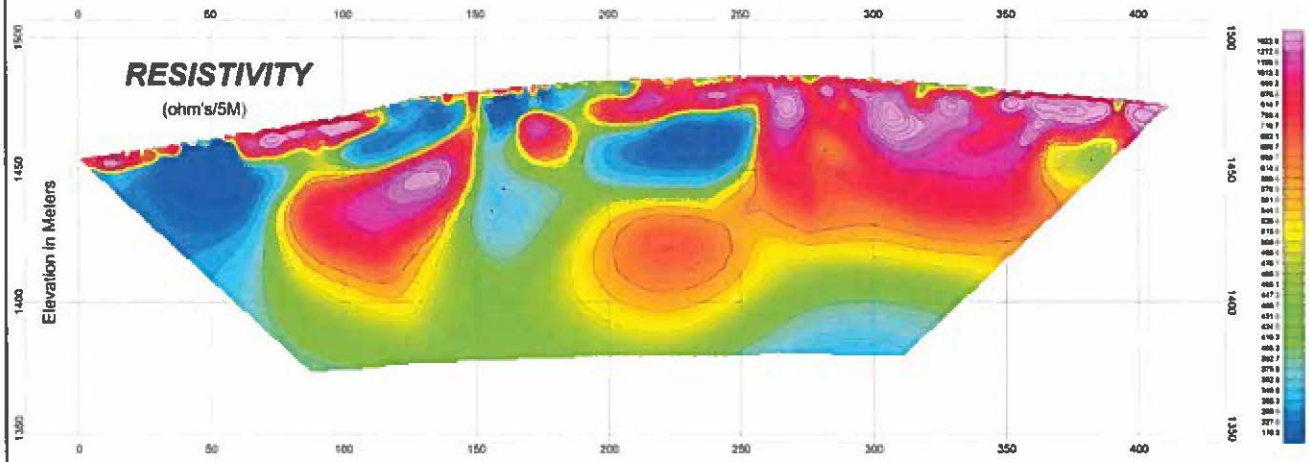
INVERSION
High Resolution Resistivity/IP Survey

Figure 11

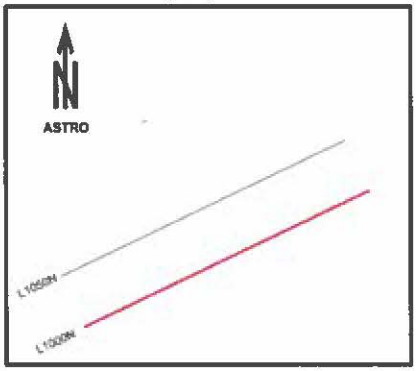


LOOKING NORTH

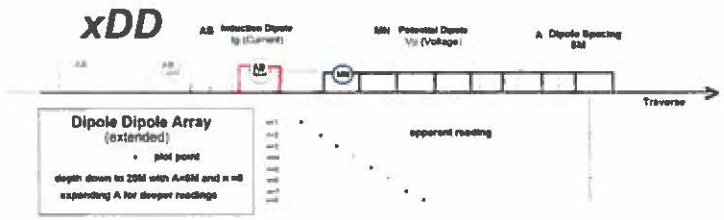




Key Map



LEGEND



Supersting by AGI (Advanced Geoscience Inc.)
Time Domain Equipment
84 Electrode System
A (spacing) = 5M, 415M Traverse

Ansell Capital Corporation

OK

Charlotte Project

Nansen Mountain Area, NTS: 115-I/03.
Whitehorse Mining District, Yukon Territories.

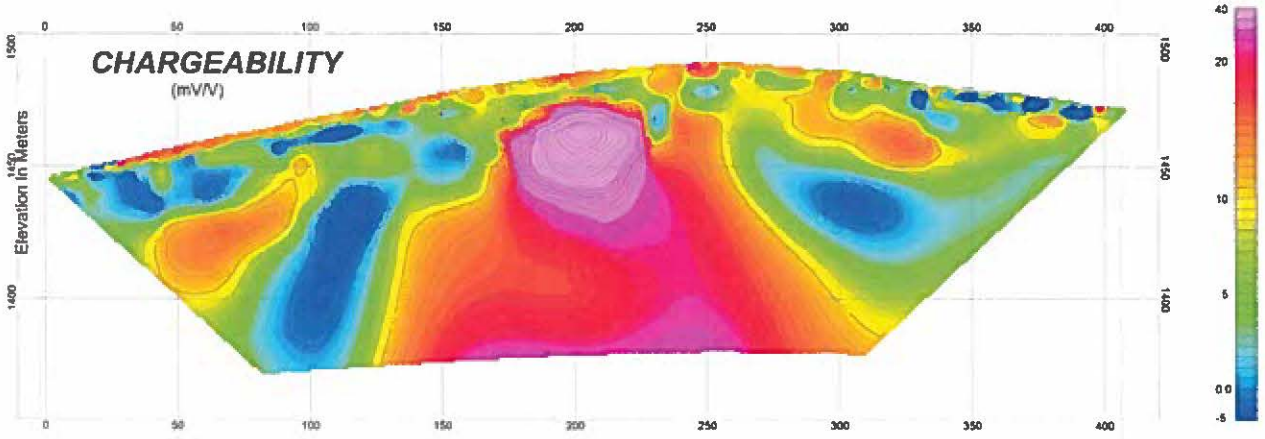
Section 1050N

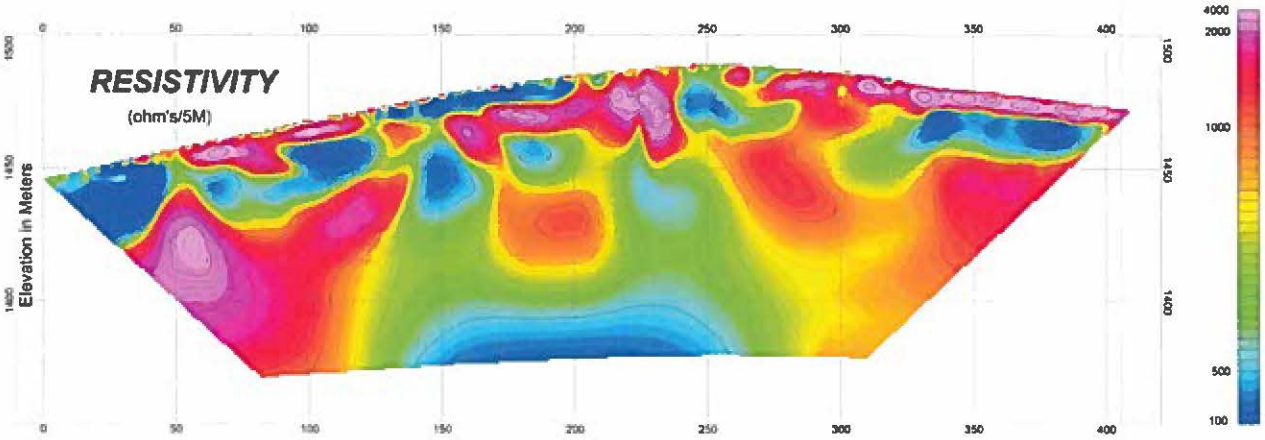
INVERSION
High Resolution Resistivity/IP Survey

Figure 12

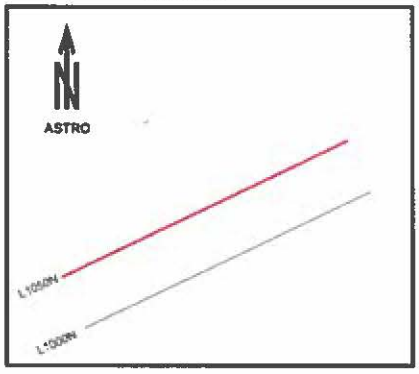


LOOKING NORTH

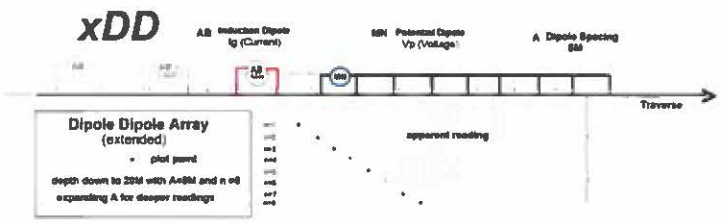




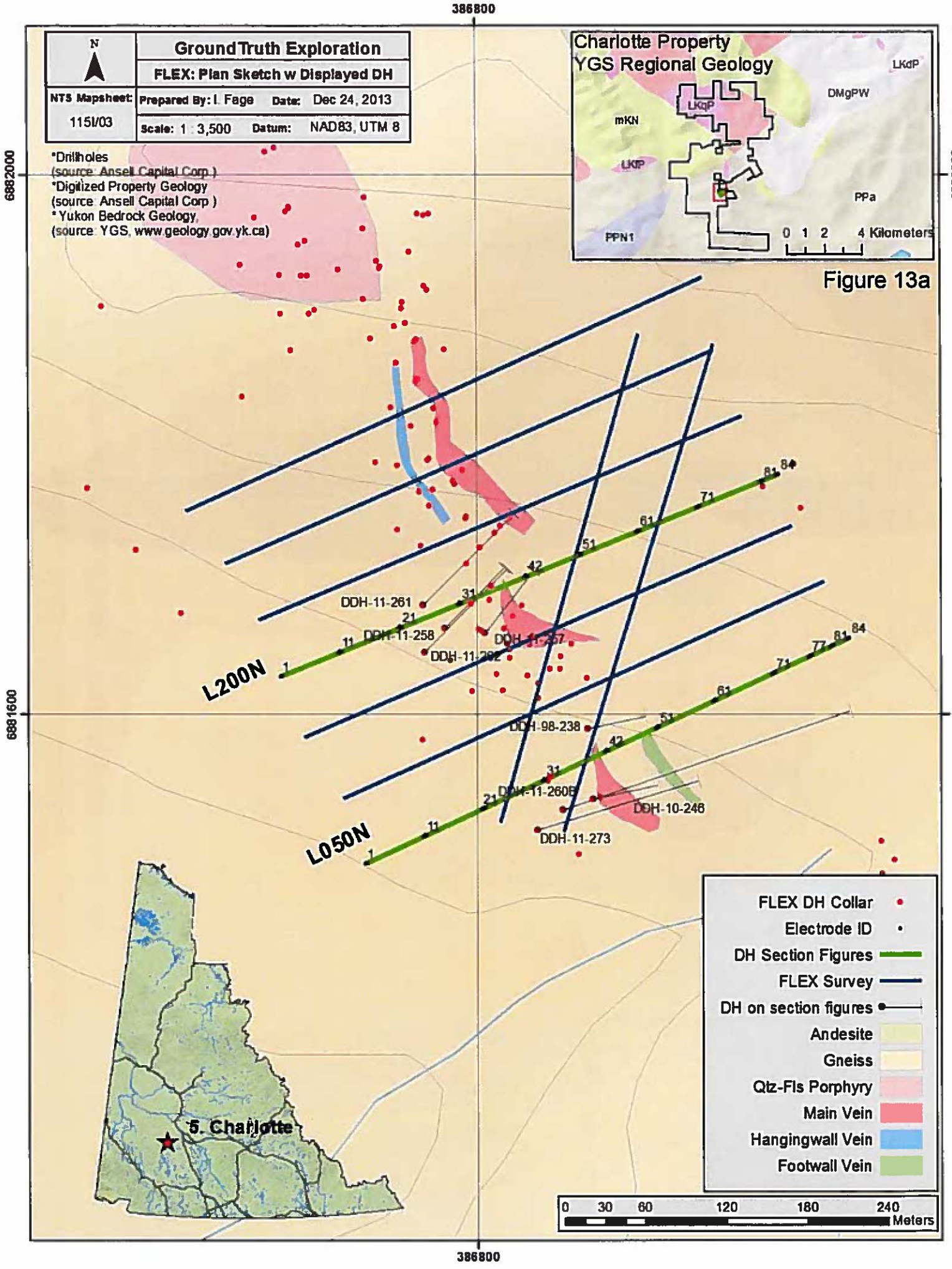
Key Map



LEGEND

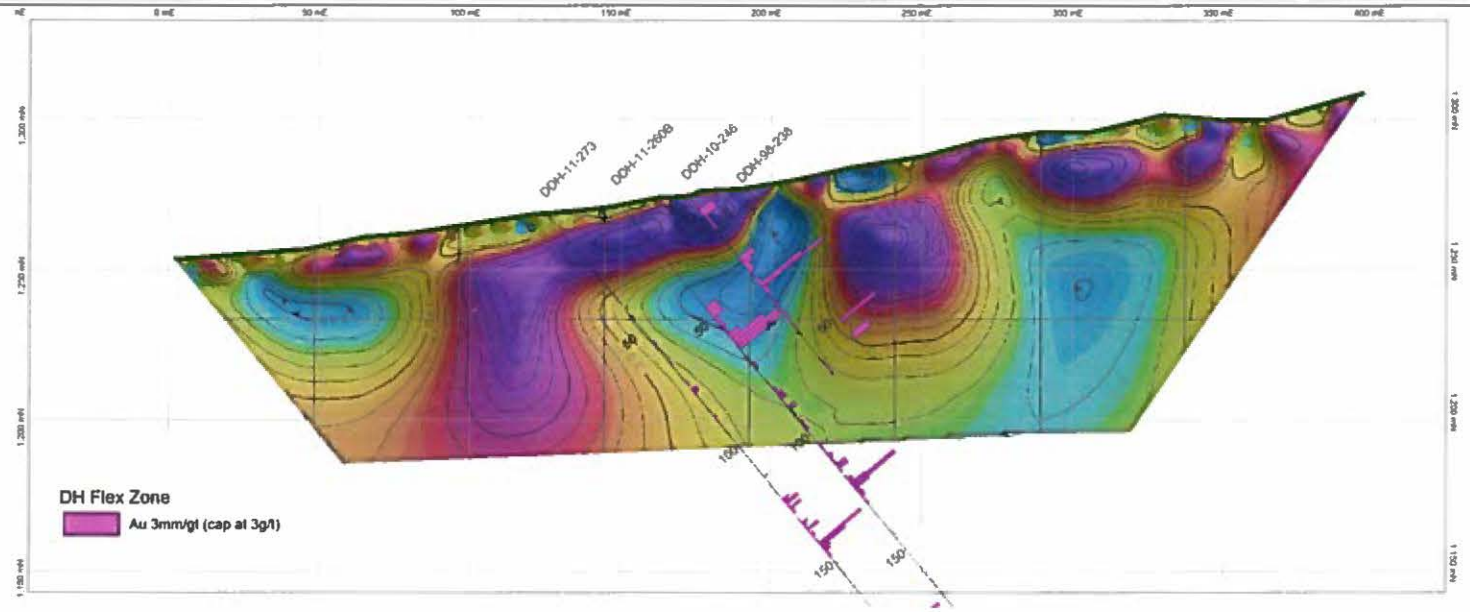


Supersting by AGI (Advanced Geoscience Inc.)
Time Domain Equipment
84 Electrode System
A (spacing) = 5M, 415M Traverse

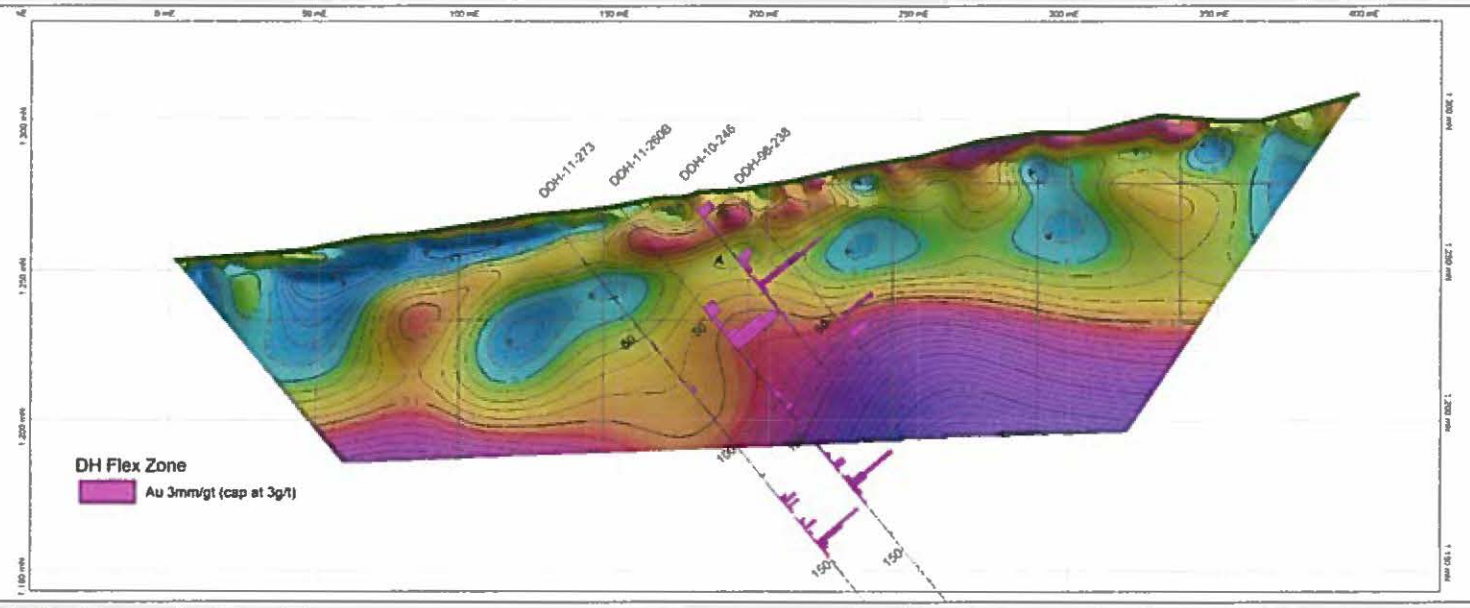

386800
6882000
6881600
386800
N
Ground Truth Exploration
FLEX: Plan Sketch w Displayed DH
NTS Mapsheet: 115I/03
Prepared By: I. Fage
Date: Dec 24, 2013
Scale: 1 : 3,500
Datum: NAD83, UTM 8
*Drillholes (source: Ansell Capital Corp.)
*Digitized Property Geology (source: Ansell Capital Corp.)
*Yukon Bedrock Geology (source: YGS, www.geology.gov.yk.ca)
Charlotte Property
YGS Regional Geology
LKdP
DMgPW
LKqP
mKN
LKfP
PPa
PPN1
0 1 2 4 Kilometers
Figure 13a
DDH-11-261
DDH-11-258
DDH-11-257
DDH-11-262
DDH-98-238
DDH-11-260B
DDH-10-246
DDH-11-273
L200N
L050N
1
11
21
31
42
51
61
71
77
81
84
5. Charlotte
FLEX DH Collar
Electrode ID
DH Section Figures
FLEX Survey
DH on section figures
Andesite
Gneiss
Qtz-Fls Porphyry
Main Vein
Hangingwall Vein
Footwall Vein
0 30 60 120 180 240
Meters

Inverted Resistivity — Extended Dipole-Dipole Array

Figure 13



Inverted Chargeability — Extended Dipole-Dipole Array



Project: Charlotte Property, Flex Zone
Line: L050N
Look Direction: North West (334 deg)
Survey Date:September 2, 2013

Projection: NAD83, UTM zone 8N
Inversion: M. Best
Plot: R. Daigle, I. Fage

GROUNDTRUTH EXPLORATION

Inverted Resistivity — Extended Dipole-Dipole Array

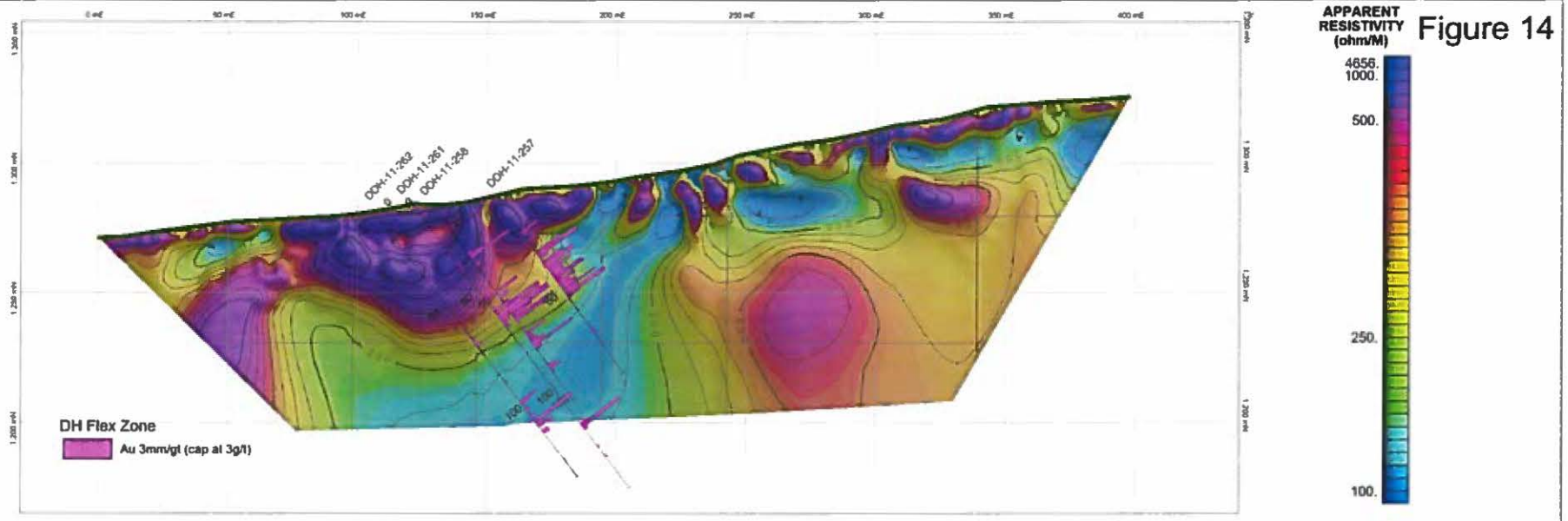
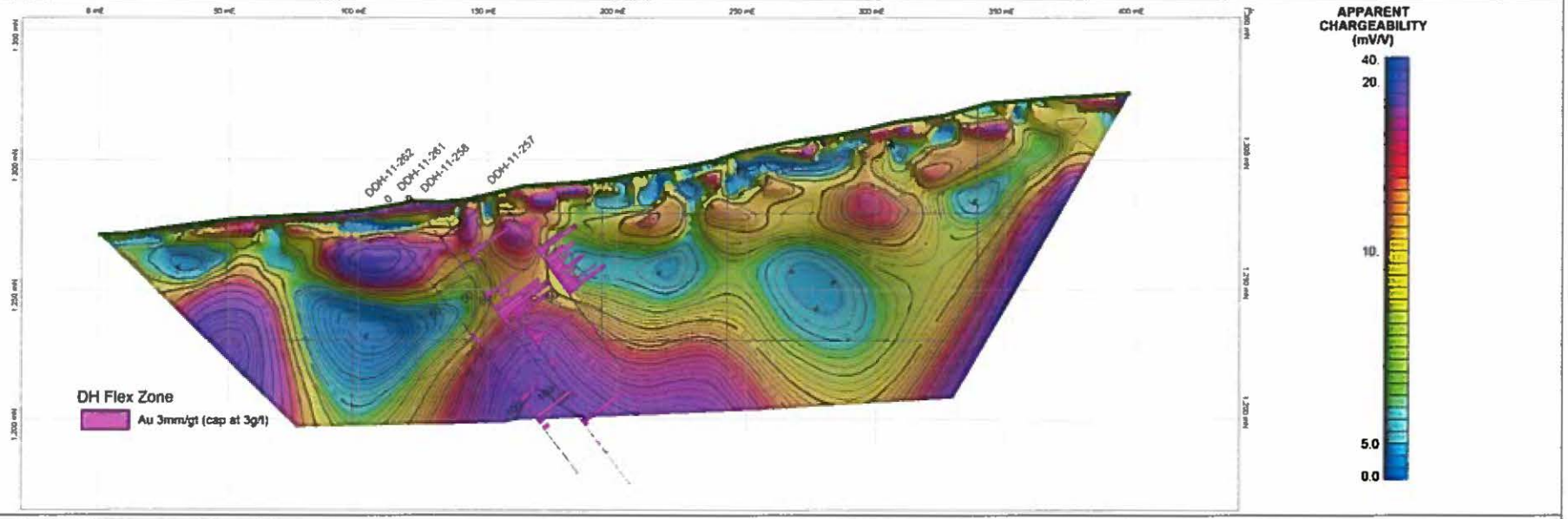


Figure 14

Inverted Chargeability — Extended Dipole-Dipole Array

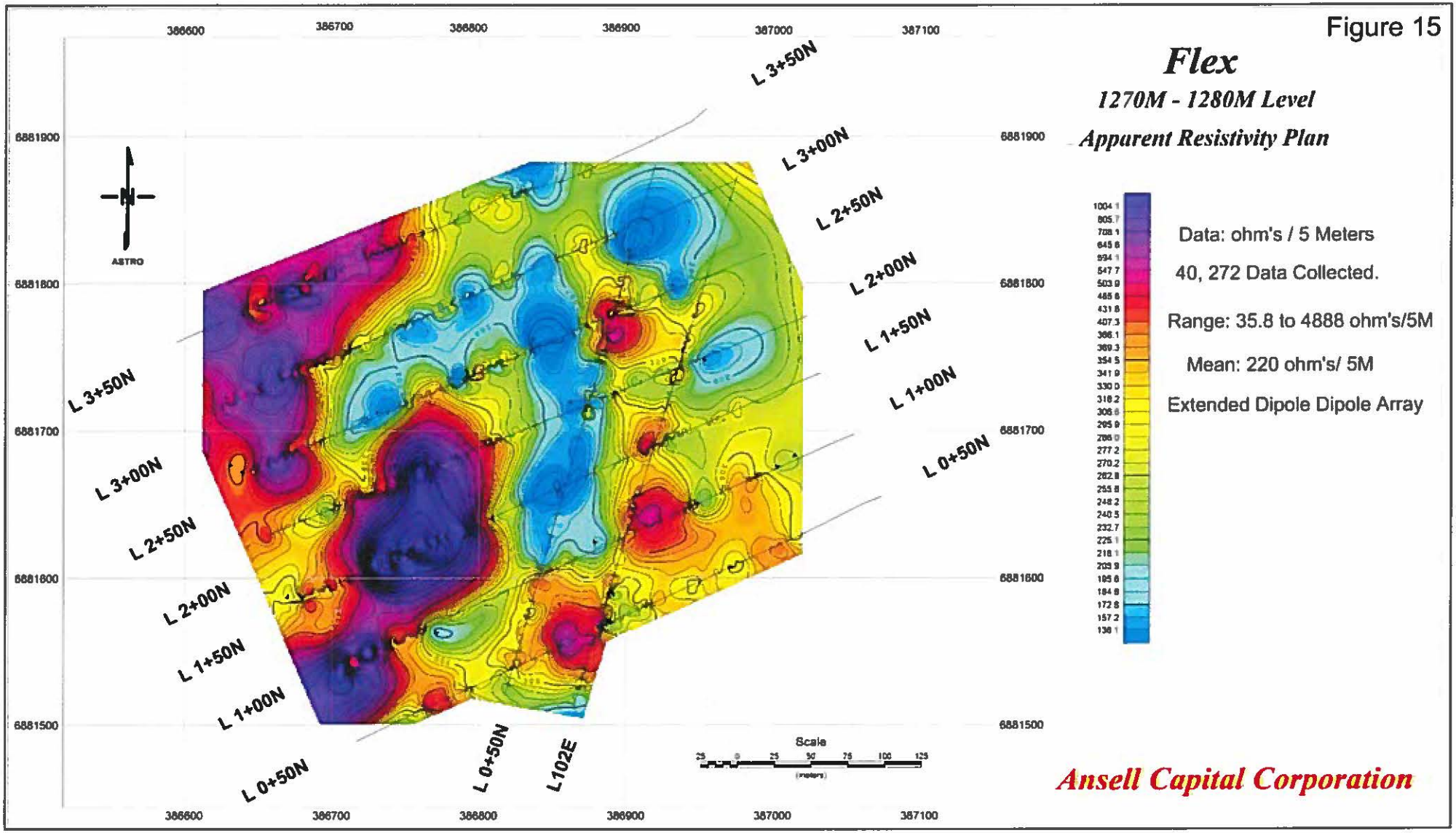


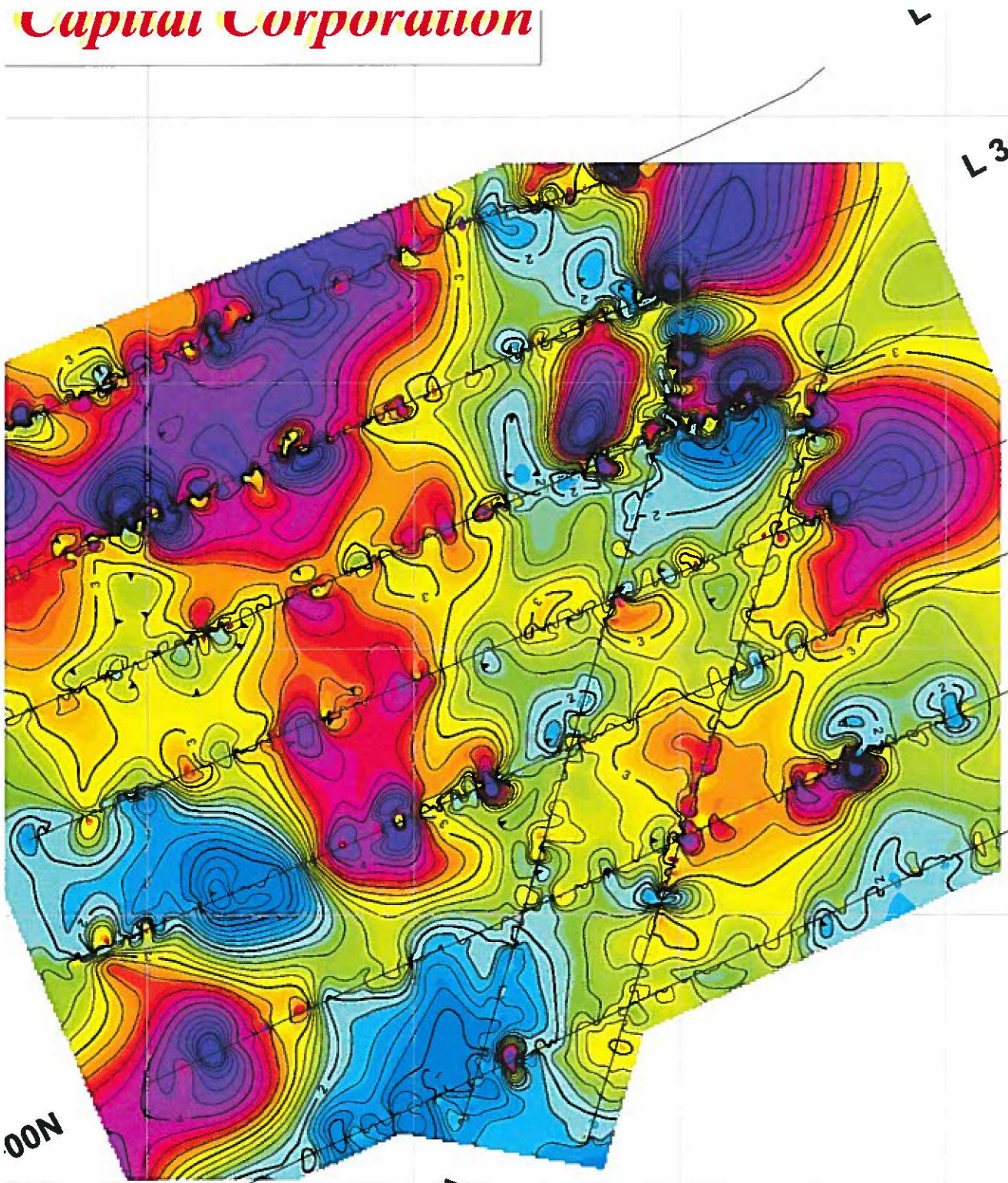
Project: Charlotte Property, Flex Zone
Line: L200N
Look Direction: North West (334 deg)
Survey Date:September 2, 2013

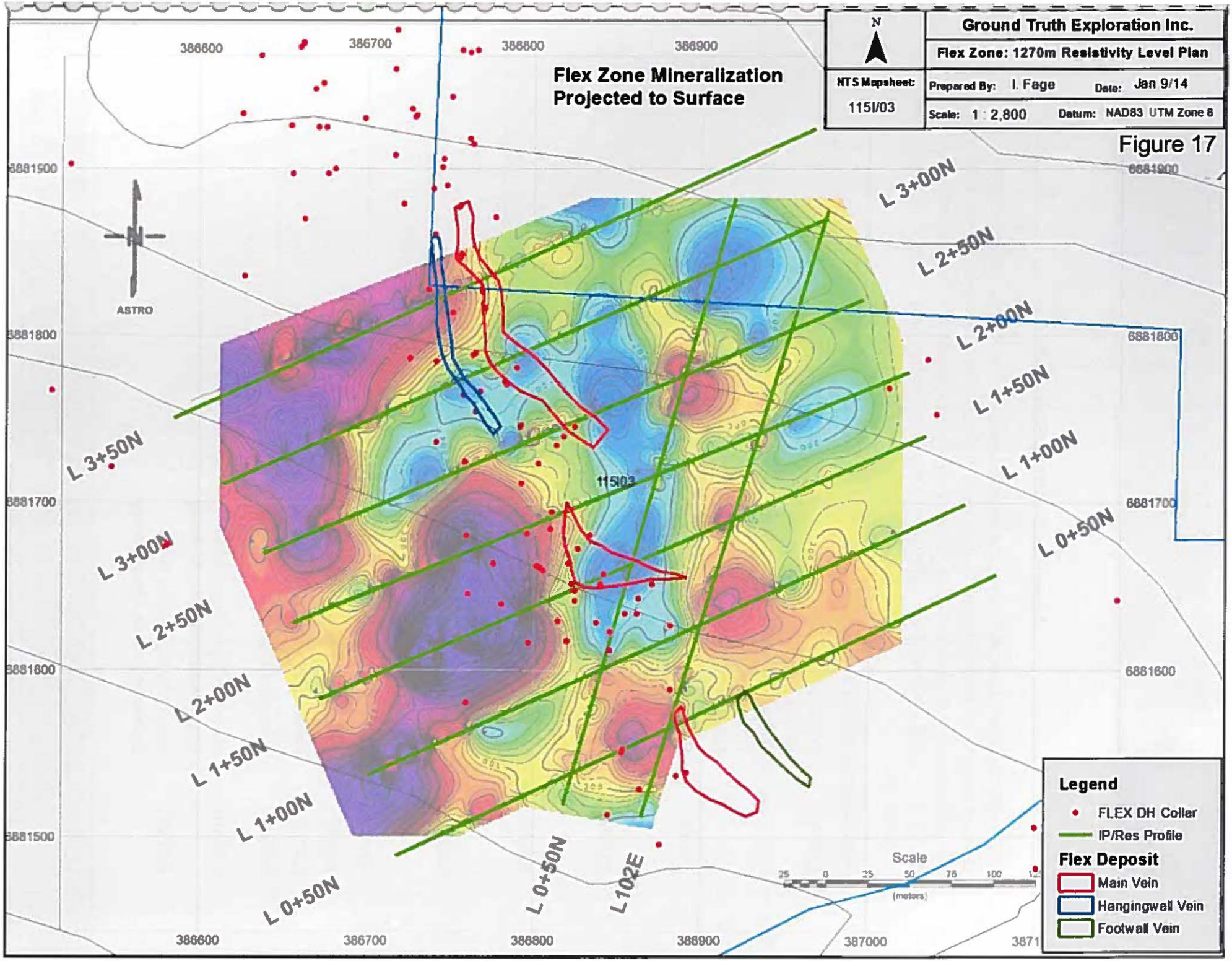
Projection: NAD83, UTM zone 8N
Inversion: M. Best
Plot: R. Daigle, I. Fage

GROUNDTRUTH EXPLORATION

Figure 15


Flex
1270M - 1280M Level
Apparent Resistivity Plan
Data: ohm's / 5 Meters
40, 272 Data Collected.
Range: 35.8 to 4888 ohm's/5M
Mean: 220 ohm's/ 5M
Extended Dipole Dipole Array
Ansell Capital Corporation
Scale
ASTRO
386600
386700
386800
386900
387000
387100
6881900
6881800
6881700
6881600
6881500
L 3+50N
L 3+00N
L 2+50N
L 2+00N
L 1+50N
L 1+00N
L 0+50N
L102E


L 3+00N
L 2+50N
L 2+00N
L 1+50N
L 1+00N
L 0+50N
6881900
6881800
6881700
6881600
6881500
Data:
Range:
Mean:
Extende


Ground Truth Exploration Inc.
Flex Zone: 1270m Resistivity Level Plan
NTS Mapsheet: 115I/03
Prepared By: I. Fage
Date: Jan 9/14
Scale: 1 : 2,800
Datum: NAD83 UTM Zone 8
Figure 17
Flex Zone Mineralization Projected to Surface
ASTRO
L 3+00N
L 2+50N
L 2+00N
L 1+50N
L 1+00N
L 0+50N
L 3+50N
L 102E
115I/03
386600
386700
386800
386900
387000
6881500
6881600
6881700
6881800
6881900
Scale
(meters)
Legend
FLEX DH Collar
IP/Res Profile
Flex Deposit
Main Vein
Hangingwall Vein
Footwall Vein

Appendix A- Arrays Surveyed

This table outlines the arrays surveyed on each traverse. xDD was selected at the optimal array to be presented on all traverses in this report. Inversions of the xDD array are cataloged in the `Inverted Data` folder in final data submission that accompanies this report. All other arrays are cataloged in the `Instrument Data` folder in the final data submission.

FLEX and Orloff King Surveyed Arrays:

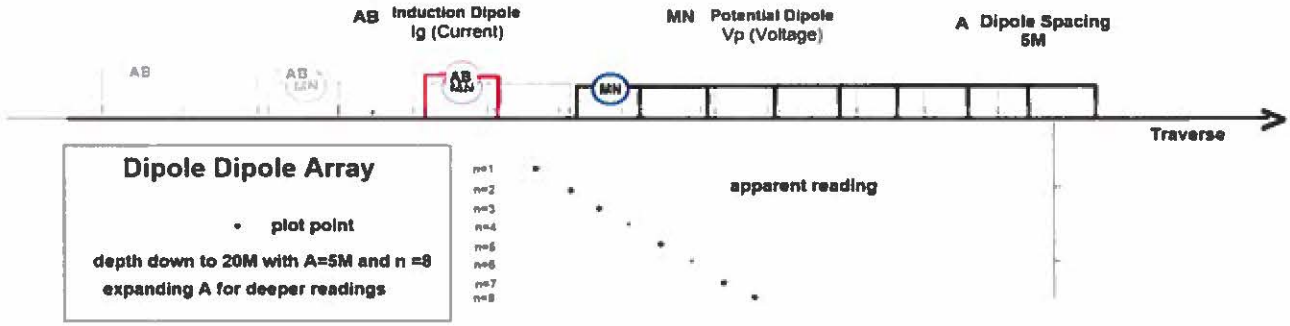
L050N	Pole-Dipole Array Strong Gradient Array Inverse Schlumberger Array Wenner Array **Extended Dipole-Dipole Array**
L100N	Pole-Dipole Array Strong Gradient Array **Extended Dipole-Dipole Array**
L150N	Pole-Dipole Array Strong Gradient Array **Extended Dipole-Dipole Array**
L200N	Strong Gradient Array Inverse Schlumberger Array **Extended Dipole-Dipole Array**
L250N	Pole-Dipole Array Strong Gradient Array **Extended Dipole-Dipole Array**
L300N	**Extended Dipole-Dipole Array**
L350N	**Extended Dipole-Dipole Array**
L101E	**Extended Dipole-Dipole Array**
L102E	**Extended Dipole-Dipole Array**
L1000N	Inverse Schlumberger Array **Extended Dipole-Dipole Array**
L1050N	Inverse Schlumberger Array **Extended Dipole-Dipole Array**

Box 70, DAWSON, YT
Y0B 1G0

Appendix B - Survey Theory

This section outlines the arrays utilized in the Charlotte IP/Res Survey

1. Dipole-Dipole Array (presented Array)

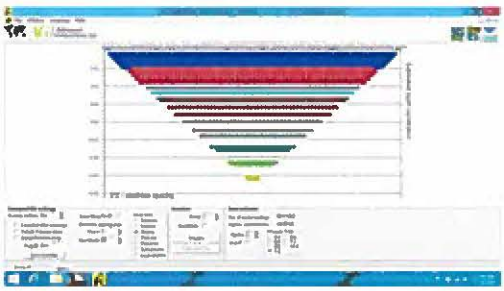


geometry

Most common of arrays, directional current inductions mainly favored to delineate bodies having dip(s). Current electrodes always lagging potential electrodes. Attention to direction of current inductions important when interpreting data. Known to produce typical pant-leg anomalies when both AB and MN electrodes cross a zone.

Set-up

Once a designated traverse is located, 84 electrodes are put into the ground pre extending 6 x cables of 14 connections amounting to a **415M Traverse.** The **Supersting** Transmitter/ Receiver (Tx/Rx) along with power-pack and switch-box are always centrally positioned.



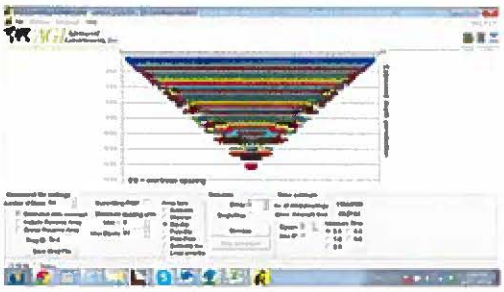
A designated Dipole Dipole Array command file was loaded in the Supersting performing:

1453 sample points, with an estimated 57.29min lapse-time, Maximum n (depth level) kept at 8 for best Signal/Noise, and Maximum dipoles of 26.

AB: 5,10,15,20,25,and 30M, **5 x expansions** reversed to traverse direction

MN: 5M till n=8, then 10M until n=8, then 20M until EOL

Extended Dipole Dipole



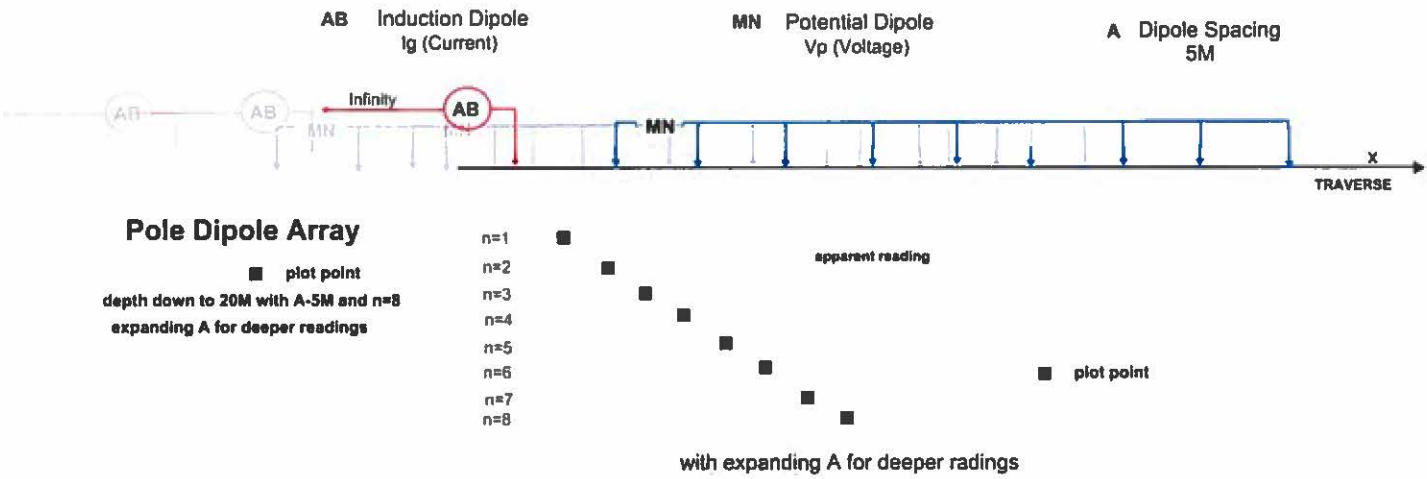
Extended Option

4709 sample points, with an estimated 3hr:27Min lapse-time. Maximum n (depth level) kept at 8 for best Signal/Noise, and Maximum Dipoles of 26.

AB: 5,10,15... up to95M, **19 expansions** reversed to traverse direction

MN: 5,10,15,25, and 50M, 5 x expansions.

2. Pole-Dipole Array



Geometry

Most common of arrays, directional current inductions mainly favored to delineate bodies having dip(s). Current electrodes always lagging potential electrodes. Attention to of current inductions direction important when interpreting data. Known to produce typical pant-leg anomalies when both AB and MN electrodes cross a zone.

Set-up

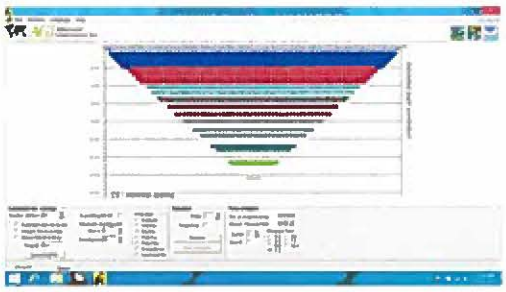
Once a designated traverse is located, 84 electrodes are put into the ground pre extending 6x cables of 14 connections amounting to a 415M Traverse. The Supersting Transmitter/ Receiver (Tx/Rx) along with power-pack and switch-box are always centrally positioned.

A designated Dipole-Dipole Array command file was loaded in the Supersting performing:

1453 sample points, with an estimated 57.29min lapse-time, Maximum n (depth level) kept at 8 for best Signal/Noise, and Maximum dipoles of 26.

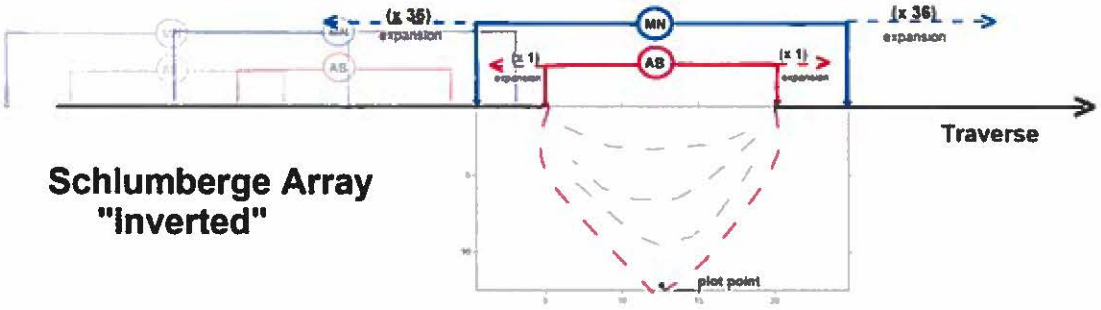
AB: 5,10,15,20,25,and 30M, 5 x expansions reversed to traverse direction

MN: 5M till n=8, then 10M until n=8, then 20M until EOL



3. Inverse Schlumberger Array

AB Induction Dipole Ig (Current) MN Potential Dipole Vp (Voltage) A Dipole Spacing 5M



Schlumberge Array "Inverted"

Geometry

Symmetric, vertical sounding technique is reliable delineating axis of zones. Termed inverted because the original design of the Schlumberger has inducing current electrodes outside potential electrodes. Also very useful isolating narrow, weak zones.

"Si-1" AB = 5M MN= 15M to 360M (36 expansions both directions). Narrow Zones Favored.

"Si-2" AB= 5M MN= 15M to 65M first four levels. Shallow (limited depth extent) Zones Favored.

AB=15M MN= 15M to 360M

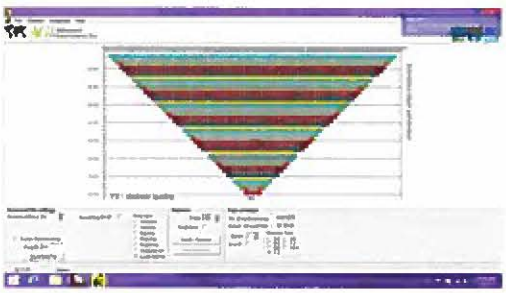
"Si-3" AB= 5M to 95M and MN 15M to 360M. Best penetration of all three.

Set-up

Once a designated traverse is located, 84 electrodes are put into the ground pre extending 6x cables of 14 connections amounting to a 415M Traverse. The Supersting Transmitter/ Receiver (Tx/Rx) along with power-pack and switch-box are always centrally positioned.

A designated Schlumberger Array command file was loaded in the Supersting performing:

1679 sample points, with an estimated 80:48min lapse-time, Maximum n kept at 8 (for best Signal/Noise), and Maximum dipoles of 26.



Appendix C - Equipment Specifications

(www.agiusa.com)

SuperSting R1/IP Technical Specifications

Measurement modes: apparent resistivity, resistance, self-potential (SP), induced polarization (IP), battery voltage
Measurement range: +/- 10V
Measuring resolution: max 30 nV, depends on voltage level
Screen resolution: 4 digits in engineering notation
Output current: 1mA – 2 A continuous, measured to high accuracy
Output voltage: 800 Vp-p, actual electrode voltage depends on transmitted current and ground resistivity
Output power: 200 W
Input gain ranging: automatic, always uses full dynamic range of receiver
Input impedance: >20 MΩ
SP compensation: automatic cancellation of SP voltages during resistivity measurement; constant and linearly varying SP cancels completely
Type of IP measurement: Time domain chargeability (M), six time slots measured and stored in memory
IP current transmission: ON+, OFF, ON-, OFF
IP time cycles: 0.5, 1, 2, 4 and 8 seconds (combined resistivity/IP mode)
Measure cycles: running average of measurement displayed after each cycle; automatic cycle stop when reading errors fall below user set limit or user set max cycles are done
Resistivity time cycles: basic measure time is 0.4, 0.8, 1.2, 3.6, 7.2 or 14.4 seconds as selected by user via keyboard, auto-ranging and commutation adds about 1.4 s
Signal processing: continuous averaging after each complete cycle; noise errors calculated and displayed as percentage of reading; reading displayed as resistance (ΔV/I) and apparent resistivity (Ωm); resistivity is calculated using user entered electrode array coordinates
Noise suppression: better than 100 dB at f>20 Hz; better than 120 dB at power line frequencies (16 2/3, 20, 50 and 60 Hz) for measure cycles of 1.2 s and above
Total accuracy: better than 1% of reading in most cases (lab measurements). Field measurement accuracy depends on ground noise and resistivity. Instrument will calculate and display running estimate of measuring accuracy
System calibration: calibration is done digitally by the microprocessor based on correction values stored in memory
Supported manual: resistance, Schlumberger, Wenner, dipole-dipole, pole-dipole, pole-pole, SP absolute, SP-gradient configurations
Operating system: Stored in re-programmable flash memory; new version can be downloaded from our web site and stored in the flash memory
Data storage: full resolution reading average and error are stored along with user entered coordinates and time of day for each measurement; storage is effected automatically in a job oriented file system
Data display: apparent resistivity (Ohmmeter), injected current (mAmp) and measured voltage (mVolt) are displayed and stored in memory for each measurement
Memory capacity: the memory can store 24,468 measurements in Resistivity Mode and 14,966 measurements in combined Resistivity/IP Mode
Data transmission: RS-232C channel available to dump data from the instrument to a Windows type computer on user command.
Automatic multi-electrodes: the SuperSting is designed to run dipole-dipole, pole-dipole, pole-pole, Wenner and Schlumberger surveys including roll-along surveys completely automatic with the Swift Dual Mode Automatic Multi-electrode system (patent 6,404,203) or with switch box and passive cables; the SuperSting can run any other array by using user programmed command files; these files are ASCII files and can be created using a regular text editor; the command files are downloaded to the SuperSting RAM memory and can at any time be recalled and run; therefore there is no need for a fragile computer in the field.
Manual measurements: the instrument has four banana pole screws for connecting current and potential electrodes during manual measurements
User controls: 20 key tactile, weather proof keyboard with alpha numeric entry keys and function keys; On/off switch; Measure button; integrated within main keyboard; LCD night light switch (push to light)
Display: Graphics LCD display (16 lines x 30 characters) with night light.
Power supply, field: 12V or 2x12 V DC external power (one or two 12 V batteries), connector on front panel.
Power supply, office: DC power supply
Operating time: depends on survey conditions and size of battery used; internal circuitry in auto mode adjusts current to save energy
Operating temperature: -5 to +50°C
Weight: 10.9 kg (24 lb.)
Dimensions: Width 184 mm (7.25"), length 406 mm (16") and height 273 mm (10.75")

16 Appendix 2- Mineralogical report

Charlotte Property Au-Ag Polished Sections:

Mineralogical Report

November 2013

Completed for Ansell Capital Corp.

By

M.L. Dalsin, M.Sc.

Table of Contents

1. Objectives 14

2. Experimental Methods 15

3. Mineralogical Results 16

MIN-001A 17

MIN-001B 20

MIN-002 23

MIN-003A 27

MIN-003B 28

MIN-004 30

MIN-005A 33

MIN-005B 35

MIN-006 38

MIN-007 40

MIN-008A 42

MIN-008B 45

MIN-009 47

MIN-010 49

MIN-011 51

MIN-012 53

MIN-013 55

MIN-014 58

MIN-015 59

MIN-016 64

MIN-017 66

MIN-018 68
MIN-019 72
MIN-020 75
MIN-021 77
MIN-022 82
MIN-023 84
MIN-024A 86
MIN-024B 88
MIN-025 92
MIN-026 94
MIN-027 96
MIN-028 98
MIN-029 100
4. Discussion 102
Statement of Qualifications 105
References 106
Appendix A: Polished section scans in plane polarized and crossed polarized light 107
Appendix B: EDX spectra of minerals observed in polished section 142

Table of Figures

Figure 1. Photomicrographs of the quartz matrix with some grains showing recrystallized rims in transmitted light, plane-polars (left) and crossed polars (right) (4x mag., F.O.V. ~3 mm)..... 17
Figure 2. Photomicrographs of the sulphide mineralization in reflected light (4x mag., F.O.V. ~3mm)..... 18
Figure 3. Backscattered electron image of quartz, and carbonate mineralization. 18
Figure 4. Backscattered electron image of arsenopyrite, sphalerite and galena. 19
Figure 5. Photomicrographs of the quartz matrix with some grains showing recrystallized rims in transmitted light, plane-polars (left) and crossed polars (right) (4x mag., F.O.V. ~3 mm)..... 20
Figure 6. Photomicrographs of the sulphide mineralization in reflected light (4x mag., F.O.V. ~3mm)..... 21
Figure 7. Photomicrograph of freibergite, bournonite, and pyrite in reflected light (4x mag., F.O.V. ~3mm)..... 21
Figure 8. Backscattered electron image of Figure 7, showing freibergite, bournonite, and galena. 22
Figure 9. Photomicrographs of the quartz matrix with some grains showing recrystallized rims in transmitted light, plane-polars (left) and crossed polars (right) (4x mag., F.O.V. ~3 mm)..... 23
Figure 10. Photomicrograph of arsenopyrite, sphalerite and chalcopyrite in reflected light (4x mag., F.O.V. ~3mm)..... 24
Figure 11. Photomicrograph in reflected light (4x mag., F.O.V. ~3mm) (left), and backscattered electron image (right) of arsenopyrite, sphalerite, galena, and boulangerite..... 24
Figure 12. Backscattered electron image of galena and boulangerite. 25
Figure 13. Backscattered electron image of arsenopyrite, sphalerite, galena and freibergite. Arsenopyrite is possibly being replaced by galena..... 25
Figure 14. Photomicrograph of arsenopyrite, galena, and Sb-sulphosalt minerals in reflected light (4x mag., F.O.V. ~3mm)..... 26
Figure 15. Backscattered electron image of Figure 14 showing the Sb-sulphosalts bournonite and boulangerite..... 26
Figure 16. Photomicrographs of the quartz matrix, muscovite alteration, and ankerite in transmitted light, plane-polars (left) and crossed polars (right) (4x mag., F.O.V. ~3 mm)..... 27

Figure 17. Photomicrograph of pyrite in reflected light (4x mag., F.O.V. ~3mm). 27
Figure 18. Photomicrographs of the quartz matrix, and muscovite alteration in transmitted light, plane-polars (left) and crossed polars (right) (2x mag., F.O.V. ~6 mm). 28
Figure 19. Photomicrographs of pyrite (left) and pyrite, sphalerite, and arsenopyrite (right) in reflected light (4x mag., F.O.V. ~3mm). 29
Figure 20. Photomicrographs of the quartz matrix, calcite, ankerite, and dolomite in transmitted light, plane-polars (left) and crossed polars (right) (4x mag., F.O.V. ~3 mm)..... 30
Figure 21. Backscattered electron image of Figure 21, showing quartz, calcite, ankerite, dolomite and arsenopyrite. 31
Figure 22. Photomicrographs of the quartz matrix, calcite, and ankerite in transmitted light, plane-polars (left) and crossed polars (right) (4x mag., F.O.V. ~3 mm). 31
Figure 23. Photomicrograph of pyrite, and arsenopyrite in reflected light (4x mag., F.O.V. ~3mm). 32
Figure 24. Backscattered electron image of arsenopyrite, pyrite, galena and sphalerite. 32
Figure 25. Photomicrographs of the quartz matrix, muscovite, and Fe-oxide in transmitted light, plane-polars (left) and crossed polars (right) (20x mag., F.O.V. ~0.6 mm). 33
Figure 26. Photomicrographs of the quartz matrix, muscovite, and Fe-oxide replacing pyrite in transmitted light (plane-polars (left), crossed polars (right)), and reflected light (bottom) (4x mag., F.O.V. ~3 mm). 34
Figure 27. Photomicrographs of the quartz matrix, muscovite, and K-Fe-sulphate alteration in transmitted light, plane-polars (left) and crossed polars (right) (4x mag., F.O.V. ~3mm)..... 35
Figure 28. Backscattered electron image of Figure 27 showing the alteration of pyrite to K-Fe-sulphate, and muscovite alteration. 36
Figure 29. Photomicrograph of pyrite being altered in reflected light (4x mag., F.O.V. ~3 mm). 37
Figure 30. Photomicrographs of the quartz matrix in transmitted light, plane-polars (left) and crossed polars (right) (4x mag., F.O.V. ~3mm)..... 38
Figure 31. Photomicrograph of pyrite, arsenopyrite, sphalerite and galena in reflected light (4x mag., F.O.V. ~3 mm). 39
Figure 32. Backscattered electron image of pyrite, arsenopyrite, and galena. 39

Figure 33. Photomicrographs of the quartz matrix in transmitted light, plane-polars (left) and crossed polars (right) (4x mag., F.O.V. ~3mm)..... 40
Figure 34. Photomicrographs of the quartz matrix and ankerite veinlet in transmitted light, plane-polars (left) and crossed polars (right) (4x mag., F.O.V. ~3mm). 41
Figure 35. Photomicrograph s of arsenopyrite, sphalerite and galena in reflected light (4x mag., F.O.V. ~3 mm). 41
Figure 36. Photomicrographs of the quartz matrix and muscovite alteration in transmitted light, plane-polars (left) and crossed polars (right) (10x mag., F.O.V. ~1.2mm). 42
Figure 37. Photomicrographs of quartz matrix in transmitted light, plane polars (left), and crossed polars (right) (4x mag., F.O.V. ~3mm)..... 43
Figure 38. Photomicrograph of arsenopyrite, pyrite, sphalerite and galena in reflected light (4x mag., F.O.V. ~3 mm). 43
Figure 39. Backscattered electron image of arsenopyrite, pyrite, and sphalerite. 44
Figure 40. Photomicrographs of the quartz matrix and muscovite alteration in transmitted light, plane-polars (left) and crossed polars (right) (10x mag., F.O.V. ~1.2mm). 45
Figure 41. Photomicrographs of quartz matrix in transmitted light, plane polars (left), and crossed polars (right) (4x mag., F.O.V. ~3mm)..... 46
Figure 42. Photomicrograph of arsenopyrite, pyrite, and sphalerite in reflected light (4x mag., F.O.V. ~3 mm). 46
Figure 43. Photomicrographs of the quartz matrix and muscovite alteration in transmitted light, plane-polars (left) and crossed polars (right) (10x mag., F.O.V. ~1.2mm). 47
Figure 44. Photomicrographs of the quartz matrix being weakly altered by muscovite in transmitted light, plane-polars (left) and crossed polars (right) (10x mag., F.O.V. ~1.2mm)..... 48
Figure 45. Photomicrographs of arsenopyrite, pyrite, and sphalerite in reflected light (4x mag., F.O.V. ~3 mm). 48
Figure 46. Backscattered electron images of arsenopyrite, pyrite, sphalerite and galena. 48
Figure 47. Photomicrographs of the quartz matrix and areas of aphanitic quartz and muscovite alteration in transmitted light, plane-polars (left) and crossed polars (right) (2x mag., F.O.V. ~6mm). 49
Figure 48. Photomicrograph pyrite, galena and boulangerite in reflected light (10x mag., F.O.V. ~1.2mm). 50

Figure 49. Backscattered electron images of Figure 48. 50
Figure 50. Photomicrographs showing the differences in the two halves of the section and the formation and appearance of quartz, muscovite and oxide alteration in transmitted light, plane-polars (left) and crossed polars (right) (4x mag., F.O.V. ~3mm). 51
Figure 51. Photomicrograph of sphalerite, pyrite, and arsenopyrite in reflected light (10x mag., F.O.V. ~1.2mm). 52
Figure 52. Photomicrographs of quartz being altered by Fe-oxide and muscovite in transmitted light, plane-polars (left) and crossed polars (right) (4x mag., F.O.V. ~3mm). 53
Figure 53. Backscattered electron images of the alteration of the quartz in this section, this includes Fe-oxide nodules, very fine-grained, fibrous Fe-oxide, and muscovite. 54
Figure 54. Photomicrographs of two stages of quartz being altered muscovite in transmitted light, plane-polars (left) and crossed polars (right) (4x mag., F.O.V. ~3mm). 55
Figure 55. Photomicrographs of quartz being altered by a brown-orange oxide and possible pyrite or arsenopyrite that has been replaced by a greenish mineral (may be a Fe-As-oxide) in transmitted light, plane-polars (top) and crossed polars (bottom) (4x mag., F.O.V. ~3mm). 56
Figure 56. Photomicrograph of arsenopyrite, and pyrite in reflected light (10x mag., F.O.V. ~1.2mm). 57
Figure 57. Photomicrographs of quartz being altered by a brown-orange oxide in transmitted light, plane-polars (top) and crossed polars (bottom) (4x mag., F.O.V. ~3mm). 58
Figure 58. Photomicrograph of arsenopyrite, sphalerite, boulangerite and a Ca-Fe-Cu-As-Au-S-Si-O-mineral in reflected light (4x mag., F.O.V. ~3mm). 60
Figure 59. Backscattered electron image (left) and elemental map (right) of Figure 58 showing a Ca-Fe-Cu-As-Au-S-Si-O-mineral, arsenopyrite (blue), sphalerite (red), and boulangerite (pink). 60
Figure 60. Photomicrograph of arsenopyrite, sphalerite, boulangerite, bournonite, and freibergite in reflected light (4x mag., F.O.V. ~3mm). 61
Figure 61. Backscattered electron images of Figure 60 showing arsenopyrite, galena, freibergite, boulangerite and bournonite. 61
Figure 62. Photomicrograph of arsenopyrite, sphalerite, galena and a Ca-Fe-Cu-As-Au-S-Si-O-mineral in reflected light (10x mag., F.O.V. ~1.2mm). 62

Figure 63. Backscattered electron images of Figure 62 showing arsenopyrite, galena, sphalerite, and a Ca-Fe-Cu-As-S-Si-O-mineral. 62
Figure 64. Backscattered electron images of arsenopyrite, sphalerite, galena, an As-Pb-sulphide and a Fe-As-Sb-Au-Pb-sulphate. 63
Figure 65. Photomicrographs of the first and second stages of quartz in transmitted light, plane-polars (left) and crossed polars (right) (2x mag., F.O.V. ~6mm). 64
Figure 66. Photomicrographs of the second and third stages of quartz in transmitted light, plane-polars (left) and crossed polars (right) (4x mag., F.O.V. ~3mm). 65
Figure 67. Photomicrograph of arsenopyrite in reflected light (4x mag., F.O.V. ~3mm). 65
Figure 68. Photomicrographs of quartz and muscovite in the host rock in transmitted light, plane-polars (left) and crossed polars (right) (4x mag., F.O.V. ~3mm). 66
Figure 69. Photomicrographs of the quartz in the vein in transmitted light, plane-polars (left) and crossed polars (right) (4x mag., F.O.V. ~3mm) 67
Figure 70. Photomicrographs of arsenopyrite, pyrite, sphalerite and galena in reflected light (4x mag., F.O.V. ~3mm). 67
Figure 71. Photomicrographs of the quartz in the vein, muscovite, and brownish alteration in transmitted light, plane-polars (left) and crossed polars (right) (4x mag., F.O.V. ~3mm). 68
Figure 72. Photomicrographs of a relatively unaltered quartz pod in the host rock surrounded by muscovite and some very fine-grained quartz in transmitted light, plane-polars (left) and crossed polars (right) (4x mag., F.O.V. ~3mm) 69
Figure 73. Backscattered electron image of pyrite altering to a Fe-As-oxide. 69
Figure 74. Backscattered electron image of pyrargyrite, and boulangerite. 70
Figure 75. Photomicrograph of pyrite, arsenopyrite, and Ag-minerals in reflected light. 70
Figure 76. Backscattered electron images of pyrite and arsenopyrite with a small pod of freibergite and pyrargyrite. 71
Figure 77. Photomicrographs of the fine-grained quartz with opaque minerals in transmitted light, plane-polars (left) and crossed polars (right) (4x mag., F.O.V. ~3mm). 72
Figure 78. Photomicrographs of altered pyrite in the altered host rock in transmitted light, plane-polars (left) and crossed polars (right) (4x mag., F.O.V. ~3mm). 73
Figure 79. Backscattered electron image of Figure 80, showing pyrite altering to a K-Fe-sulphate and muscovite altering the quartz matrix. 73

Figure 80. Photomicrograph of galena, arsenopyrite, Pb-sulphate, and an As-Pb-sulphate in reflected light (10x mag., F.O.V. 1.2mm). 74
Figure 81. Backscattered electron image of Figure 78, showing galena, Pb-sulphate and Pb-As-sulphate. 74
Figure 82. Photomicrographs of quartz among the sulphides and a Pb-sulphate mineral in transmitted light, plane-polars (left) and crossed polars (right) (4x mag., F.O.V. ~3mm)..... 75
Figure 83. Photomicrographs of quartz with very fine-grained, recrystallized quartz in transmitted light, plane-polars (left) and crossed polars (right) (4x mag., F.O.V. ~3mm)..... 76
Figure 84. Photomicrographs of arsenopyrite, sphalerite, pyrite, and galena in reflected light (4x mag., F.O.V. ~3mm). 76
Figure 85. Backscattered electron images of arsenopyrite pyrite, galena and Pb-sulphate..... 76
Figure 86. Photomicrographs of a fine-grained quartz pod in the host rock in transmitted light, plane-polars (left) and crossed polars (right) (2x mag., F.O.V. ~6mm). 78
Figure 87. Photomicrograph of arsenopyrite and pyrite in reflected light (4x mag., F.O.V. ~3 mm). 78
Figure 88. Backscattered electron image of an As-Fe-oxide mineral replacing a sulphide mineral. 79
Figure 89. Backscattered electron image of acanthite, a Fe-As-Sb-Pb-oxide, and a Fe-As-Ag-Sb-Au-Pb-sulphate. 79
Figure 90. Photomicrographs of Fe-As-oxide grains with pods of aphanitic quartz in transmitted light, plane-polars (left) and crossed polars (right) (10x mag., F.O.V. ~1.2mm)..... 80
Figure 91. Backscattered electron image of Fe-As-oxide grains, and Fe-As-Au-Pb-sulphate..... 80
Figure 92. Photomicrographs of the Fe-As-oxide mineral symplesite (light brown to green) in transmitted light, plane-polars (left) and crossed polars (right) (4x mag., F.O.V. ~3mm)..... 81
Figure 93. Backscattered electron image of Figure 91 showing symplesite and a Fe-As-Sb-Au-Pb-oxide. 81
Figure 94. Photomicrographs of sphalerite (brown), quartz and muscovite enriched areas in transmitted light, plane-polars (left) and crossed polars (right) (2x mag., F.O.V. ~6mm)..... 82
Figure 95. Backscattered electron image (left) and electron map (right) showing pyrite, arsenopyrite, and muscovite..... 83

Figure 96. Photomicrograph of sphalerite, arsenopyrite and pyrite in reflected light (4x mag., F.O.V. ~3mm). 83
Figure 97. Photomicrographs of the host rock with quartz, and muscovite alteration in transmitted light, plane-polars (left) and crossed polars (right) (4x mag., F.O.V. ~3mm). 84
Figure 98. Photomicrographs of the cross-cutting quartz vein with ankerite at the contact between the host rock and sulphide vein in transmitted light, plane-polars (left) and crossed polars (right) (2x mag., F.O.V. ~6mm). 85
Figure 99. Photomicrograph of arsenopyrite, pyrite, and sphalerite within the sulphide vein in reflected light (4x mag., F.O.V. ~3mm). 85
Figure 100. Photomicrographs of the host rock with quartz, and areas of concentrated muscovite alteration in transmitted light, plane-polars (left) and crossed polars (right) (4x mag., F.O.V. ~3mm). 86
Figure 101. Photomicrograph of the arsenopyrite, sphalerite and galena within the vein in reflected light (4x mag., F.O.V. ~3mm). 87
Figure 102. Photomicrographs of the quartz and sphalerite within the sulphide vein, in transmitted light, plane-polars (left) and crossed polars (right) (4x mag., F.O.V. ~3mm). 89
Figure 103. Photomicrographs of the host rock in an area that is concentrated with fine-grained quartz, muscovite alteration, and little pyrite in transmitted light, plane-polars (left) and crossed polars (right) (4x mag., F.O.V. ~3mm). 89
Figure 104.Electron map (top) and backscattered electron images (bottom) of muscovite alteration (blue), pyrite, arsenopyrite, boulangerite, bournonite, and pyrargite. 90
Figure 105. Photomicrographs of sulphide mineralization within the vein in reflected light: left: arsenopyrite, pyrite, and boulangerite (10x mag., F.O.V. ~1.2mm). right: arsenopyrite, pyrite, sphalerite and boulangerite (4x mag., F.O.V. ~3mm). 91
Figure 106.Backscattered electron image (left) and electron map (right) of arsenopyrite, sphalerite, pyrite, and boulangerite. 91
Figure 107. Photomicrographs of the dominant aphanitic rock and a local pod of very fine-grained quartz in transmitted light, plane-polars (left) and crossed polars (right) (2x mag., F.O.V. ~6mm). 92
Figure 108. Photomicrograph of pyrite, in reflected light (4x mag., F.O.V. ~3mm). 93
Figure 109. Backscattered electron image of pyrite and arsenopyrite. 93

Figure 110. Photomicrographs of three areas within the section showing different degrees of alteration and the preferential occurrence of pyrite or arsenopyrite within these units, in transmitted light, plane-polars (left) and crossed polars (right) (2x mag., F.O.V. ~6mm)..... 94
Figure 111. Photomicrographs of two areas within the section that show different degrees of alteration and the preferential occurrence of pyrite or arsenopyrite, in transmitted light, plane-polars (left) and crossed polars (right) (2x mag., F.O.V. ~6mm). 95
Figure 112. Photomicrograph of arsenopyrite in one unit and pyrite in another, in reflected light (4x mag., F.O.V. ~3mm)..... 95
Figure 113. Photomicrographs of the quartz vein and fracture, in transmitted light, plane-polars (left) and crossed polars (right) (4x mag., F.O.V. ~3mm). 96
Figure 114. Photomicrograph of arsenopyrite, sphalerite, galena and a Sb-sulphosalt, in reflected light (4x mag., F.O.V. ~3mm). 97
Figure 115. Photomicrographs of quartz infilling around sphalerite, in transmitted light, plane-polars (left) and crossed polars (right) (4x mag., F.O.V. ~3mm). 98
Figure 116. Photomicrographs in reflected light of: (left) sphalerite, arsenopyrite, and galena (4x mag., F.O.V. ~3mm); (right) sphalerite with small inclusions of pyrite (10x mag., F.O.V. ~1.2mm)..... 99
Figure 117. Photomicrographs of quartz, with local grains that are partially recrystallized, and sphalerite, in transmitted light, plane-polars (left) and crossed polars (right) (4x mag., F.O.V. ~3mm). 100
Figure 118. Photomicrograph of sphalerite, pyrite, arsenopyrite, and galena, in reflected light (4x mag., F.O.V. ~3mm). 101
Figure 119. Polished section scan of MIN-01A..... 108
Figure 120. Polished section scan of MIN-01B. 109
Figure 121. Polished section scan of MIN-02. 110
Figure 122. Polished section scan of MIN-03A..... 111
Figure 123. Polished section scan of MIN-03B. 112
Figure 124. Polished section scan of MIN-04. 113
Figure 125. Polished section scan of MIN-05A..... 114
Figure 126. Polished section scan of MIN-05B. 115
Figure 127. Polished section scan of MIN-06. 116

Figure 128. Polished section scan of MIN-07. 117
Figure 129. Polished section scan of MIN-08A. 118
Figure 130. Polished section scan of MIN-08B. 119
Figure 131. Polished section scan of MIN-09 120
Figure 132. Polished section scan of MIN-10. 121
Figure 133. Polished section scan of MIN-11. 122
Figure 134. Polished section scan of MIN-12 123
Figure 135. Polished section scan of MIN-13. 124
Figure 136. Polished section scan of MIN-14. 125
Figure 137. Polished section scan of MIN-15. 126
Figure 138. Polished section scan of MIN-16. 127
Figure 139. Polished section scan of MIN-17. 128
Figure 140. Polished section scan of MIN-18. 129
Figure 141. Polished section scan of MIN-19. 130
Figure 142. Polished section scan of MIN-20. 131
Figure 143. Polished section scan of MIN-21. 132
Figure 144. Polished section scan of MIN-22. 133
Figure 145. Polished section scan of MIN-23. 134
Figure 146. Polished section scan of MIN-24A. 135
Figure 147. Polished section scan of MIN-24B. 136
Figure 148. Polished section scan of MIN-25. 137
Figure 149. Polished section scan of MIN-26. 138
Figure 150. Polished section scan of MIN-27. 139
Figure 151. Polished section scan of MIN-28. 140
Figure 152. Polished section scan of MIN-29. 141
Figure 153. EDX spectrum of quartz. 143
Figure 154. EDX spectrum of calcite. 143
Figure 155. EDX spectrum of ankerite. 144
Figure 156. EDX spectrum of dolomite with a small Fe peak. 144
Figure 157. EDX spectrum of dolomite with no Fe peak. 145
Figure 158. EDX spectrum of muscovite. 145

Figure 159. EDX spectrum of pyrite. 146
Figure 160. EDX spectrum of arsenopyrite. 146
Figure 161. EDX spectrum of arsenopyrite with a possible, very small, Au peak. 147
Figure 162. EDX spectrum of chalcopyrite. 147
Figure 163. EDX spectrum of sphalerite. 148
Figure 164. EDX spectrum of galena. 148
Figure 165. EDX spectrum of stibnite. 149
Figure 166. EDX spectrum of boulangerite. 149
Figure 167. EDX spectrum of bournonite. 150
Figure 168. EDX spectrum of freibergite. 150
Figure 169. EDX spectrum of pyrargrite with small Pb peak. 151
Figure 170. Spectrum of an As-Pb-sulphide. 151
Figure 171. Spectrum of a Fe-oxide. 152
Figure 172. Spectrum of a Fe-As-oxide with a potential small Au peak. 152
Figure 173. Spectrum of a Pb-oxide. 153
Figure 174. Spectrum of an As-Pb-oxide. 153
Figure 175. Spectrum of a Fe-As-Sb-Au-Pb-oxide. 154
Figure 176. Spectrum of a Fe-As-Ag-Sb-Au-Pb-oxide. 154
Figure 177. Spectrum of a K-Fe-sulphate. 155
Figure 178. Spectrum of a Fe-As-Sb-Au-Pb-sulphate. 155
Figure 179. Spectrum of a Ca-Fe-Cu-As-Au-S-silicate. 156
Figure 180. Spectrum of apatite. 156
Figure 181. Spectrum of monazite-(Ce) 157

Table of Tables

Table 1. Name, abbreviation, and formula of the minerals described in the following descriptions. 16

1. Objectives

The objective of this report is to present mineralogical data. Particular attention was focused on the identities of mineralogical phases hosting high contents of Au, Ag, Cu, and Sb, as well as the abundances, textures, and paragenetic relationships of these phases.

2. Experimental Methods

Twenty-nine rock samples were obtained from Ansell Capital, and 34 areas for polished sections were picked by the author. The samples were sent to Vancouver Petrographics to be prepared for polished section. The polished sections were then scanned using a Nikon slide scanner, and high resolution images in plane-polarized and cross-polarized light were obtained. These scans were used as navigational maps when utilizing the microscopes. Optical petrography was conducted using the authors Olympus CX-31P petrographic microscope (transmitted and reflected light with camera capability). The Phillips XL30 scanning electron microscope (SEM) at the University of British Columbia, equipped with an energy-dispersion X-ray spectrometer, was utilized for more detailed mineralogical investigation on selected polished section. The 18 selected polished sections were carbon coated prior to observation with the SEM. Detailed investigation consisted of backscattered electron (BSE) images and energy-dispersive X-ray spectra (EDX). During SEM analysis, a beam spot size of 6 μm was used with an excitation

3. Mineralogical Results

Thirty-four polished sections were studied via the methods described above. All percentages are estimates approximated by eye, and every attempt was made to remain consistent throughout the sections. Where possible IUGS recommended mineral abbreviations were used. Appendix A shows the section scans in plane polarized and cross polarized light.

Several sulphide, sulphosalt, sulphate and oxide phases related to Ag and Au mineralization were identified. Some of these phases could not be identified as a known mineral. Appendix B shows the EDX spectra of the minerals analyzed using energy dispersive X-ray spectrometry. There is a large variety of sulphosalt minerals and many of these minerals have a similar chemistry and are difficult to distinguish using petrography, and EDX spectra. The minerals identified in this report are the most commonly identified minerals with the chemistry determined, but it is possible that further advanced analysis may yield a different mineral with the same chemistry. However, for exploration and metallurgy purposes this exact identification may not be necessary as the overall chemistry stays the same.

	Mineral Name	Abbreviation	Formula
Rock Forming Minerals	quartz	qtz	SiO_2
	calcite	cal	$CaCO_3$
	ankerite	ank	$Ca(Fe, Mg, Mn)(CO_3)_2$
	dolomite	dol	$CaMg(CO_3)_2$
	muscovite	ms	$KAl_2(AlSi_3O_{10})(OH)_2$
Sulphide and Sulphosalt Minerals	acanthite	acan	Ag_2S
	arsenopyrite	apy	FeAsS
	boulangerite	boul	$Pb_5Sb_4S_{11}$
	bournonite	bour	$CuPbSbS_3$
	chalcopyrite	ccp	$CuFeS_2$
	freibergite	frei	$Ag_6(Cu_4Fe_2)Sb_4S_{13-x}$
	galena	gn	PbS
	pyrargyrite	pyra	Ag3SbS3
	pyrite	py	FeS_2
	sphalerite	sp	ZnS
	stibnite	stib	Sb_2S_3

Table 1. Name, abbreviation, and formula of the minerals described in the following descriptions.

MIN-001A

This section contains approximately 54% quartz, 45% opaque minerals, and 1% carbonate minerals. The opaque minerals include approximately 35% pyrite, 7% sphalerite, 2% galena, and 1% arsenopyrite.

The quartz occurs as fine- to medium-grained, anhedral to subhedral crystals. The grain size of the quartz commonly decreases closer to the sulphide minerals. Locally the quartz appears to have recrystallized rims (Fig. 1). The carbonate minerals are very fine-grained dolomite and ankerite (Fig. 3). Backscattered electron images show that the dolomite is mottled, representing changes in Fe content, and ankerite rimming the dolomite.

Sulphide minerals are mostly found in a large aggregate on one side of the polished section, with a few grains throughout the rest. They are found as fine- to medium-grained, generally anhedral crystals (Fig. 2 and 4). The exception is arsenopyrite, which is subhedral to euhedral. Sphalerite is reddish-brown and has a small Fe-peak on EDX.



Figure 1. Photomicrographs of the quartz matrix with some grains showing recrystallized rims in transmitted light, plane-polars (left) and crossed polars (right) (4x mag., F.O.V. ~3 mm).

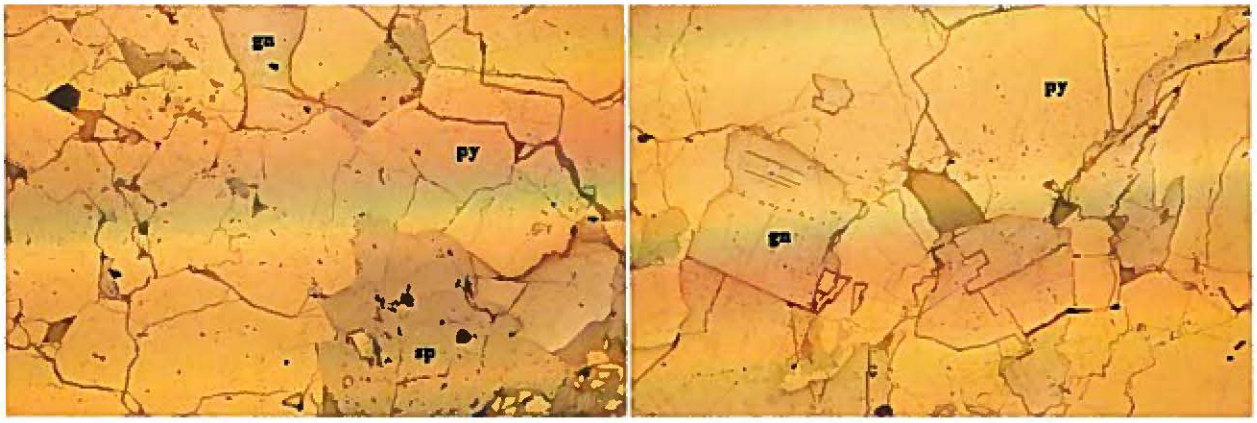


Figure 2. Photomicrographs of the sulphide mineralization in reflected light (4x mag., F.O.V. ~3mm).

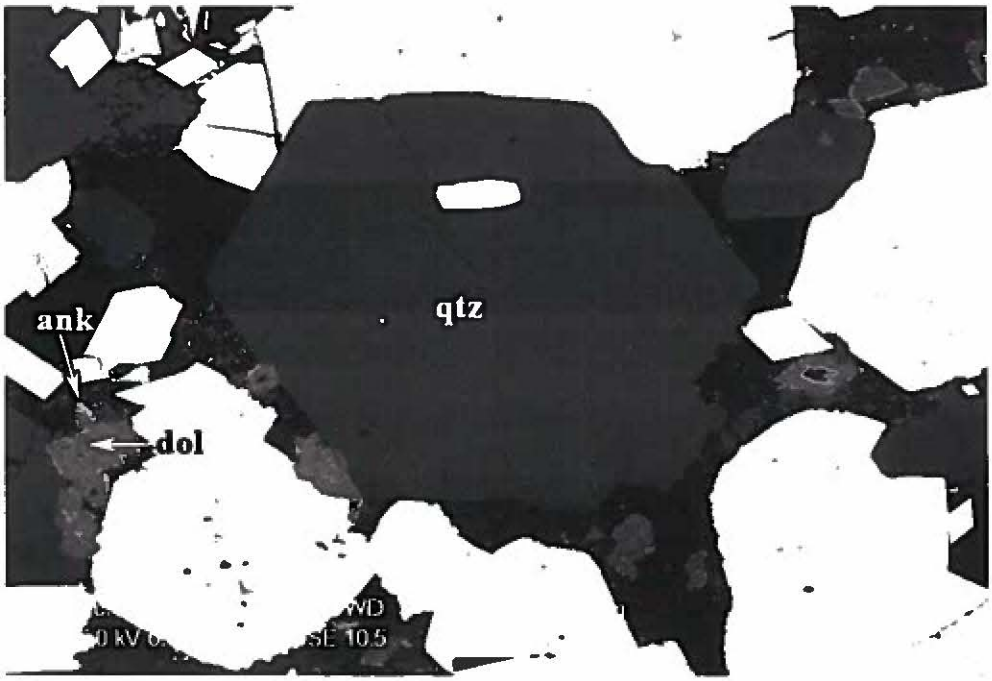


Figure 3. Backscattered electron image of quartz, and carbonate mineralization.

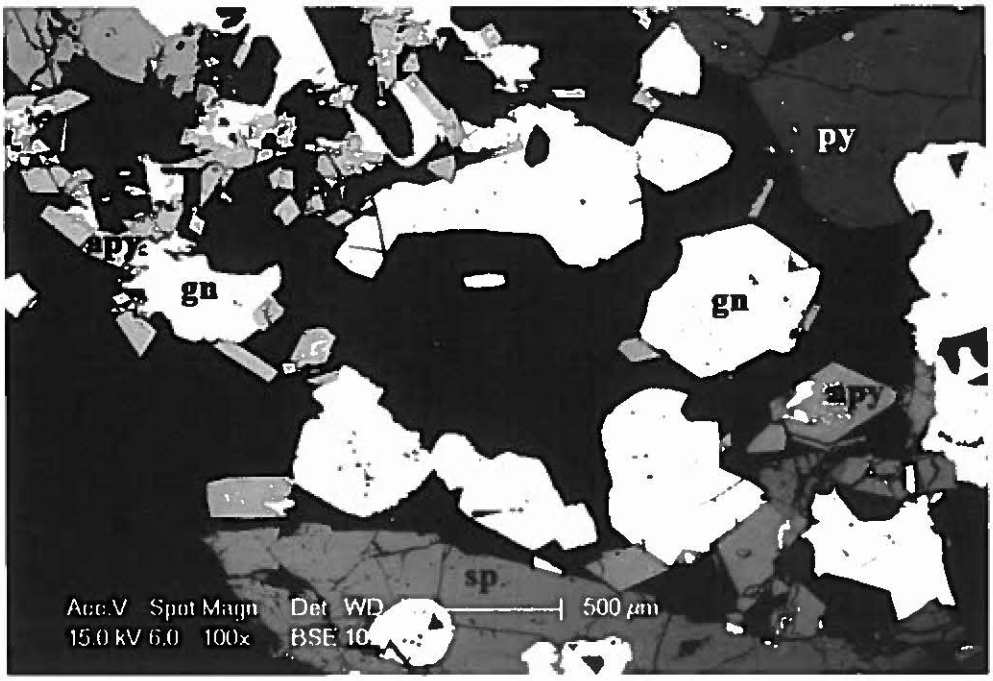


Figure 4. Backscattered electron image of arsenopyrite, sphalerite and galena.

MIN-001B

This section contains approximately 70% quartz and 30% opaque minerals. The opaque minerals include 23% pyrite, 4% Sb-sulphosalts (freibergite, and bournonite), 2% sphalerite, 1% galena, and trace arsenopyrite.

The quartz occurs as fine- to medium-grained, anhedral to subhedral crystals. The grain size of the quartz commonly decreases closer to the sulphide minerals. Locally, the quartz appears to have recrystallized rims (Fig. 5).

Sulphide and sulphosalt minerals are generally found in small aggregates (Fig. 6). Pyrite occurs as fine- to medium- grained subhedral to anhedral crystals. Arsenopyrite occurs locally as very fine-grained, euhedral to subhedral crystals. Sphalerite is fine- to medium-grained, anhedral, reddish-brown crystals and has a small Fe-peak on EDX. The sulphosalts are fine- to very fine-grained, anhedral crystals (Fig. 7 and 8). Galena is commonly associated with the bournonite, and occurs as very fine-grained anhedral crystals amongst larger, anhedral bournonite crystals. Freibergite has a few very fine-grained bournonite crystals at its crystal edges. These sulphosalts were not able to be distinguished in reflected light (Fig. 7).

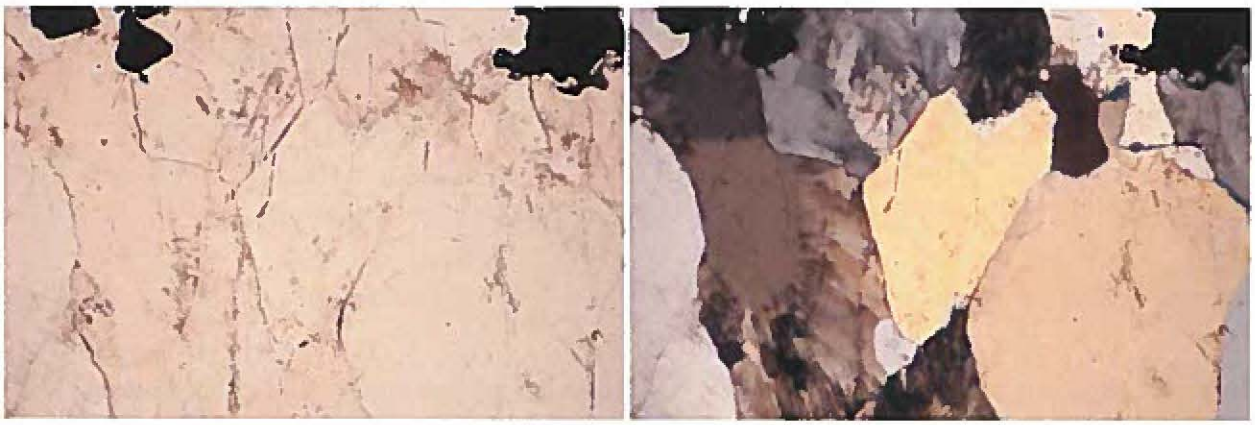


Figure 5. Photomicrographs of the quartz matrix with some grains showing recrystallized rims in transmitted light, plane-polars (left) and crossed polars (right) (4x mag., F.O.V. ~3 mm).

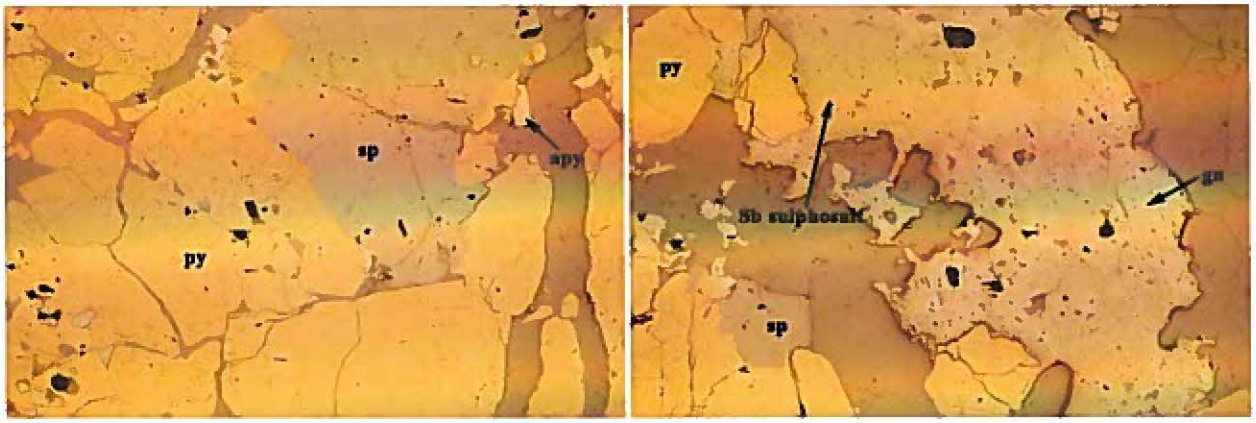


Figure 6. Photomicrographs of the sulphide mineralization in reflected light (4x mag., F.O.V. ~3mm).

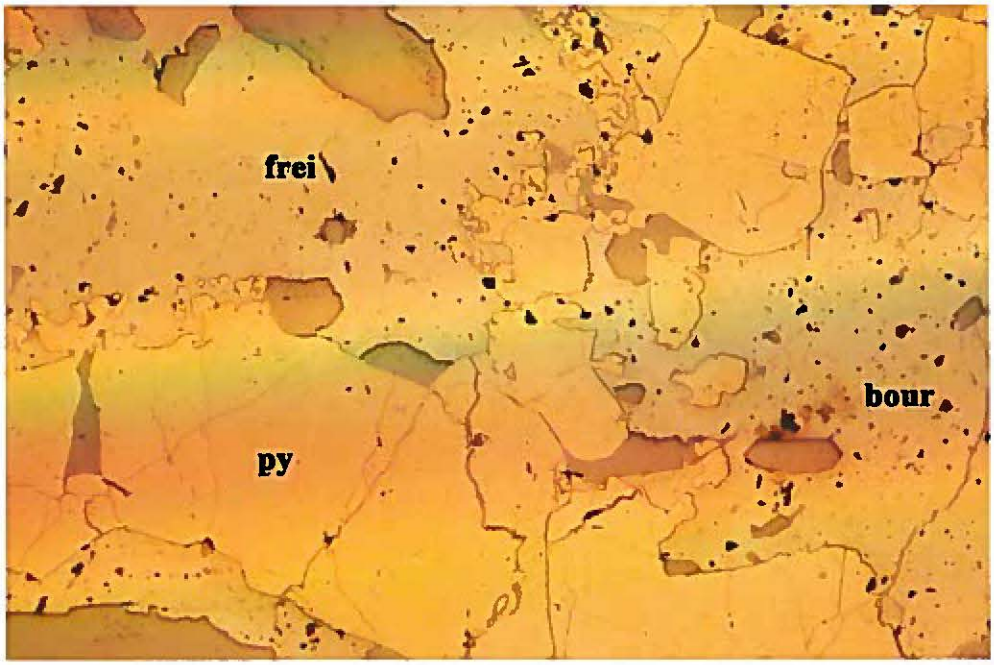


Figure 7. Photomicrograph of freibergite, bournonite, and pyrite in reflected light (4x mag., F.O.V. ~3mm).

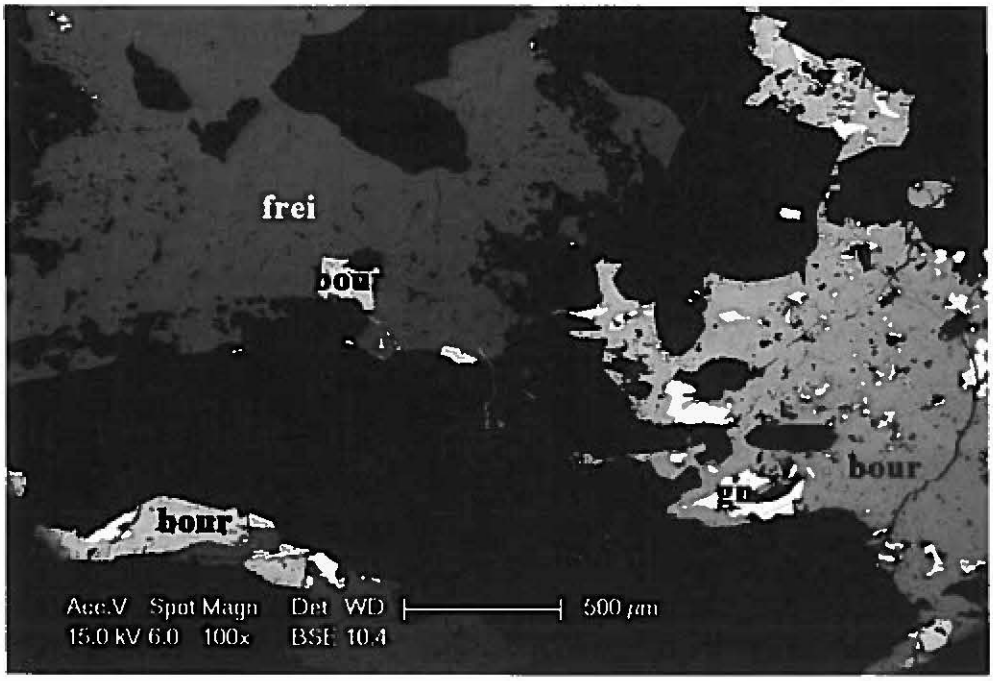


Figure 8. Backscattered electron image of Figure 7, showing freibergite, bournonite, and galena.

MIN-002

This section contains approximately 60% quartz, and 40% opaque minerals. The opaque minerals include approximately 25% arsenopyrite, 7% galena, 5% Sb-sulphosalts (freibergite, boulangerite, and bournonite), 3% sphalerite, and trace chalcopyrite, and pyrite. Distinguishing between the galena and sulphosalt minerals in reflected light can be difficult as the minerals are fine-grained, and occur together. Generally, galena does not appear as altered so it has a fresher looking surface, and locally cleavage planes are observed.

The quartz occurs as fine- to medium-grained, subhedral to euhedral crystals (Fig. 9). Commonly the quartz has recrystallized rims.

Sulphide and sulphosalt minerals are found together, but the sulphosalts appear to be more closely associated with galena. Sphalerite has anhedral, reddish-brown crystals and has a small Fe-peak on EDX (Fig. 9 and 10). The arsenopyrite occurs as fine- to very fine-grained, subhedral to euhedral crystals (Fig. 11, 13, and 14)). Chalcopyrite and pyrite are very fine-grained, and occur locally (Fig. 10). Galena consists of very fine-grained, subhedral crystals. Boulangerite consists of very fine-grained, subhedral to euhedral crystals that form in areas together with galena (Fig. 11, 12, 14 and 15). Locally, you can see boulangerite forming acicular crystals (Fig. 12). Bournonite was observed as very fine-grained crystals associated with boulangerite, and galena (Fig. 15). Freibergite occurs locally as very-fine grained, anhedral crystals, associated with galena (Fig. 13).

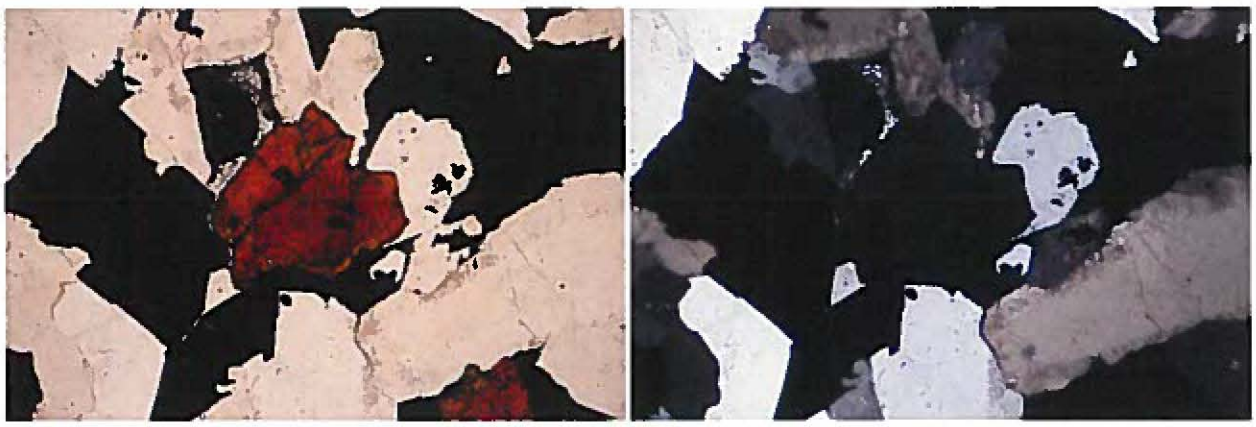


Figure 9. Photomicrographs of the quartz matrix with some grains showing recrystallized rims in transmitted light, plane-polars (left) and crossed polars (right) (4x mag., F.O.V. ~3 mm).

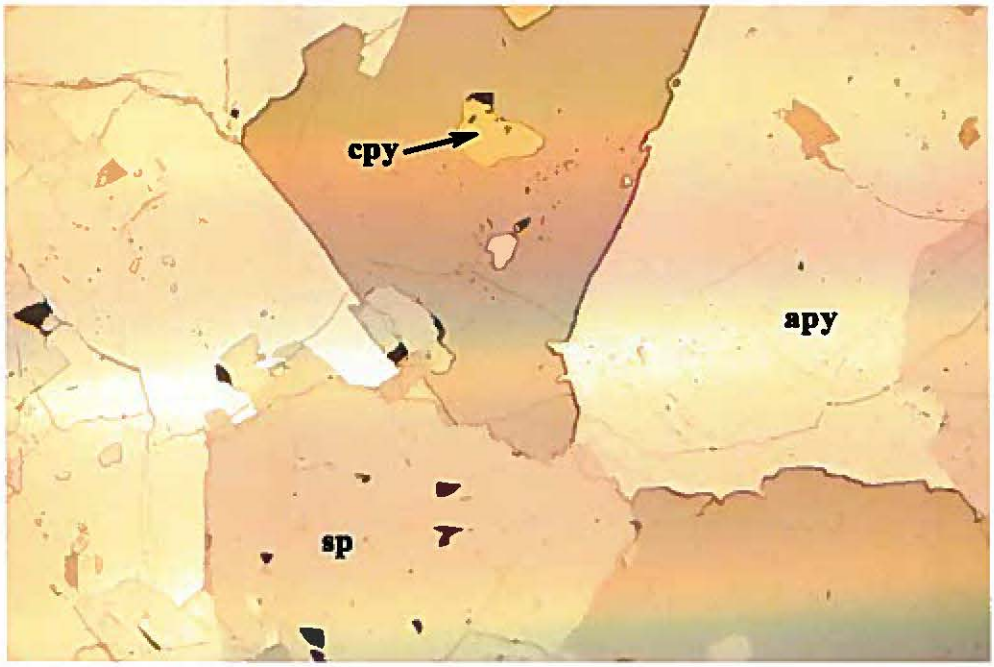


Figure 10. Photomicrograph of arsenopyrite, sphalerite and chalcopyrite in reflected light (4x mag., F.O.V. ~3mm).

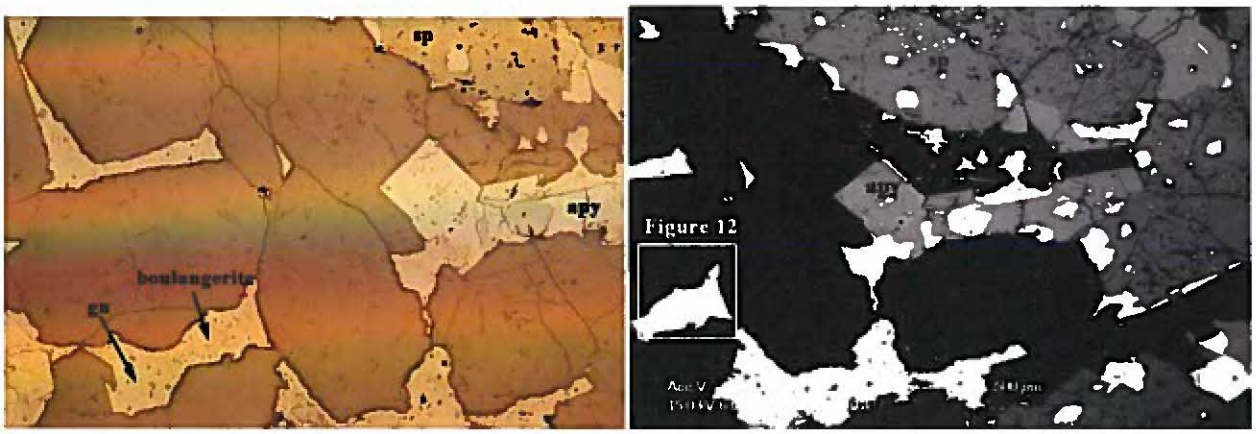


Figure 11. Photomicrograph in reflected light (4x mag., F.O.V. ~3mm) (left), and backscattered electron image (right) of arsenopyrite, sphalerite, galena, and boulangerite.

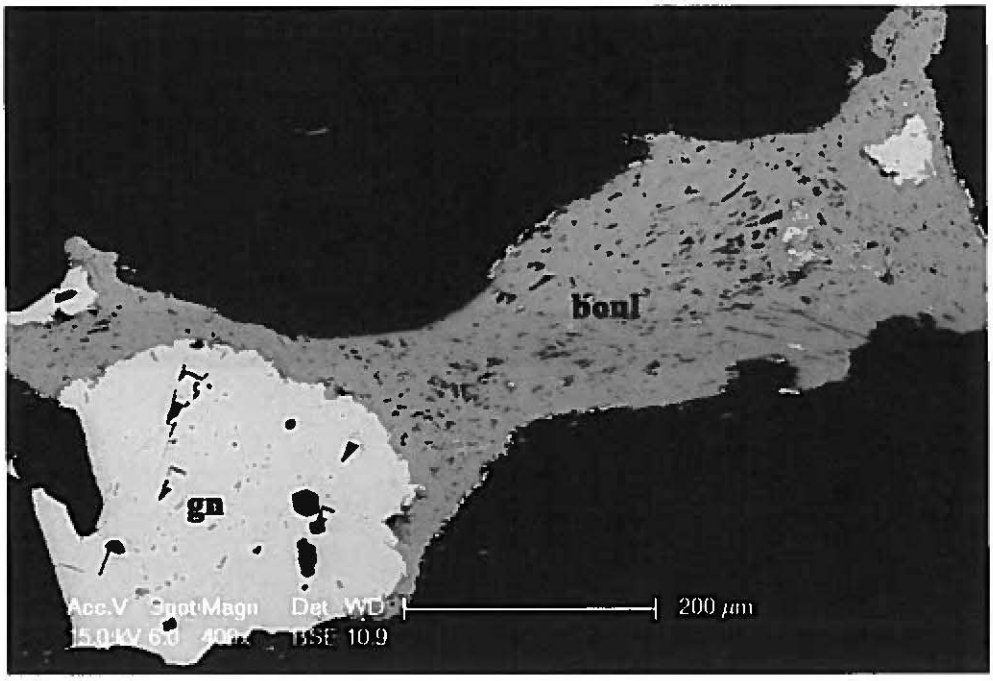


Figure 12. Backscattered electron image of galena and boulangerite.

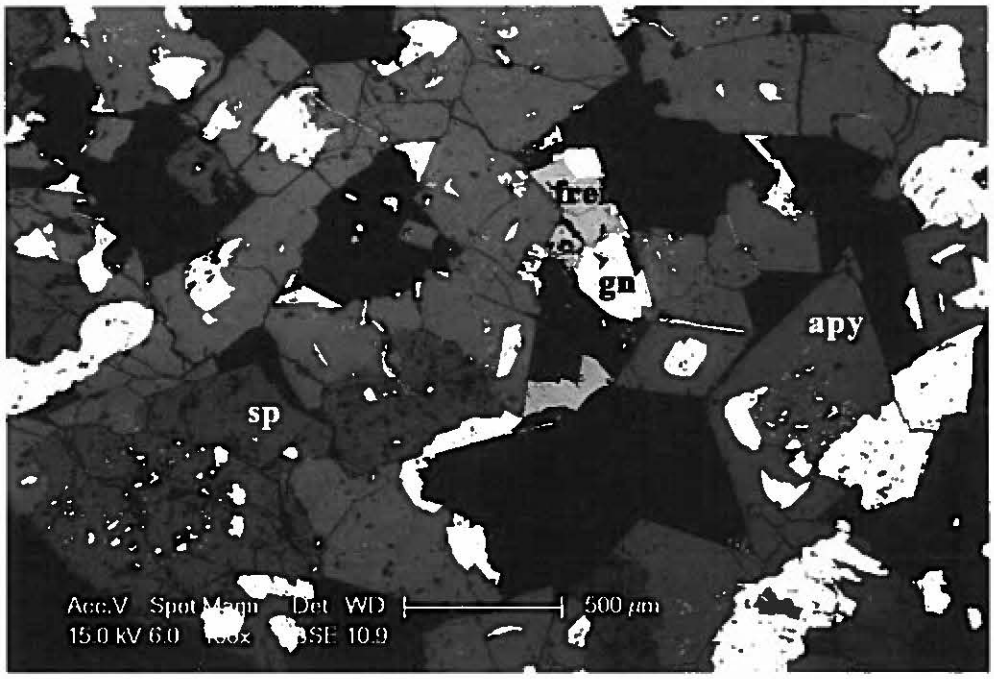


Figure 13. Backscattered electron image of arsenopyrite, sphalerite, galena and freibergite. Arsenopyrite is possibly being replaced by galena.

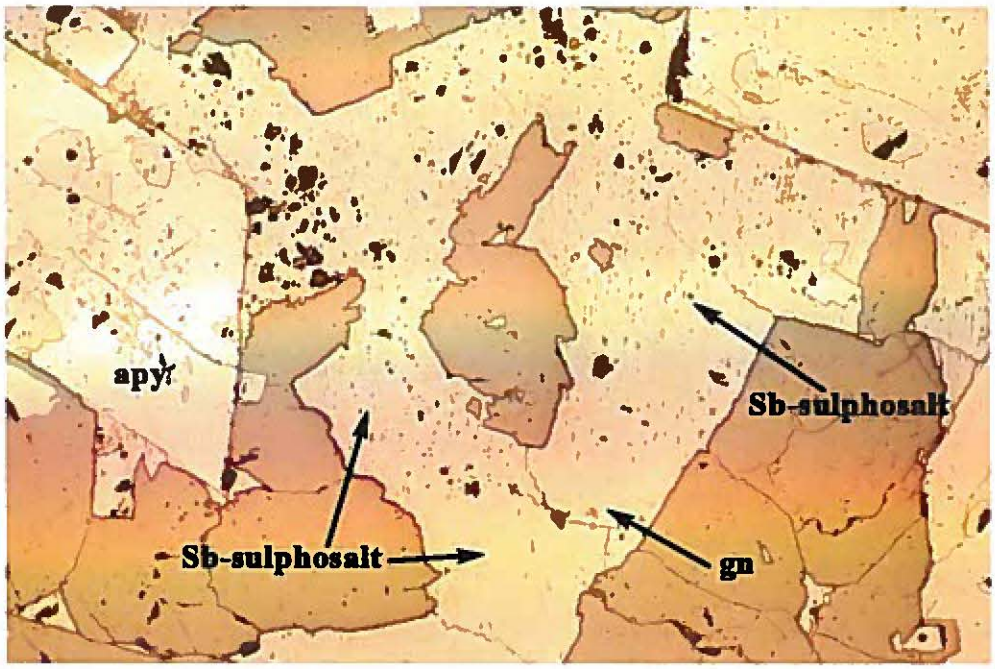


Figure 14. Photomicrograph of arsenopyrite, galena, and Sb-sulphosalt minerals in reflected light (4x mag., F.O.V. ~3mm).

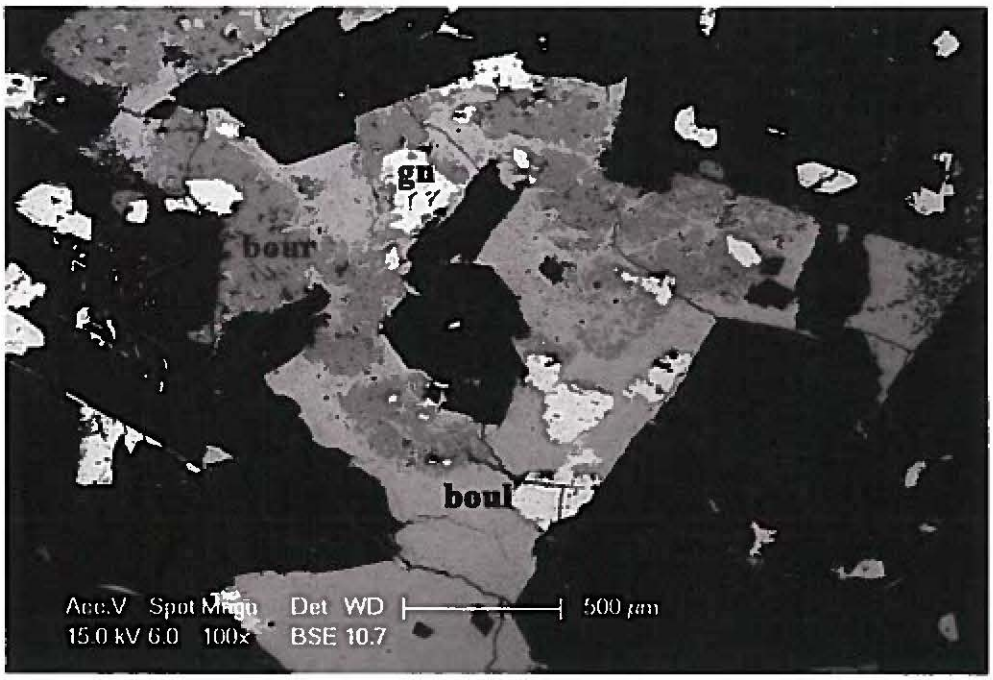


Figure 15. Backscattered electron image of Figure 14 showing the Sb-sulphosalts bournonite and boulangerite.

MIN-003A

This section contains approximately 85% quartz, 12% muscovite, 1.5% pyrite, 1% dolomite, and 0.5% sphalerite.

The quartz ranges in grain size from aphanitic to very fine-grained, with a local coarse-grained crystal. The quartz is locally recrystallized. There are local pods of very fine-grained ankerite (Fig. 16). Alteration is caused by muscovite, which varies locally in concentration.

Pyrite mineralization is fine- to very fine-grained, subhedral to anhedral crystals (Fig. 17). Sphalerite occurs locally as fine- to medium-grained, anhedral crystals.

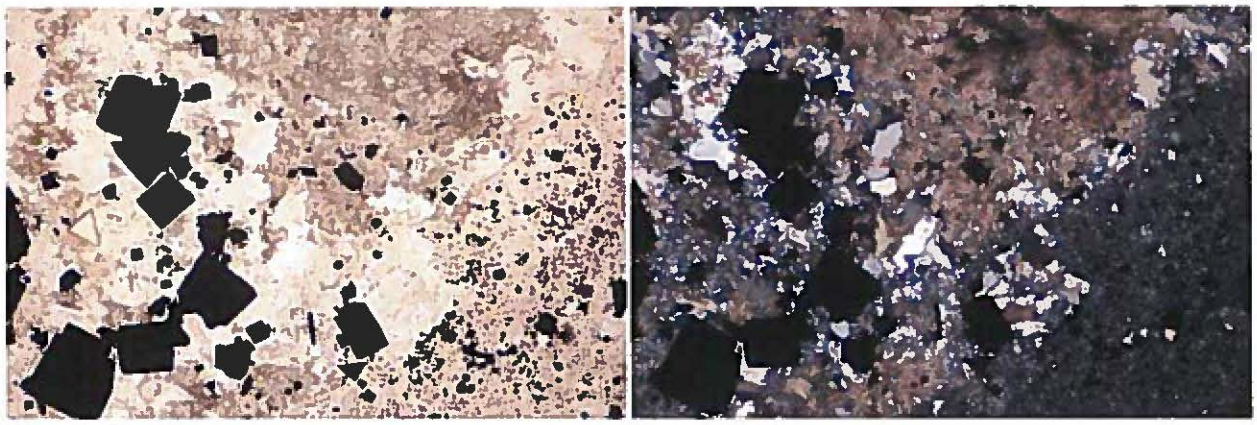


Figure 16. Photomicrographs of the quartz matrix, muscovite alteration, and ankerite in transmitted light, plane-polars (left) and crossed polars (right) (4x mag., F.O.V. ~3 mm).

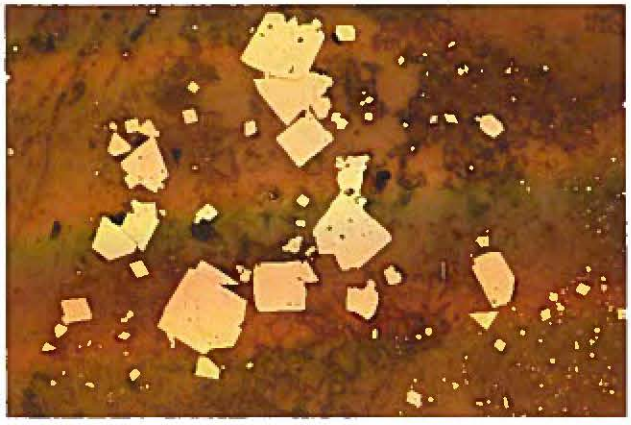


Figure 17. Photomicrograph of pyrite in reflected light (4x mag., F.O.V. ~3mm).

MIN-003B

This section consists of approximately 60% quartz, 39% alteration zones and 1% opaque minerals. Opaque minerals include approximately 1% pyrite and trace sphalerite, arsenopyrite, and galena.

The quartz is very fine- to fine-grained, anhedral crystals, likely caused by alteration. The aphanitic alteration appears to be composed of quartz, muscovite, and local carbonate. It is observed cross-cutting through the quartz (Fig. 18). Muscovite is the dominant alteration mineral.

Pyrite is found as very fine- to fine-grained, euhedral crystals disseminated throughout the section (Fig. 19). Local clusters of arsenopyrite, sphalerite and galena also occur. The arsenopyrite is fine-grained and euhedral. The sphalerite is anhedral and has very small inclusions of pyrite in the crystal (Fig. 19). Galena is very fine-grained.

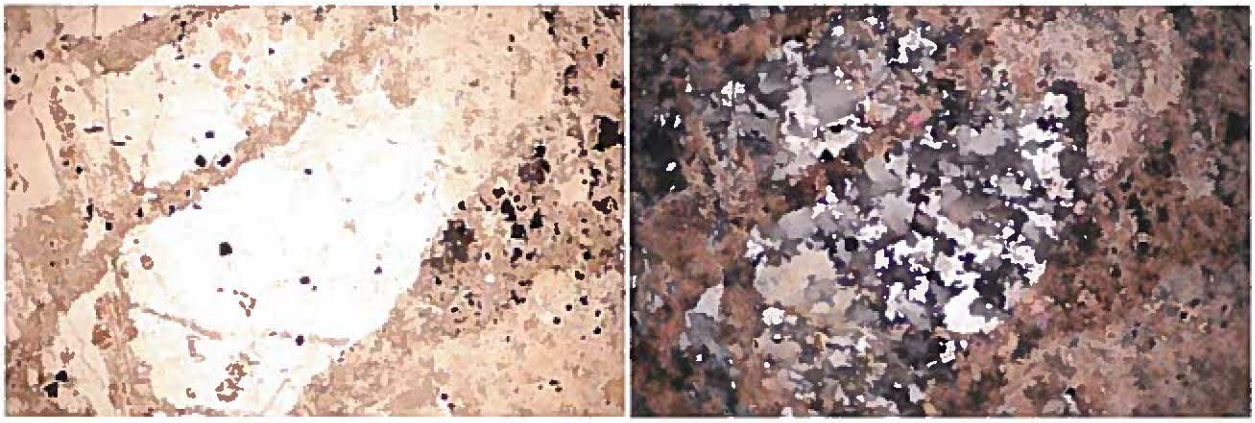


Figure 18. Photomicrographs of the quartz matrix, and muscovite alteration in transmitted light, plane-polars (left) and crossed polars (right) (2x mag., F.O.V. ~6 mm).

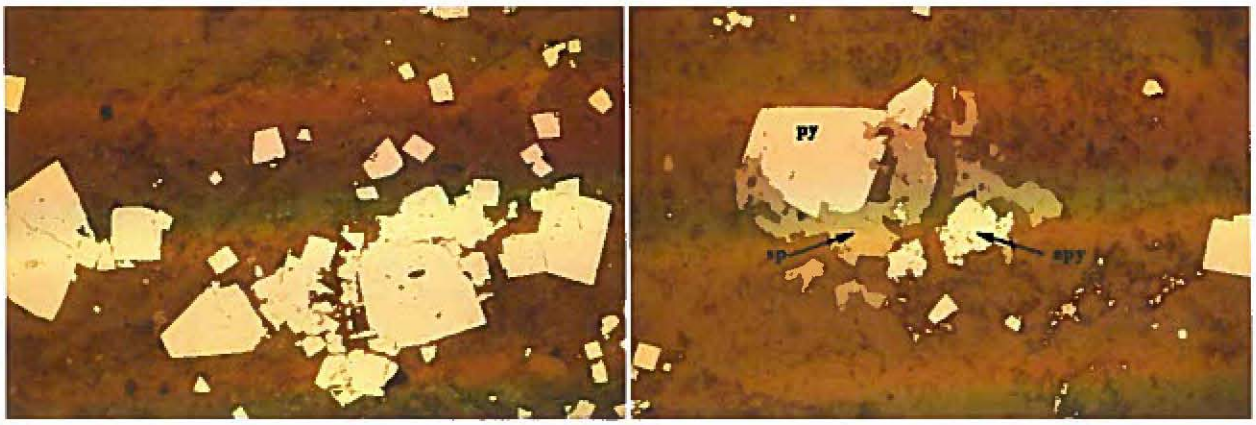


Figure 19. Photomicrographs of pyrite (left) and pyrite, sphalerite, and arsenopyrite (right) in reflected light (4x mag., F.O.V. ~3mm).

MIN-004

This section consists of approximately 75% opaque minerals, 17% carbonate, and 8% quartz. The opaque minerals include approximately 69% arsenopyrite, 3% pyrite, 2% sphalerite, and 1% galena.

The quartz is fine-grained, anhedral crystals (Figs. 20 to 22). There are three phases of carbonate mineralization. The first is very fine-grained dolomite, and it forms in the center of the second carbonate phase which is ankerite. The ankerite is very fine-grained to fine-grained and forms the rest of the vein (Fig. 20 and 21). The third phase is fine- to medium-grained calcite, and it generally rims the areas of quartz, and locally infill's through the opaque minerals (Figs. 20 to 22).

The sulphide minerals form as large aggregates with each other (Fig. 23 and 24). Sphalerite is a reddish-brown in colour, forms fine-grained, anhedral crystals, and has a small Fe-peak on EDX. Arsenopyrite is fine-grained, subhedral to euhedral crystals and forms large masses. Galena forms fine-grained, euhedral crystals. Pyrite occurs locally as fine-grained, subhedral crystals.

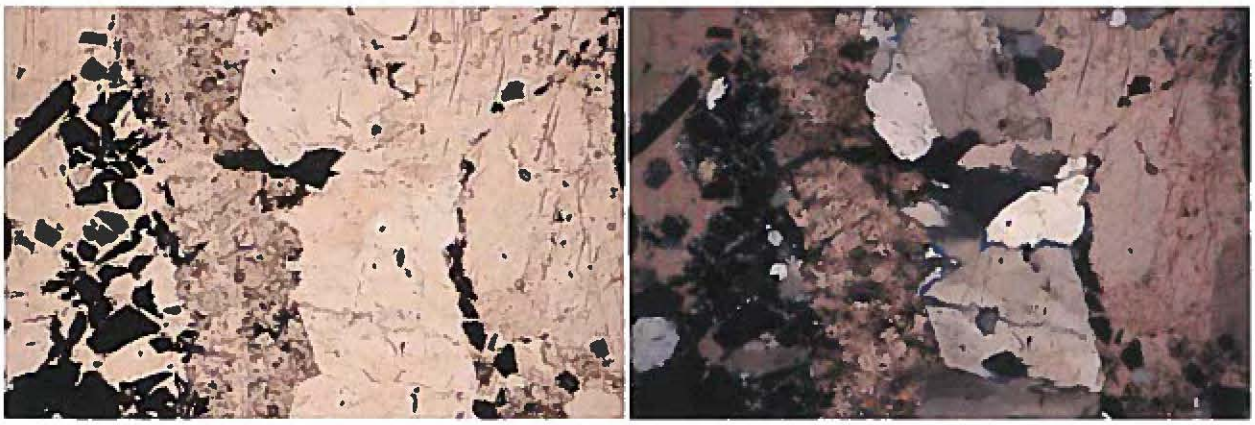


Figure 20. Photomicrographs of the quartz matrix, calcite, ankerite, and dolomite in transmitted light, plane-polars (left) and crossed polars (right) (4x mag., F.O.V. ~3 mm).

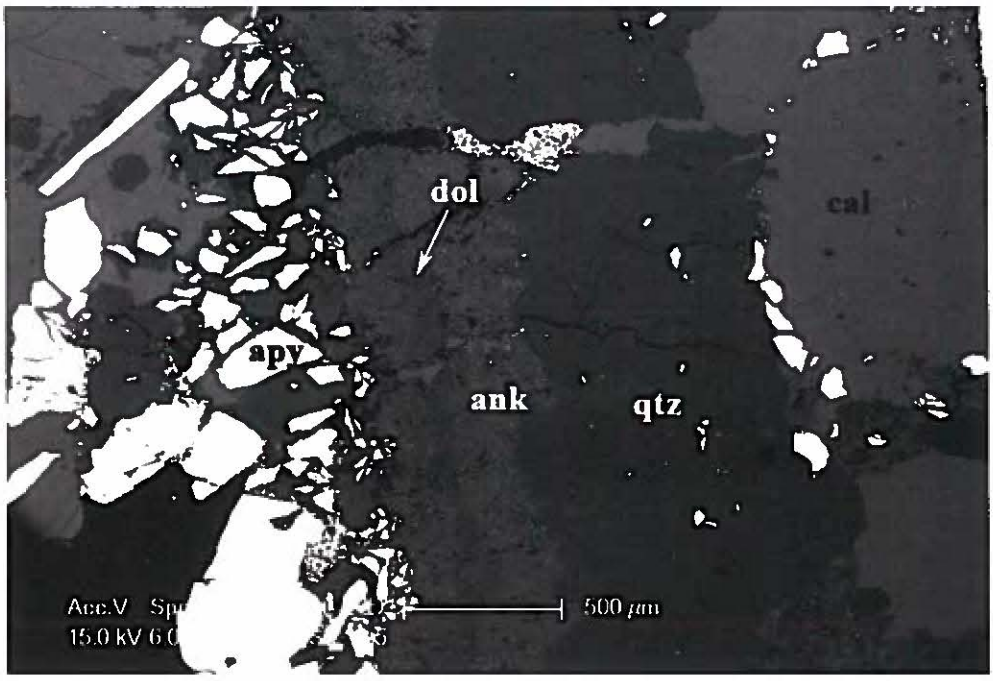


Figure 21. Backscattered electron image of Figure 21, showing quartz, calcite, ankerite, dolomite and arsenopyrite.



Figure 22. Photomicrographs of the quartz matrix, calcite, and ankerite in transmitted light, plane-polars (left) and crossed polars (right) (4x mag., F.O.V. ~3 mm).

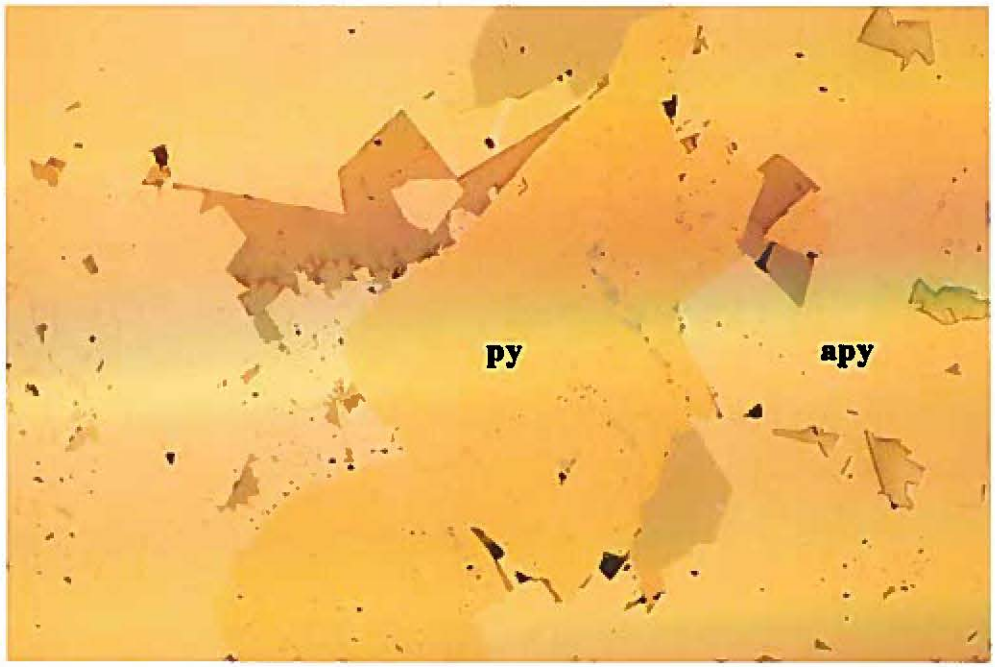


Figure 23. Photomicrograph of pyrite, and arsenopyrite in reflected light (4x mag., F.O.V. ~3mm).

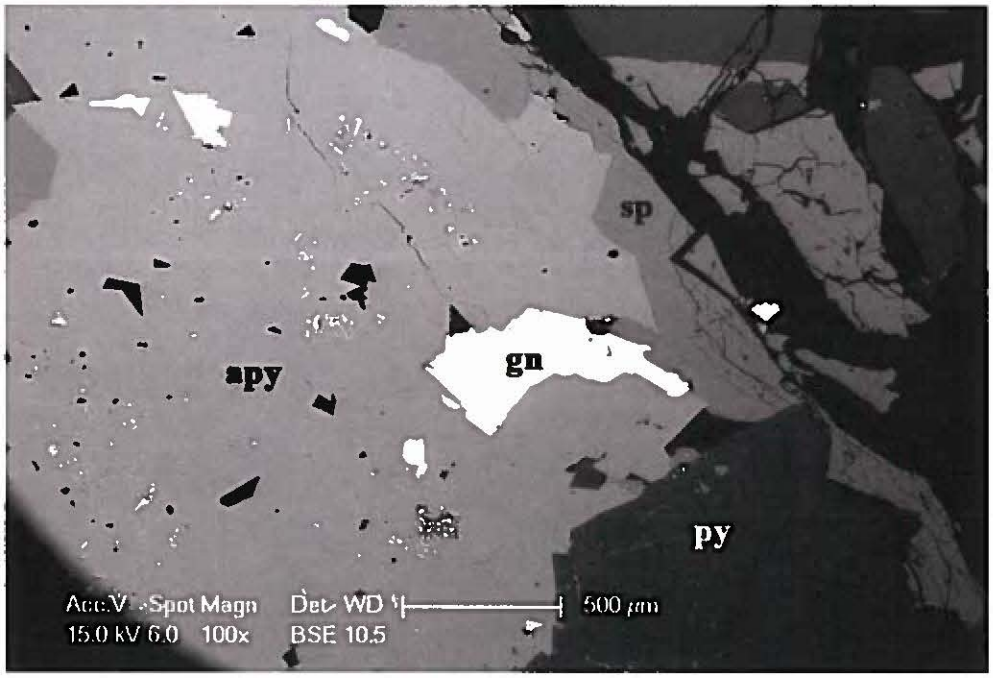


Figure 24. Backscattered electron image of arsenopyrite, pyrite, galena and sphalerite.

MIN-005A

This section consists of approximately 50% quartz, 49% alteration with the remaining 1% as void space and altered pyrite.

The quartz is very fine-grained to fine grained, anhedral crystals. Locally the quartz appears to be recrystallized to a nearly aphanitic grain size. The alteration consists of an opaque mineral, and muscovite with quartz (Fig. 25 and 26). The majority of the alteration minerals are generally aphanitic, but locally very fine-grained muscovite is observed. The pyrite is fine-grained, and generally replaced (Fig. 26).

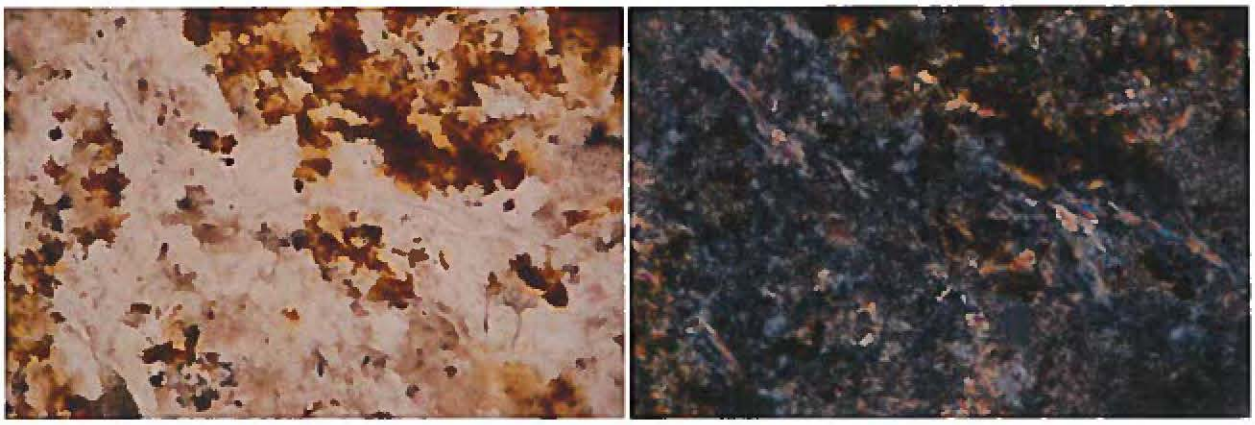


Figure 25. Photomicrographs of the quartz matrix, muscovite, and Fe-oxide in transmitted light, plane-polars (left) and crossed polars (right) (20x mag., F.O.V. ~0.6 mm).

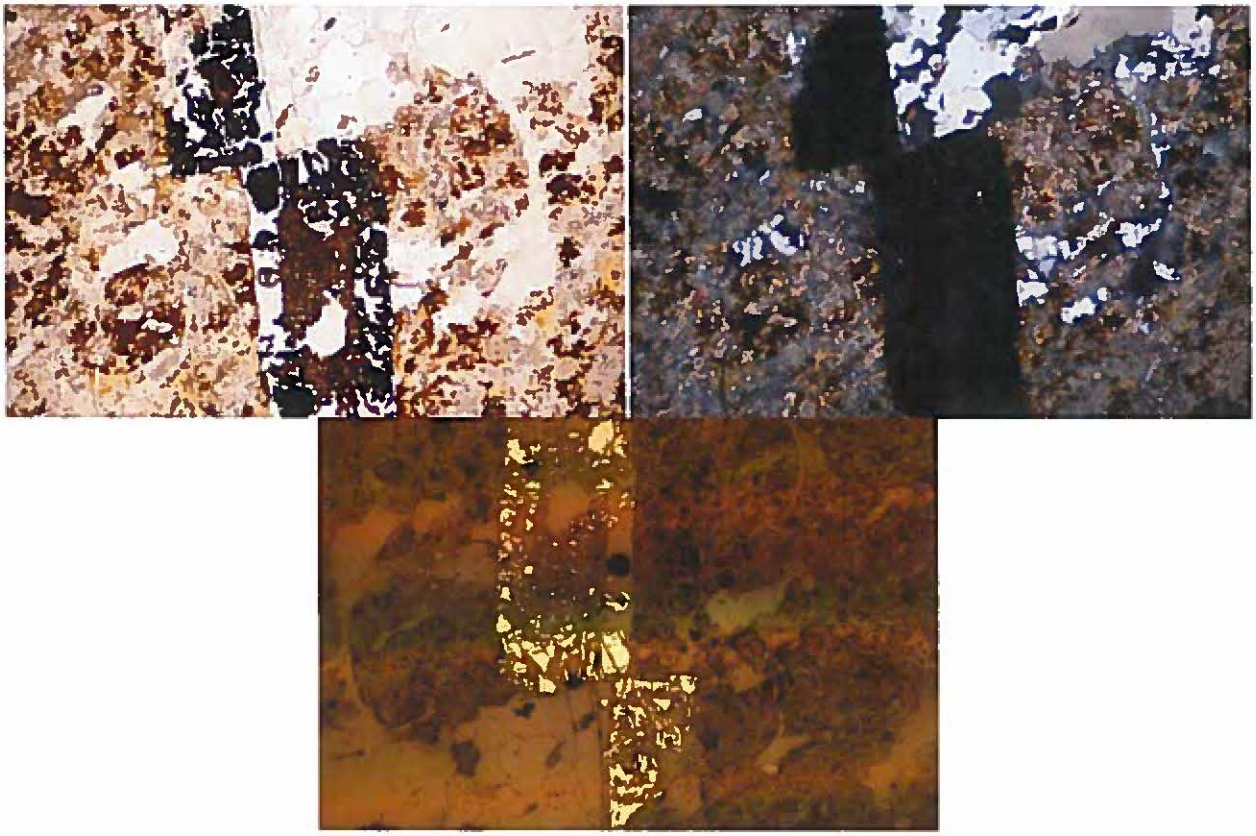


Figure 26. Photomicrographs of the quartz matrix, muscovite, and Fe-oxide replacing pyrite in transmitted light (plane-polars (left), crossed polars (right)), and reflected light (bottom) (4x mag., F.O.V. ~3 mm).

MIN-005B

This section consists of approximately 65% quartz, 34% alteration with the remaining 1% as altered pyrite.

The quartz is very fine-grained to fine grained, anhedral crystals (Fig. 27). Locally the quartz is aphanitic, and these areas were confirmed with BSE imaging and EDX spectra. The alteration consists of oxide and clay minerals with quartz. The majority of the alteration minerals are generally aphanitic, and could only be confirmed through the use of EDX spectra. The alteration was found to consist of a K-Fe-sulphate and muscovite (Fig. 27 and 28). Locally the muscovite was very fine-grained rather than aphanitic, and it is the most prominent of the alteration minerals. Pyrite was very fine-grained to locally fine-grained, and was being replaced by the K-Fe-sulphate (Fig. 28 and 29). The muscovite was found locally in patches and replacing quartz crystals.

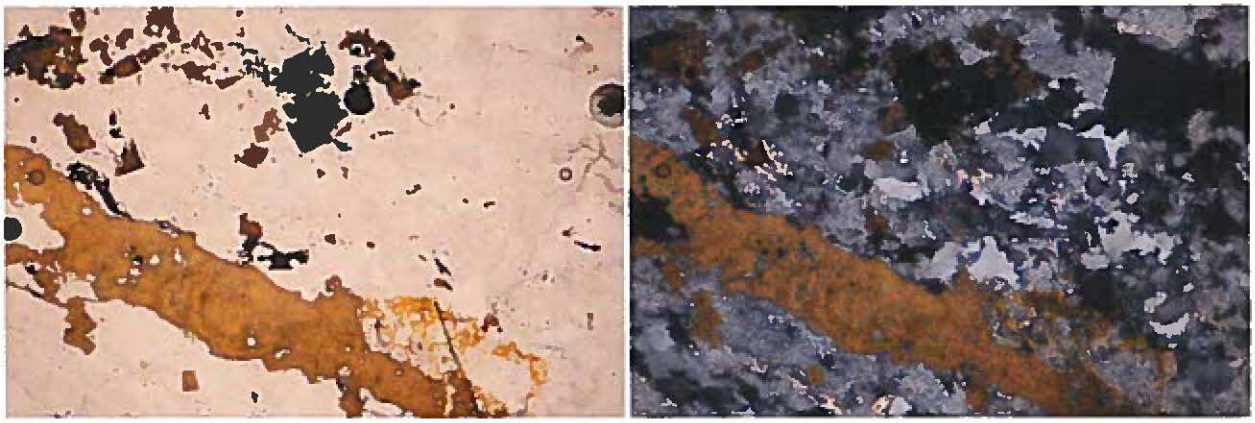


Figure 27. Photomicrographs of the quartz matrix, muscovite, and K-Fe-sulphate alteration in transmitted light, plane-polars (left) and crossed polars (right) (4x mag., F.O.V. ~3mm).

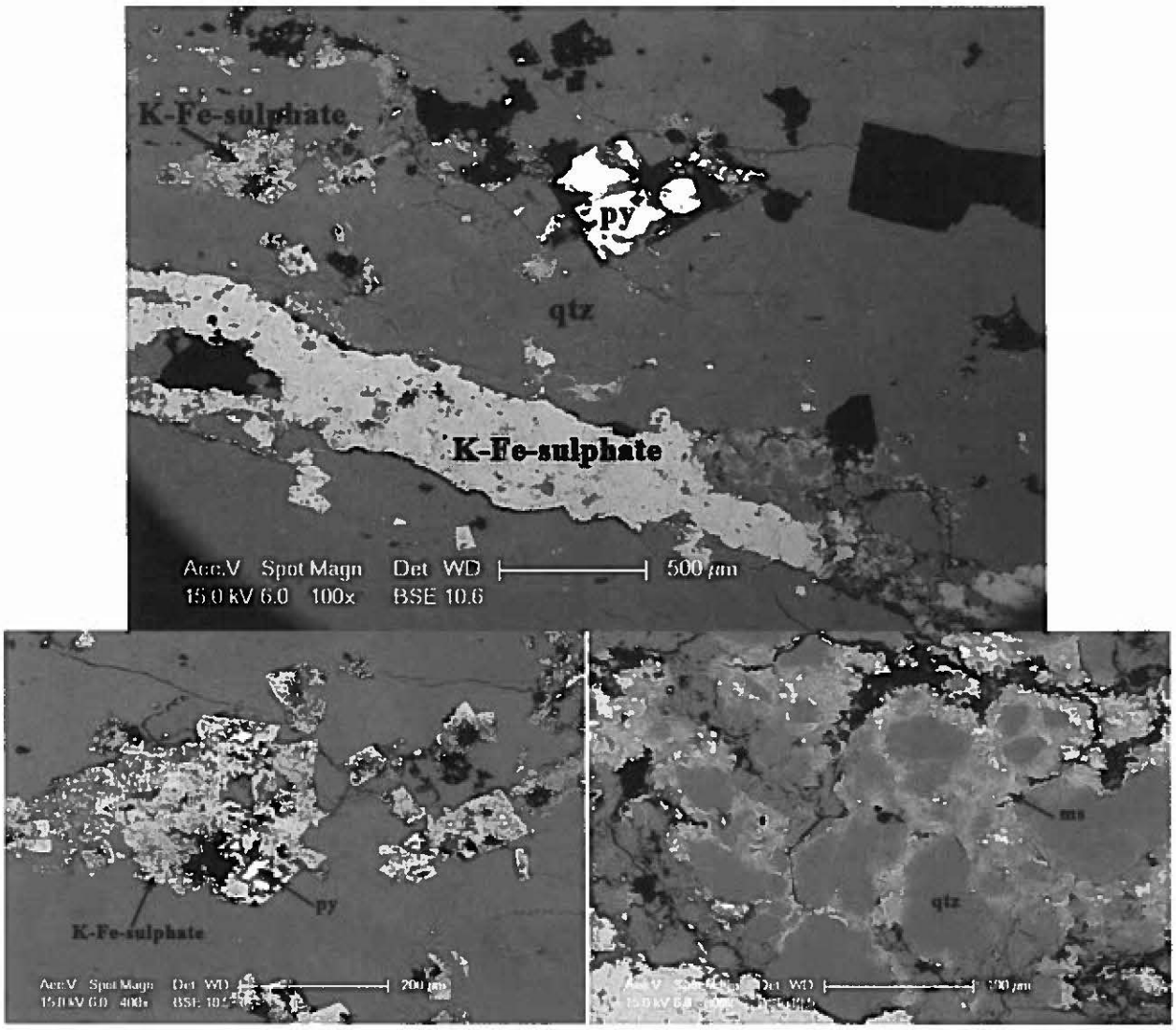


Figure 28. Backscattered electron image of Figure 27 showing the alteration of pyrite to K-Fe-sulphate, and muscovite alteration.

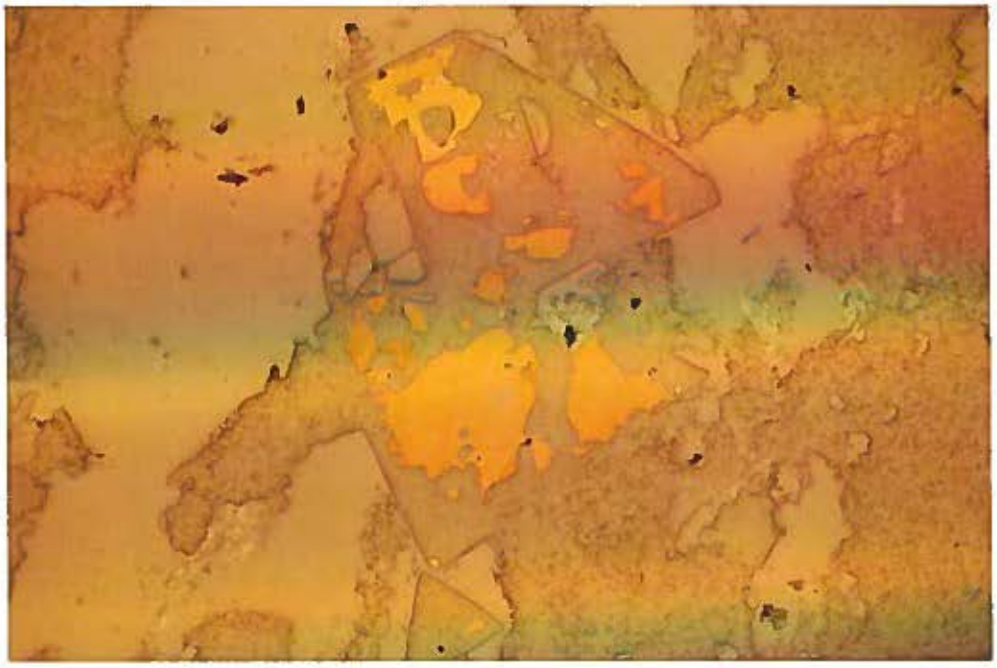


Figure 29. Photomicrograph of pyrite being altered in reflected light (4x mag., F.O.V. ~3 mm).

MIN-006

This section consists of approximately 90% opaque minerals, and 10% quartz. The opaque minerals consist of approximately 40% pyrite, 35% arsenopyrite, 9% sphalerite, and 6% galena.

The quartz is very fine- to fine-grained, anhedral crystals and appears to be infilling between the sulphide grains (Fig. 30).

The sulphide minerals are composed of one large aggregate (Fig. 31 and 32). The pyrite is fine- to medium-grained, subhedral to anhedral crystals. The arsenopyrite is fine-grained, subhedral to anhedral crystals. Sphalerite is reddish-brown in colour, medium- to fine-grained, anhedral crystals that have a small Fe peak on EDX spectrum. Galena is fine-grained, generally rounded masses and, generally appears to be infilling around the arsenopyrite and pyrite.

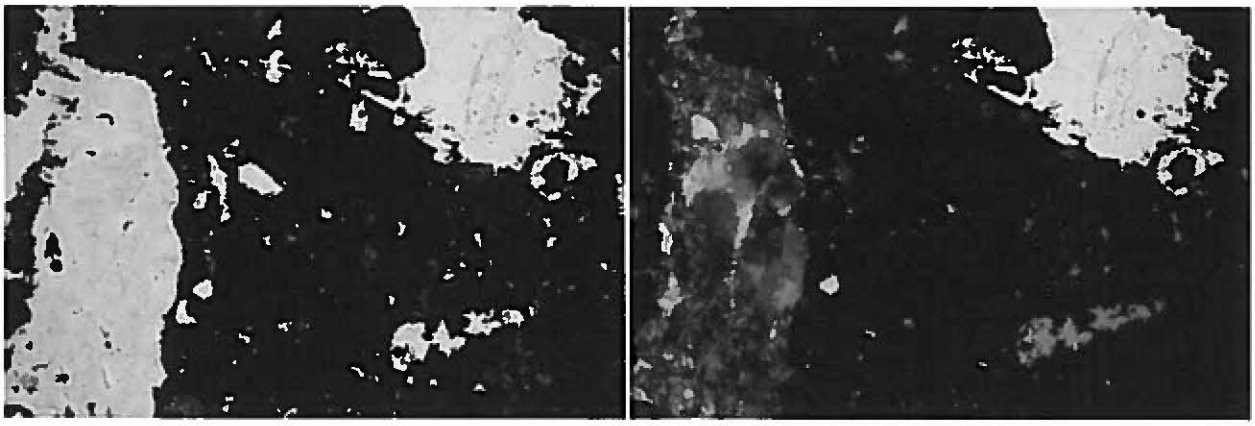


Figure 30. Photomicrographs of the quartz matrix in transmitted light, plane-polars (left) and crossed polars (right) (4x mag., F.O.V. ~3mm).

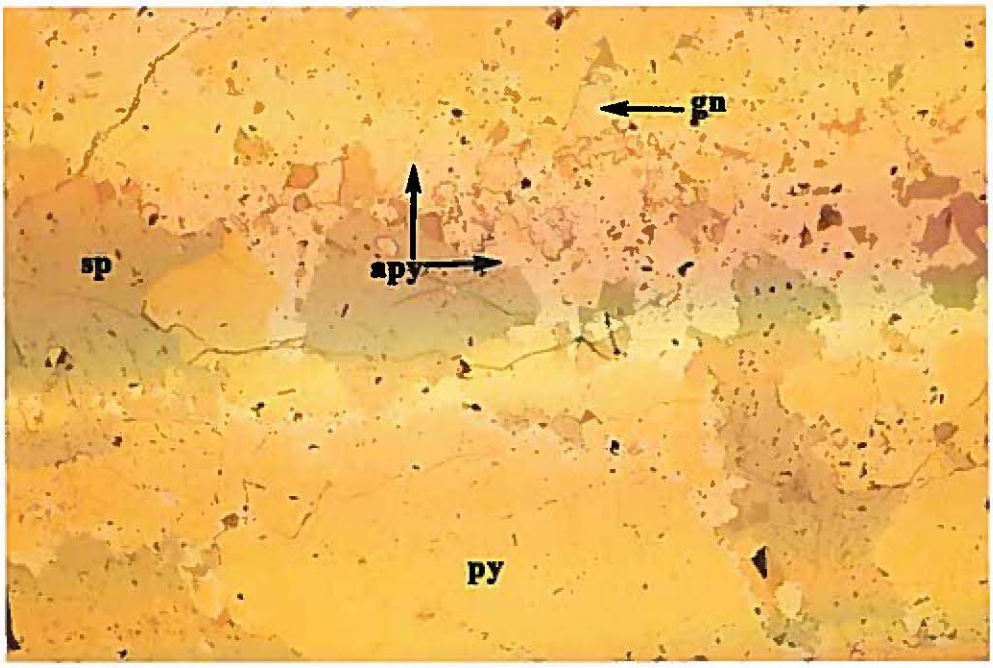


Figure 31. Photomicrograph of pyrite, arsenopyrite, sphalerite and galena in reflected light (4x mag., F.O.V. ~3 mm).

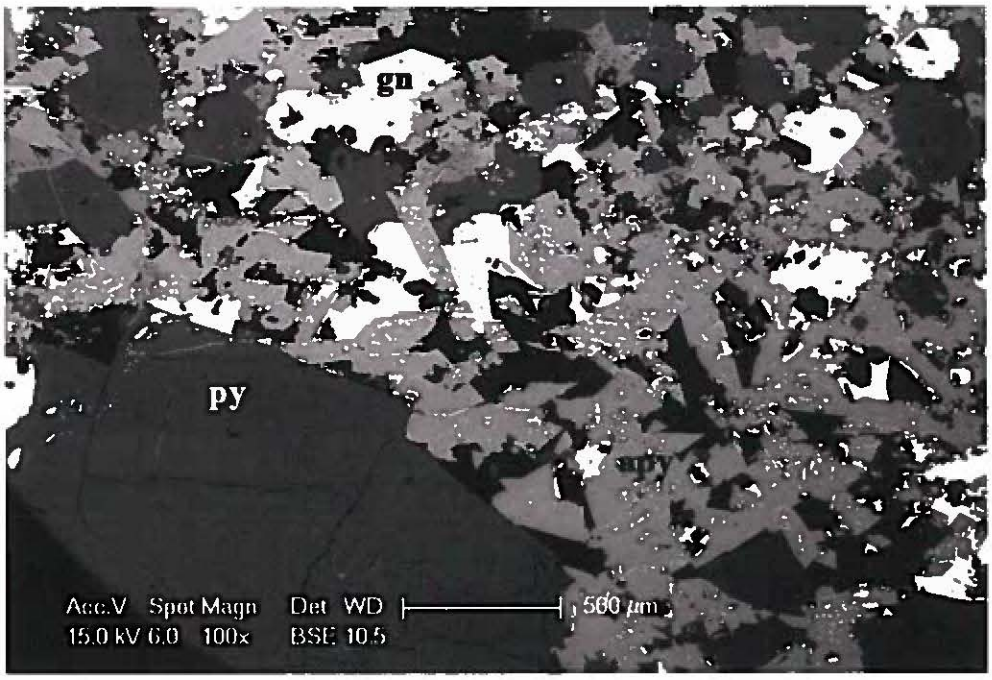


Figure 32. Backscattered electron image of pyrite, arsenopyrite, and galena.

MIN-007

This section consists of approximately 60% opaque minerals, 39% quartz and 1% ankerite. The opaque minerals consist of 45% arsenopyrite, 8% galena, 7% sphalerite, and trace pyrite.

The quartz is generally fine- to very fine-grained, anhedral to subhedral crystals. Locally some of the very fine-grained quartz rims the sulphides (Fig. 33). The more subhedral quartz grains form outside of the main area of sulphide mineralisation. The ankerite is very fine-grained, and occurs as a veinlet, cross-cutting through the section (Fig. 34).

The arsenopyrite is fine-grained, subhedral to anhedral crystals, and occurs in large masses (Fig. 35). The galena occurs amongst the main body of sulphide mineralization as well as infilling between quartz grains (Fig. 34). Sphalerite occurs as medium- to coarse-grained, anhedral crystals. Locally the sphalerite has very small inclusions of pyrite. Local, very fine-grained pyrite also was observed.

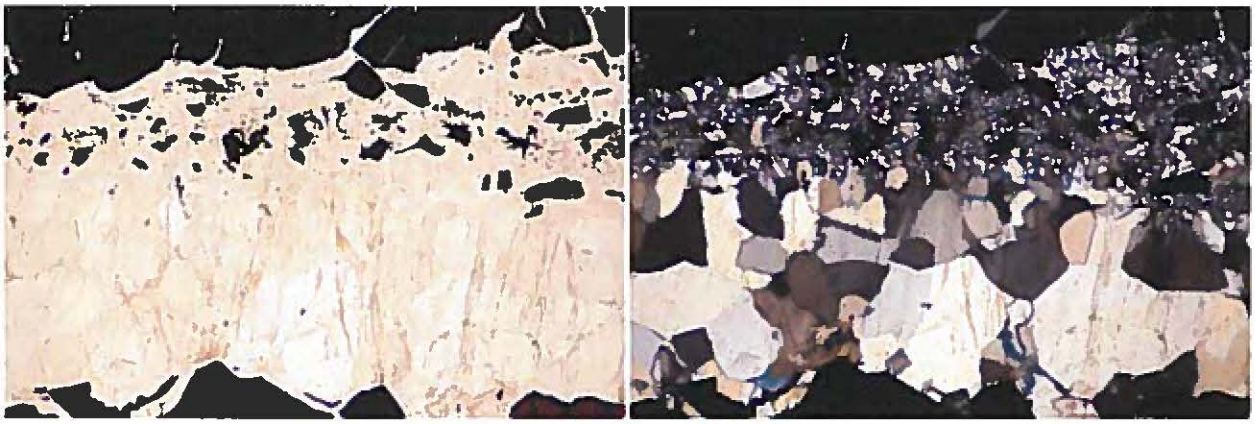


Figure 33. Photomicrographs of the quartz matrix in transmitted light, plane-polars (left) and crossed polars (right) (4x mag., F.O.V. ~3mm).

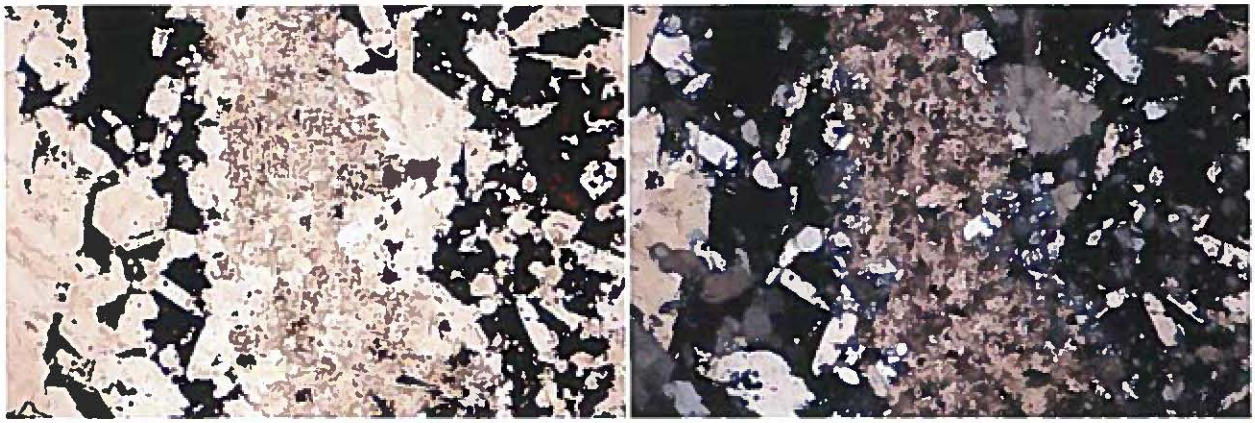


Figure 34. Photomicrographs of the quartz matrix and ankerite veinlet in transmitted light, plane-polars (left) and crossed polars (right) (4x mag., F.O.V. ~3mm).

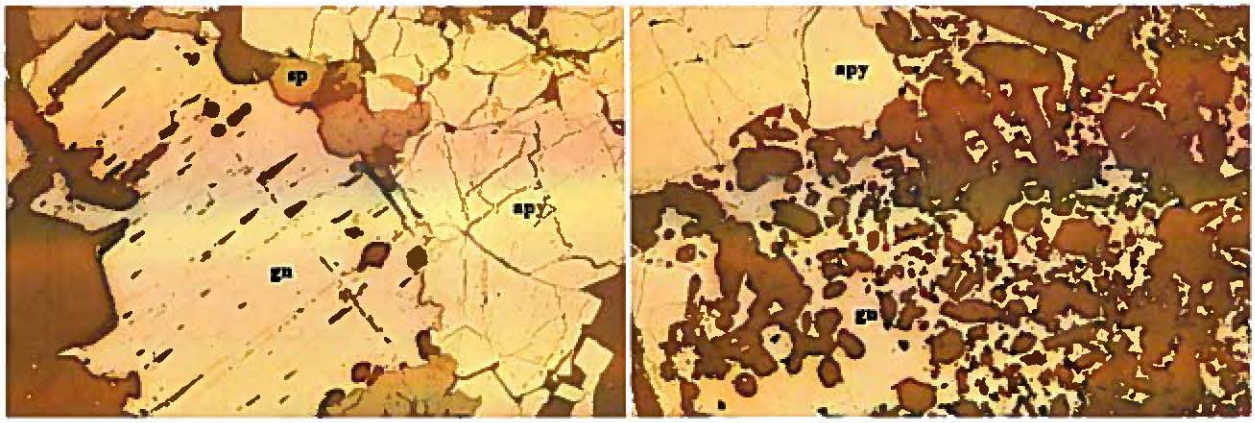


Figure 35. Photomicrograph s of arsenopyrite, sphalerite and galena in reflected light (4x mag., F.O.V. ~3 mm).

MIN-008A

This section consists of a quartz-sulphide vein cross-cutting through the altered host rock. This section consists of approximately 70% quartz, and alteration minerals, and 30% opaque minerals. The opaque minerals consist of 13% pyrite, 10% sphalerite, 5% arsenopyrite, and 2% galena.

The quartz occurs within the alteration as well as in the sulphide vein. Within the sulphide vein, the quartz is fine-grained, and anhedral (Fig. 37). Very fine-grained quartz rims the sulphide vein on one side and partially rims it on the other. Within the host rock is a combination of aphanitic to very fine-grained quartz, and muscovite (Fig. 36). This was easiest to determine through BSE imaging.

Sulphide minerals include pyrite, sphalerite, arsenopyrite, and galena (Fig. 38 and 39). The pyrite is fine- to medium-grained, subhedral to anhedral crystals. The arsenopyrite is fine-grained, subhedral to anhedral crystals, which locally appear to be fractured. Sphalerite is reddish-brown in colour, medium- to fine-grained, anhedral crystals. Galena generally appears to be infilling fractures around the sphalerite.

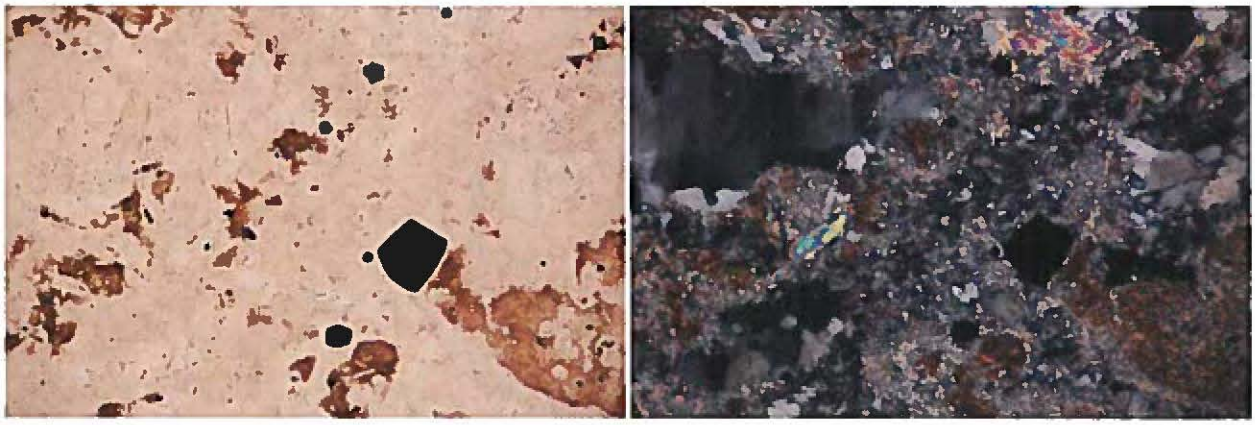


Figure 36. Photomicrographs of the quartz matrix and muscovite alteration in transmitted light, plane-polars (left) and crossed polars (right) (10x mag., F.O.V. ~1.2mm).

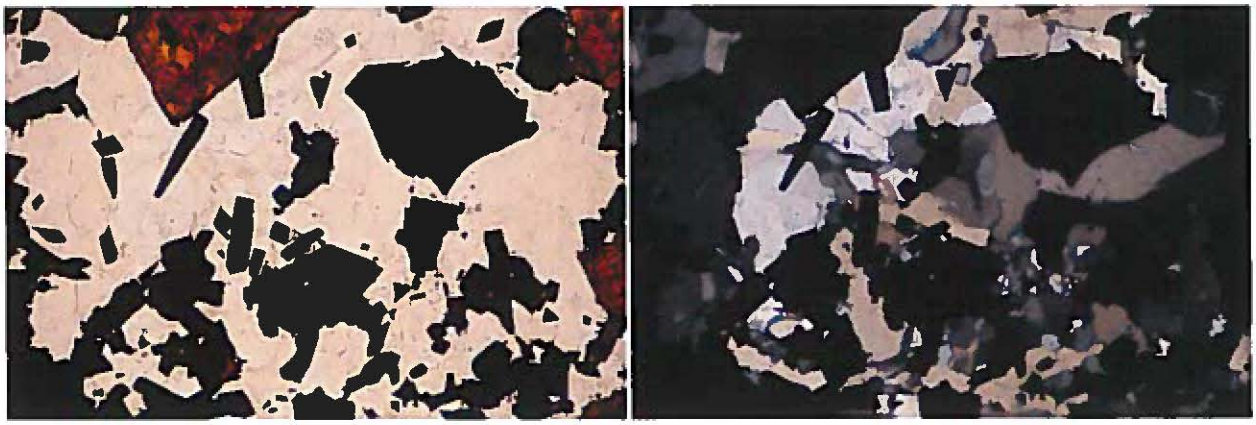


Figure 37. Photomicrographs of quartz matrix in transmitted light, plane polars (left), and crossed polars (right) (4x mag., F.O.V. ~3mm).

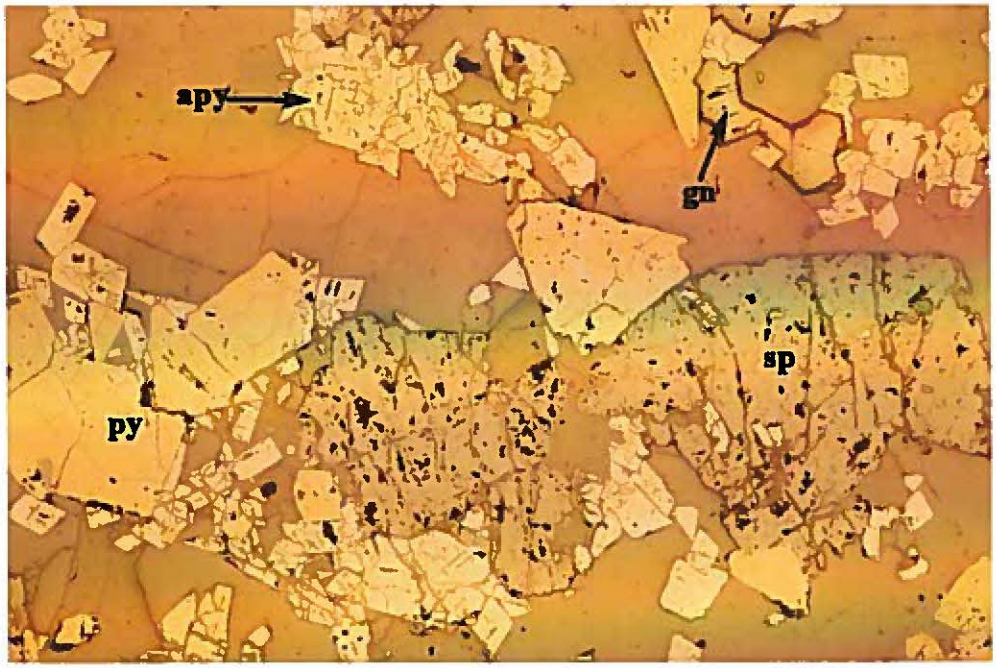


Figure 38. Photomicrograph of arsenopyrite, pyrite, sphalerite and galena in reflected light (4x mag., F.O.V. ~3 mm).

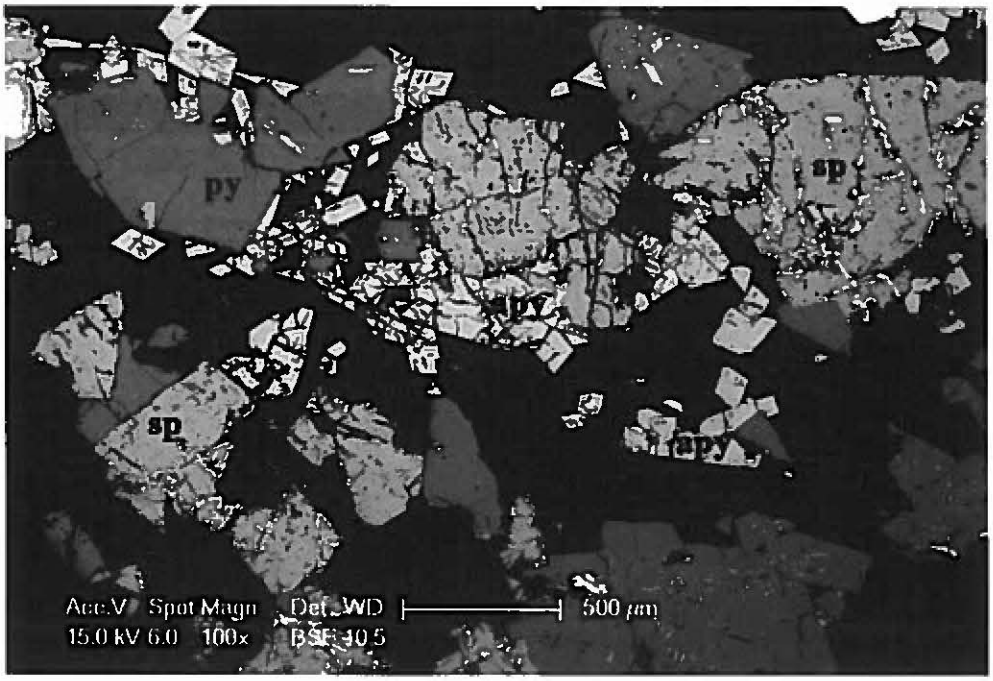


Figure 39. Backscattered electron image of arsenopyrite, pyrite, and sphalerite.

MIN-008B

This section consists of approximately 45% quartz, and alteration minerals, 35% opaque minerals and 10% quartz. Opaque minerals include approximately 15% arsenopyrite, 15% sphalerite, 4% pyrite and 1% galena.

The quartz forms as medium- to fine-grained, anhedral to subhedral crystals in the sulphide vein and locally very fine-grained quartz is observed rimming parts of the sulphide vein (Fig. 41). The host rock is formed of aphanitic to very fine-grained quartz and altered by muscovite (Fig. 40). Generally the muscovite is aphanitic, but locally observed as very fine-grained.

The sulphide mineral occur as masses within a vein as well as rimming the vein where it contacts the host rock (Fig. 42). Sphalerite occurs as reddish-brown, medium- to coarse-grained, anhedral crystals. Arsenopyrite occurs as masses of fine- to very fine-grained, subhedral to euhedral crystals. Local very fine-grained, subhedral pyrite crystals. Galena is very fine-grained, rounded crystals.

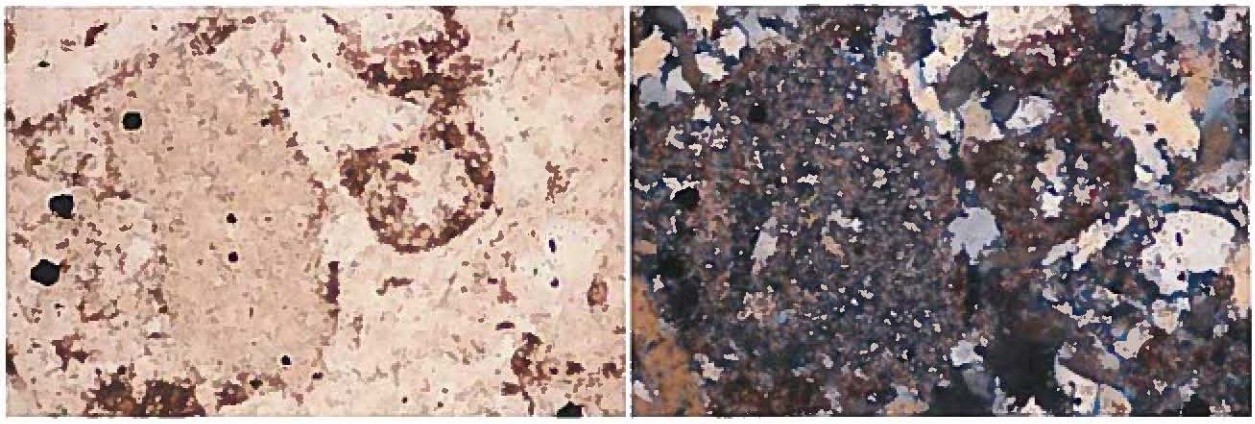


Figure 40. Photomicrographs of the quartz matrix and muscovite alteration in transmitted light, plane-polars (left) and crossed polars (right) (10x mag., F.O.V. ~1.2mm).



Figure 41. Photomicrographs of quartz matrix in transmitted light, plane polars (left), and crossed polars (right) (4x mag., F.O.V. ~3mm).

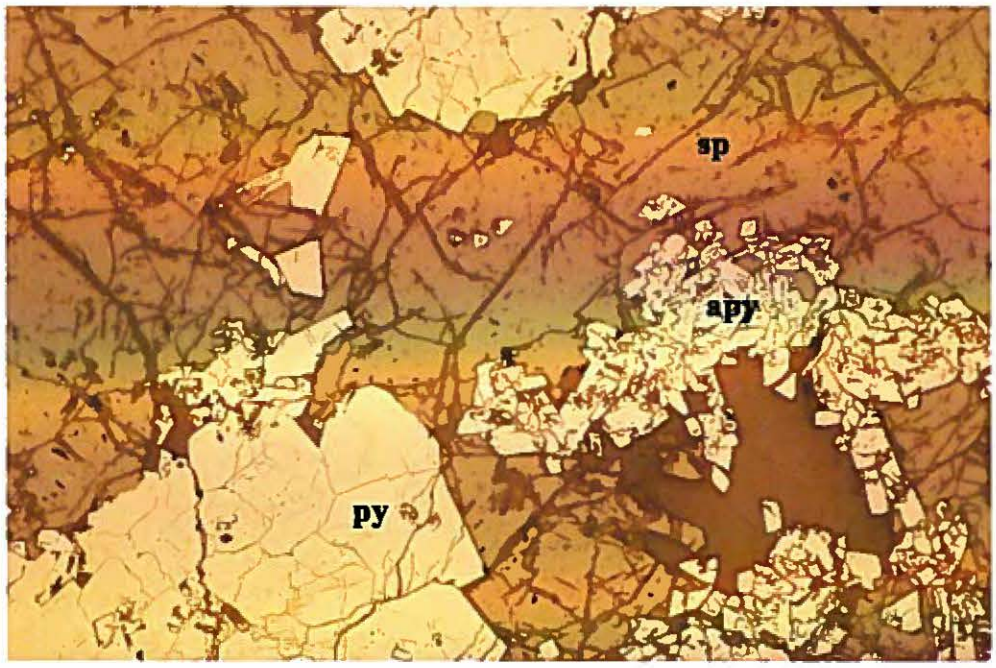


Figure 42. Photomicrograph of arsenopyrite, pyrite, and sphalerite in reflected light (4x mag., F.O.V. ~3 mm).

MIN-009

This section consists of approximately 40% quartz, 30% quartz, and alteration minerals, and 30% opaque minerals. The opaque minerals consist of approximately12% pyrite, 10% arsenopyrite, 7% sphalerite, and 1% galena.

The quartz occurs as a vein and in a veinlet cross-cutting through the alteration. The quartz is fine-grained, subhedral to euhedral grains (Fig. 44). The host rock is formed of aphanitic to very fine-grained quartz and altered by muscovite (Fig. 43). Generally the muscovite is aphanitic, but locally observed as very fine-grained. Muscovite is weakly altering the quartz within the vein.

These minerals occur mostly as aggregates within the quartz vein (Fig. 45 and 46). There are a few disseminated sulphides disseminated throughout the alteration. Pyrite is generally very fine- to fine-grained, anhedral to locally subhedral crystals through the vein. Within the host rock pyrite is very fine- to fine-grained, subhedral, subhedral, disseminated crystals. Arsenopyrite is fine-grained, locally fractured, euhedral to subhedral crystals. Sphalerite is a reddish-brown colour in transmitted light, very fine-grained and anhedral crystals. Sphalerite also shows a small Fe peak on EDX spectrum. Galena is very fine-grained and is observed locally infilling fractures and amongst the sulphide crystals.

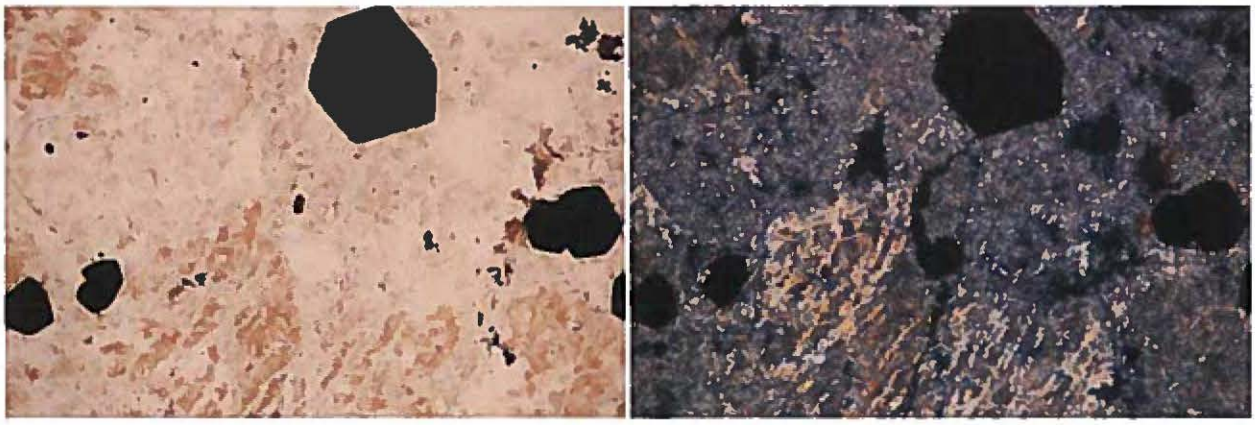


Figure 43. Photomicrographs of the quartz matrix and muscovite alteration in transmitted light, plane-polars (left) and crossed polars (right) (10x mag., F.O.V. ~1.2mm).

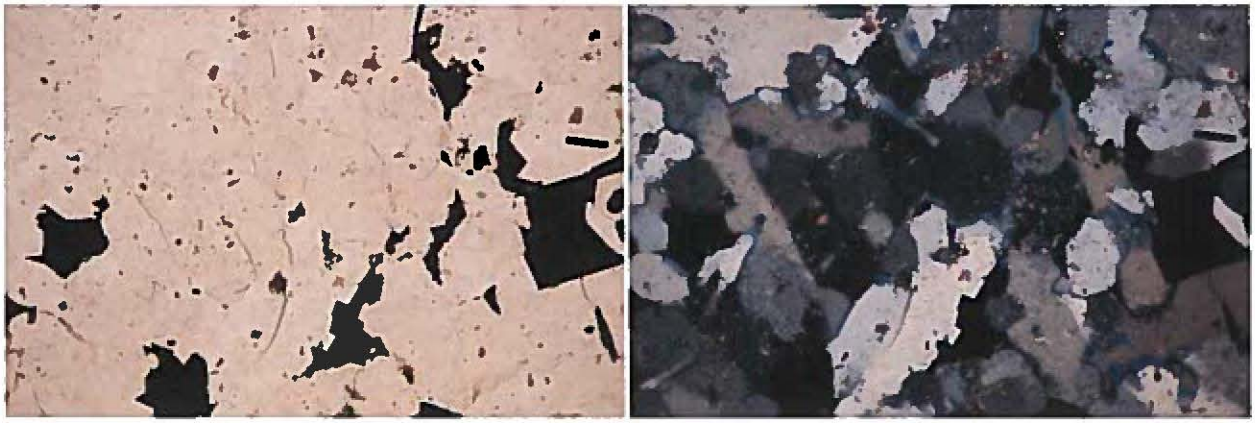


Figure 44. Photomicrographs of the quartz matrix being weakly altered by muscovite in transmitted light, plane-polars (left) and crossed polars (right) (10x mag., F.O.V. ~1.2mm).

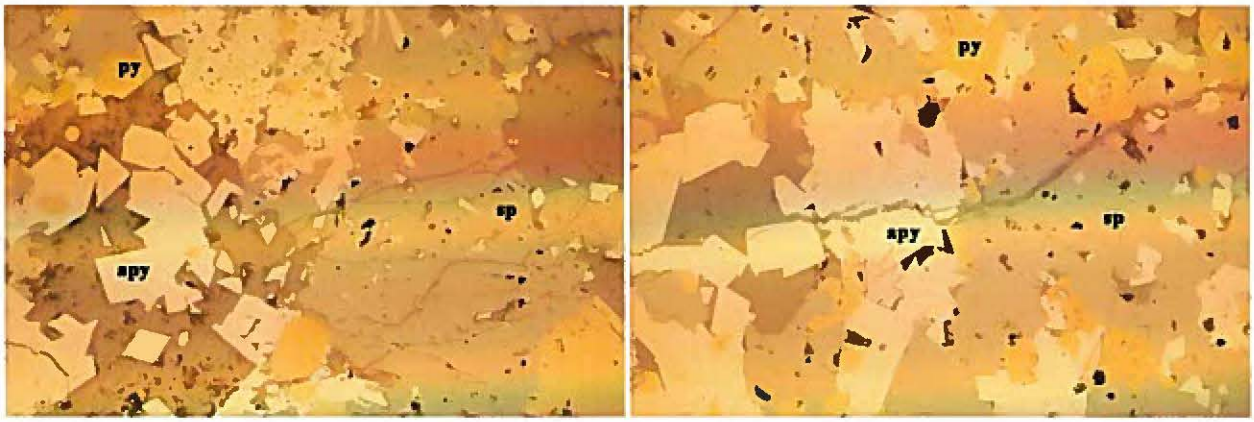


Figure 45. Photomicrographs of arsenopyrite, pyrite, and sphalerite in reflected light (4x mag., F.O.V. ~3 mm).

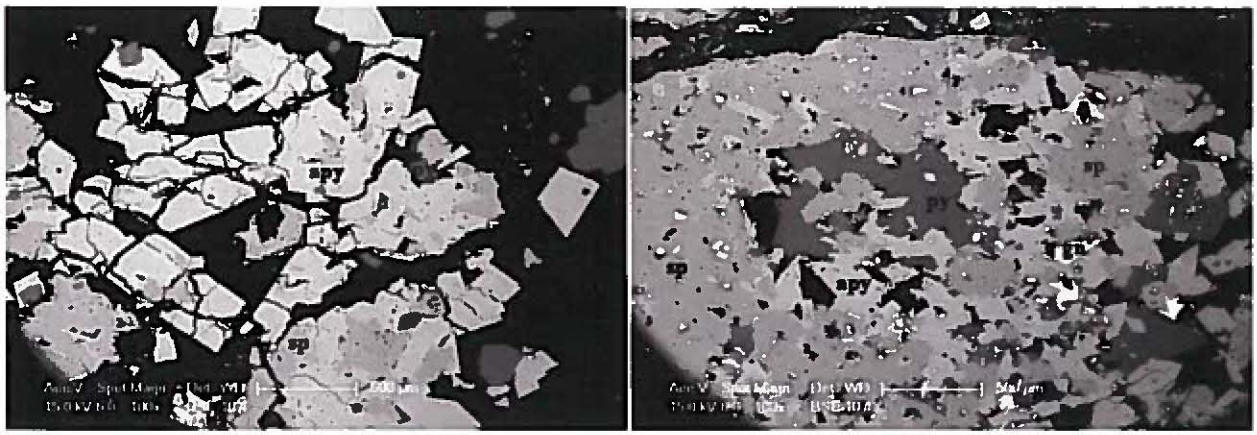


Figure 46. Backscattered electron images of arsenopyrite, pyrite, sphalerite and galena.

MIN-010

The section consists of approximately 54% quartz, 44% quartz, and alteration minerals, and the remaining 2% is opaque minerals and open space. The opaque minerals are mostly pyrite, with trace amounts of arsenopyrite, galena and boulangerite.

The quartz occurs in a vein with multiple stages of mineralization. The mineralization varies from areas of very fine-grained to aphanitic quartz to fine- to medium-grained quartz (Fig. 47). The majority of the sulphides are hosted within the vein. The quartz also occurs locally within the alteration as very fine-grained anhedral crystals. Using backscattered electron imaging and EDX spectra the alteration appears to be largely muscovite.

The sulphide and sulphosalt minerals occur predominately within the vein. Pyrite occurs as fine-grained, subhedral crystals. Pyrite is the only mineral found within the host rock. Galena is very fine-grained. Boulangerite is very fine-grained, anhedral crystals, and found associated with galena (Fig. 48 and 49). Arsenopyrite forms as fine-grained, subhedral to euhedral crystals.

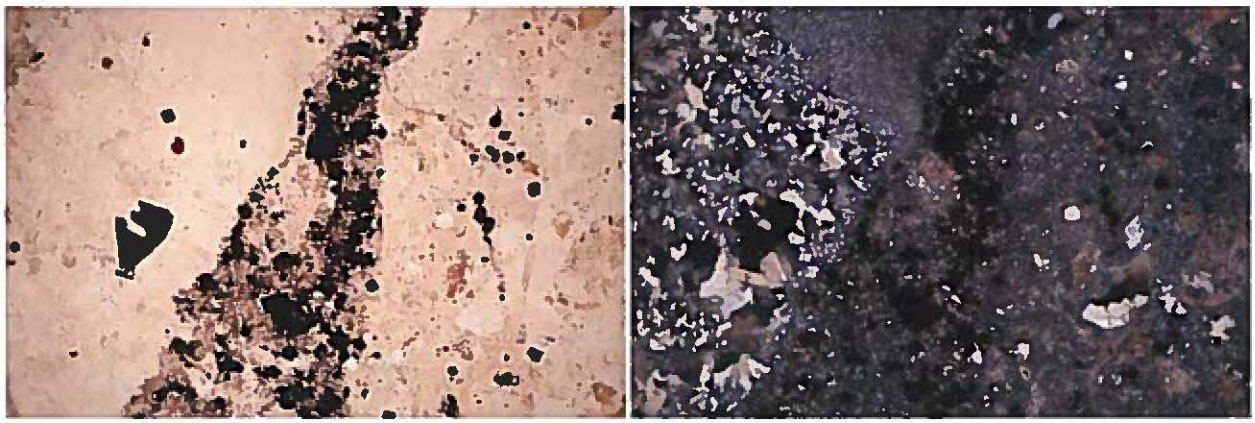


Figure 47. Photomicrographs of the quartz matrix and areas of aphanitic quartz and muscovite alteration in transmitted light, plane-polars (left) and crossed polars (right) (2x mag., F.O.V. ~6mm).

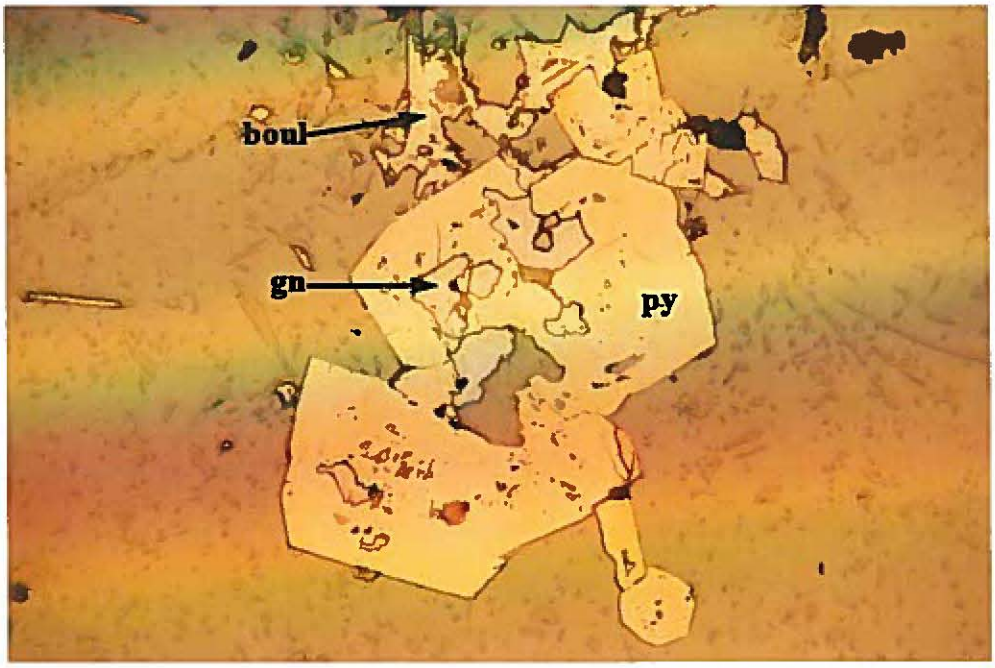


Figure 48. Photomicrograph pyrite, galena and boulangerite in reflected light (10x mag., F.O.V. ~1.2mm).

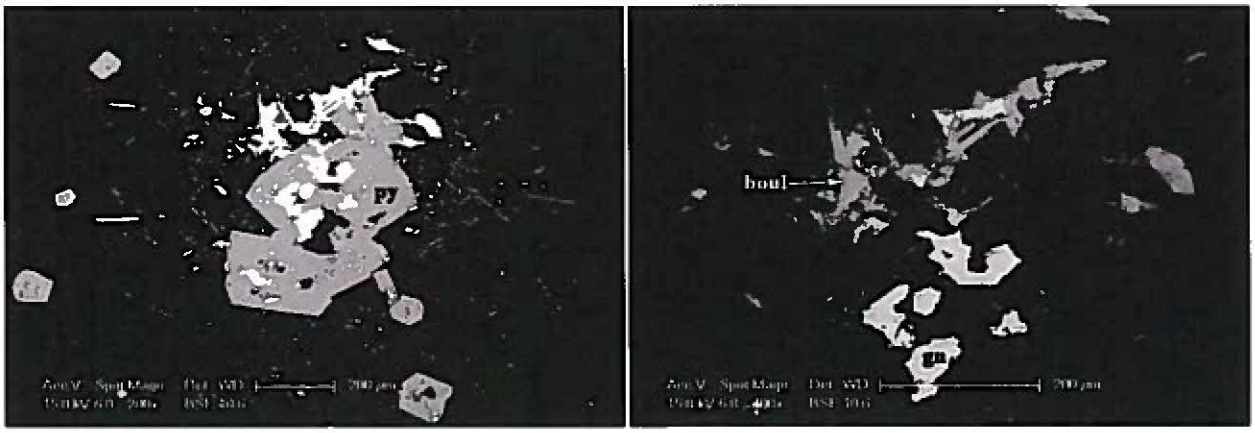


Figure 49. Backscattered electron images of Figure 48.

MIN-011

The section consists of approximately 55% quartz, 44% quartz, and alteration minerals, and 1% opaque minerals. The opaque minerals consist of approximately 1% pyrite, and trace sphalerite and arsenopyrite.

Two stages of quartz and alteration occur in this section, each taking up about half of the section (Fig. 50). Both sides consist of quartz and alteration by muscovite, and an unknown oxide. The muscovite is aphanitic to very fine-grained on both halves of the section. The one half has fine-grained quartz making up small pods amongst a matrix of aphanitic to very fine-grained quartz, and muscovite. The second half is more altered, and does not have the quartz pods but does some local larger grains. There is more oxide alteration and the quartz is very fine-grained to aphanitic on this side.

Pyrite is very fine-grained, subhedral crystals that locally occur as inclusions within sphalerite. Sphalerite occurs locally as very fine-grained, anhedral crystals (Fig. 51). Arsenopyrite occurs locally as very fine-grained, subhedral crystals.

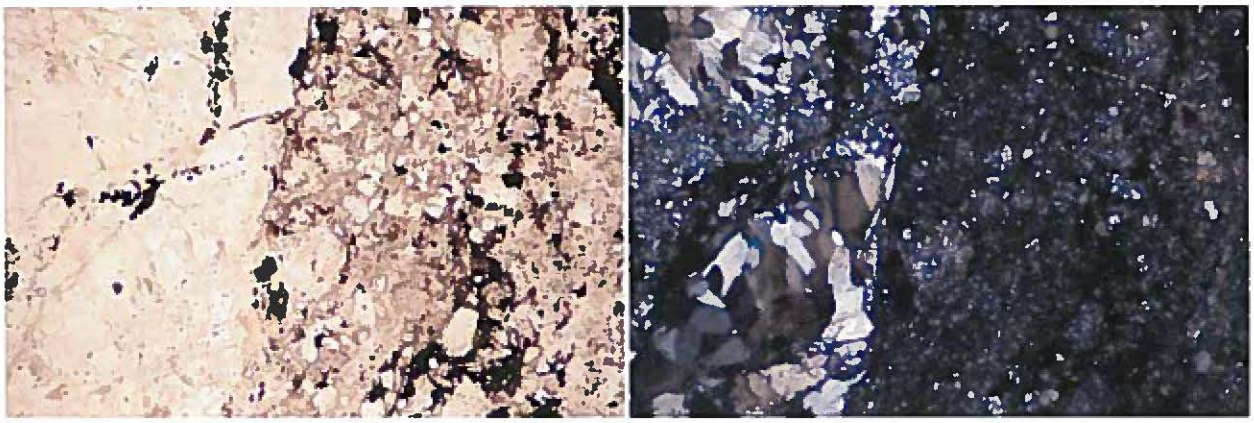


Figure 50. Photomicrographs showing the differences in the two halves of the section and the formation and appearance of quartz, muscovite and oxide alteration in transmitted light, plane-polars (left) and crossed polars (right) (4x mag., F.O.V. ~3mm).

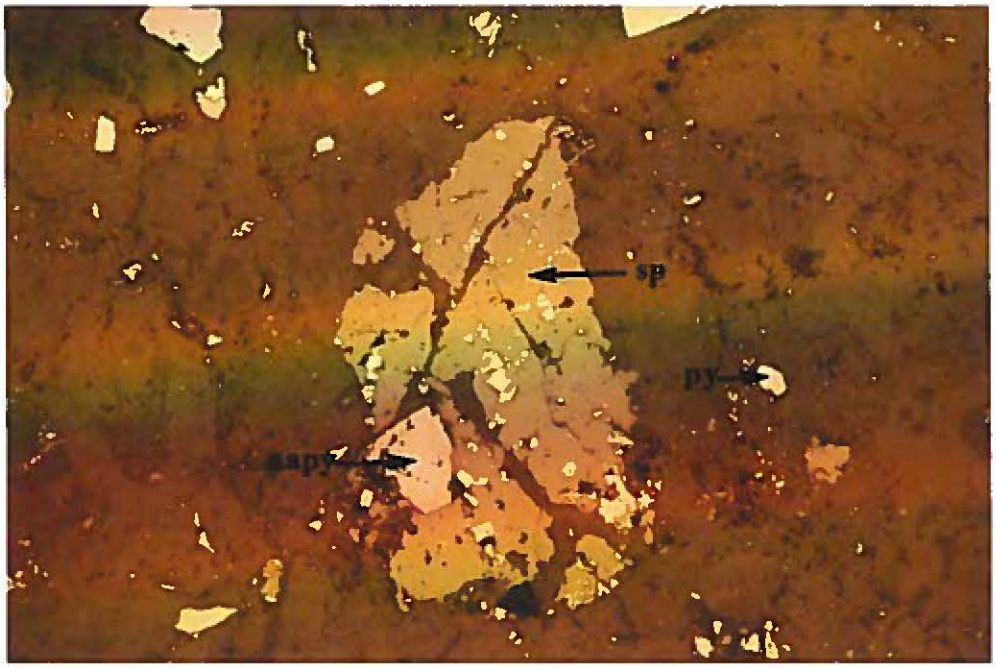


Figure 51. Photomicrograph of sphalerite, pyrite, and arsenopyrite in reflected light (10x mag., F.O.V. ~1.2mm).

MIN-012

This section is very altered, and the exact mineral amounts are difficult to determine. There is approximately 10% observable, very fine-grained, quartz. Using backscattered electron imaging and EDX the section is found to consist largely of quartz. The alteration within the section consists of Fe-oxide, and muscovite (Fig. 52). From BSE imaging there appears to be two types of Fe-oxide (Fig. 53). The first type occurs as very fine-grained nodules, and locally appears to rim around void space. The second type is very fine-grained, and appears fibrous in nature. The second type has a larger Fe-peak on EDX.

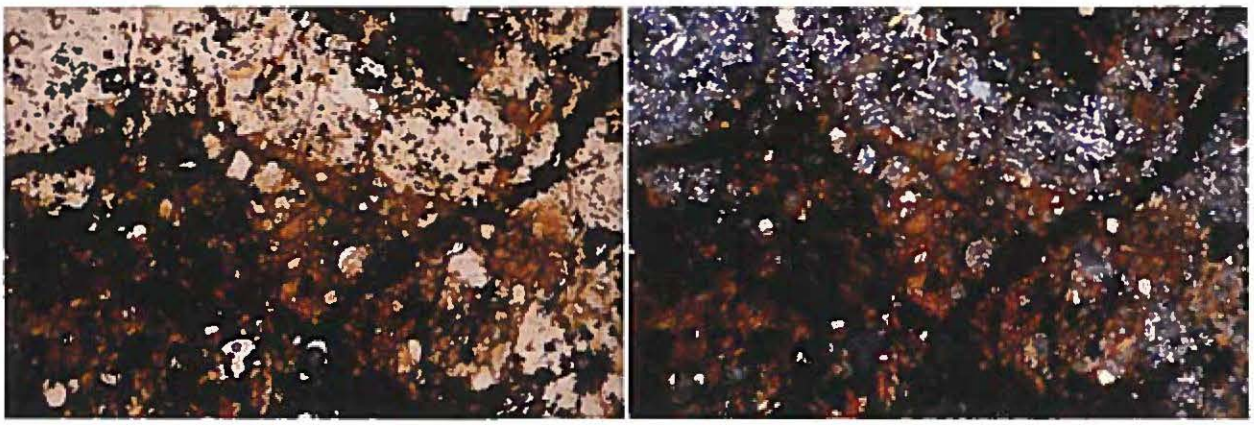


Figure 52. Photomicrographs of quartz being altered by Fe-oxide and muscovite in transmitted light, plane-polars (left) and crossed polars (right) (4x mag., F.O.V. ~3mm).

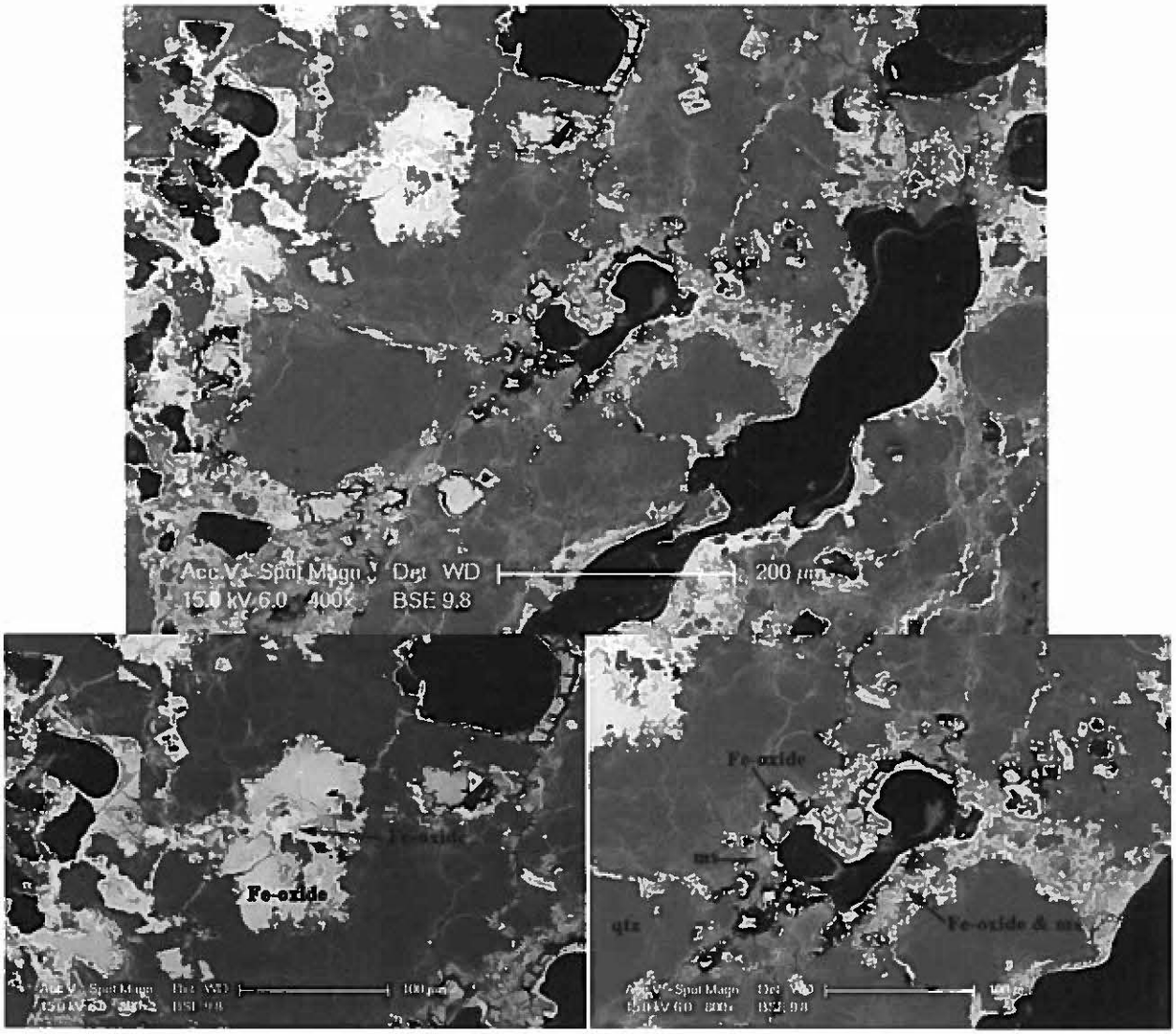


Figure 53. Backscattered electron images of the alteration of the quartz in this section, this includes Fe-oxide nodules, very fine-grained, fibrous Fe-oxide, and muscovite.

MIN-013

This section has a cross-cutting quartz vein through multiple alteration phases. It consists of approximately 73% aphanitic alteration mineralization, 25% observable quartz, and 2% opaque minerals and void space.

The quartz within the vein is medium- to coarse-grained subhedral crystals. There are local pods of fine- to very fine-grained quartz throughout the host rock (Fig. 54). Within the host rock quartz is anhedral, aphanitic to very fine-grained crystals. The alteration consists of an unknown brownish-orange oxide, muscovite, and a greenish mineral, that may be a Fe-As-oxide, replacing a sulphide mineral (Fig. 55). One band through the section hosts the majority of the Fe-oxide mineralization. The oxide minerals are aphanitic so their exact identities could not be determined. Muscovite is aphanitic to very fine-grained. The opaque minerals consist mostly of pyrite with trace arsenopyrite (Fig. 56). Pyrite is fine-grained, and subhedral, whereas arsenopyrite is fine-grained and subhedral to euhedral.

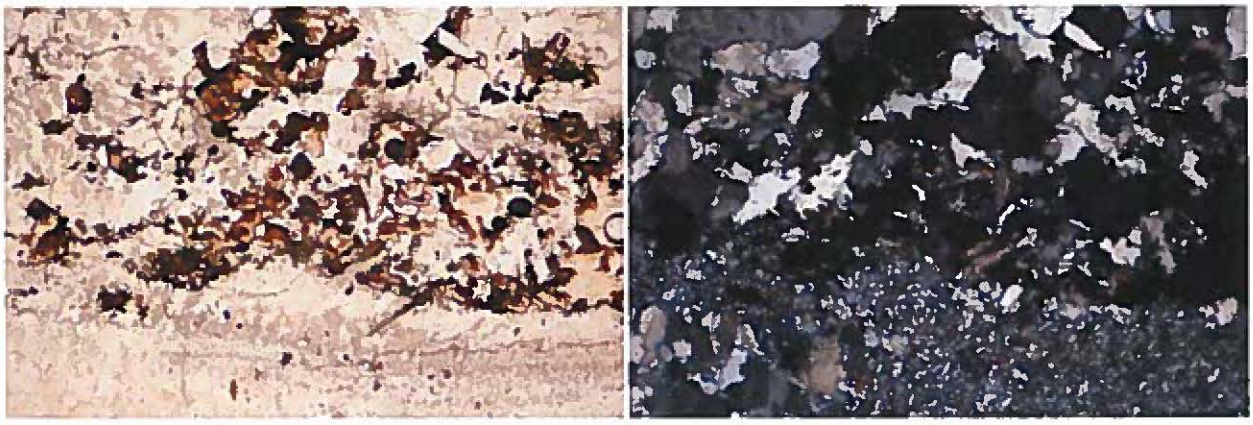


Figure 54. Photomicrographs of two stages of quartz being altered muscovite in transmitted light, plane-polars (left) and crossed polars (right) (4x mag., F.O.V. ~3mm).

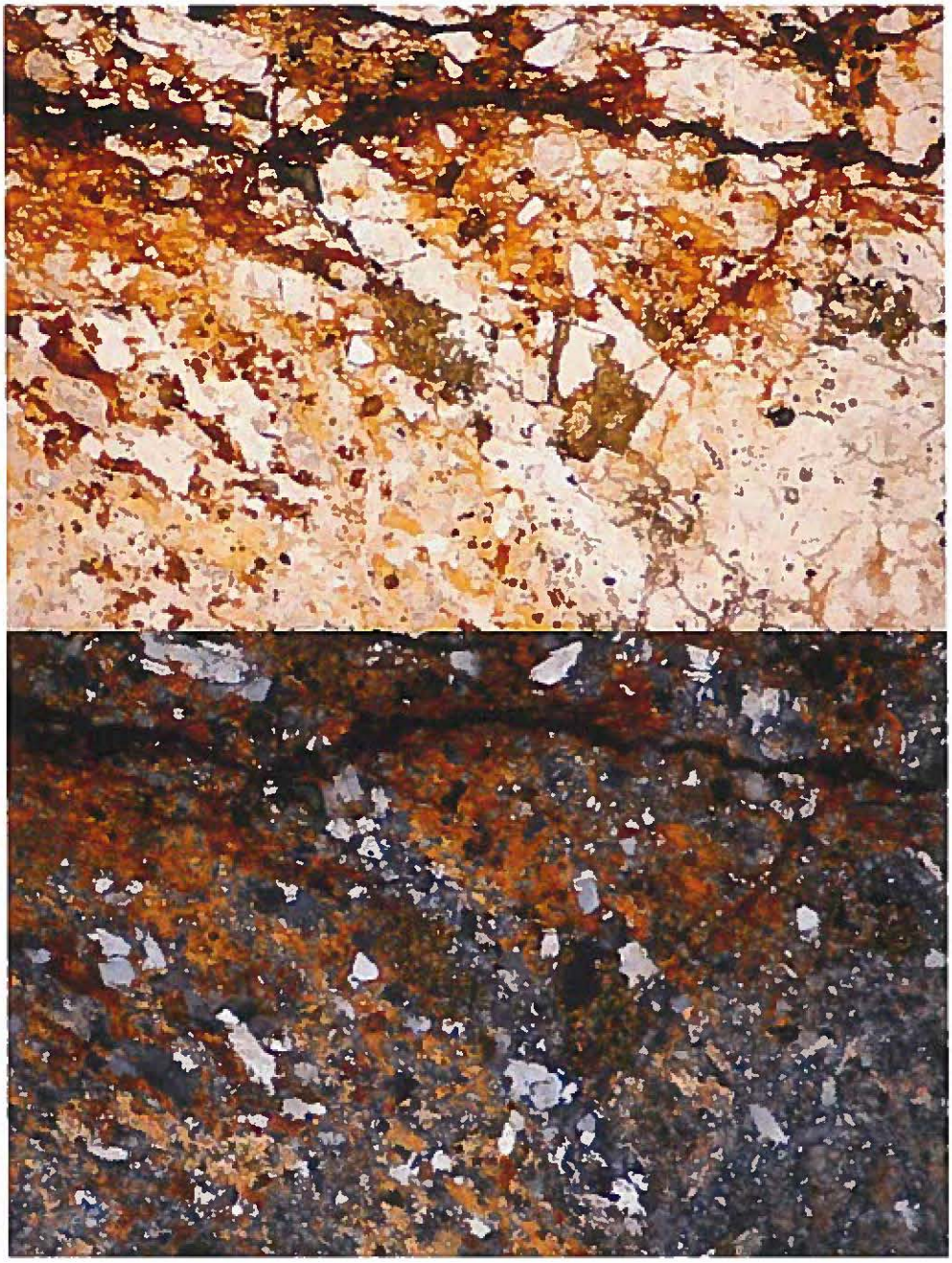


Figure 55. Photomicrographs of quartz being altered by a brown-orange oxide and possible pyrite or arsenopyrite that has been replaced by a greenish mineral (may be a Fe-As-oxide) in transmitted light, plane-polars (top) and crossed polars (bottom) (4x mag., F.O.V. ~3mm).

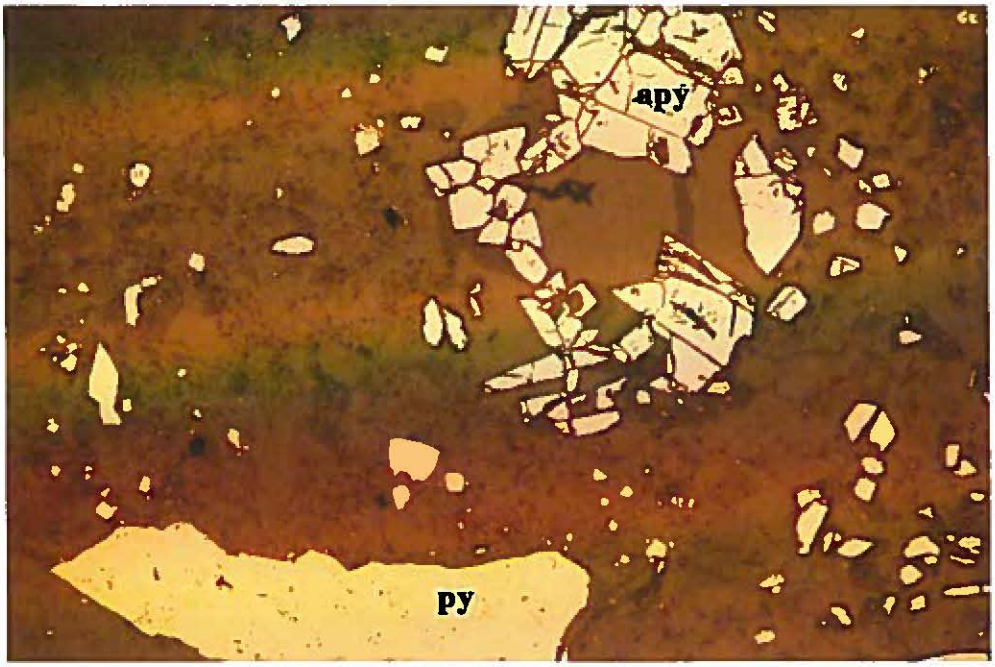


Figure 56. Photomicrograph of arsenopyrite, and pyrite in reflected light (10x mag., F.O.V. ~1.2mm).

MIN-014

This section is very altered. It consists of approximately 99% aphanitic alteration mineralization, and 1% local fine-grained, anhedral quartz. The alteration consists of an unknown orange-brown, likely Fe-oxide and aphanitic to very fine-grained muscovite. The Fe-oxide mineralization is especially strong along fractures (Fig. 57). The quartz throughout the alteration is very fine-grained to aphanitic, rounded grains.

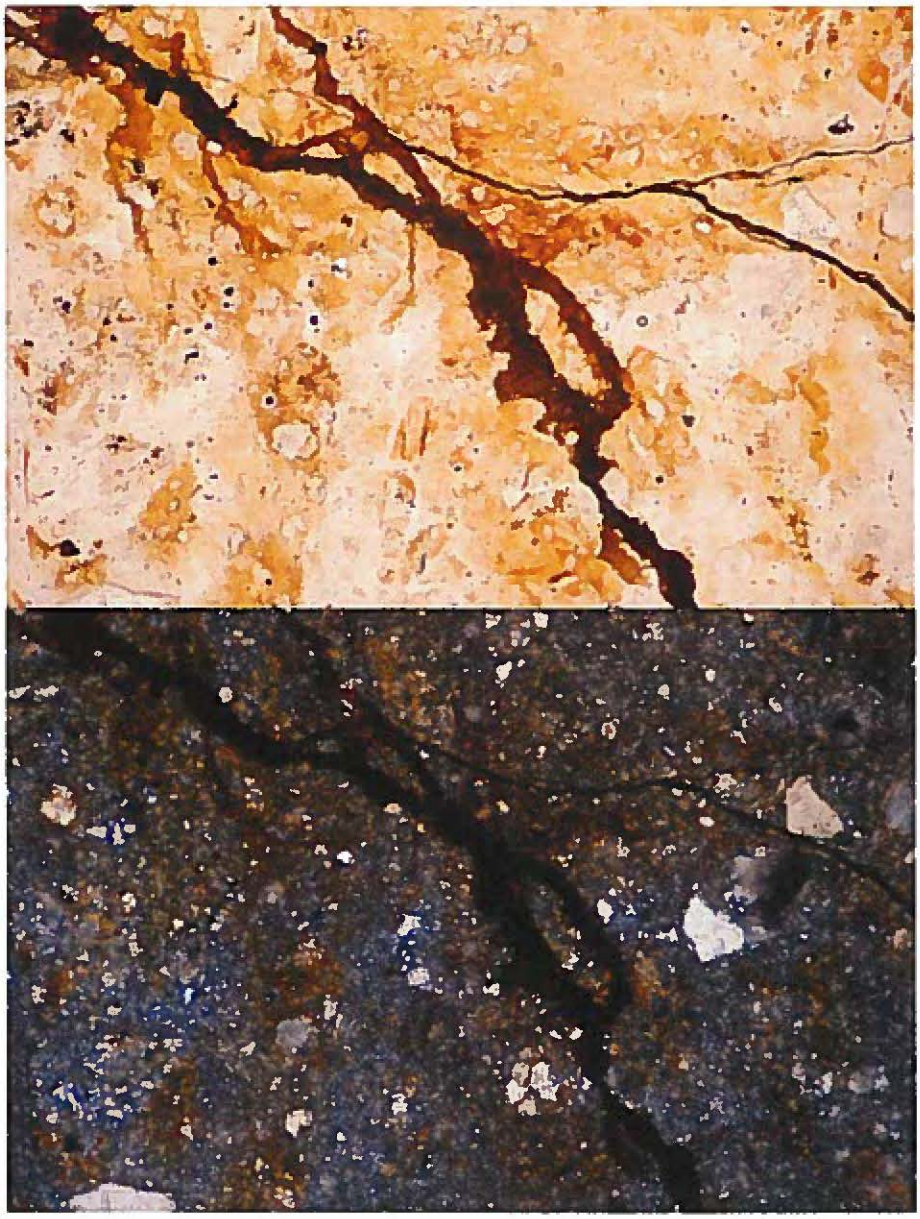


Figure 57. Photomicrographs of quartz being altered by a brown-orange oxide in transmitted light, plane-polars (top) and crossed polars (bottom) (4x mag., F.O.V. ~3mm).

MIN-015

This section consists of approximately 85% opaque minerals, and 15% quartz. The opaque minerals consist of approximately 68% arsenopyrite, 12% sphalerite, 3% Sb-sulphosalt minerals, 1% pyrite, 1% galena, and trace unknowns. The thickness of the slide is questionable as the quartz shows second order birefringence colours, and because of this no transmitted light photos were taken. It was identified using EDX spectrum. The quartz is fine- to very fine-grained, anhedral crystals.

Sulphide and sulphosalt minerals include pyrite, sphalerite, arsenopyrite, galena, boulangerite, bournonite, and freibergite. The sphalerite occurs as fine- to medium-grained, anhedral, reddish-brown crystals. The arsenopyrite occurs as fine-grained, subhedral to euhedral crystals (Figs. 59 to 64). Galena, bournonite, boulangerite, and freibergite, are generally very fine-grained to fine-grained, and occur infilling amongst the arsenopyrite and sphalerite (Figs. 59 to 61). Locally boulangerite forms as larger masses infilling amongst the arsenopyrite and pyrite.

Several unknown minerals also exist in this section. The first is an As-Pb-sulphide that is associated with galena (Fig. 64). There are several possibilities for what mineral this could be. The second is a Fe-As-Sb-Au-Pb-sulphate mineral (Fig. 64). On EDX the Au peak is small and it may be replacing another element rather than part of the mineral itself, however, even removing Au from the possible formula no known mineral could be identified from the chemistry. The third unknown appears to be a Ca-Fe-Cu-As-Au-S-Si-O mineral, which may be a silicate or sulphate mineral (Figs. 58, 59, 62, and 63). No known analogue could be found with this chemistry. The Au peak for this mineral is quite large. This mineral appears to be an alteration product of the sulphide and sulphosalt minerals. It was observed at the edges of the minerals as well as replacing the center, and edges of galena crystals. It is possible that unknown sulphate and S-Si-O minerals may be a combination of two or more extremely fine-grained minerals, but the BSE imaging shows a fairly uniform texture for both. None of these minerals could be observed in transmitted light.

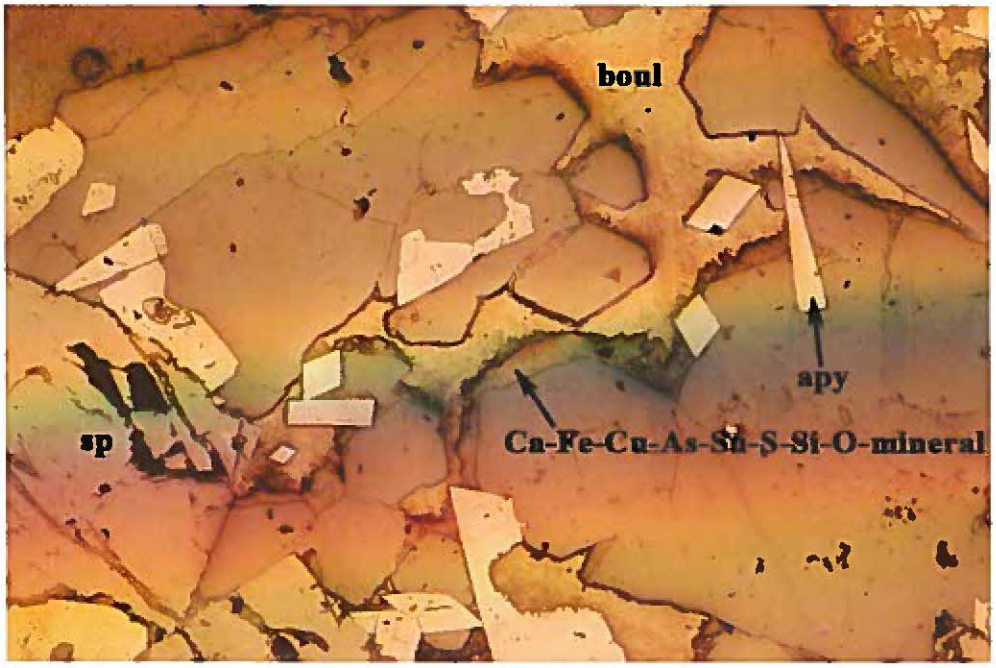


Figure 58. Photomicrograph of arsenopyrite, sphalerite, boulangerite and a Ca-Fe-Cu-As-Au-S-Si-O-mineral in reflected light (4x mag., F.O.V. ~3mm).

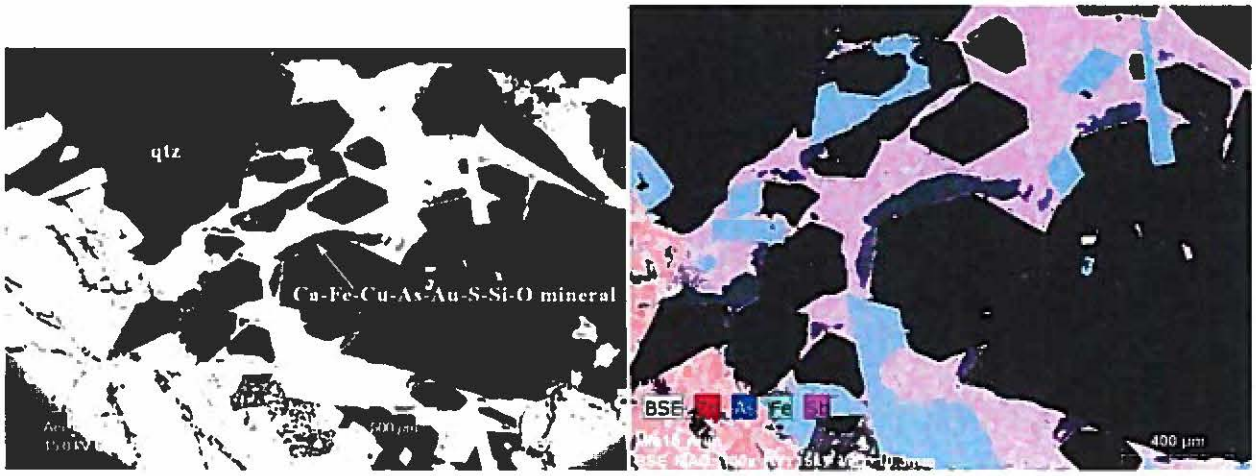


Figure 59. Backscattered electron image (left) and elemental map (right) of Figure 58 showing a Ca-Fe-Cu-As-Au-S-Si-O-mineral, arsenopyrite (blue), sphalerite (red), and boulangerite (pink).

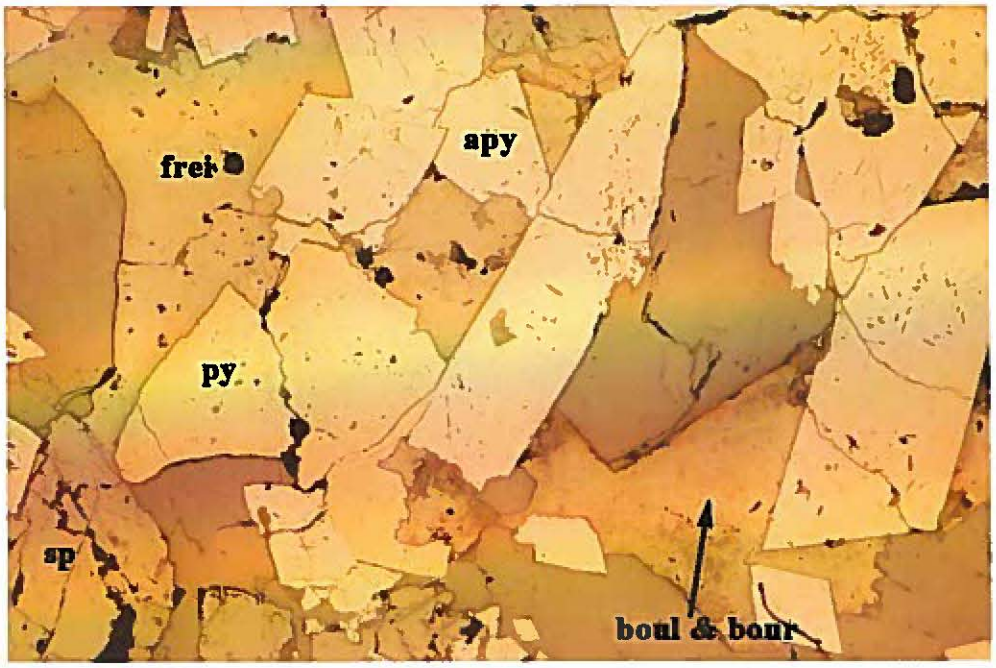


Figure 60. Photomicrograph of arsenopyrite, sphalerite, boulangerite, bournonite, and freibergite in reflected light (4x mag., F.O.V. ~3mm).

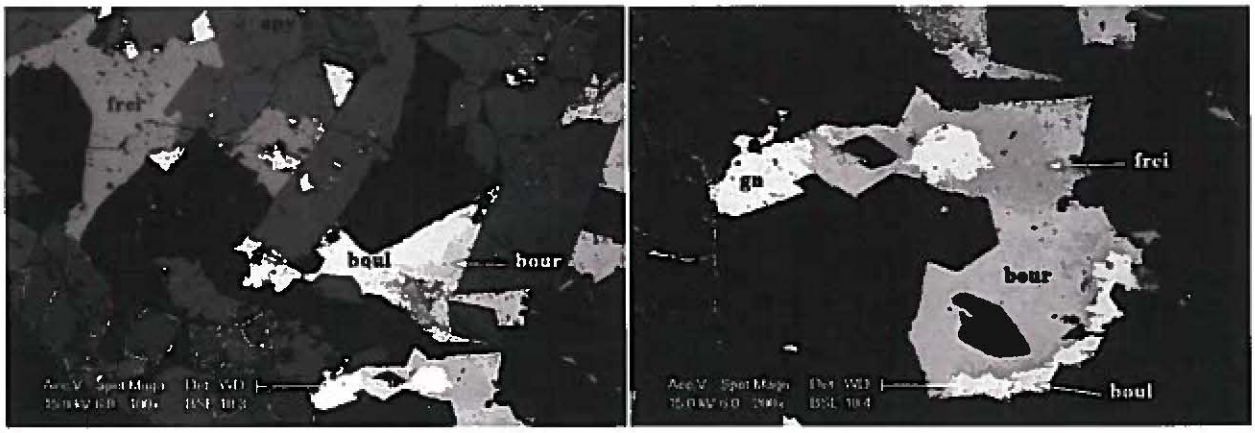


Figure 61. Backscattered electron images of Figure 60 showing arsenopyrite, galena, freibergite, boulangerite and bournonite.

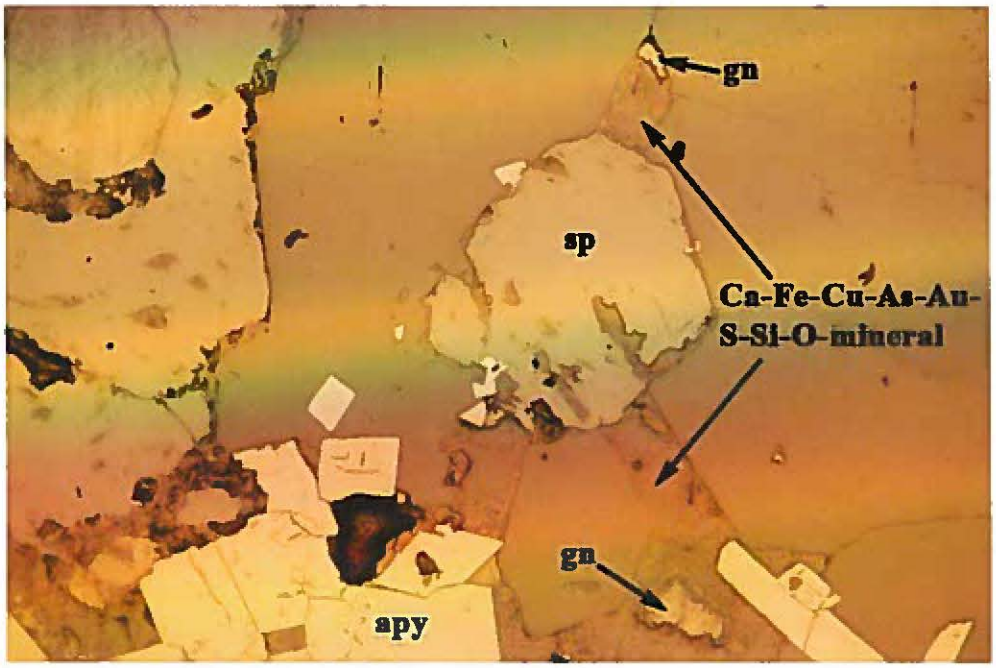


Figure 62. Photomicrograph of arsenopyrite, sphalerite, galena and a Ca-Fe-Cu-As-Au-S-Si-O-mineral in reflected light (10x mag., F.O.V. ~1.2mm).

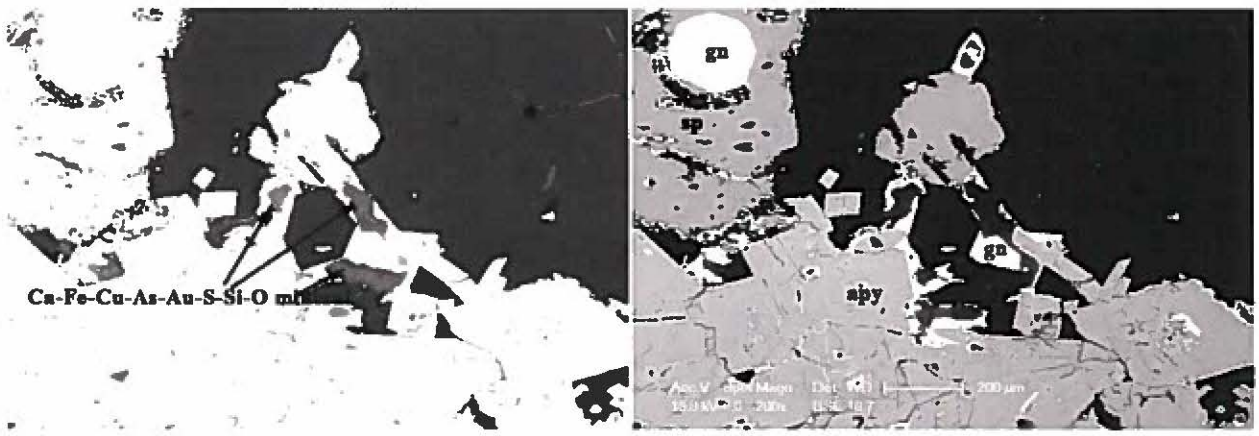


Figure 63. Backscattered electron images of Figure 62 showing arsenopyrite, galena, sphalerite, and a Ca-Fe-Cu-As-S-Si-O-mineral.

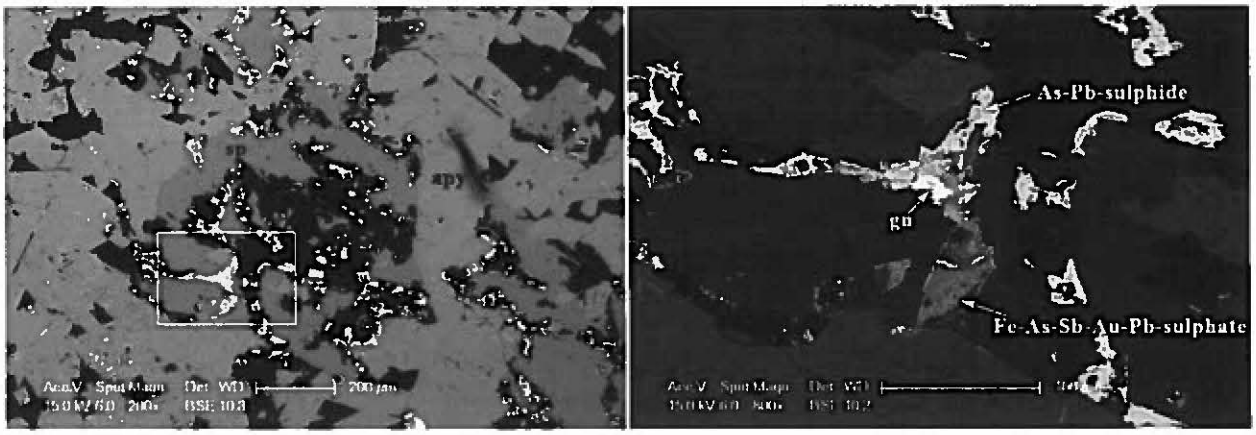


Figure 64. Backscattered electron images of arsenopyrite, sphalerite, galena, an As-Pb-sulphide and a Fe-As-Sb-Au-Pb-sulphate.

MIN-016

This section consists of 95% quartz and 5% arsenopyrite. The quartz ranges from coarse-grained, subhedral to euhedral crystals, to very fine-grained, anhedral crystals. There are three distinct groups of quartz mineralization. The first is coarse-grained, and generally euhedral crystals that are aligned in the same direction (Fig. 65). The second forms around these and locally infill's and forms around the rims of the first group (Fig. 65 and 66). This second group is fine-grained, and does not show any preferential alignment. It also hosts the majority of the sulphide mineralization. The third group is very fine-grained to aphanitic and infill's the remaining pockets in the section (Fig. 66). The arsenopyrite is very fine-grained, subhedral to euhedral, locally fractured crystals (Fig. 67).



Figure 65. Photomicrographs of the first and second stages of quartz in transmitted light, plane-polars (left) and crossed polars (right) (2x mag., F.O.V. ~6mm).

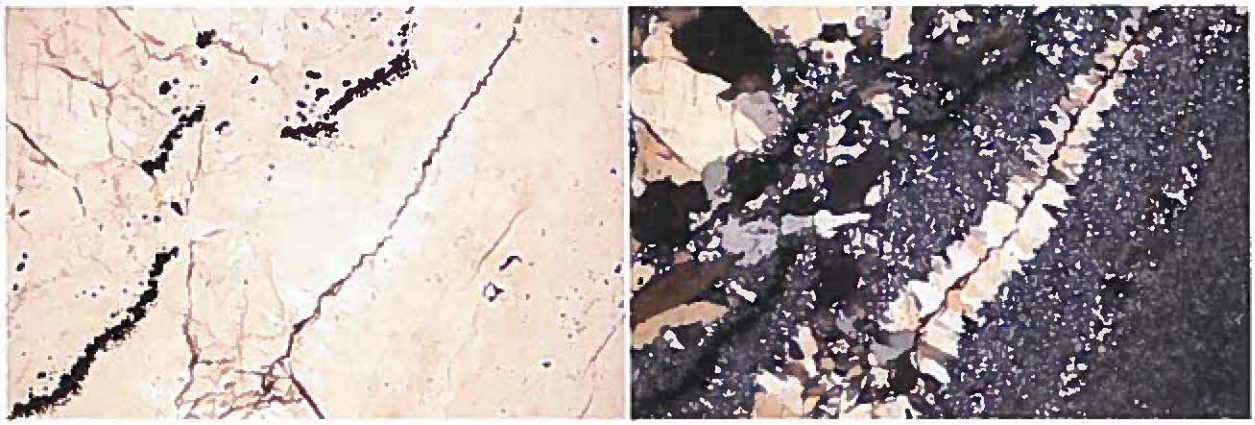


Figure 66. Photomicrographs of the second and third stages of quartz in transmitted light, plane-polars (left) and crossed polars (right) (4x mag., F.O.V. ~3mm).



Figure 67. Photomicrograph of arsenopyrite in reflected light (4x mag., F.O.V. ~3mm).

MIN-017

This section shows a vein cross-cutting through altered host rock. The section consists of approximately 45% quartz, 28% opaque minerals, 25% quartz and muscovite alteration mineralization, and 2% void space. The opaque minerals consist of approximately 10% arsenopyrite, 8% pyrite, 5% sphalerite, and 2% galena.

The quartz vein consists of fine- to medium-grained, subhedral to anhedral crystals (Fig. 69). The host rock consists of aphanitic to very fine-grained quartz and generally aphanitic to locally very fine-grained muscovite (Fig. 68).

The sulphide mineralization occurs within the vein and the host rock (Fig. 69). Pyrite occurs dominantly in the host rock; no other sulphide was observed in the host rock. It is very fine- to fine-grained, subhedral to euhedral crystals. Arsenopyrite forms within the vein as very fine- to fine-grained subhedral crystals. Sphalerite is reddish-brown in colour, fine-grained, anhedral crystals that locally appear fractured. Locally the sphalerite has small inclusions of pyrite within it. Galena is very fine-grained and locally it appears to be infilling around the quartz crystals.

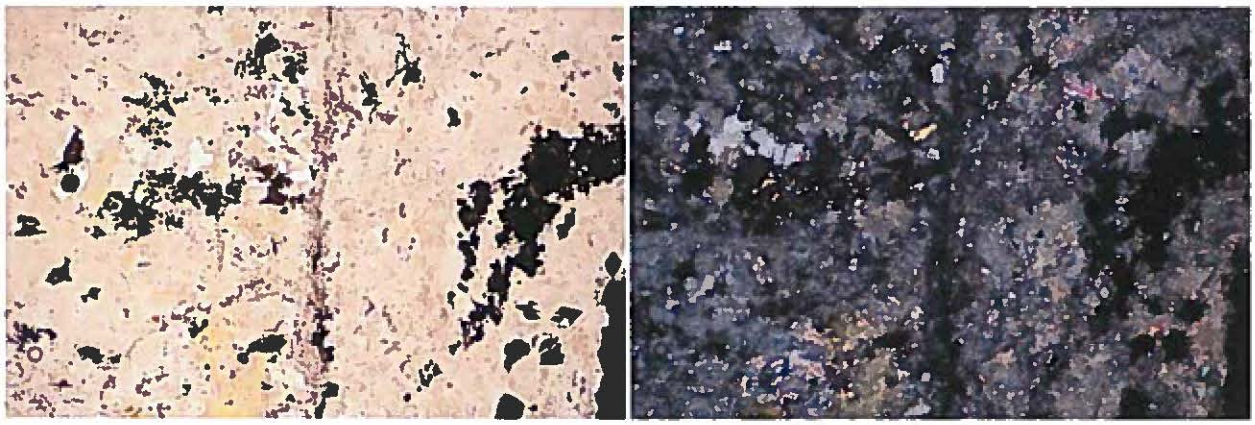


Figure 68. Photomicrographs of quartz and muscovite in the host rock in transmitted light, plane-polars (left) and crossed polars (right) (4x mag., F.O.V. ~3mm).

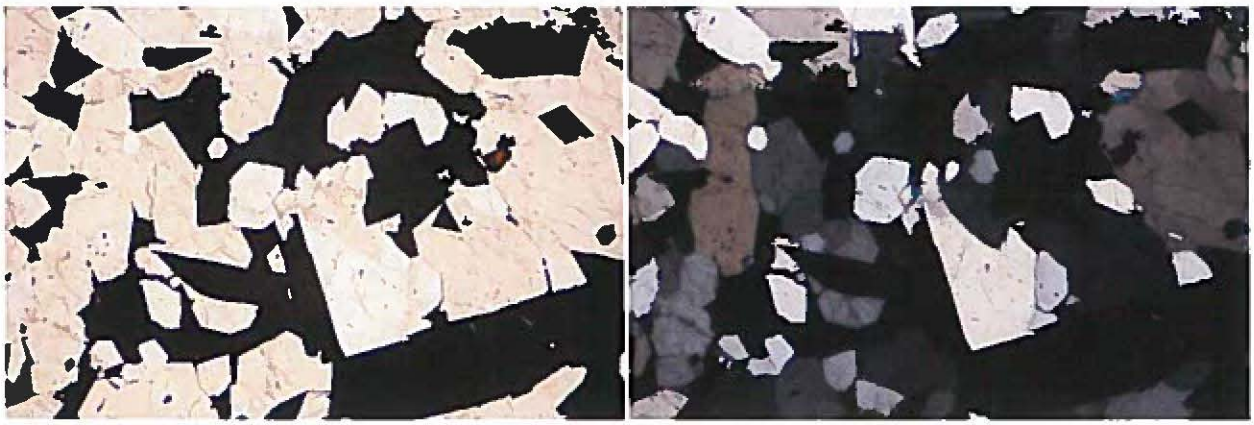


Figure 69. Photomicrographs of the quartz in the vein in transmitted light, plane-polars (left) and crossed polars (right) (4x mag., F.O.V. ~3mm).

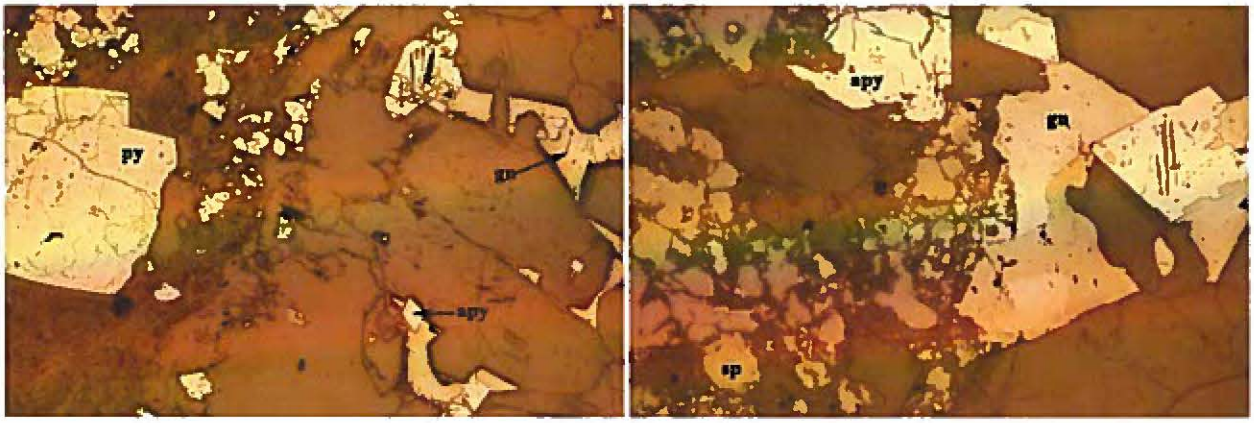


Figure 70. Photomicrographs of arsenopyrite, pyrite, sphalerite and galena in reflected light (4x mag., F.O.V. ~3mm).

MIN-018

This section consists of an altered quartz vein cross-cutting a very altered host rock. The section consists of approximately 60% quartz, 33% quartz and muscovite alteration mineralization, and 7% opaque minerals. The opaque minerals consist of 5% pyrite, 1% arsenopyrite, 1% sphalerite, and trace sulphosalt minerals.

Within the vein the quartz is fine- to very fine-grained, subhedral to anhedral crystals. Locally they are altered by an extremely fine-grained, brownish mineral that could not be identified, as well as alteration by muscovite (Fig. 71). Within the host rock the quartz is aphanitic to very fine-grained and is being altered by muscovite (Fig. 72).

Sulphide and sulphosalt minerals include pyrite, arsenopyrite, sphalerite, freibergite, boulangerite, and pyrargyrite. Locally they appear to be infilling around quartz crystals. The pyrite occurs as fine-grained, anhedral crystals that are commonly being replaced by a Fe-As-oxide or rimmed by arsenopyrite (Figs. 73, 75, and 76). Pyrite occurs both in the host rock and the vein. Arsenopyrite is very fine-grained, subhedral to euhedral crystals, and is commonly observed rimming the pyrite. Sphalerite occurs as very fine-grained, anhedral crystals. Pyrargyrite is fine-grained, anhedral, and has a small Pb peak on EDX (Fig. 74). Boulangerite is very fine-grained and found associated with the possible pyrargyrite (Fig. 74). Freibergite occurs locally as very fine-grained, anhedral crystals (Fig. 75 and 76).

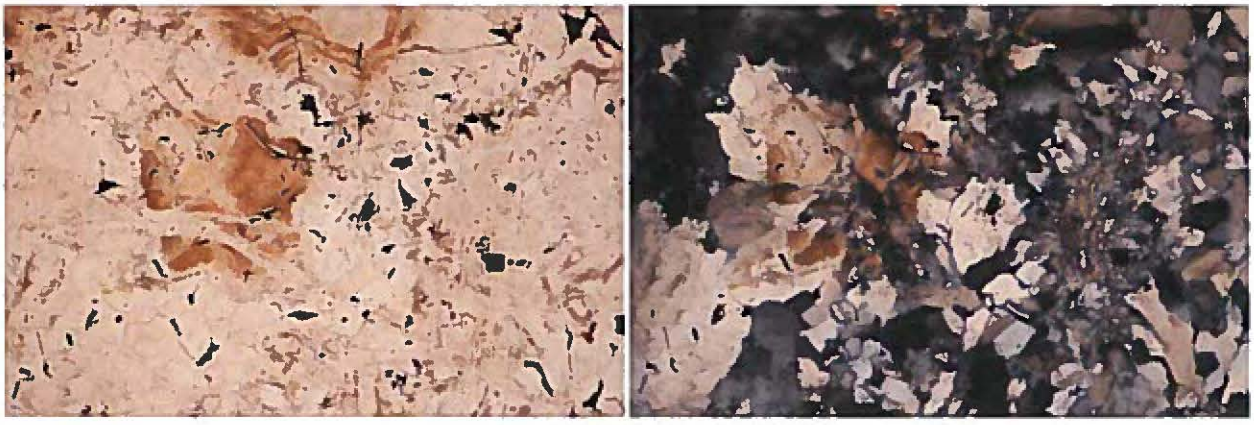


Figure 71. Photomicrographs of the quartz in the vein, muscovite, and brownish alteration in transmitted light, plane-polars (left) and crossed polars (right) (4x mag., F.O.V. ~3mm).

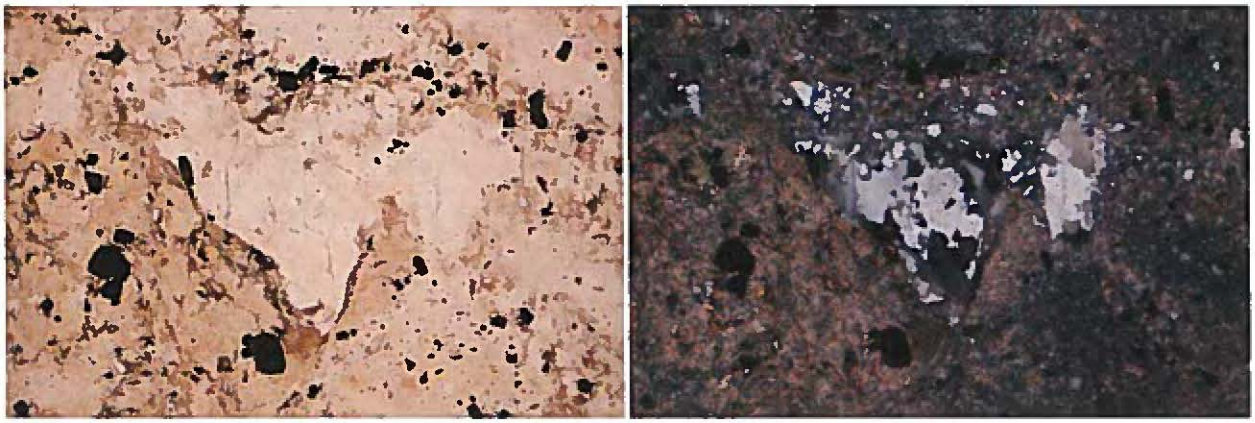


Figure 72. Photomicrographs of a relatively unaltered quartz pod in the host rock surrounded by muscovite and some very fine-grained quartz in transmitted light, plane-polars (left) and crossed polars (right) (4x mag., F.O.V. ~3mm).

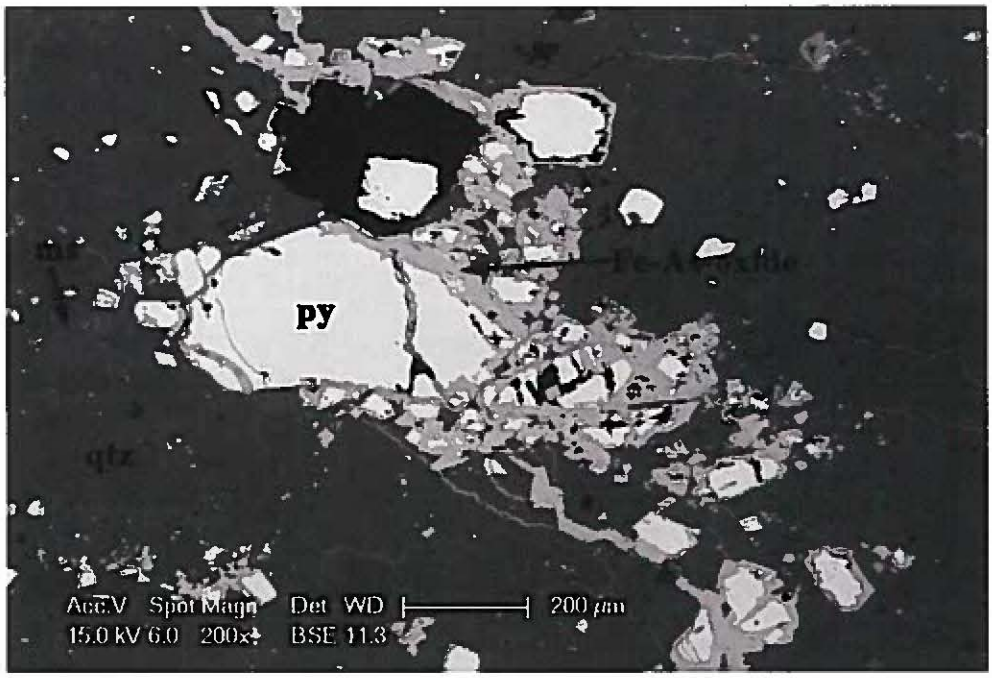


Figure 73. Backscattered electron image of pyrite altering to a Fe-As-oxide.

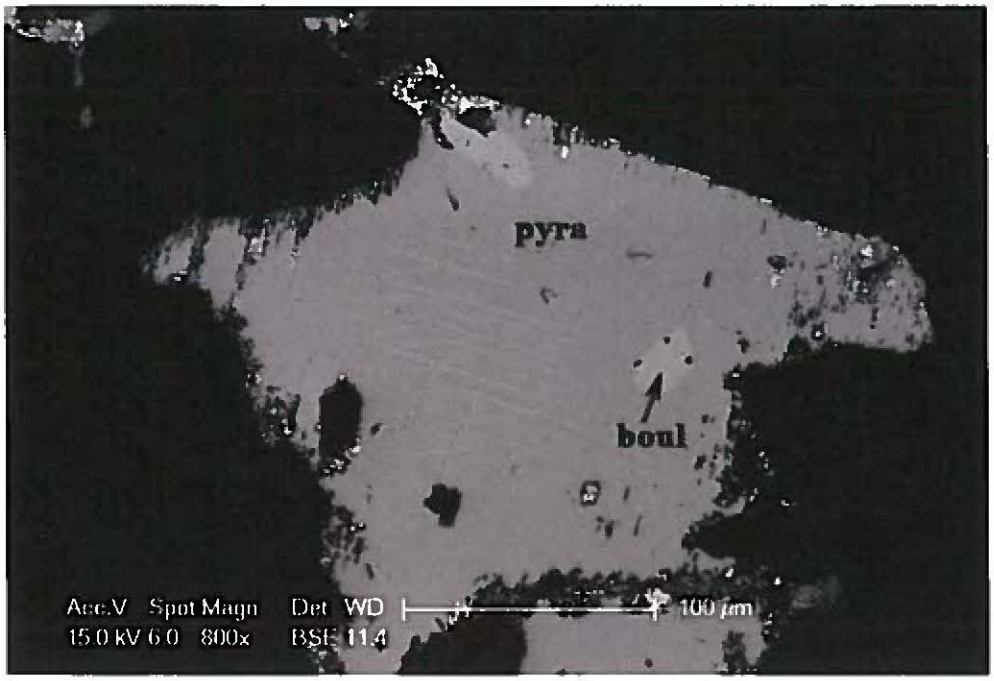


Figure 74. Backscattered electron image of pyrargyrite, and boulangerite.

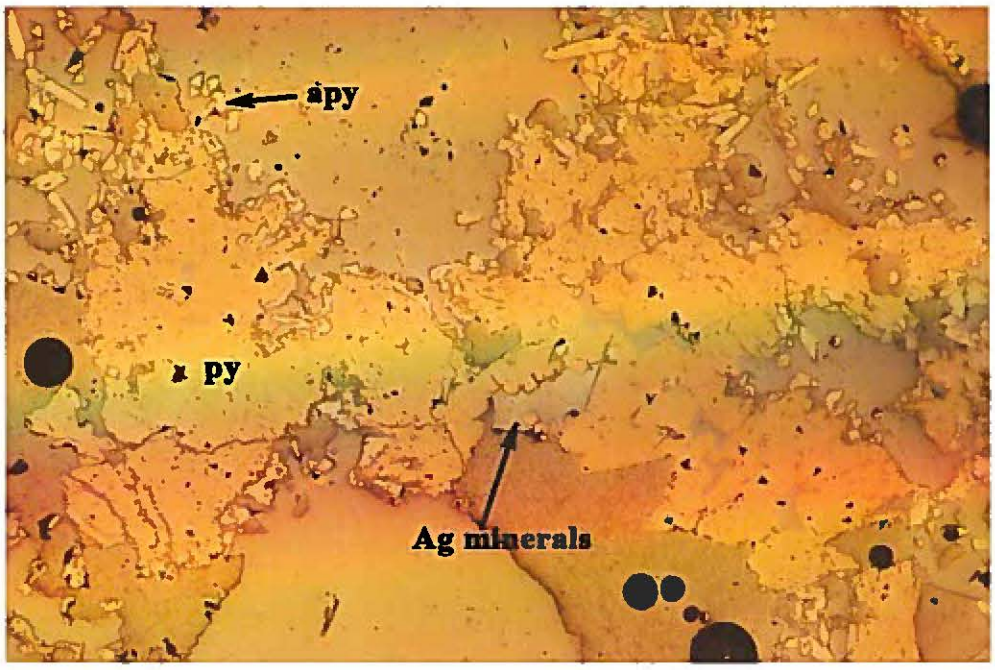


Figure 75. Photomicrograph of pyrite, arsenopyrite, and Ag-minerals in reflected light.

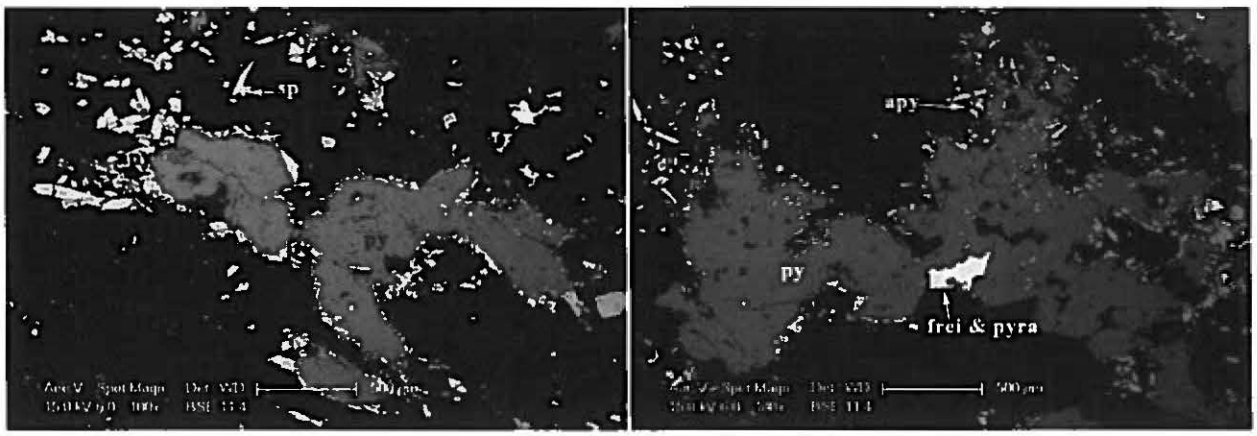


Figure 76. Backscattered electron images of pyrite and arsenopyrite with a small pod of freibergite and pyrargyrite.

MIN-019

The section consists of 57% quartz and muscovite alteration mineralization, 33% quartz and 10% opaque minerals. The opaque minerals consist of 6% pyrite, 3% arsenopyrite, and 1% galena.

The quartz in this section is largely aphanitic to very fine-grained (Fig. 77). There is one area and several pockets of fine-grained, subhedral to anhedral quartz. This may represent a former vein cutting through the host rock that has since been altered. The alteration mineralization consists of muscovite. This was confirmed using backscattered electron imaging and EDX.

Sulphide minerals include pyrite, arsenopyrite, and galena. Pyrite is very fine-grained and disseminated throughout as well as very fine-grained anhedral crystals being altered to a Fe-sulphate (Figs. 78 and 79). Local void space appears to be where pyrite may have once existed and has been altered away. Arsenopyrite occurs as very fine-grained clusters locally. Galena is very fine- to fine-grained, and is locally altered to a Pb-sulphate and a Pb-As-sulphate (Figs. 80 and 81).

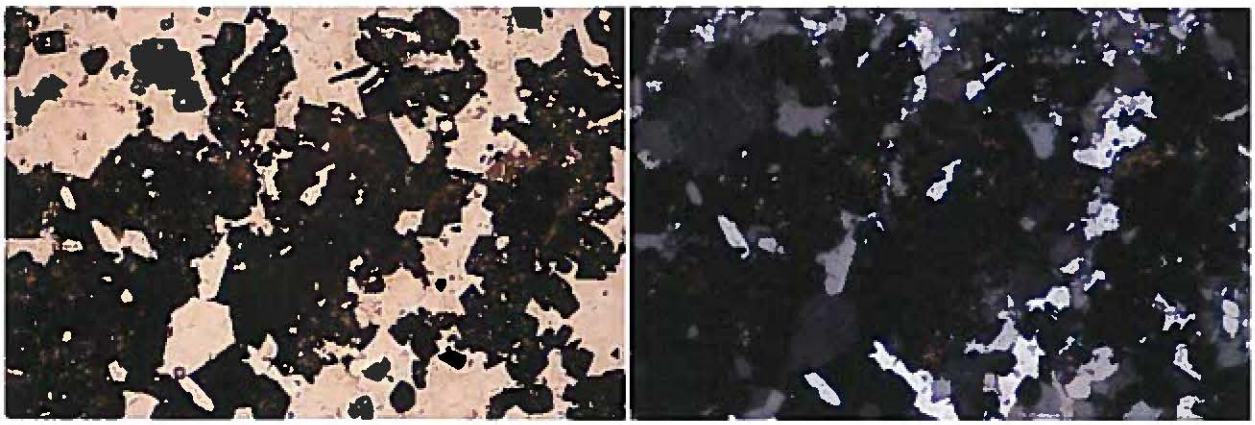


Figure 77. Photomicrographs of the fine-grained quartz with opaque minerals in transmitted light, plane-polars (left) and crossed polars (right) (4x mag., F.O.V. ~3mm).

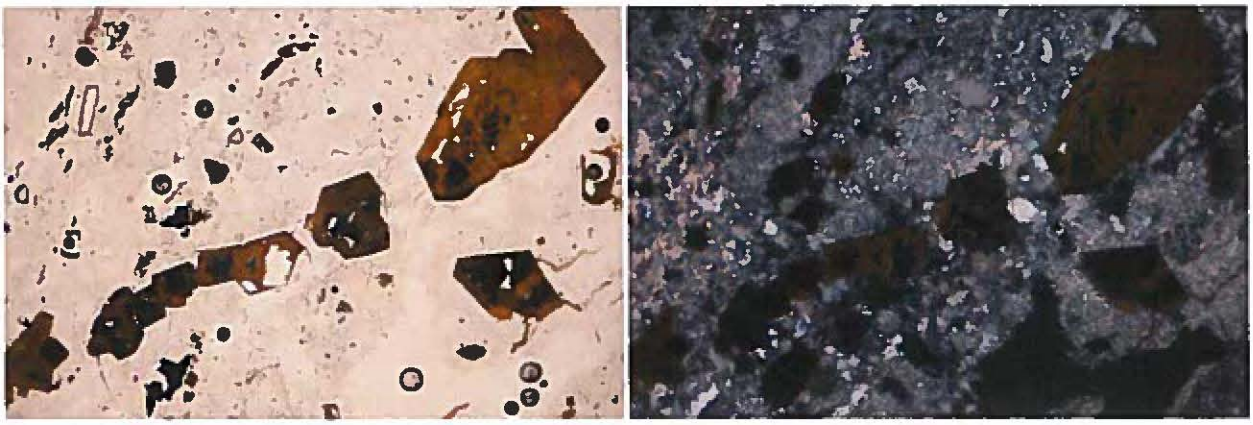


Figure 78. Photomicrographs of altered pyrite in the altered host rock in transmitted light, plane-polars (left) and crossed polars (right) (4x mag., F.O.V. ~3mm).

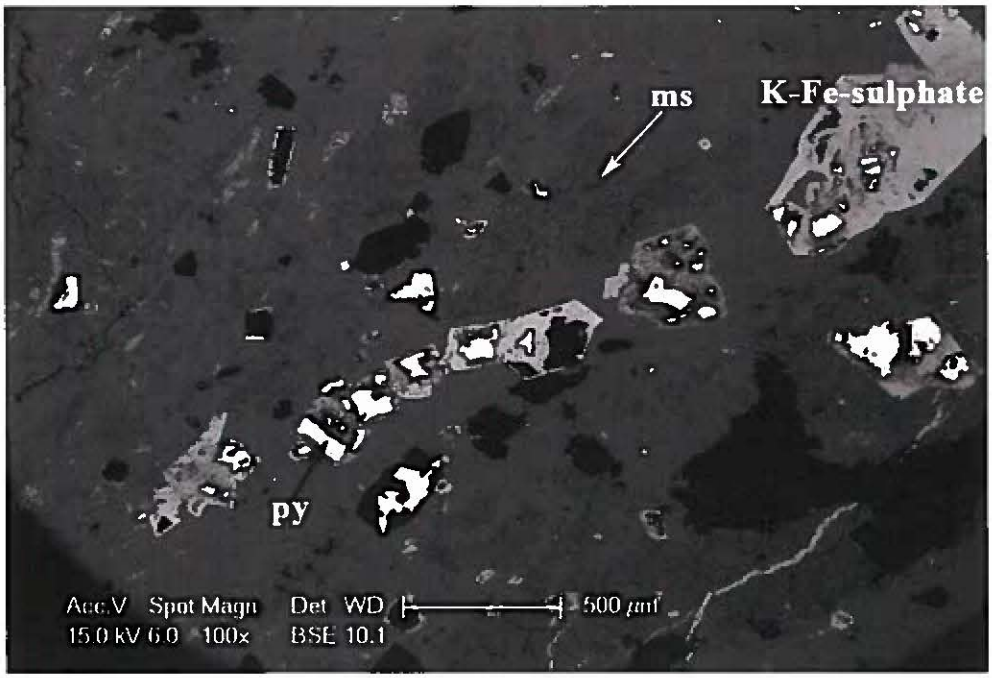


Figure 79. Backscattered electron image of Figure 80, showing pyrite altering to a K-Fe-sulphate and muscovite altering the quartz matrix.

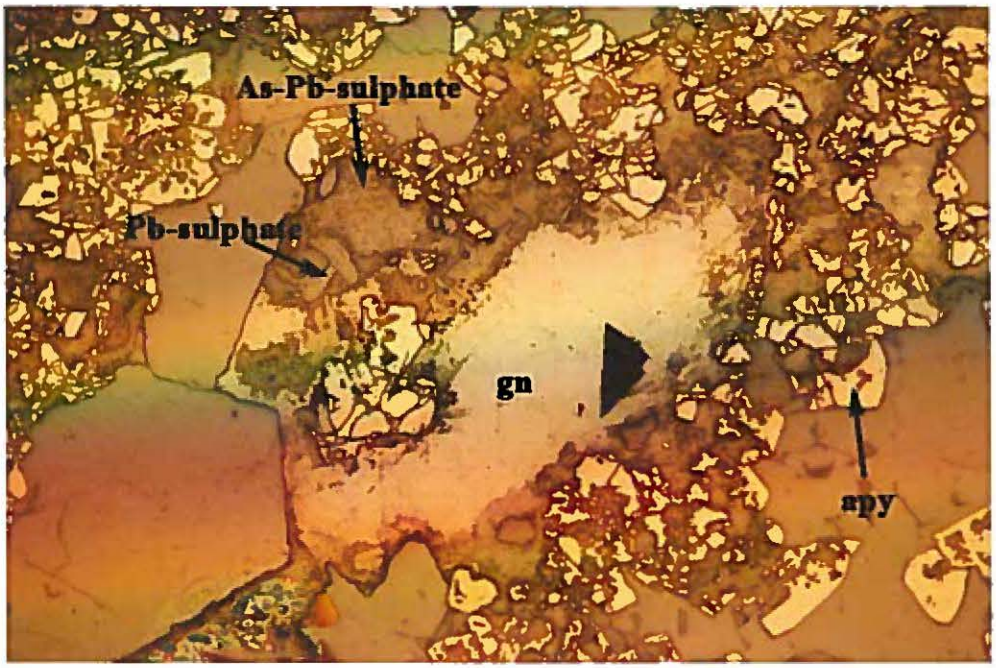


Figure 80. Photomicrograph of galena, arsenopyrite, Pb-sulphate, and an As-Pb-sulphate in reflected light (10x mag., F.O.V. 1.2mm).

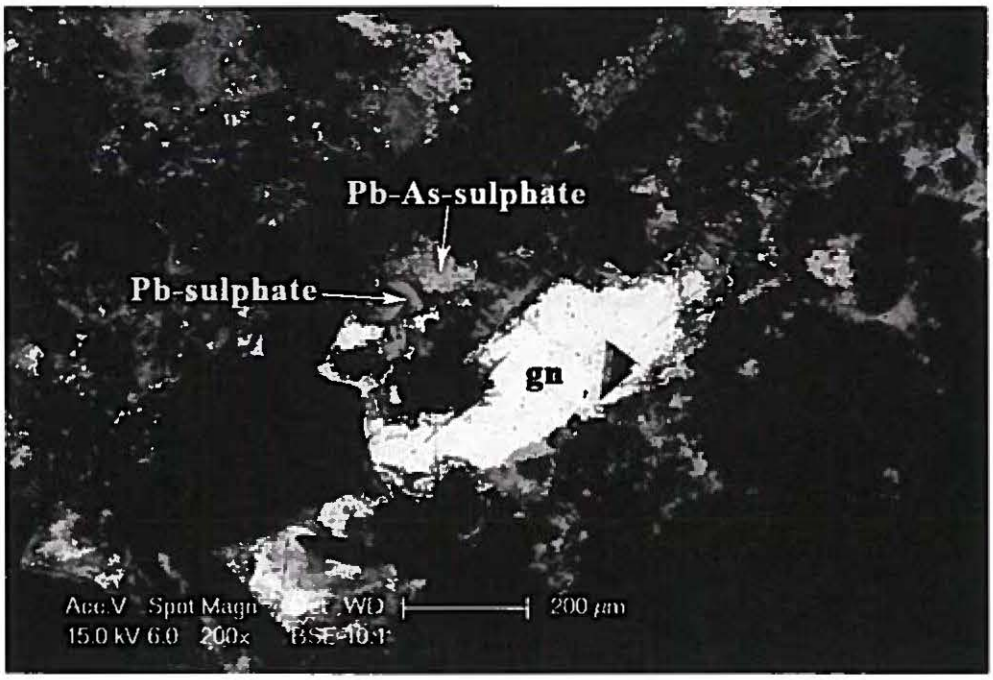


Figure 81. Backscattered electron image of Figure 78, showing galena, Pb-sulphate and Pb-As-sulphate.

MIN-020

This section has the majority of the opaque mineralization on one side of the section. The section consists of approximately 65% quartz and 35% opaque minerals. The opaque minerals include approximately 19% arsenopyrite, 10% pyrite, 5% sphalerite, 1% galena, and trace bournonite.

The quartz is fine- to very fine-grained around the opaque minerals (Fig. 82). The grain size increases from fine- to coarse-grained away from the opaque minerals. All of the quarts are anhedral to subhedral. Local, very fine-grained, recrystallized quartz occurs around some of the quartz crystals (Fig. 83).

Sulphide and sulphosalt minerals are concentrated on one half of the section (Fig. 84). Arsenopyrite is fine- to medium-grained subhedral to anhedral crystals that locally appear weakly fractured. Pyrite occurs locally as fine-grained, subhedral to euhedral crystals. The majority of the pyrite occurs in the quartz rich or near the quartz rich part of the section. Galena occurs as fine-grained crystals that are locally altered to a Pb-sulphate (Fig. 85). Local, very fine-grained, anhedral bournonite occurs.

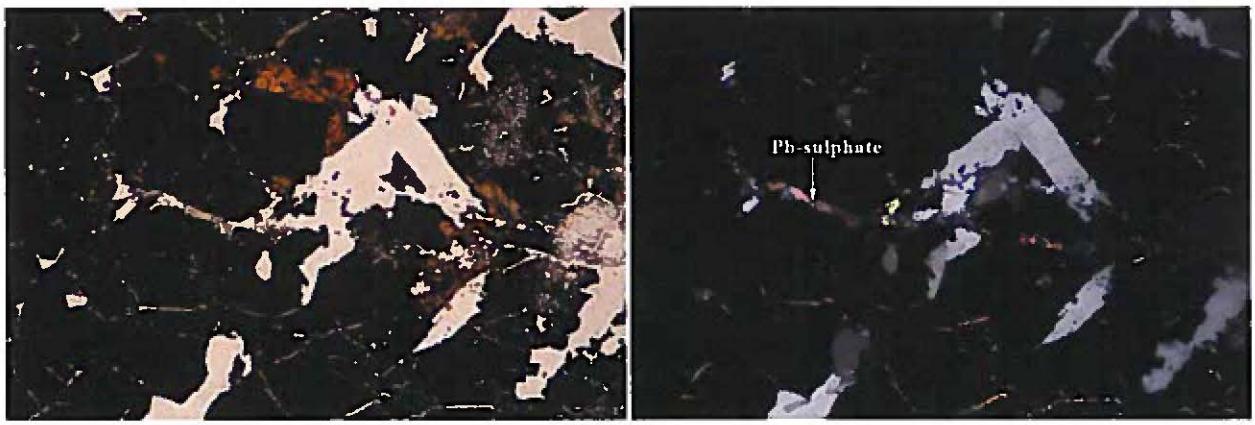


Figure 82. Photomicrographs of quartz among the sulphides and a Pb-sulphate mineral in transmitted light, plane-polars (left) and crossed polars (right) (4x mag., F.O.V. ~3mm).

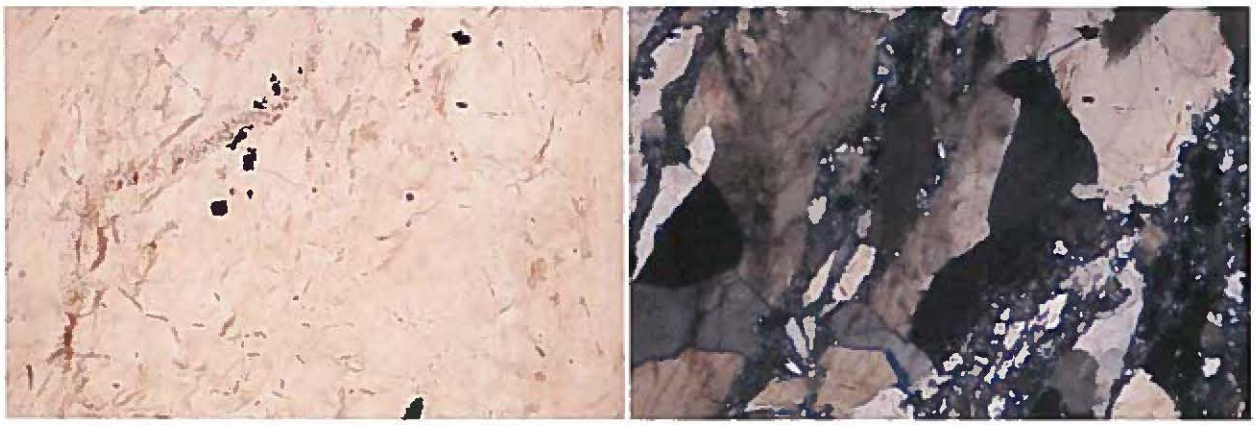


Figure 83. Photomicrographs of quartz with very fine-grained, recrystallized quartz in transmitted light, plane-polars (left) and crossed polars (right) (4x mag., F.O.V. ~3mm).

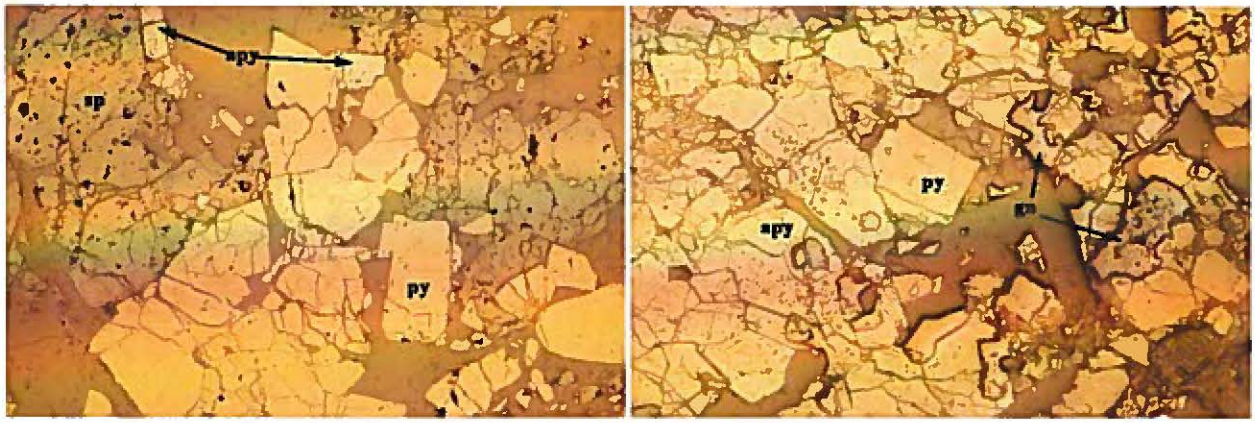


Figure 84. Photomicrographs of arsenopyrite, sphalerite, pyrite, and galena in reflected light (4x mag., F.O.V. ~3mm).

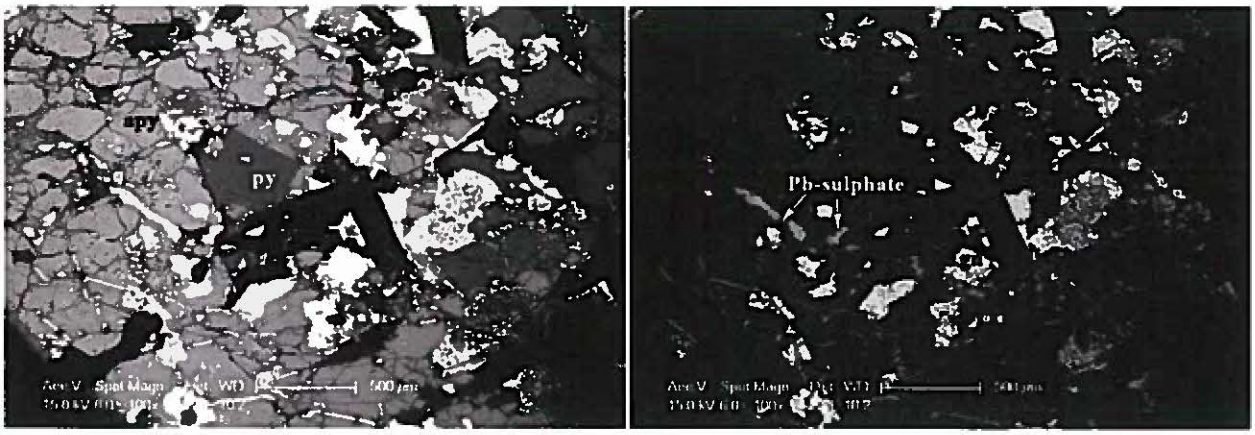


Figure 85. Backscattered electron images of arsenopyrite pyrite, galena and Pb-sulphate.

MIN-021

This section is very altered, and the alteration is complex. The section consists of approximately 75% quartz, and muscovite alteration mineralization, 12% quartz, 10% void space, and 3% opaque minerals. The opaque minerals consist of approximately 2% arsenopyrite, 1% pyrite and trace acanthite.

The quartz forms as fine-grained anhedral to subhedral pods, and as local crystals throughout the main type of alteration (Fig. 86). The remaining matrix is composed largely of aphanitic to very fine-grained quartz that is being altered by muscovite, Fe-oxide and Fe-As-oxide (discussed below). The muscovite is aphanitic to very fine-grained.

Sulphide minerals include arsenopyrite, pyrite and acanthite. Arsenopyrite is fine-grained, subhedral to euhedral crystals that is commonly replaced by a Fe-As-oxide (Figs. 87, 88. and 93). Pyrite is very fine-grained and occurs locally; generally in areas of the section that are more altered. Acanthite occurs locally as extremely fine-grained crystals with an unknown oxide and sulphate minerals (Fig. 89).

Several unknown minerals exist in this section. The most common one is a Fe-As-oxide that appears to result from the alteration of arsenopyrite (Figs. 90, and 91). This oxide has replaced most of the arsenopyrite in the section. It could be any number of Fe-As-oxides. One area of Fe-As-oxide mineralization had well formed crystals enabling it to be identified as symplesite ($Fe_3(AsO_4)_2 \cdot 8H_2O$) (Figs. 92 and 93); whether the rest of the Fe-As-oxide in the section is the same is not conclusive. Another unknown oxide mineral was found with an EDX spectrum of Fe-As-Sb-Au-Pb (Fig. 91). There are two unknown sulphate minerals that using EDX spectra have a chemistry of Fe-As-Ag-Sb-Au-Pb and Fe-As-Au-Pb (Figs. 89 and 93). These latter three minerals appear to host the majority of the Au in the polished section. No known analogues could be found for the latter three minerals.

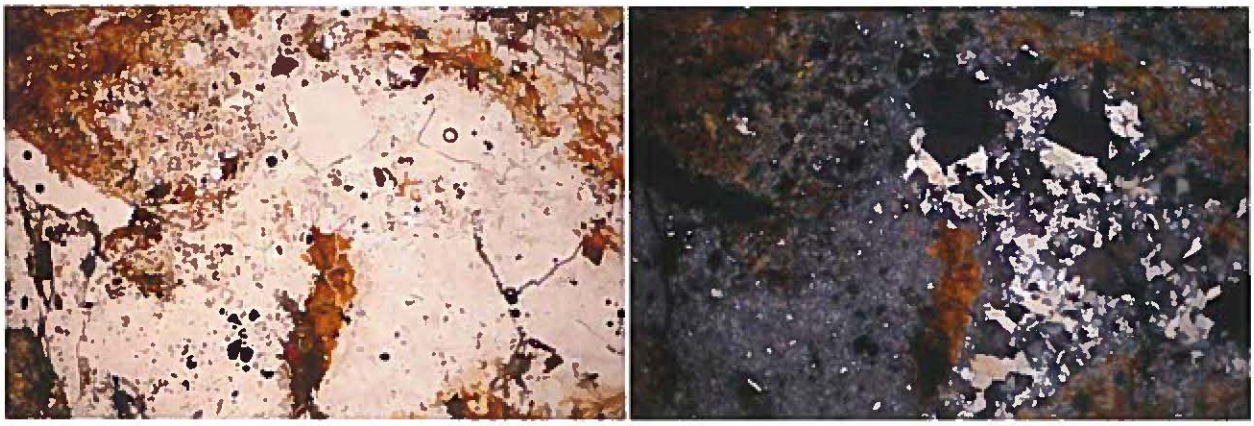


Figure 86. Photomicrographs of a fine-grained quartz pod in the host rock in transmitted light, plane-polars (left) and crossed polars (right) (2x mag., F.O.V. ~6mm).

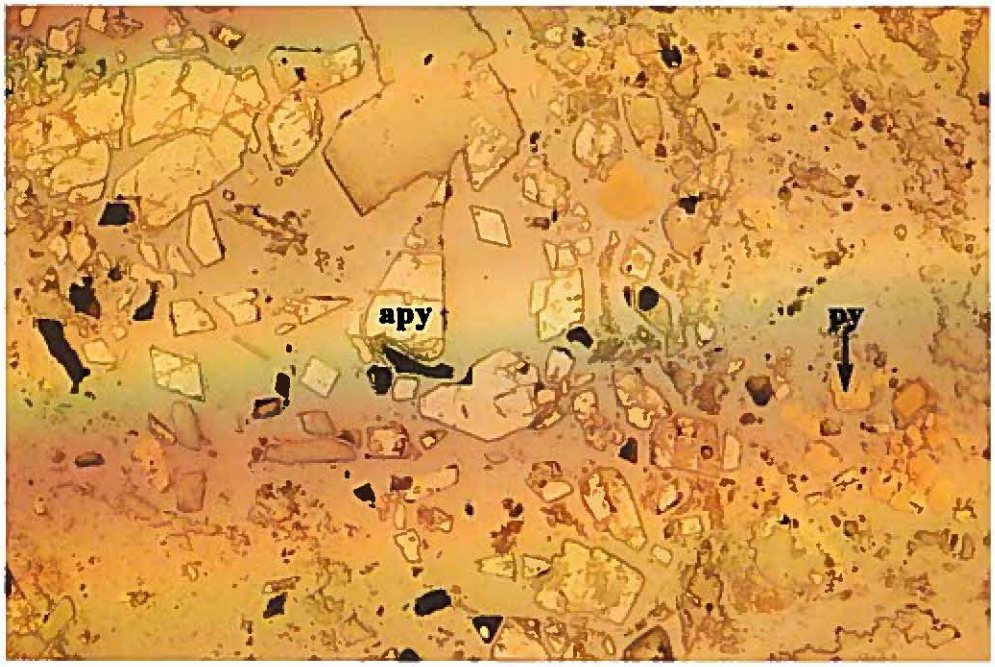


Figure 87. Photomicrograph of arsenopyrite and pyrite in reflected light (4x mag., F.O.V. ~3 mm).

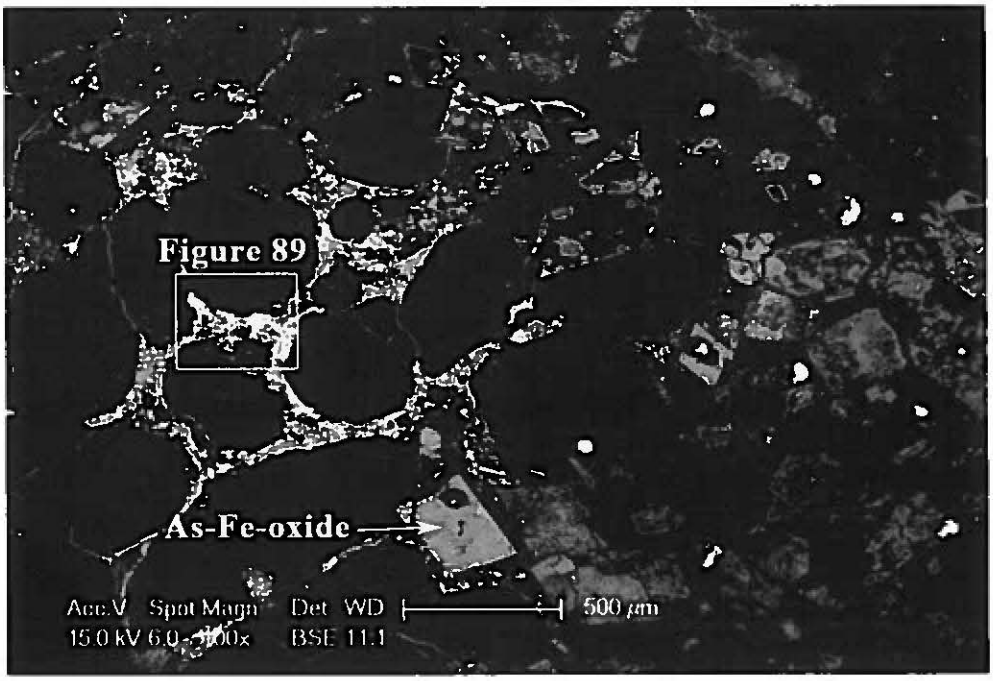


Figure 88. Backscattered electron image of an As-Fe-oxide mineral replacing a sulphide mineral.

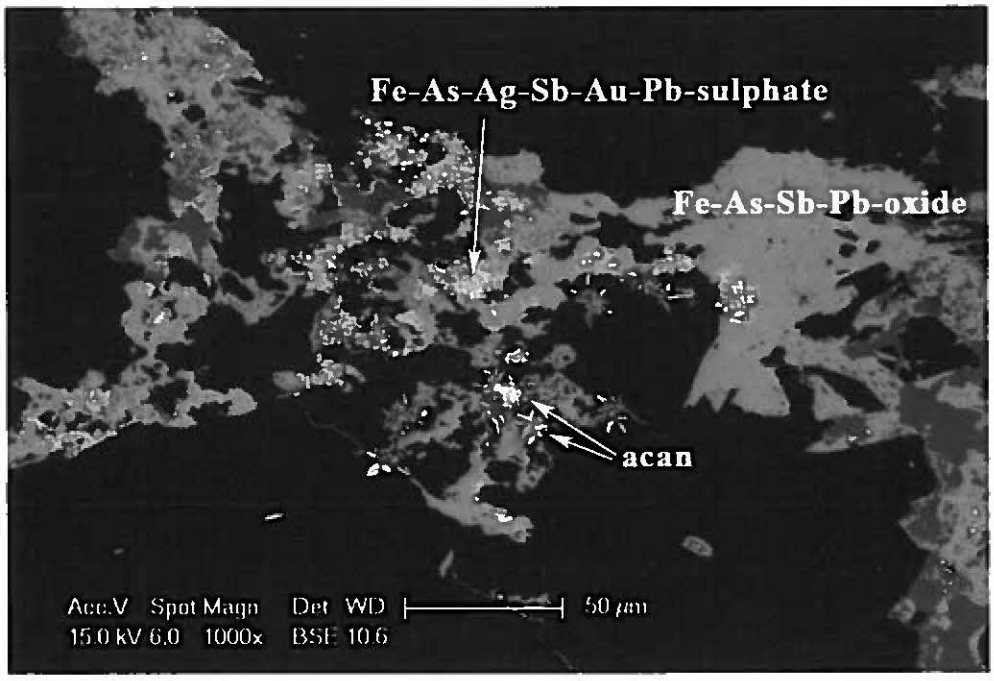


Figure 89. Backscattered electron image of acanthite, a Fe-As-Sb-Pb-oxide, and a Fe-As-Ag-Sb-Au-Pb-sulphate.

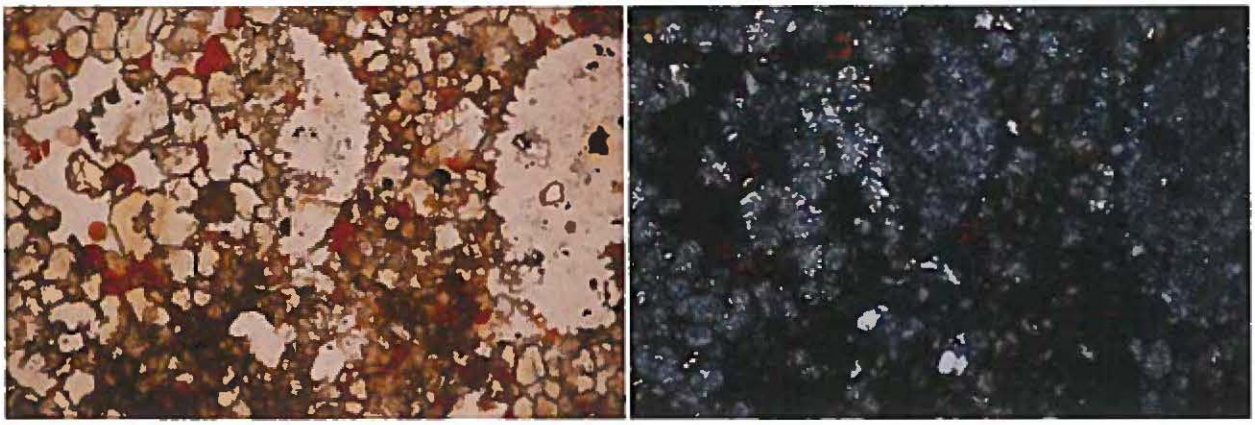


Figure 90. Photomicrographs of Fe-As-oxide grains with pods of aphanitic quartz in transmitted light, plane-polars (left) and crossed polars (right) (10x mag., F.O.V. ~1.2mm).

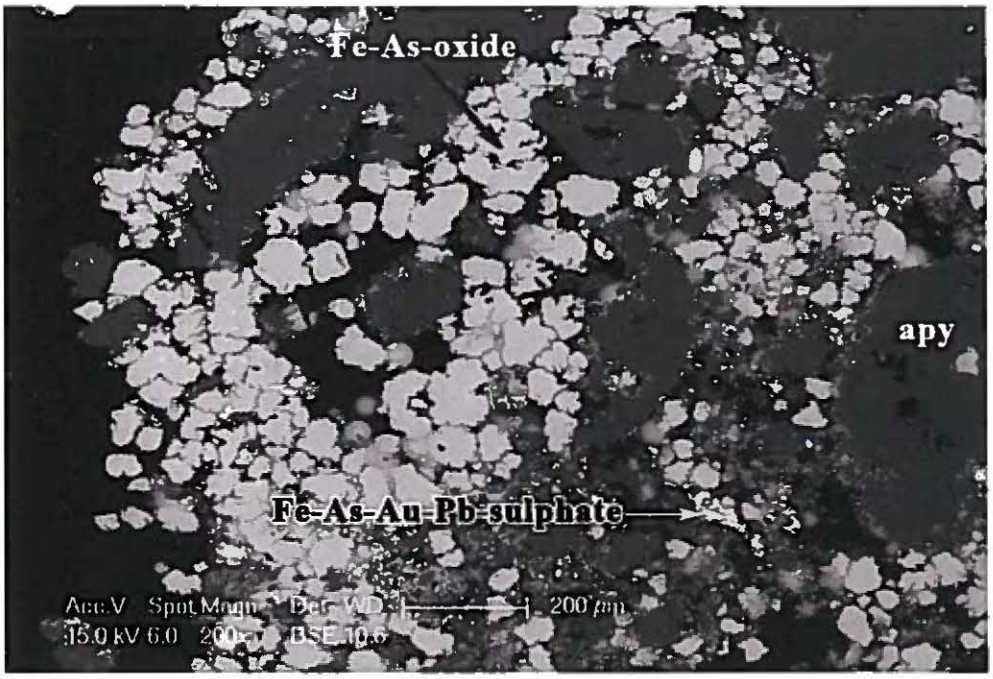


Figure 91. Backscattered electron image of Fe-As-oxide grains, and Fe-As-Au-Pb-sulphate.

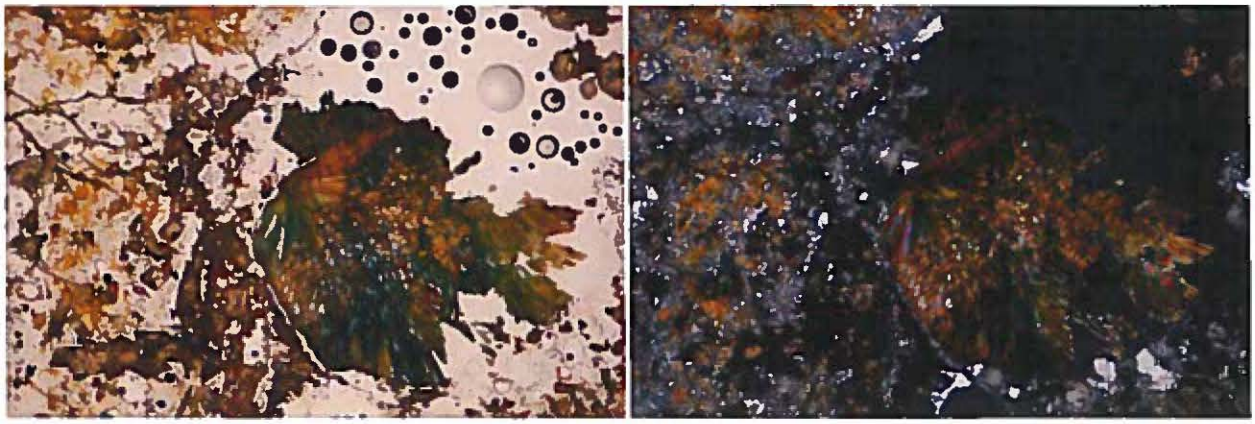


Figure 92. Photomicrographs of the Fe-As-oxide mineral symplesite (light brown to green) in transmitted light, plane-polars (left) and crossed polars (right) (4x mag., F.O.V. ~3mm).

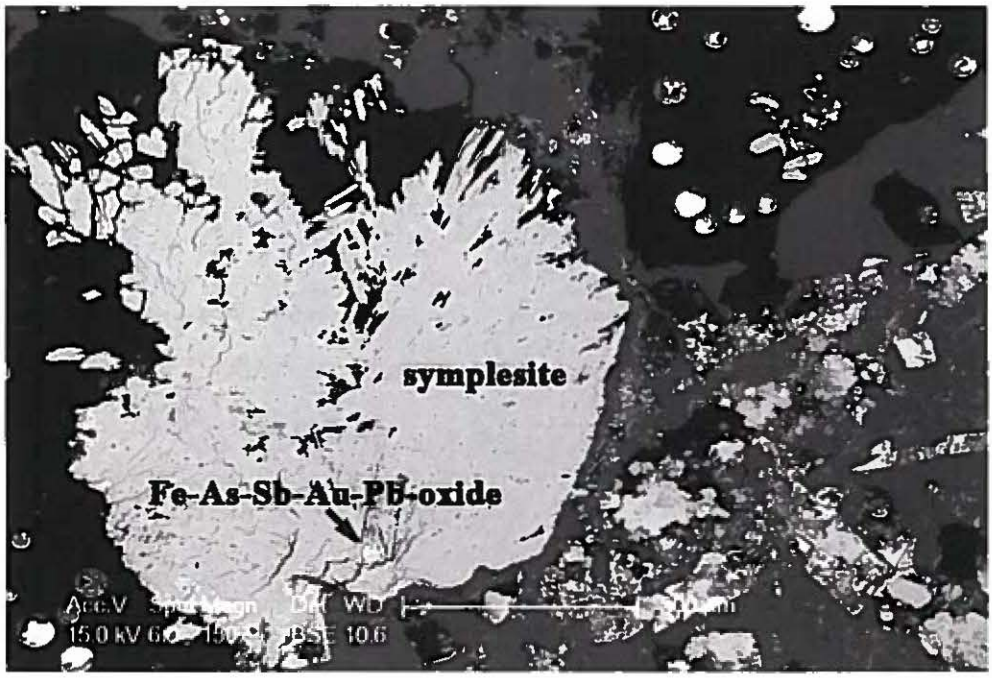


Figure 93. Backscattered electron image of Figure 91 showing symplesite and a Fe-As-Sb-Au-Pb-oxide.

MIN-022

This section consists of 55% quartz, 33% opaque minerals, 10% quartz, and muscovite alteration mineralization, and 2% calcite. The opaque minerals consist of 15% sphalerite, 9% arsenopyrite, 7% pyrite, and 2% galena.

The quartz varies from very fine- to medium-grained, anhedral to subhedral crystals (Fig. 94). The crystals appear to be more euhedral closer to the sulphides and away from the areas of increased alteration. Areas that are altered have very fine-grained to aphanitic quartz and muscovite (Fig. 95). Locally the muscovite is pervasive.

Sulphide minerals generally form in small aggregates together (Fig. 96). The sphalerite commonly appears zoned with a dark brown core and a red-brown rim. The sphalerite is coarse- to fine-grained, euhedral to anhedral crystals. The pyrite is very fine- to fine-grained, subhedral to euhedral crystals. Pyrite is the only sulphide to occur in the areas that are pervasively altered with muscovite. The arsenopyrite occurs in local clusters as fine-grained, subhedral to euhedral crystals. Local fine-grained galena also occurs, and at times it appears to infilling amongst the quartz grains.

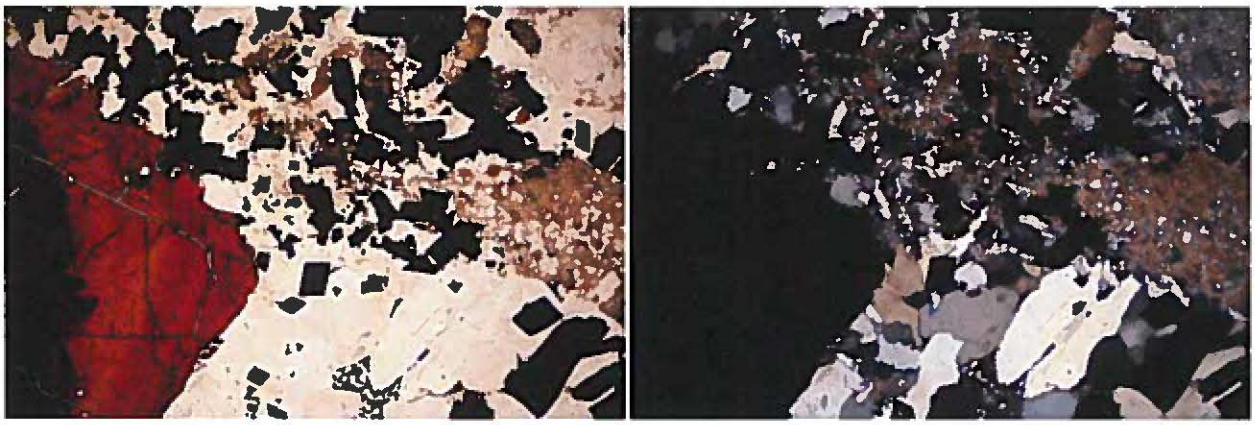


Figure 94. Photomicrographs of sphalerite (brown), quartz and muscovite enriched areas in transmitted light, plane-polars (left) and crossed polars (right) (2x mag., F.O.V. ~6mm).

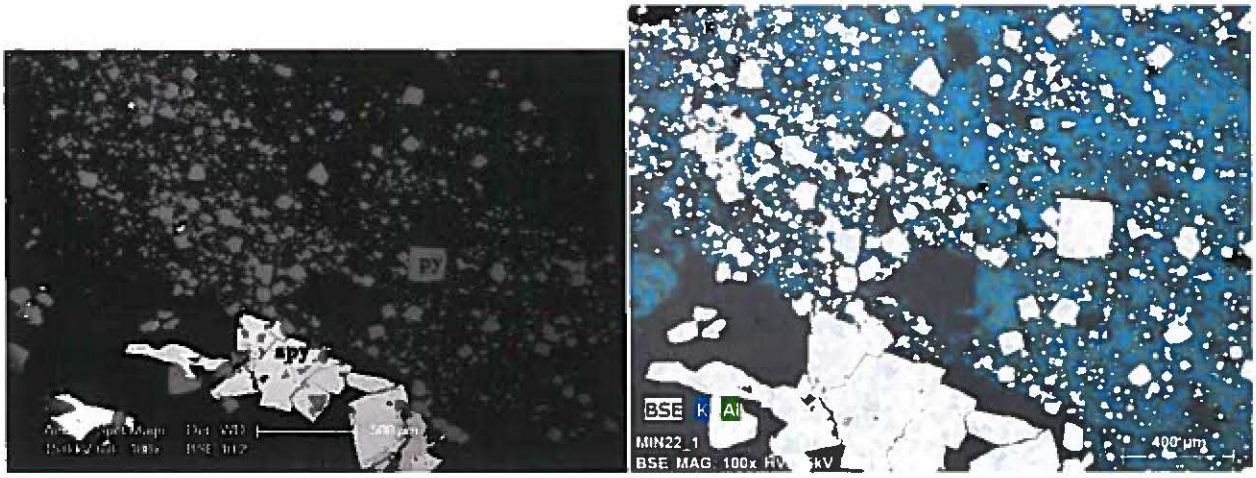


Figure 95. Backscattered electron image (left) and electron map (right) showing pyrite, arsenopyrite, and muscovite.

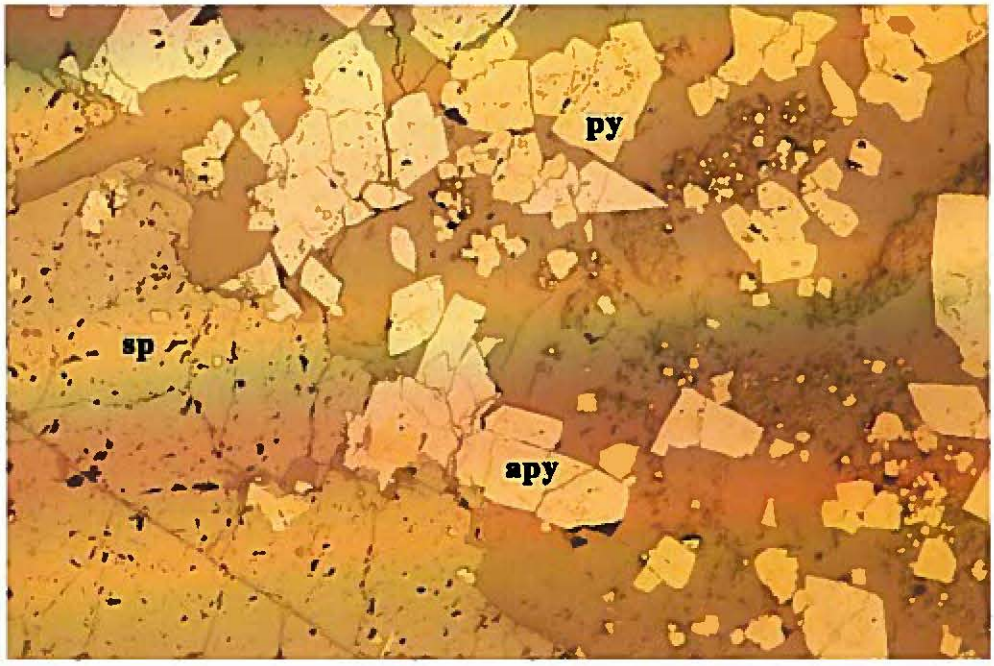


Figure 96. Photomicrograph of sphalerite, arsenopyrite and pyrite in reflected light (4x mag., F.O.V. ~3mm).

MIN-023

This section shows the altered host rock with a cross-cutting quartz veinlet and quartz-sulphide veinlet. The section consists of approximately 50% quartz and muscovite alteration mineralization, 25% opaque mineralization, 19% quartz, 3% ankerite, and 3% void space. The opaque minerals include 15% arsenopyrite, 8% pyrite, and 2% sphalerite.

The host rock consists of aphanitic to very fine-grained quartz, with aphanitic to locally very fine-grained muscovite (Fig. 97). There are local concentrated areas where the very fine-grained quartz dominates. Quartz within the veinlet separating the host rock from the sulphide vein, along with the sulphide vein itself is fine-grained. The cross-cutting veinlet is rimmed by very fine-grained, ankerite at the contact with the host rock, and sulphide vein (Fig. 98).

The sulphides predominately occur within the sulphide vein; however, pyrite is disseminated throughout the host rock. The pyrite occurs as fine-grained, subhedral crystals. Arsenopyrite occurs as fine- to very fine-grained, subhedral to euhedral crystals (Fig. 99). Sphalerite is a reddish-brown colour, with fine-grained, anhedral crystals.

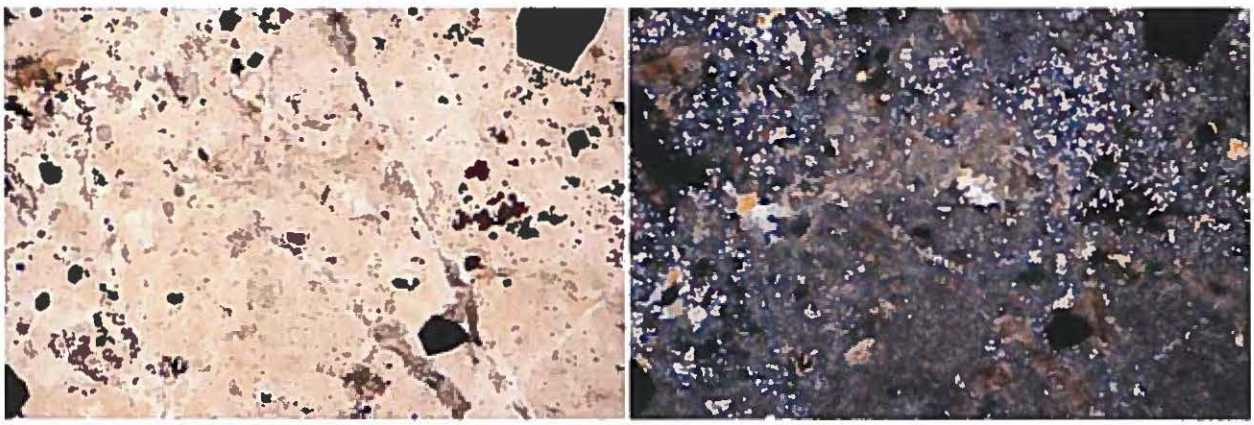


Figure 97. Photomicrographs of the host rock with quartz, and muscovite alteration in transmitted light, plane-polars (left) and crossed polars (right) (4x mag., F.O.V. ~3mm).

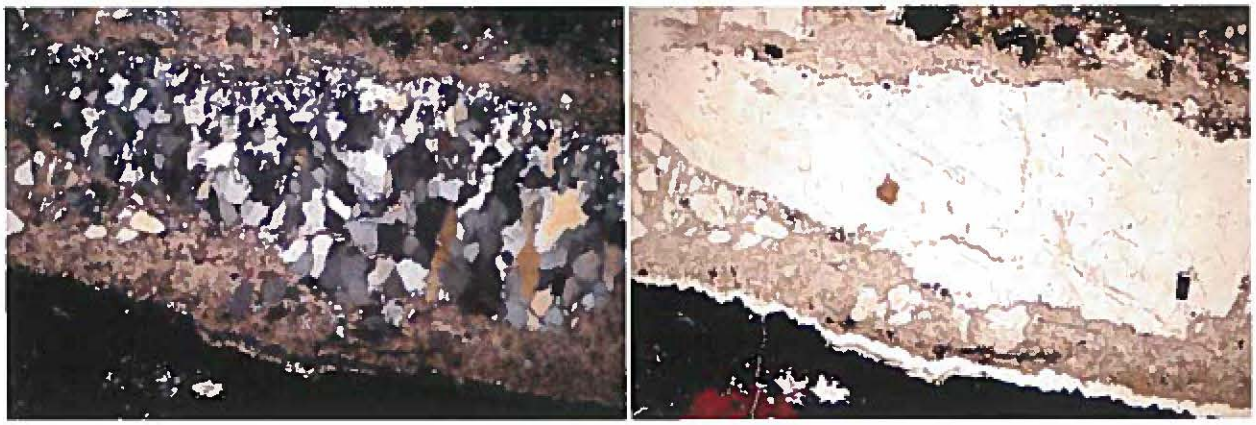


Figure 98. Photomicrographs of the cross-cutting quartz vein with ankerite at the contact between the host rock and sulphide vein in transmitted light, plane-polars (left) and crossed polars (right) (2x mag., F.O.V. ~6mm).

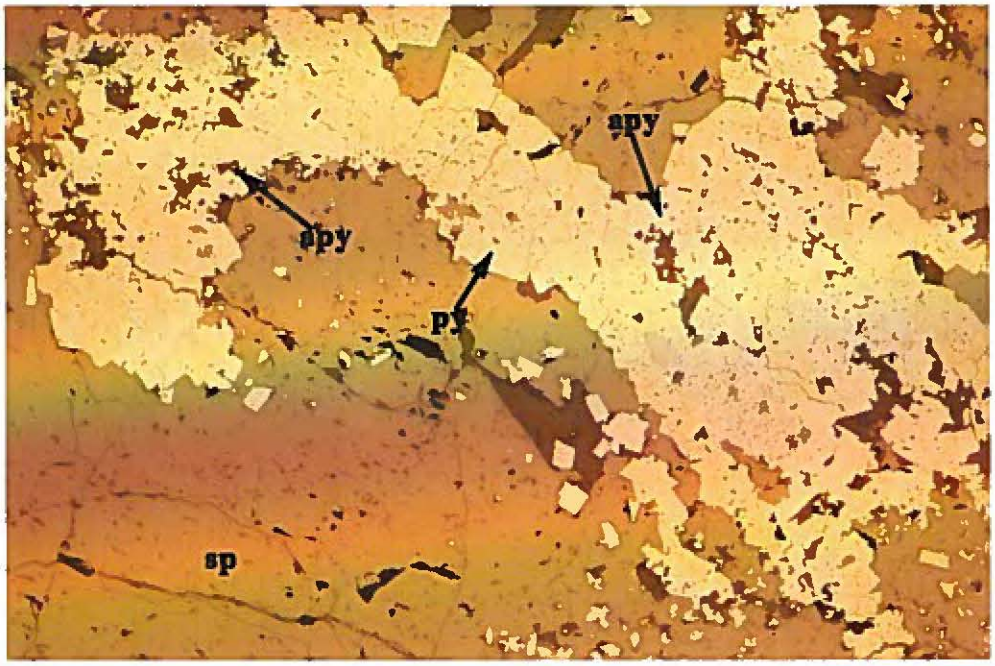


Figure 99. Photomicrograph of arsenopyrite, pyrite, and sphalerite within the sulphide vein in reflected light (4x mag., F.O.V. ~3mm).

MIN-024A

This section shows the host rock intersected by two quartz-sulphide veins. The section consists of approximately 50% aphanitic alteration mineralization, 40% quartz and 10% sulphide mineralization. The sulphide minerals consist of approximately 6% arsenopyrite, 3% pyrite, and 1% galena and sphalerite.

The host rock consists of aphanitic to very fine-grained quartz with muscovite alteration. There are areas where there are greater concentrations of very fine-grained quartz, and within these areas there is very little pyrite mineralization (Fig. 100). The muscovite is aphanitic to very fine-grained and is locally concentrated. The quartz within the veins is fine-grained, subhedral to anhedral crystals.

The sulphide mineralization occurs predominately in the veins, but pyrite does occur within the host rock and was not observed in the veins. The pyrite is most concentrated in areas of ore intense muscovite alteration, where individual quartz grains are still locally visible, rather than all aphanitic. Arsenopyrite dominates the veins as very fine-grained to fine-grained, subhedral to euhedral crystals (Fig. 101). Sphalerite occurs locally as fine-grained, anhedral crystals. Galena occurs as very fine- to fine-grained, rounded crystals infilling amongst the other minerals within the vein.

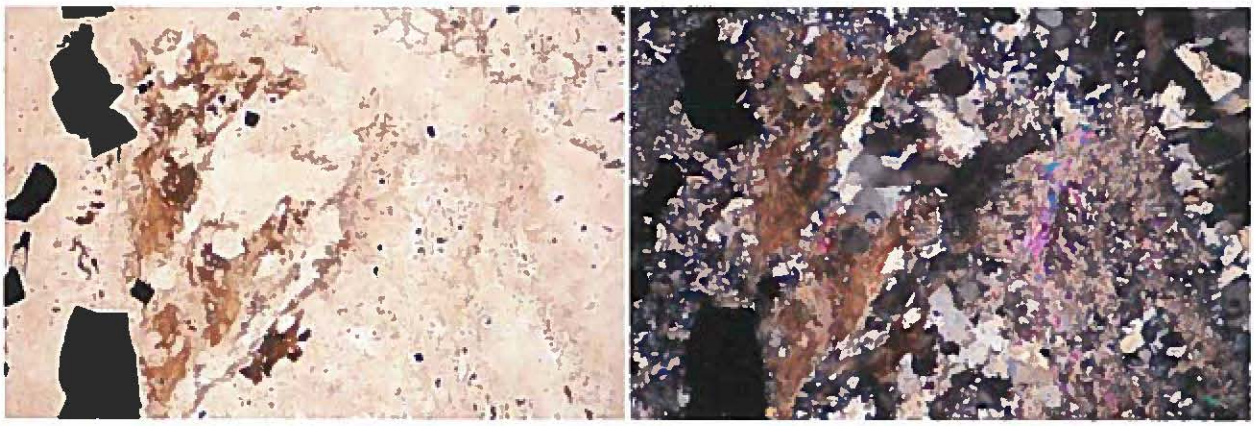


Figure 100. Photomicrographs of the host rock with quartz, and areas of concentrated muscovite alteration in transmitted light, plane-polars (left) and crossed polars (right) (4x mag., F.O.V. ~3mm).

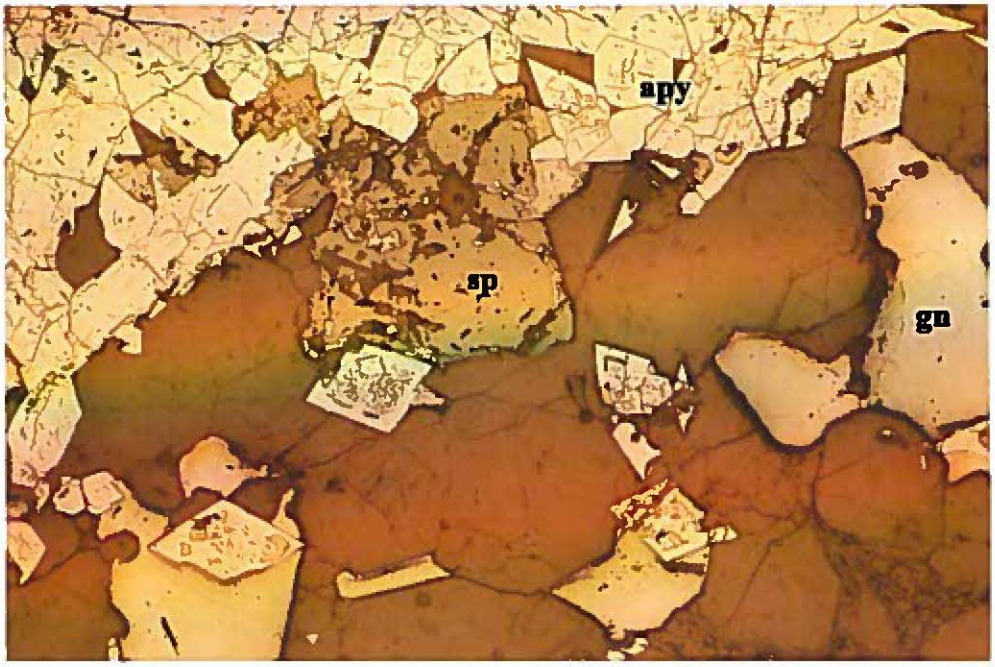


Figure 101. Photomicrograph of the arsenopyrite, sphalerite and galena within the vein in reflected light (4x mag., F.O.V. ~3mm).

MIN-024B

This section shows the host rock intersected by a quartz-sulphide vein. The section consists of approximately 50% opaque minerals, 35% quartz, and 15% aphanitic alteration mineralization. Opaque minerals consist of approximately 35% arsenopyrite, 8% pyrite, 5% boulangerite (and other sulphosalt minerals), 2% sphalerite, and trace galena.

Within the vein the quartz is very fine- to fine-grained anhedral to subhedral crystals (Fig. 102), and within the host rock the quartz is aphanitic to very fine-grained, anhedral crystals. The very fine-grained crystals are concentrated in certain areas (Fig. 103). The alteration consists predominately of muscovite.

Pyrite preferentially occurs in certain areas of strong muscovite alteration where individual quartz veins are still observed (Fig. 104). Although pyrite is the most common mineral to occur in the host rock; however, near the contact with the sulphide vein a few crystals of arsenopyrite, and boulangerite were observed. This area is also strongly altered by muscovite.

Sulphide and sulphosalt minerals include pyrite, sphalerite, arsenopyrite, galena, pyrargrite, bournonite, and boulangerite (Figs. 105 and 106). Pyrite occurs as fine-grained anhedral to subhedral crystals. Arsenopyrite occurs as fine-grained, subhedral crystals that are locally fractured. Sphalerite occurs as reddish-brown, medium- to coarse-grained, anhedral crystals. Galena is very fine-grained, and commonly occurs with the sulphosalt minerals. Boulangerite forms as very fine-grained crystals, but forms large masses infilling around the sulphide minerals (Fig. 106). Bournonite, and pyrargrite are very fine-grained, anhedral crystals that occur locally associated with boulangerite (Fig. 104).

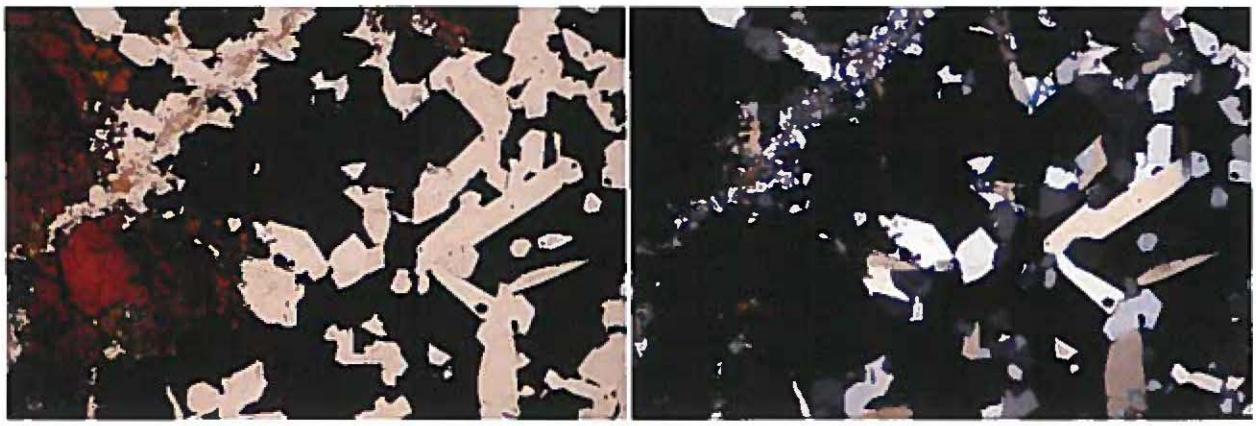


Figure 102. Photomicrographs of the quartz and sphalerite within the sulphide vein, in transmitted light, plane-polars (left) and crossed polars (right) (4x mag., F.O.V. ~3mm).

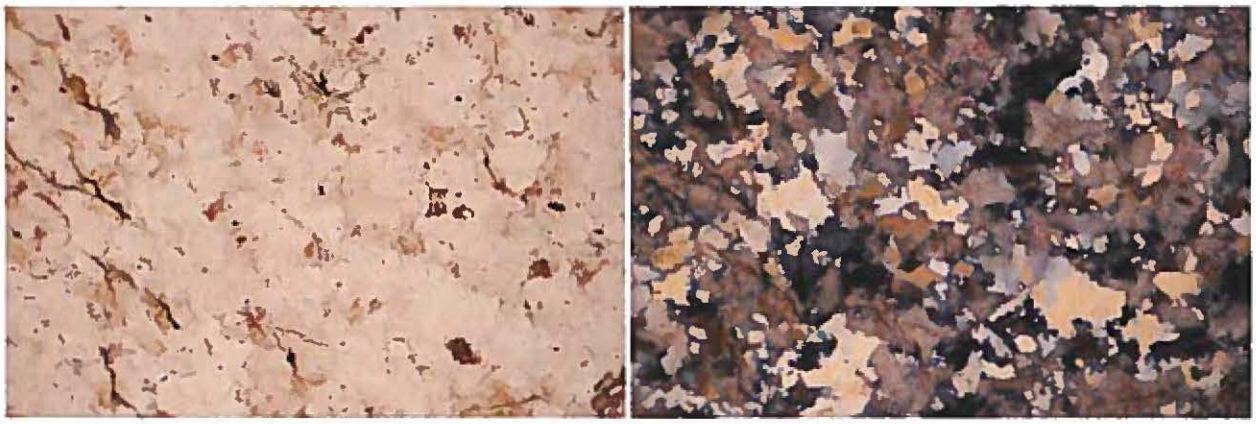


Figure 103. Photomicrographs of the host rock in an area that is concentrated with fine-grained quartz, muscovite alteration, and little pyrite in transmitted light, plane-polars (left) and crossed polars (right) (4x mag., F.O.V. ~3mm).

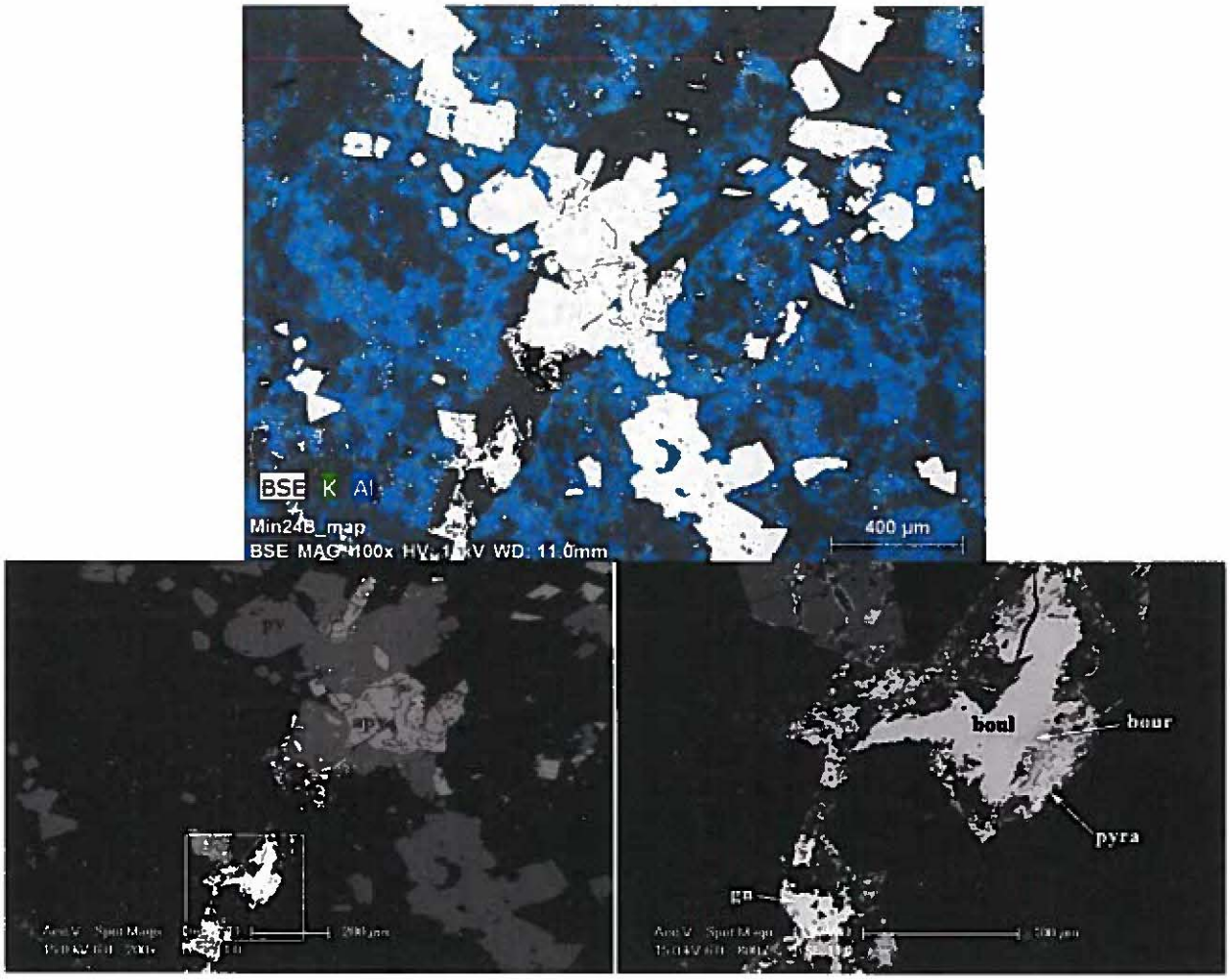


Figure 104. Electron map (top) and backscattered electron images (bottom) of muscovite alteration (blue), pyrite, arsenopyrite, boulangerite, bournonite, and pyrargite.

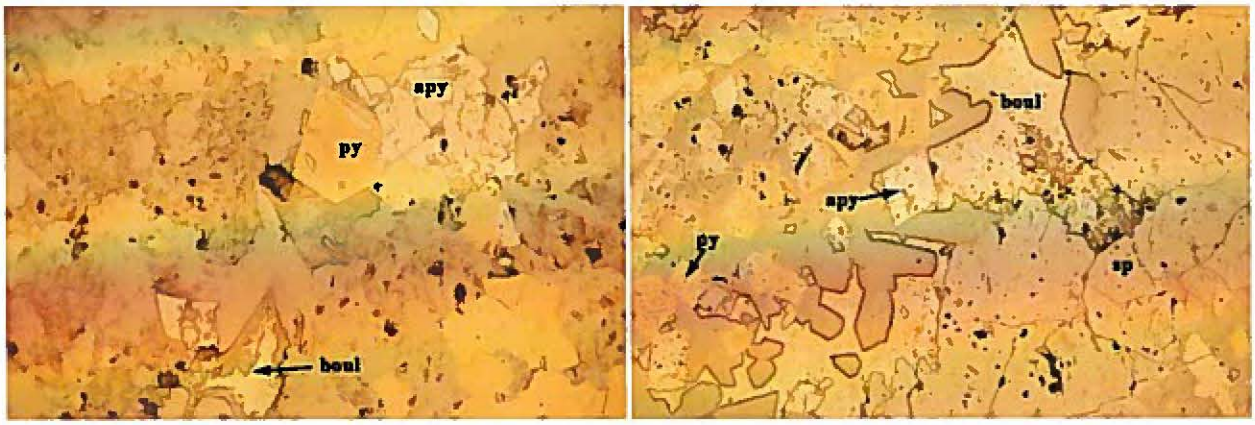


Figure 105. Photomicrographs of sulphide mineralization within the vein in reflected light: left: arsenopyrite, pyrite, and boulangerite (10x mag., F.O.V. ~1.2mm). right: arsenopyrite, pyrite, sphalerite and boulangerite (4x mag., F.O.V. ~3mm).

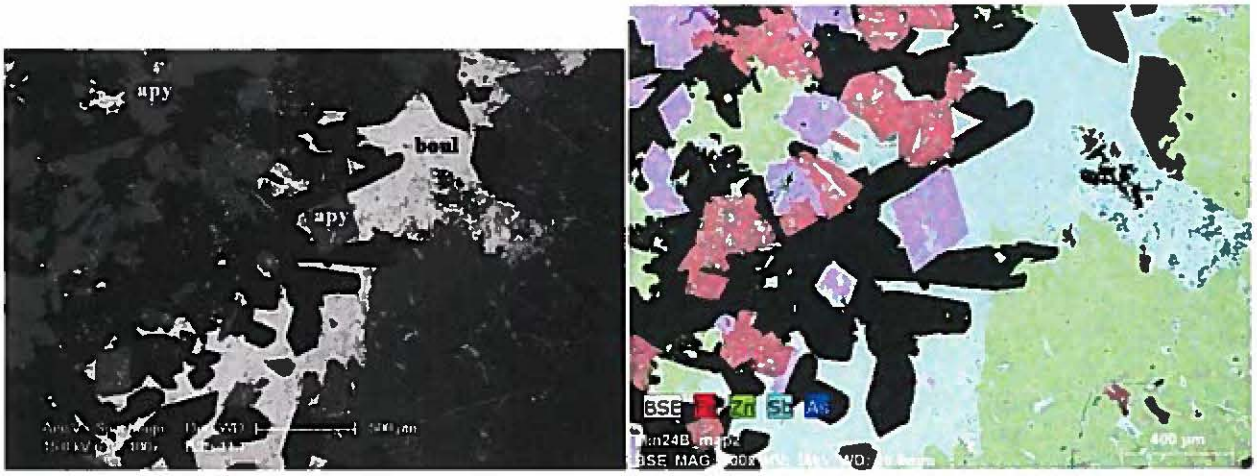


Figure 106. Backscattered electron image (left) and electron map (right) of arsenopyrite, sphalerite, pyrite, and boulangerite.

MIN-025

This section consists of 60% quartz and muscovite alteration minerals, 15% quartz, 15% opaque minerals, and trace apatite. The opaque minerals consist of 12% pyrite and 3% arsenopyrite.

The main part of the section consists of aphanitic to very fine-grained quartz and muscovite. Locally there are areas of very fine- to fine-grained quartz with little alteration (Fig. 107).

Sulphide minerals include pyrite, sphalerite, arsenopyrite, and galena. Pyrite occurs as medium- to coarse-grained, subhedral crystals that locally has very fine inclusions of sphalerite and galena (Figs. 108 and 109). Arsenopyrite occurs locally as fine-grained, euhedral to subhedral crystals.

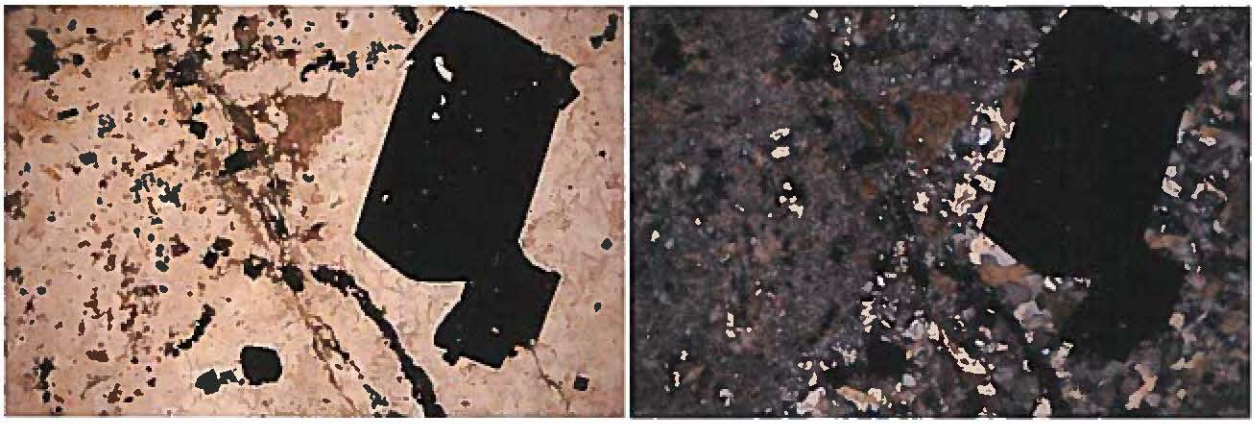


Figure 107. Photomicrographs of the dominant aphanitic rock and a local pod of very fine-grained quartz in transmitted light, plane-polars (left) and crossed polars (right) (2x mag., F.O.V. ~6mm).



Figure 108. Photomicrograph of pyrite, in reflected light (4x mag., F.O.V. ~3mm).

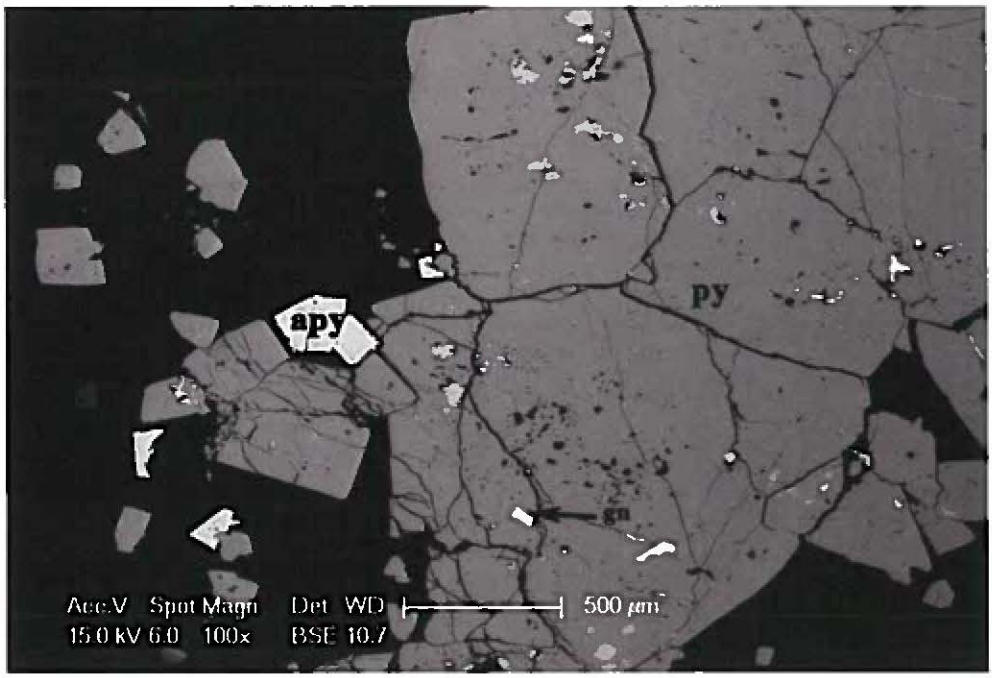


Figure 109. Backscattered electron image of pyrite and arsenopyrite.

MIN-026

This section is very altered, with multiple types of alteration. The section consists of 55% quartz, 35% aphanitic alteration mineralization, and 10% opaque minerals. The opaque minerals consist of 6% pyrite, and 4% arsenopyrite.

The section consists of three distinct areas with a combination of quartz, muscovite and sulphide mineralization (Figs. 110 to 112). The main part of the section is similar to that of the host rock of most of the previous sections; there is aphanitic to very fine-grained quartz and muscovite with very fine-grained, subhedral pyrite crystals. There are also areas of fine-grained quartz with arsenopyrite and a third area of intense muscovite alteration, where almost no quartz is visible, and arsenopyrite. The arsenopyrite in these latter two areas is continuous where they contact each other.

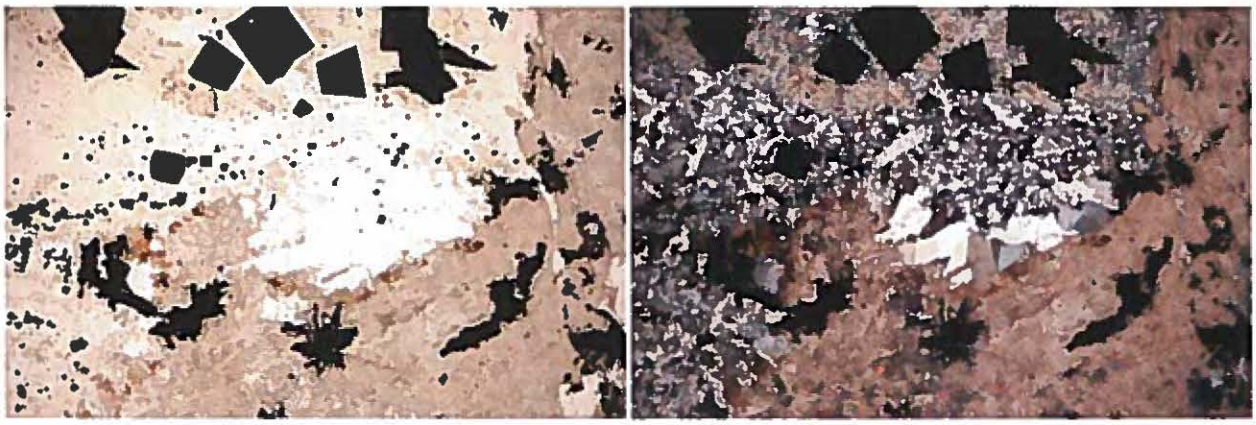


Figure 110. Photomicrographs of three areas within the section showing different degrees of alteration and the preferential occurrence of pyrite or arsenopyrite within these units, in transmitted light, plane-polars (left) and crossed polars (right) (2x mag., F.O.V. ~6mm).

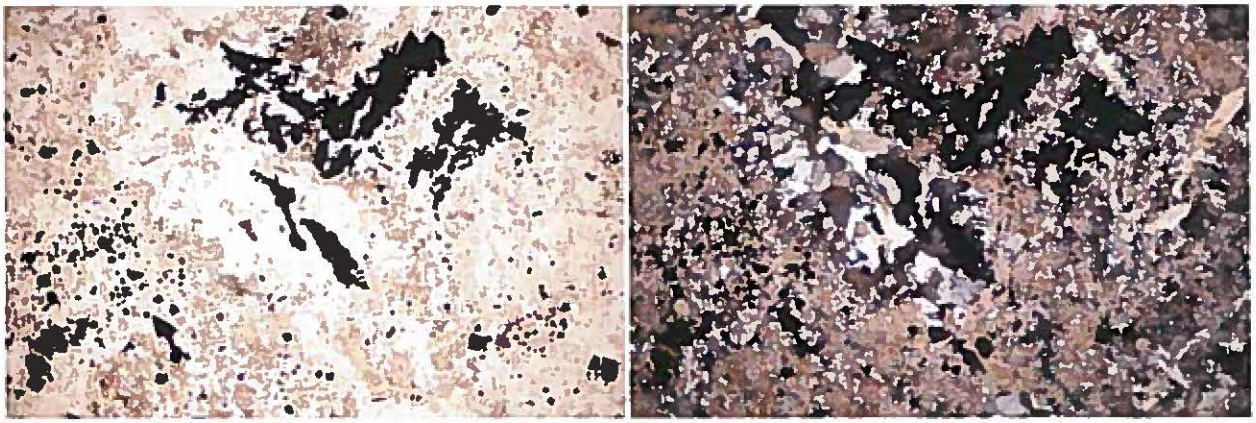


Figure 111. Photomicrographs of two areas within the section that show different degrees of alteration and the preferential occurrence of pyrite or arsenopyrite, in transmitted light, plane-polars (left) and crossed polars (right) (2x mag., F.O.V. ~6mm).

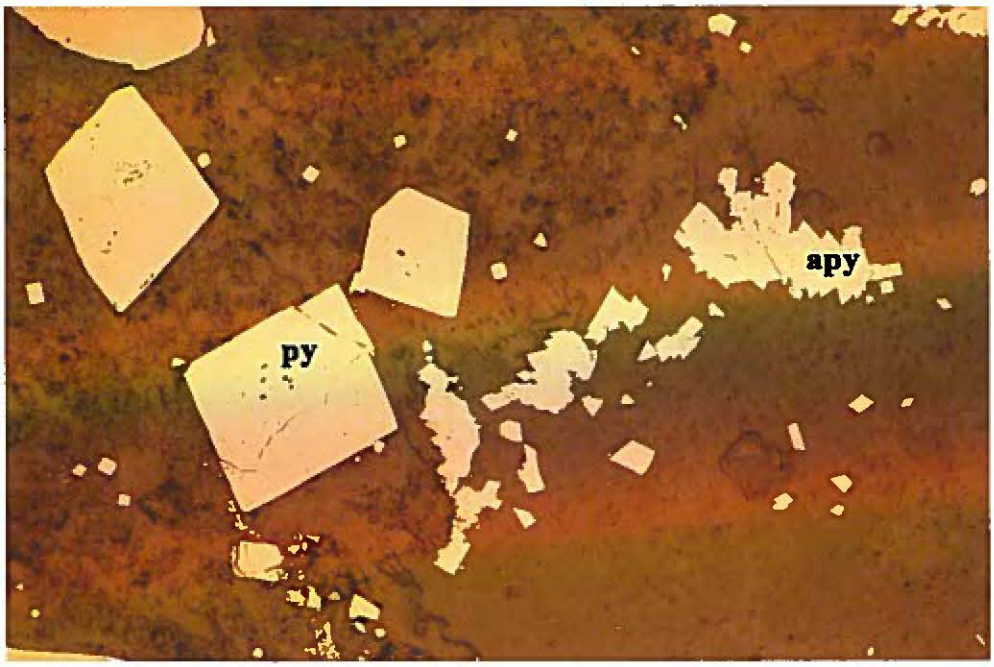


Figure 112. Photomicrograph of arsenopyrite in one unit and pyrite in another, in reflected light (4x mag., F.O.V. ~3mm).

MIN-027

This section consists of 60% quartz, 35% opaque minerals, and 5% void space. The opaque minerals consist of 28% arsenopyrite, 3% galena, 3% sphalerite, 1% Sb-sulphosalts, and trace pyrite.

The quartz is commonly fine- to medium-grained subhedral to anhedral crystals, but locally the crystals are very fine-grained. This is most commonly observed along a fracture through a portion of the section (Fig. 113). The quartz here is not only very fine-grained but appears to be brecciated.

Arsenopyrite is the dominant sulphide mineral in the section. It occurs as fine- to very fine-grained, subhedral to euhedral crystals (Fig. 114). Sphalerite occurs as fine-grained, anhedral crystals. Galena and Sb-sulphosalt mineralization appear to be infilling around the quartz crystals, and locally around the arsenopyrite, and sphalerite.

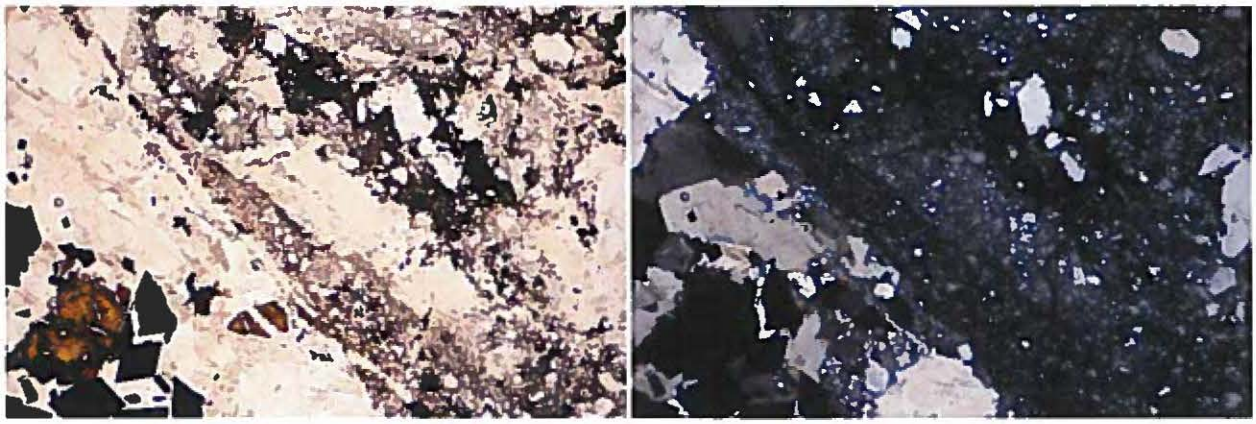


Figure 113. Photomicrographs of the quartz vein and fracture, in transmitted light, plane-polars (left) and crossed polars (right) (4x mag., F.O.V. ~3mm).



Figure 114. Photomicrograph of arsenopyrite, sphalerite, galena and a Sb-sulphosalt, in reflected light (4x mag., F.O.V. ~3mm).

MIN-028

This section consists of 60% opaque minerals, and 40% quartz. The opaque minerals consist of approximately 35% sphalerite, 22% pyrite, 3% galena, and trace arsenopyrite.

The quartz is generally very fine-grained to locally fine grained, anhedral crystals. The quartz appears to fracture the sphalerite crystals, creating sphalerite grains with sharp edges (Fig. 115). This occurs to a smaller degree with the pyrite.

The sphalerite is reddish-brown, coarse- to fine-grained, anhedral, angular crystals. The angular crystal shape may be due to fracturing from the emplacement of quartz. Some of the sphalerite crystals have inclusions of pyrite (Fig. 116). The pyrite is coarse- to medium grained, anhedral to subhedral crystals. Locally very fine-grained pyrite occurs. Galena occurs locally as fine- to very fine-grained, subhedral crystals. Arsenopyrite occurs rarely as, very fine-grained, crystals.

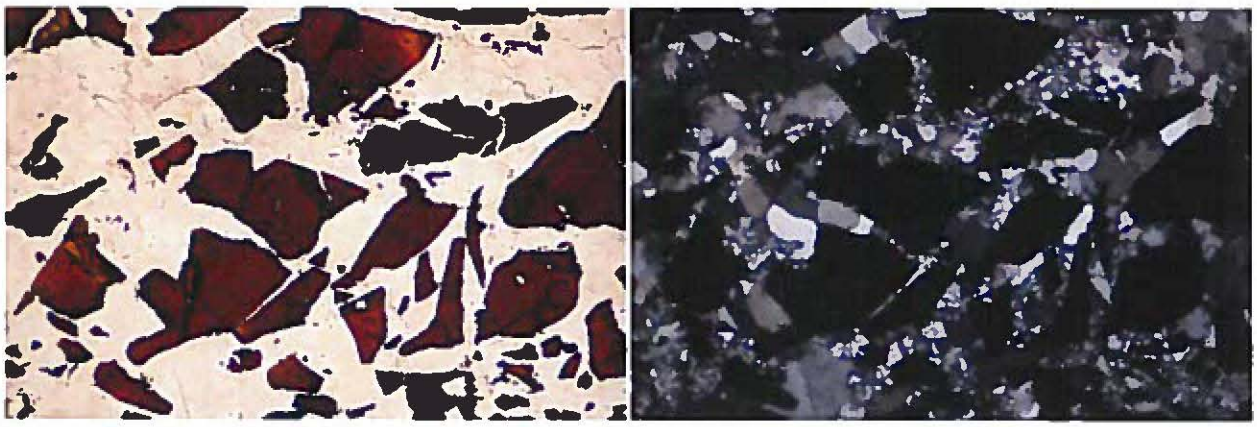


Figure 115. Photomicrographs of quartz infilling around sphalerite, in transmitted light, plane-polars (left) and crossed polars (right) (4x mag., F.O.V. ~3mm).

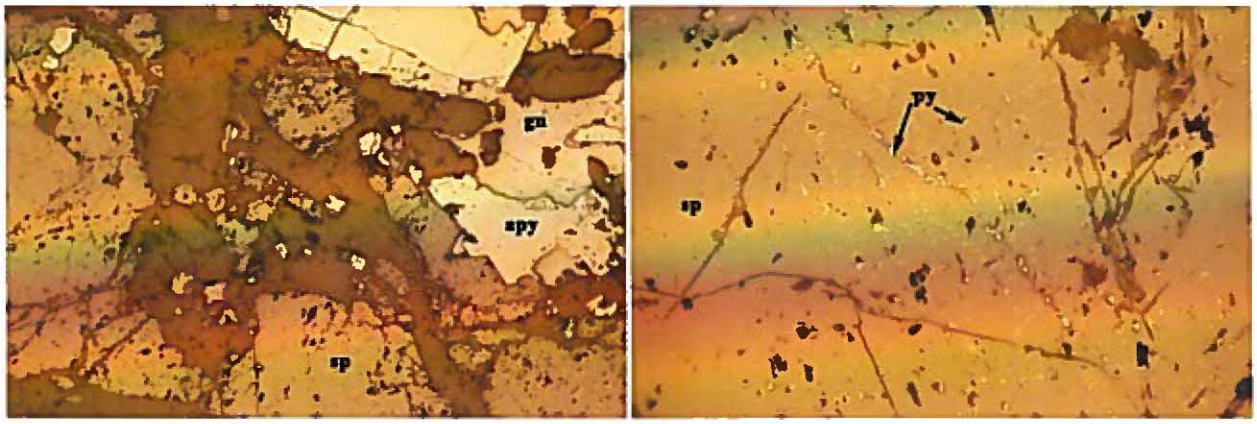


Figure 116. Photomicrographs in reflected light of: (left) sphalerite, arsenopyrite, and galena (4x mag., F.O.V. ~3mm); (right) sphalerite with small inclusions of pyrite (10x mag., F.O.V. ~1.2mm)

MIN-029

This section consists of approximately 75% opaque minerals, and 25% quartz. The opaque minerals consist of 50% sphalerite, 21% pyrite, 3% arsenopyrite, and 1% galena.

The quartz is generally medium- to fine-grained anhedral to subhedral crystals, but locally is very fine-grained (Fig. 117). Local crystals appear to be partially recrystallized.

The sulphides in this section occur as one large aggregate (Fig. 118). The sphalerite occurs as reddish-brown crystals that are coarse- to fine-grained, and anhedral. The pyrite occurs as medium- to fine-grained, subhedral to anhedral crystals. The arsenopyrite occurs locally as fine- to very fine-grained, euhedral to subhedral crystals. Galena is fine- to very fine-grained and generally occurs infilling around quartz grains, but locally individual crystals with the other sulphides.

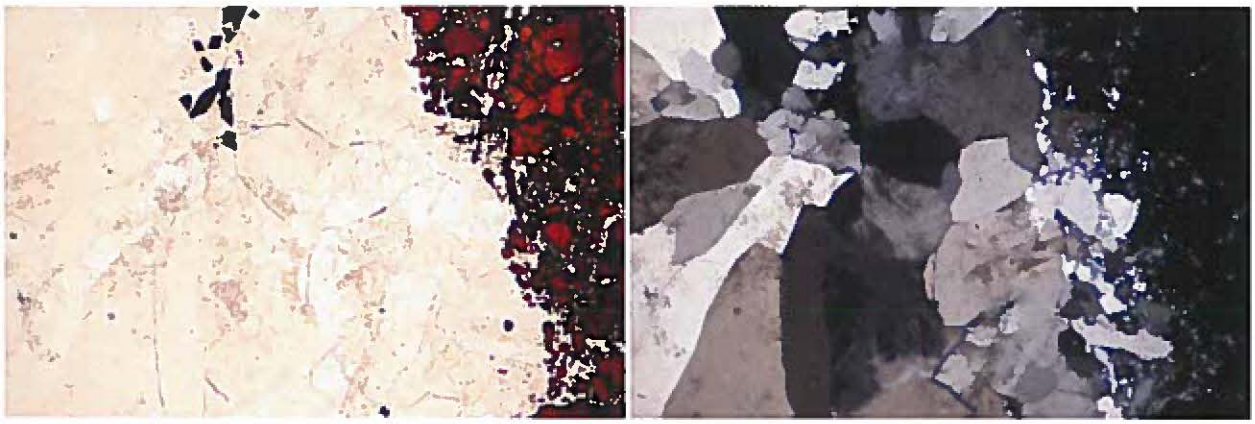


Figure 117. Photomicrographs of quartz, with local grains that are partially recrystallized, and sphalerite, in transmitted light, plane-polars (left) and crossed polars (right) (4x mag., F.O.V. ~3mm).

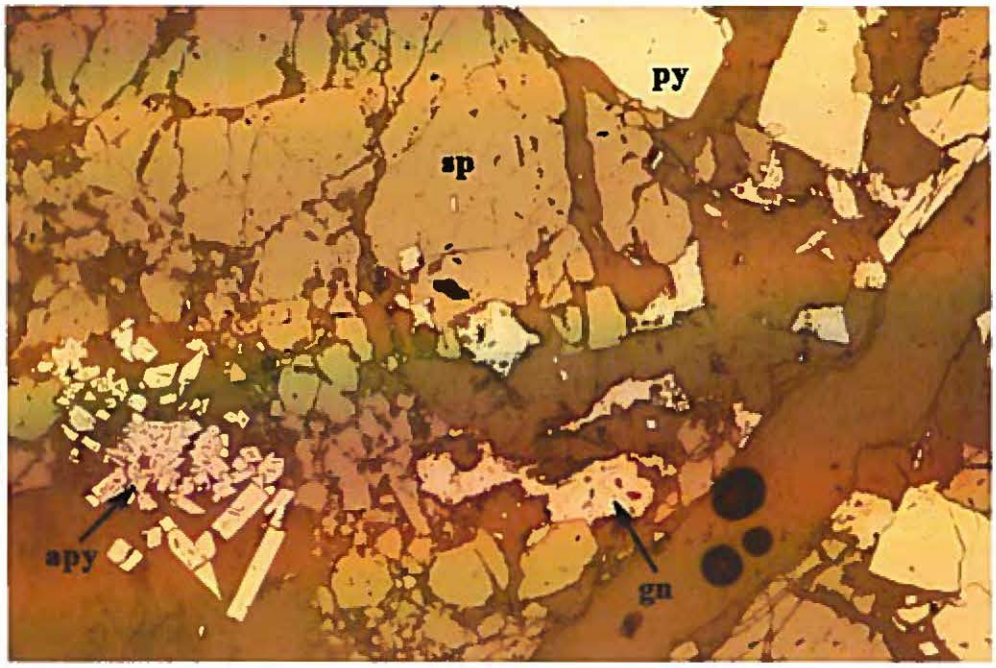


Figure 118. Photomicrograph of sphalerite, pyrite, arsenopyrite, and galena, in reflected light (4x mag., F.O.V. ~3mm).

4. Discussion

The mineralization of the above sections was carefully examined with focus on determining the phases that host Au, and Ag. Little information was provided by the client regarding the rocks the sections were cut from, thus interpretation is based solely on the observed thin sections.

Host Rock Characteristics:

In general, it appeared that most of the mineralization was hosted in quartz veins that were emplaced into a hydrothermally altered, quartz-rich host rock. The alteration consisted of muscovite, or similar K-rich mica; in field observations this would commonly be called sericite. The host rock commonly contained disseminated pyrite as discrete crystals. In some sections the host rock was altered by Fe-oxide and/or As-Fe-oxide. In section MIN-21 one group of crystals was large enough to be identified as the As-Fe-oxide, symplesite; however, in other occurrences the grains were too fine-grained to identify the mineral optically.

Vein Characteristics:

The quartz-sulphide veins consist of varying amounts of arsenopyrite, pyrite, sphalerite, galena, Sb-sulphosalts (freibergite, boulangerite, bournonite), and rarely various oxide and sulphate minerals. Arsenopyrite was the dominant mineral observed within the quartz-sulphide veins. Pyrite and sphalerite appear to form at a similar time to the arsenopyrite in these veins. The galena, and Sb-sulphosalts were commonly observed in-filling around the other sulphides and quartz grains; this is evidence that are likely forming later than arsenopyrite, pyrite and sphalerite. . The Sb-sulphosalt minerals are commonly found in epithermal systems. The oxide and sulphate minerals appear to form as a result of oxidation and alteration of the previous minerals (discussed in further detail below).

Freibergite, boulangerite and bournonite and to some extent galena, were difficult to distinguish in reflected light. Galena commonly had a higher bireflectance; the surface appeared more pristine, and locally cleavage and triangular pits were observed. In contrast, the Sb-sulphosalts commonly had small round pits due to the very fine-grained nature of the crystals. The larger crystals of boulangerite illustrated the acicular nature of the crystals better than the smaller grains, and highlighted the higher bireflectance over other Sb-sulphosalts. Bournonite

and freibergite have little to no bireflectance under reflected light, making them especially difficult to distinguish between - as shown in MIN-1B.

The Ag was observed to be hosted within the minerals freibergite, pyrargite, acanthite, and an unknown sulphate mineral (Fe-As-Ag-Sb-Au-Pb). Freibergite is the most common Ag bearing mineral observed. Pyrargite, acanthite and the unknown sulphate were observed rarely and these minerals were commonly very fine-grained.

The Au was predominately hosted in a variety of unclassified sulphates (containing Fe-As-Sb-Au-Pb, Fe-As-Au-Pb, and Fe-As-Ag-Sb-Au-Pb), and within S-Si-O (Ca-Fe-Cu-As-Au) minerals, as illustrated in sections MIN-15 and MIN-21. Small Au peaks on SEM-EDX spectra were observed in As-Fe-oxide minerals. Small peaks on EDX spectra show that Au may also exist locally within both the arsenopyrite, and the Sb-sulphosalt minerals. The Fe-As-Au-Pb-sulphate may be a form of beudantite ($PbFe_3(AsO_4)(SO_4)(OH)_6$), in which the Au has substituted for another mineral, likely As. This mineral is commonly found in the oxidized zones of polymetallic deposits. The Ca-Fe-Cu-As-Au-S-Si-O mineral may be a sulphate or silicate, further advanced analysis is required. Both the sulphate and S-Si-O minerals that host the Au are likely to form from the breakdown of the Sb-sulphosalt minerals, arsenopyrite and quartz. Sections MIN-15 and MIN-21 come from core intersections with the highest Au concentrations, and appear to host areas of sulphide mineralization that has undergone a partial degree of oxidation and alteration. This has enabled the breakdown of the minerals Au bearing primary minerals, and for the Au and other elements to mobilize into the secondary sulphate and S-Si-O minerals. If there is too much alteration then it is possible that these elements are remobilized and leached away; this would explain why sections that come from highly oxidized intersections had little Au and Ag.

Further work could be completed to better characterize some of the more unusual mineralogy; however, for the purposes of basic metallurgy what is given in this report may be sufficient. Electron probe microanalysis could be completed on arsenopyrite, freibergite, boulangerite, bournonite, and the unknown Au and Ag bearing minerals. This analysis on arsenopyrite may assist with determining how much Au is locked within the mineral. Examining the arsenopyrite on the SEM using 25kV may also help to obtain a larger Au peak to confirm the existence of Au in some of the arsenopyrite. Analysis of freibergite, boulangerite and bournonite

would confirm the optical characterization of these minerals, as there are other minerals with the same or similar chemistry and mineralogical properties that are not as common. Analysis of the unknown Au and Ag bearing minerals may help to characterize them; however, BSE imaging from the SEM shows a fairly uniform texture and it is unlikely this would assist with identifying the mineral, but it would determine the amount of Au and/or Ag within the crystal structure. Since these unknown minerals are also opaque and/or very fine-grained it is unlikely that they would be able to be extracted from the polished section for use on single crystal X-ray diffraction.

In summary, the mineralization appears to be hosted in quartz-sulphide veins that were emplaced into a quartz-rich rock. This has subsequently been altered to varying degrees by muscovite, and hosts pyrite. Sphalerite, pyrite and arsenopyrite are among the first sulphide minerals to form, followed by galena and Sb-sulphosalt minerals that infilled around the quartz, and sulphides. This stage probably included the formation of the first Ag phases. Subsequently the quartz-sulphide veins were weakly to moderately oxidized, and the sulphide and sulphosalt minerals broke down into sulphate and S-Si-O phases. This breakdown enabled the concentration of Au, and Ag. Finally, further oxidation and alteration leached Au and Ag out of the rock in varying places suggesting a late stage metasomatic overprinting.

Statement of Qualifications

I, Mallory Dalsin, graduated from The University of Alberta in 2007 with a B.Sc. in Geology (Honours), and from The University of British Columbia in 2013 with a M.Sc. in Geology. I have practiced my profession as a geologist since 2007, and have worked on mineral exploration and mining projects throughout Canada and Mexico.

References

Deer, W.A., Howie, R.A., and Zussman, J., 1992, *An Introduction to the Rock-forming Minerals*, Second Edition, Prentice Hall.

Evans, A.M., 1993, *Ore Geology and Industrial Minerals: An Introduction*, Third Edition, Blackwell Science.

Marshall, D., Anglin, C.D., and Mumin, H., 2004, *Ore Mineral Atlas*, Geological Association of Canada – Mineral Deposits Division.

Melgarejo, J.C., and Martin, R.F., 2011, *Atlas of Non-Silicate Minerals in Thin Section*, Mineralogical Association of Canada.

Appendix A: Polished section scans in plane polarized and crossed polarized light

For reference: each image represents a 2.7 by 4.6 cm wide field of view

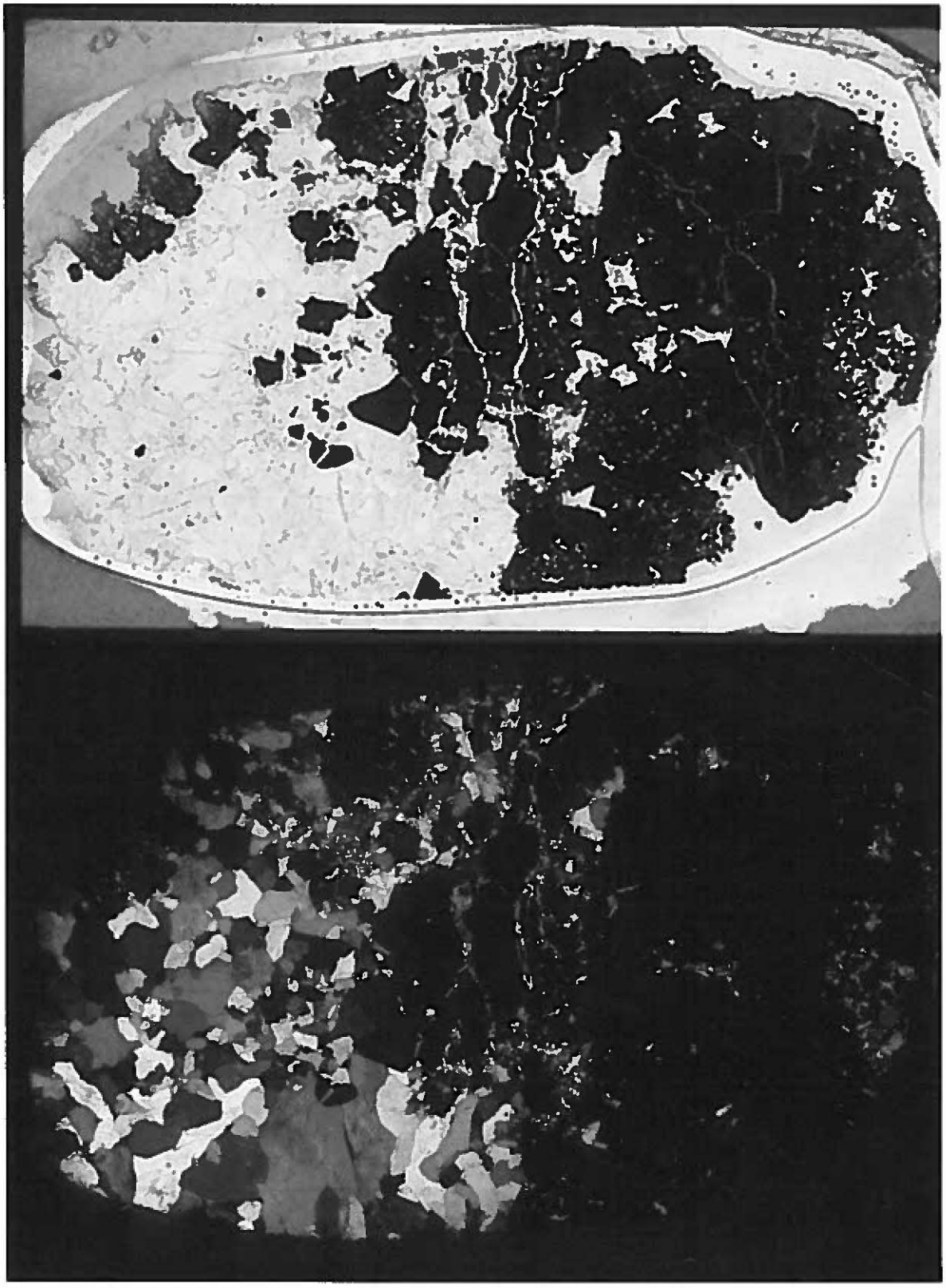


Figure 119. Polished section scan of MIN-01A.

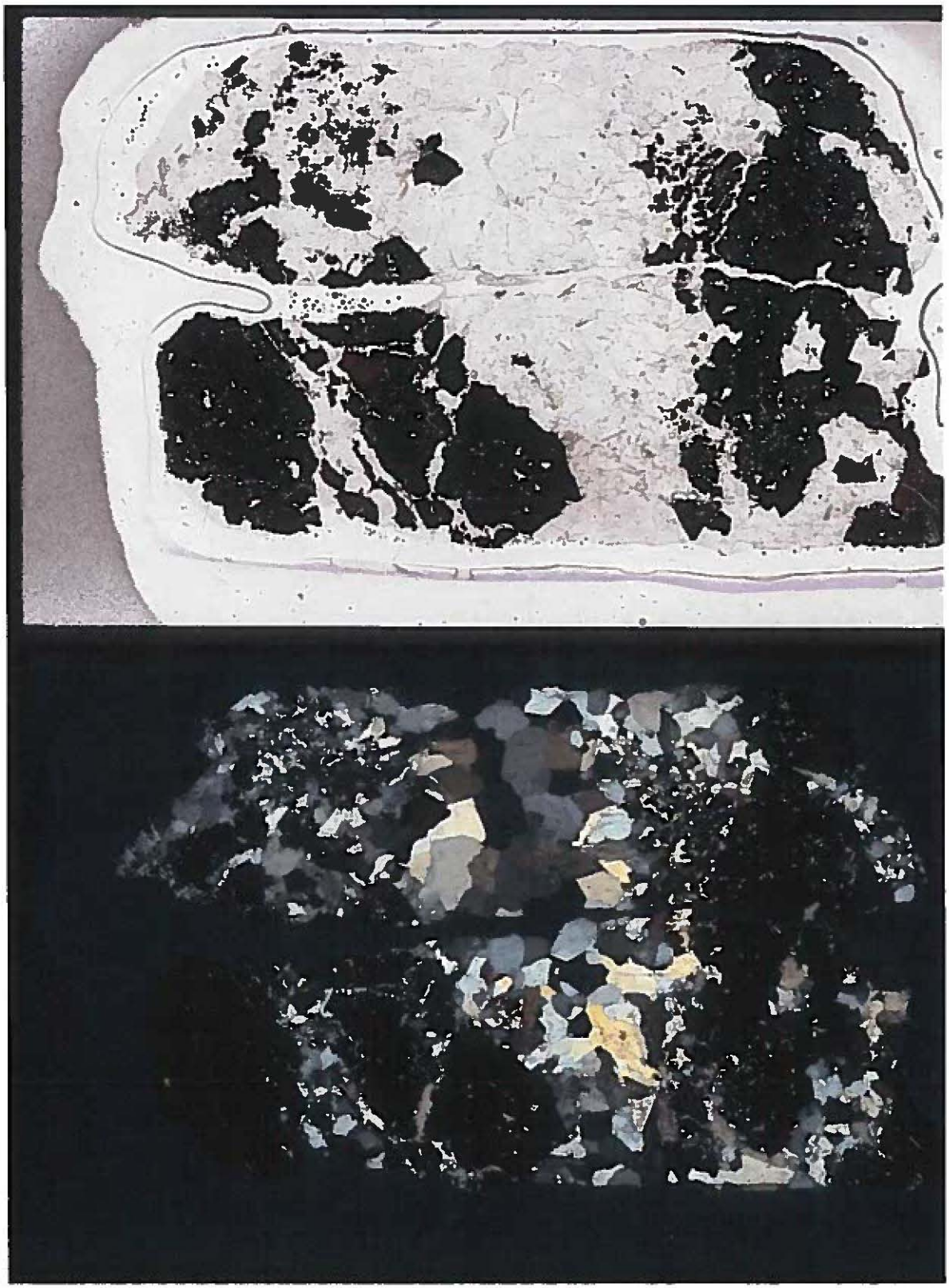


Figure 120. Polished section scan of MIN-01B.



Figure 121. Polished section scan of MIN-02.

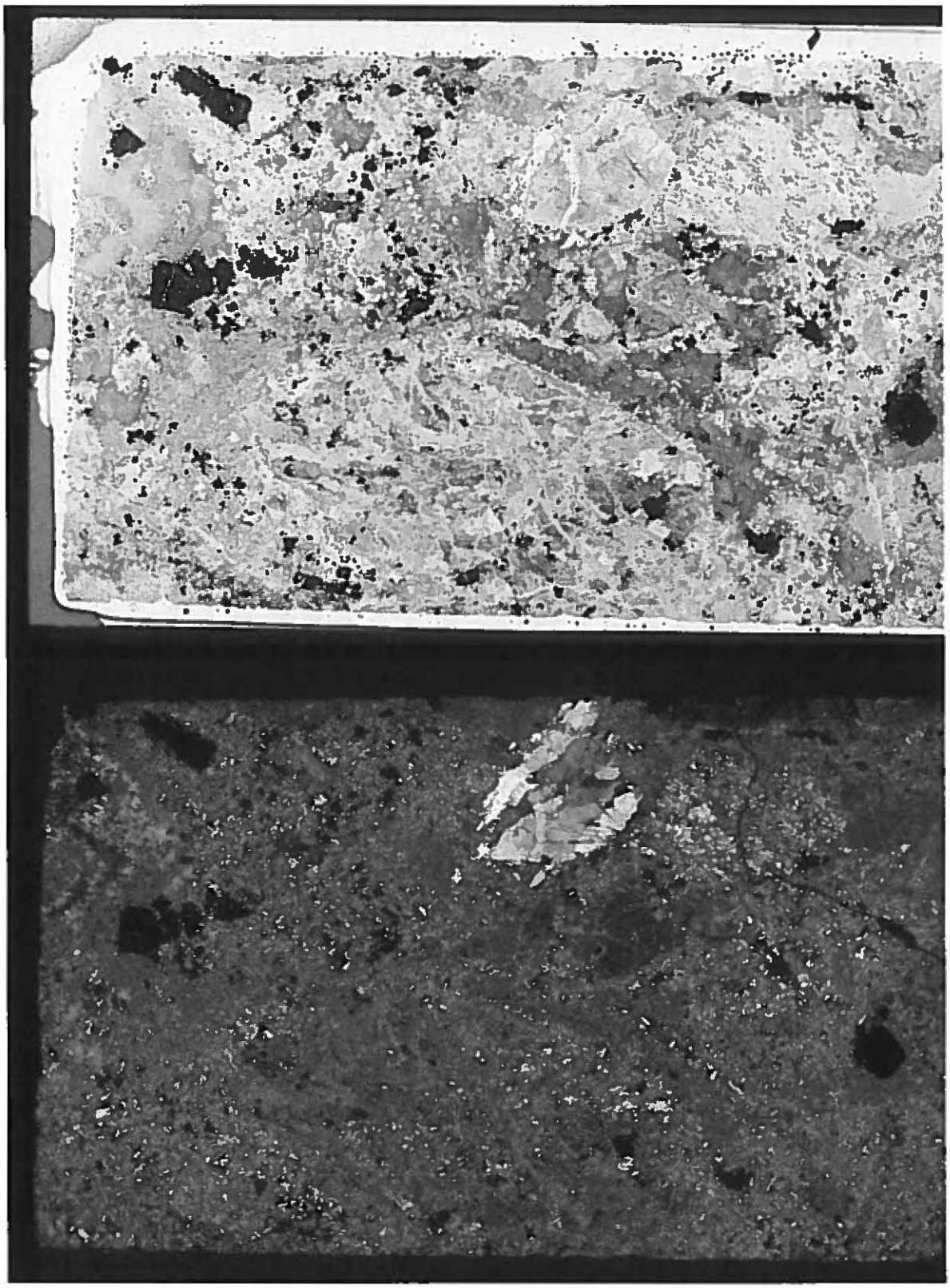


Figure 122. Polished section scan of MIN-03A.

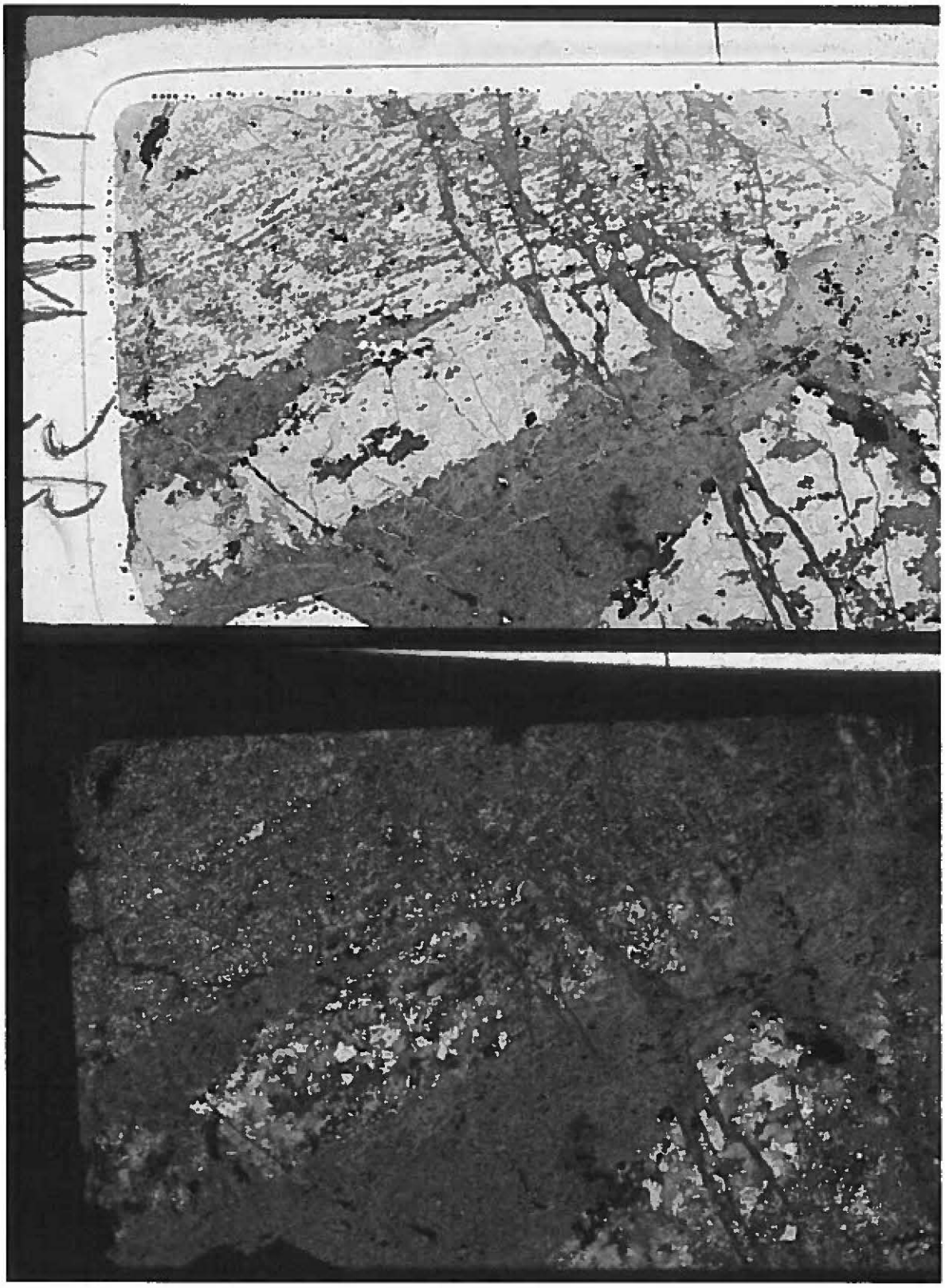


Figure 123. Polished section scan of MIN-03B.

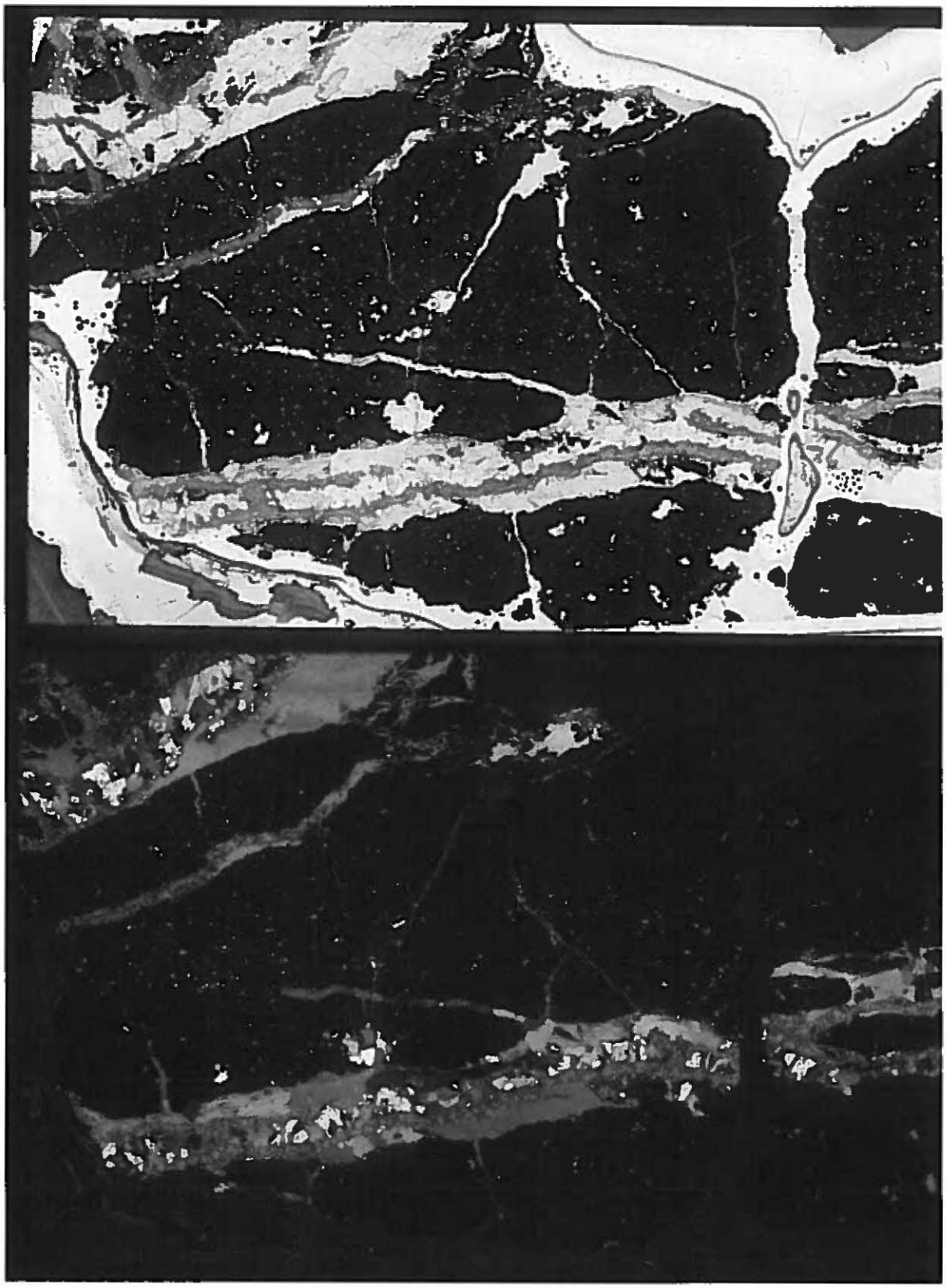


Figure 124. Polished section scan of MIN-04.

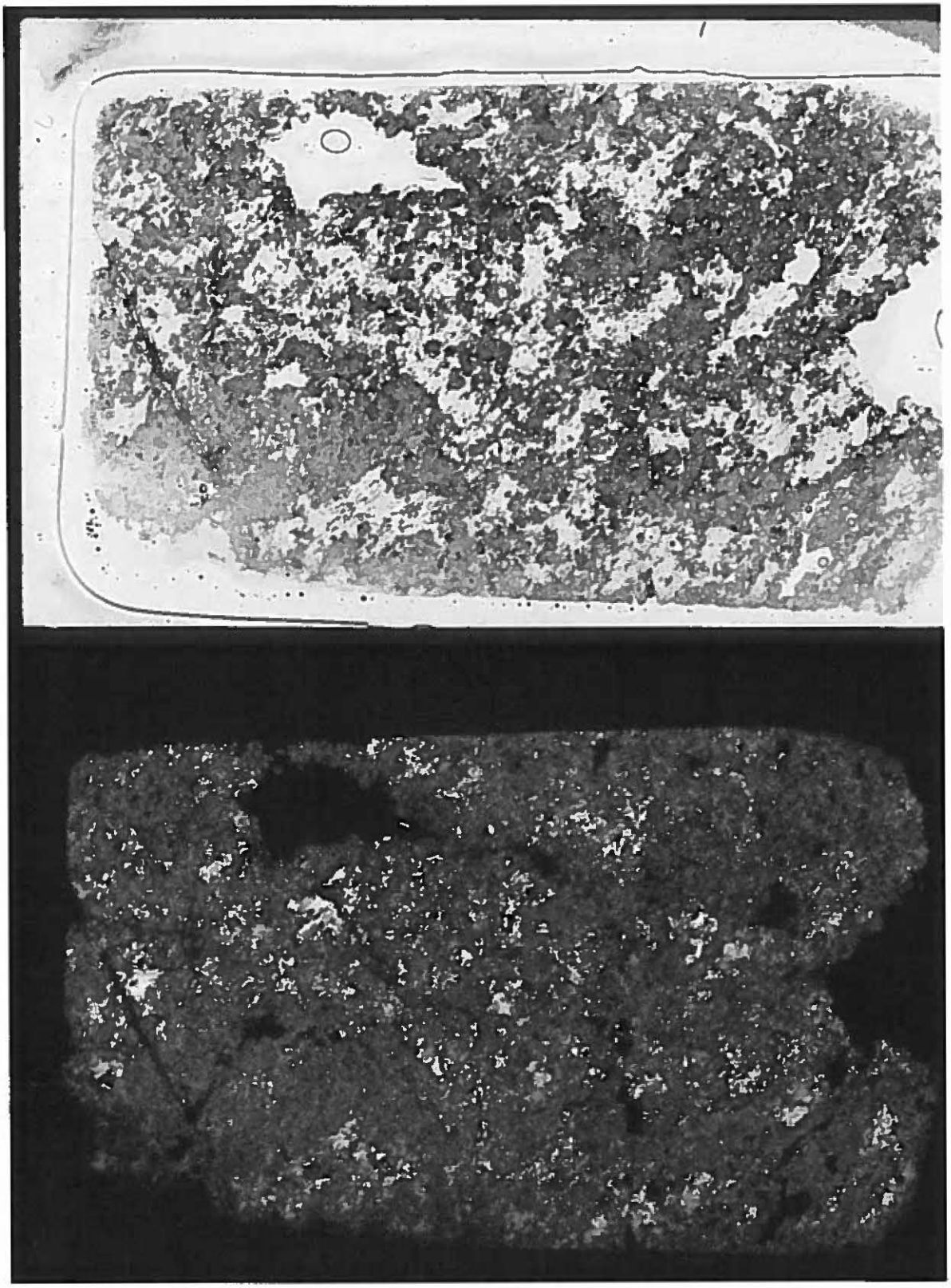


Figure 125. Polished section scan of MIN-05A.

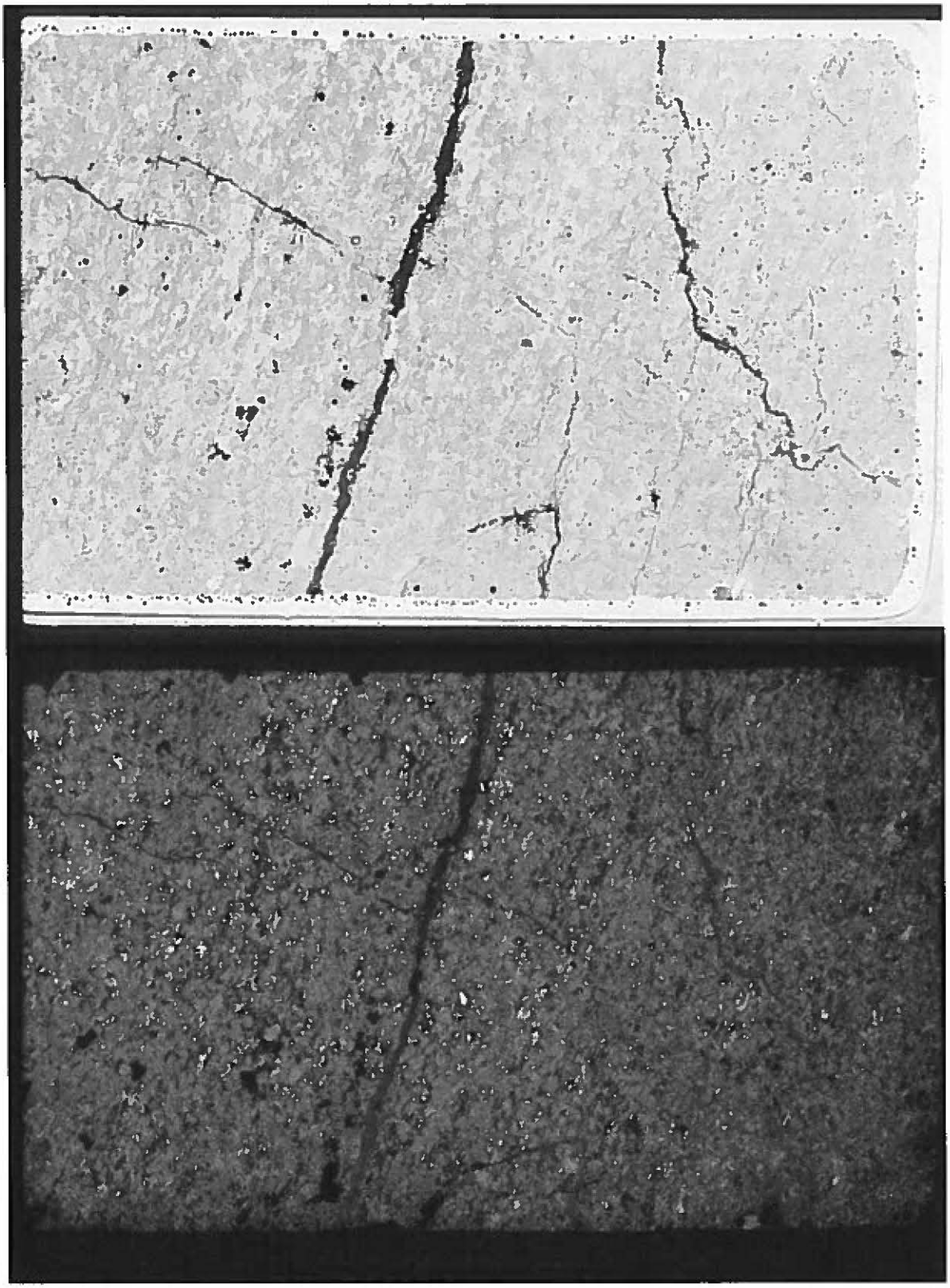


Figure 126. Polished section scan of MIN-05B.

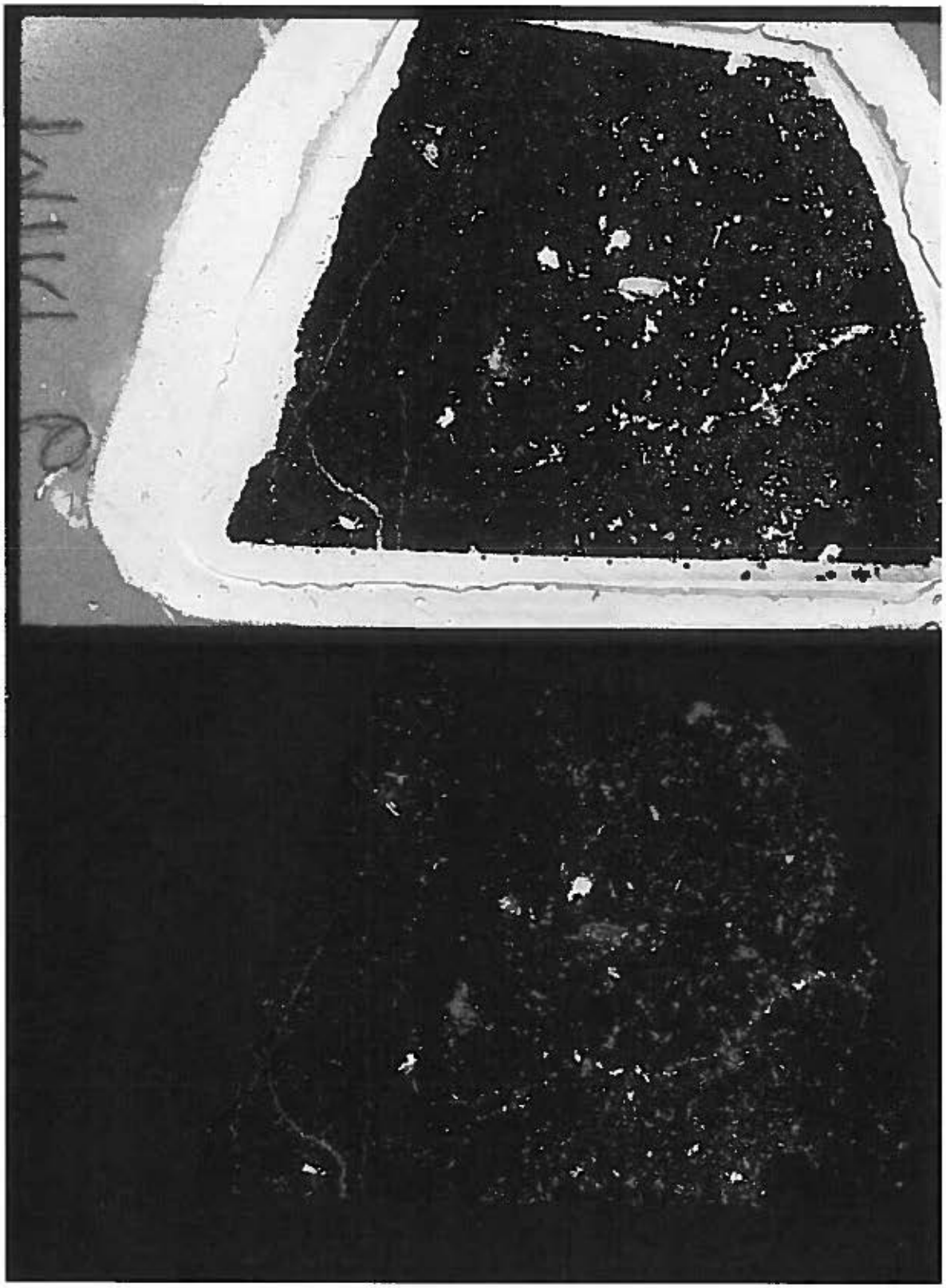


Figure 127. Polished section scan of MIN-06.

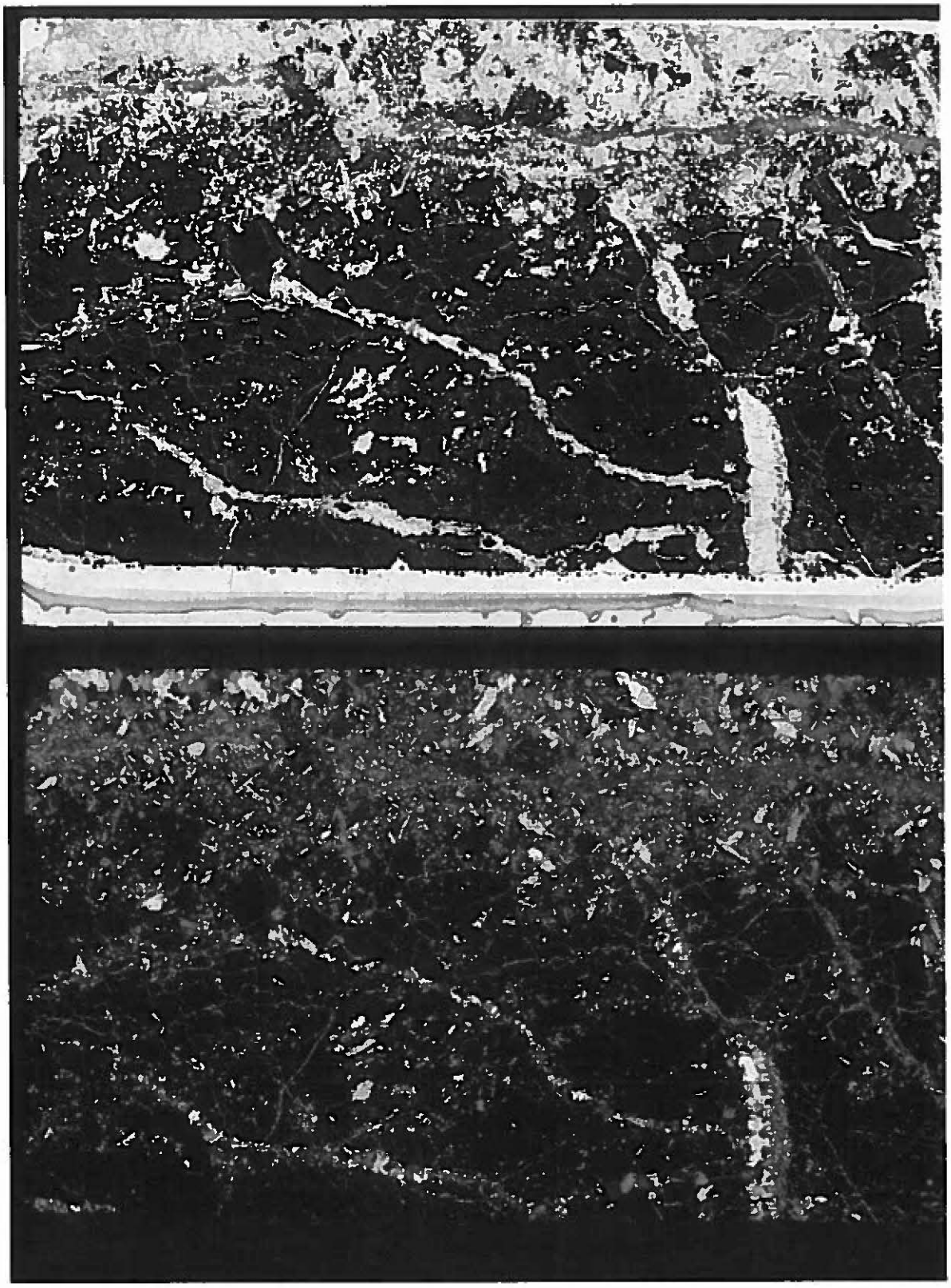


Figure 128. Polished section scan of MIN-07.

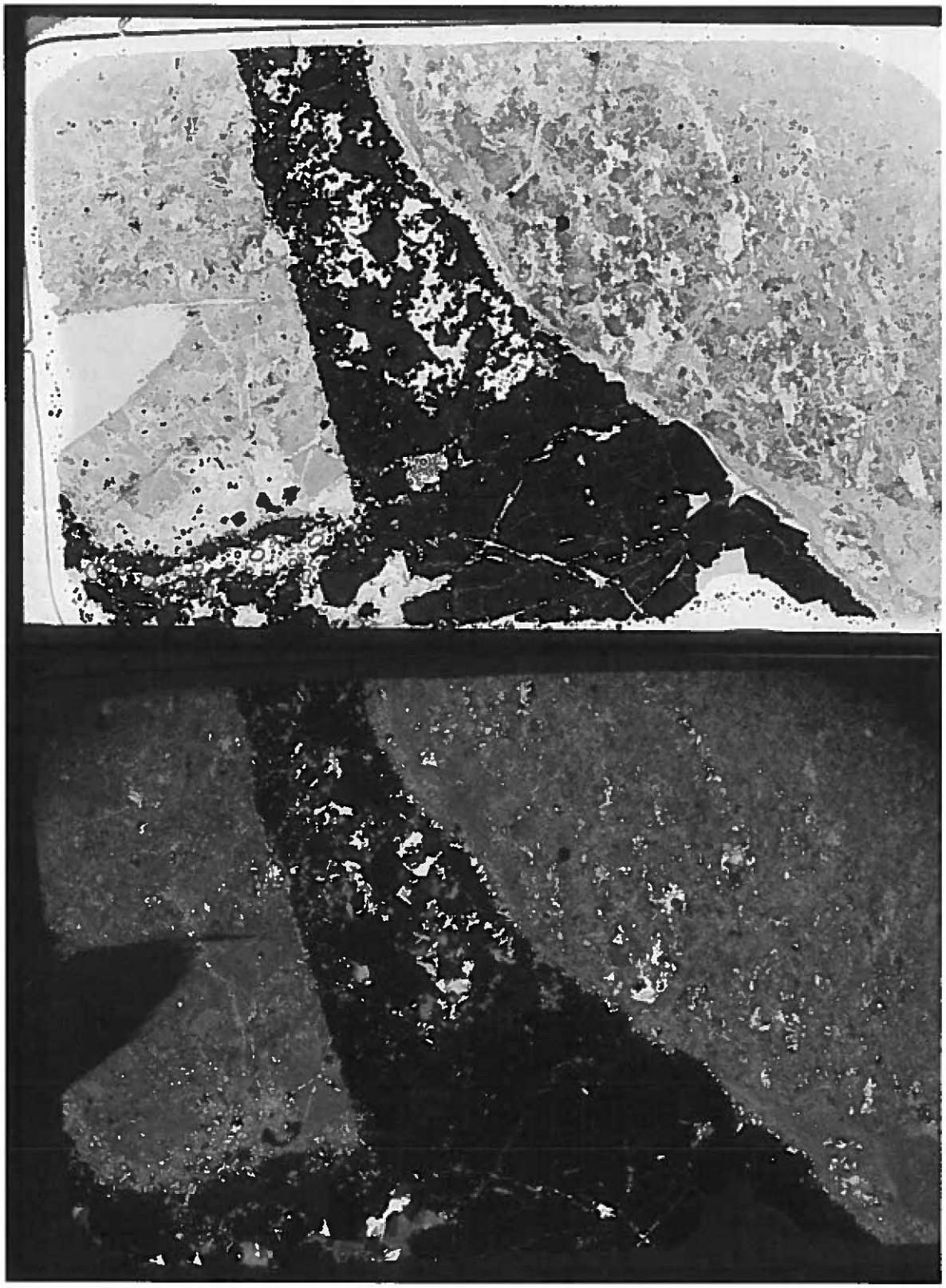


Figure 129. Polished section scan of MIN-08A.

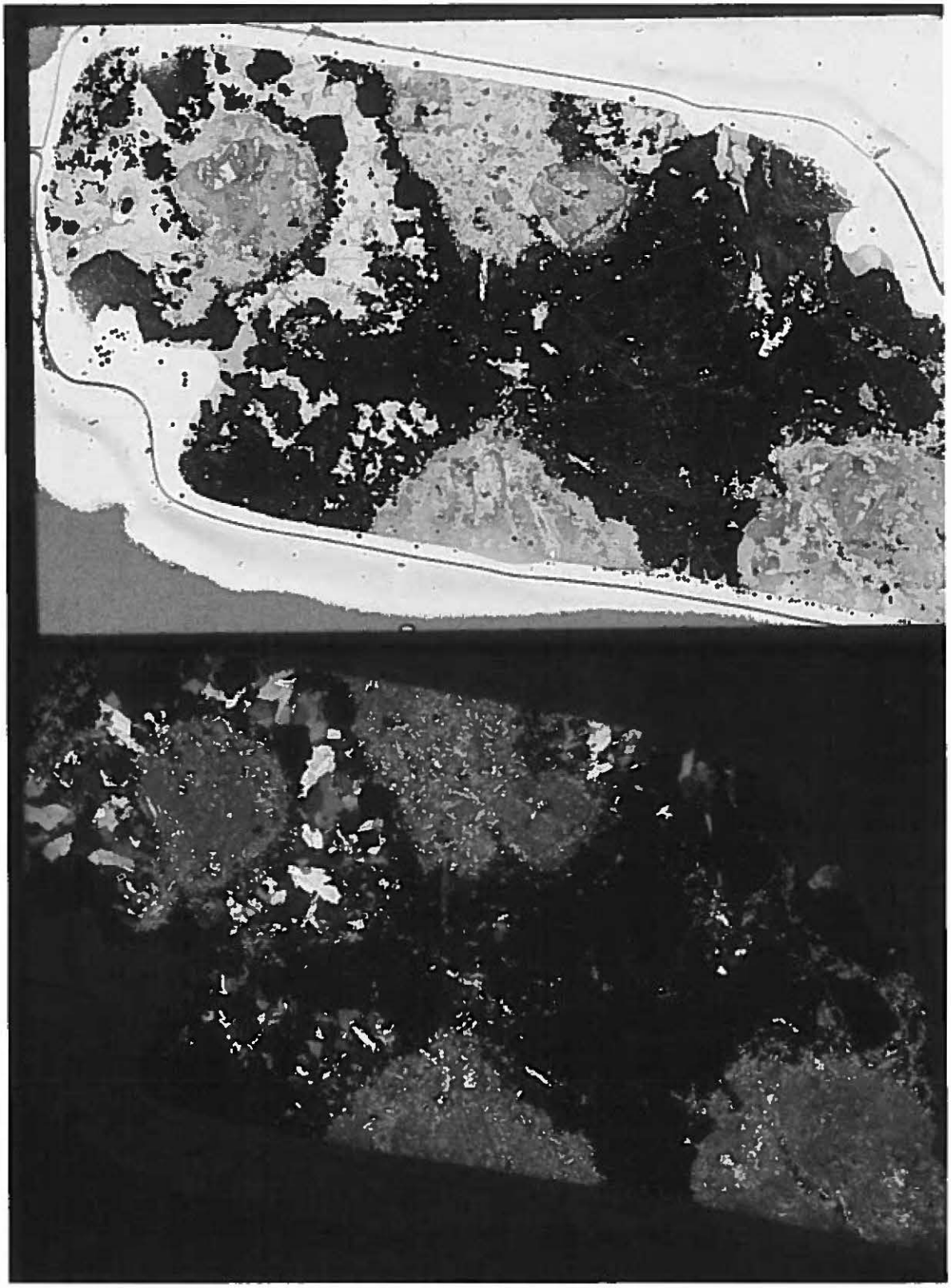


Figure 130. Polished section scan of MIN-08B.

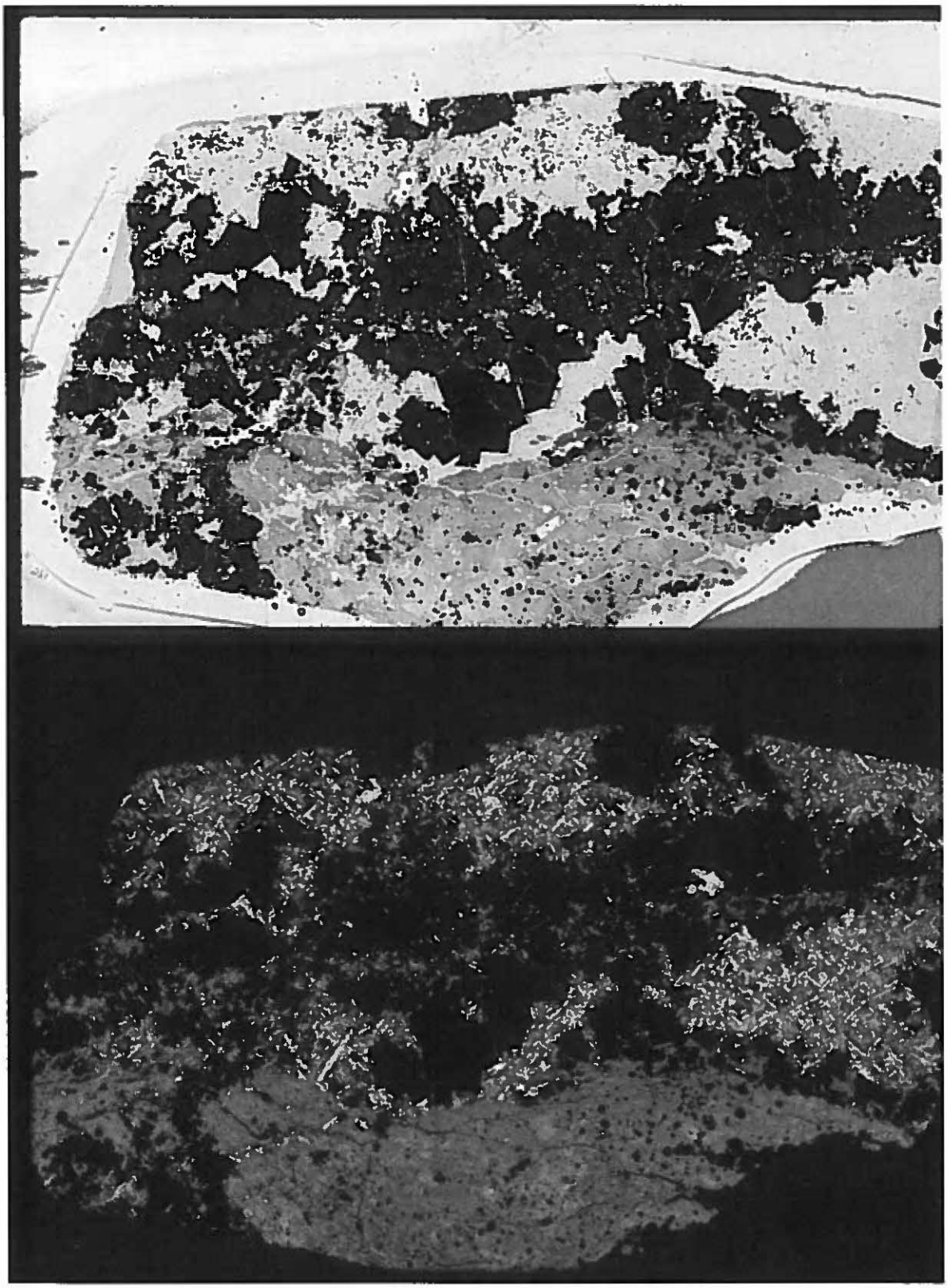


Figure 131. Polished section scan of MIN-09

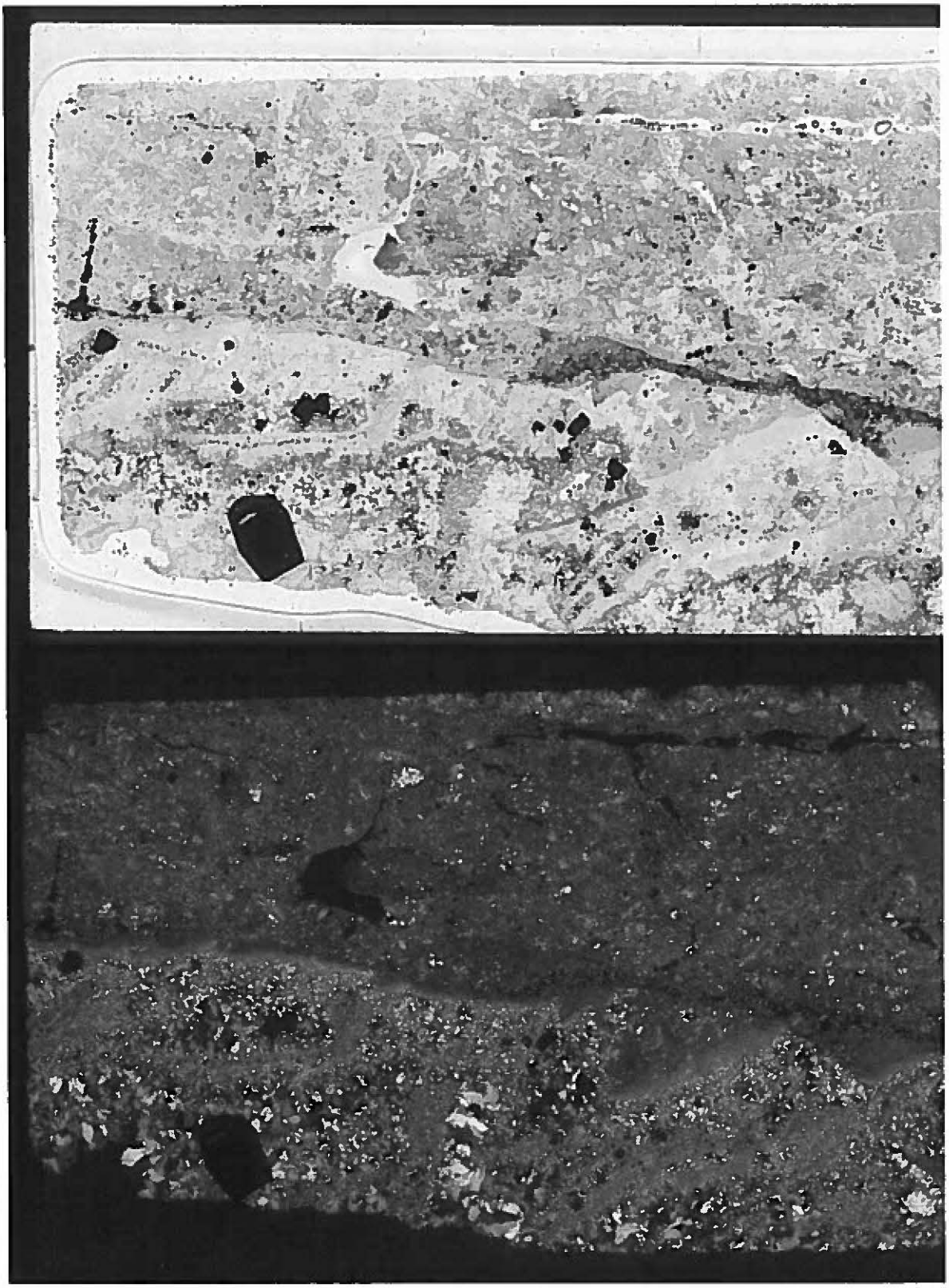


Figure 132. Polished section scan of MIN-10.



Figure 133. Polished section scan of MIN-11.

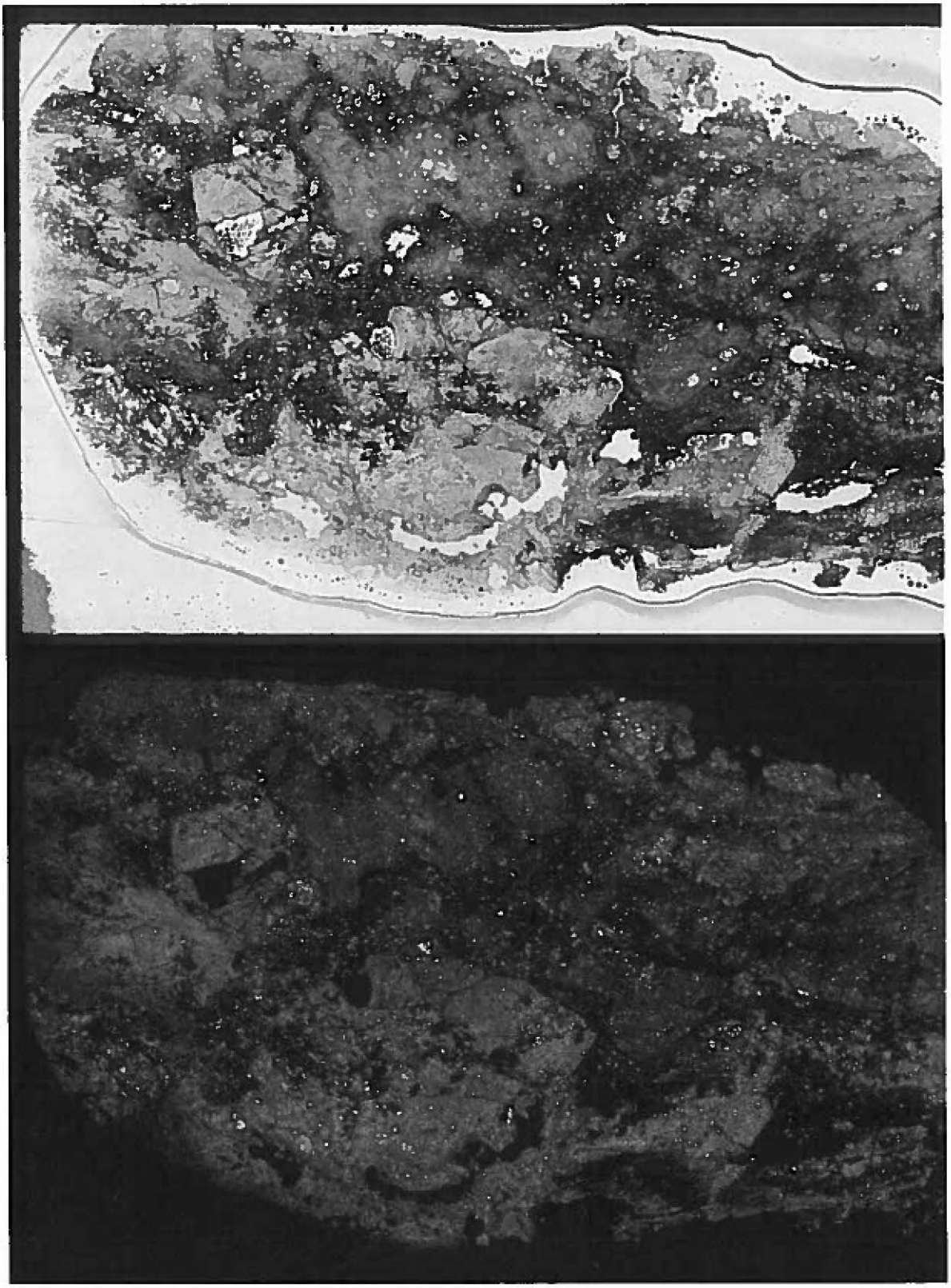


Figure 134. Polished section scan of MIN-12

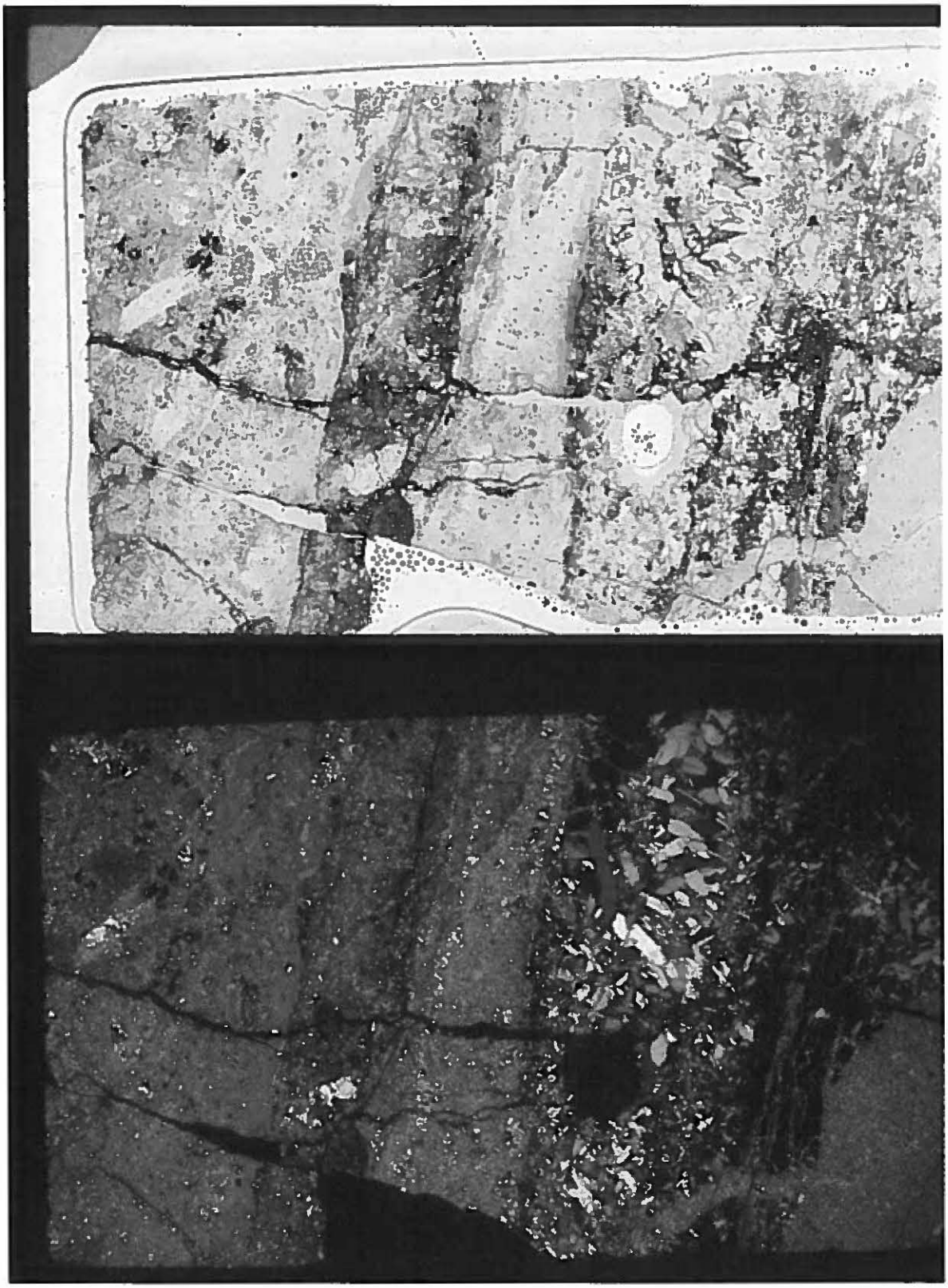


Figure 135. Polished section scan of MIN-13.



Figure 136. Polished section scan of MIN-14.

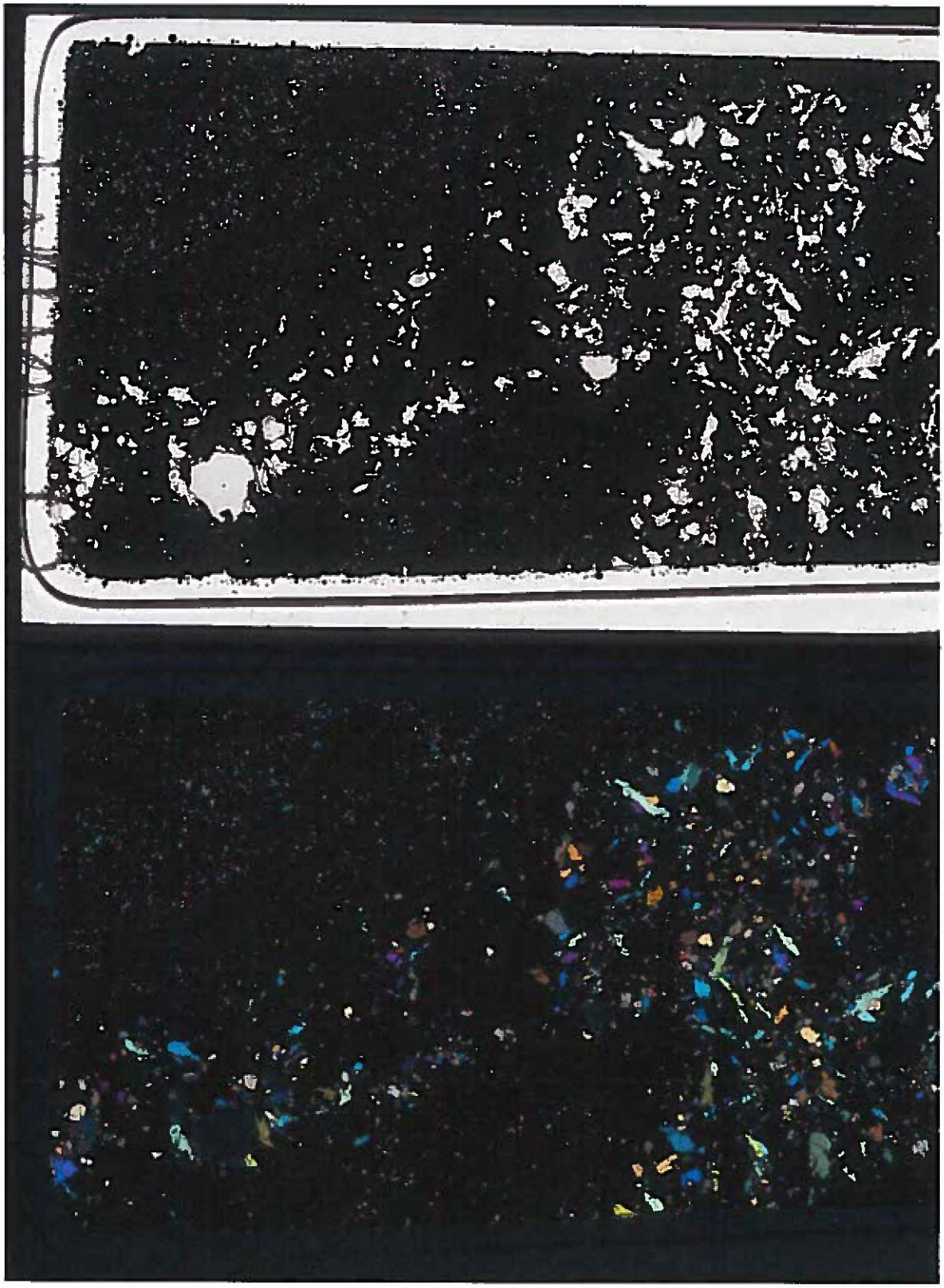


Figure 137. Polished section scan of MIN-15.



Figure 138. Polished section scan of MIN-16.

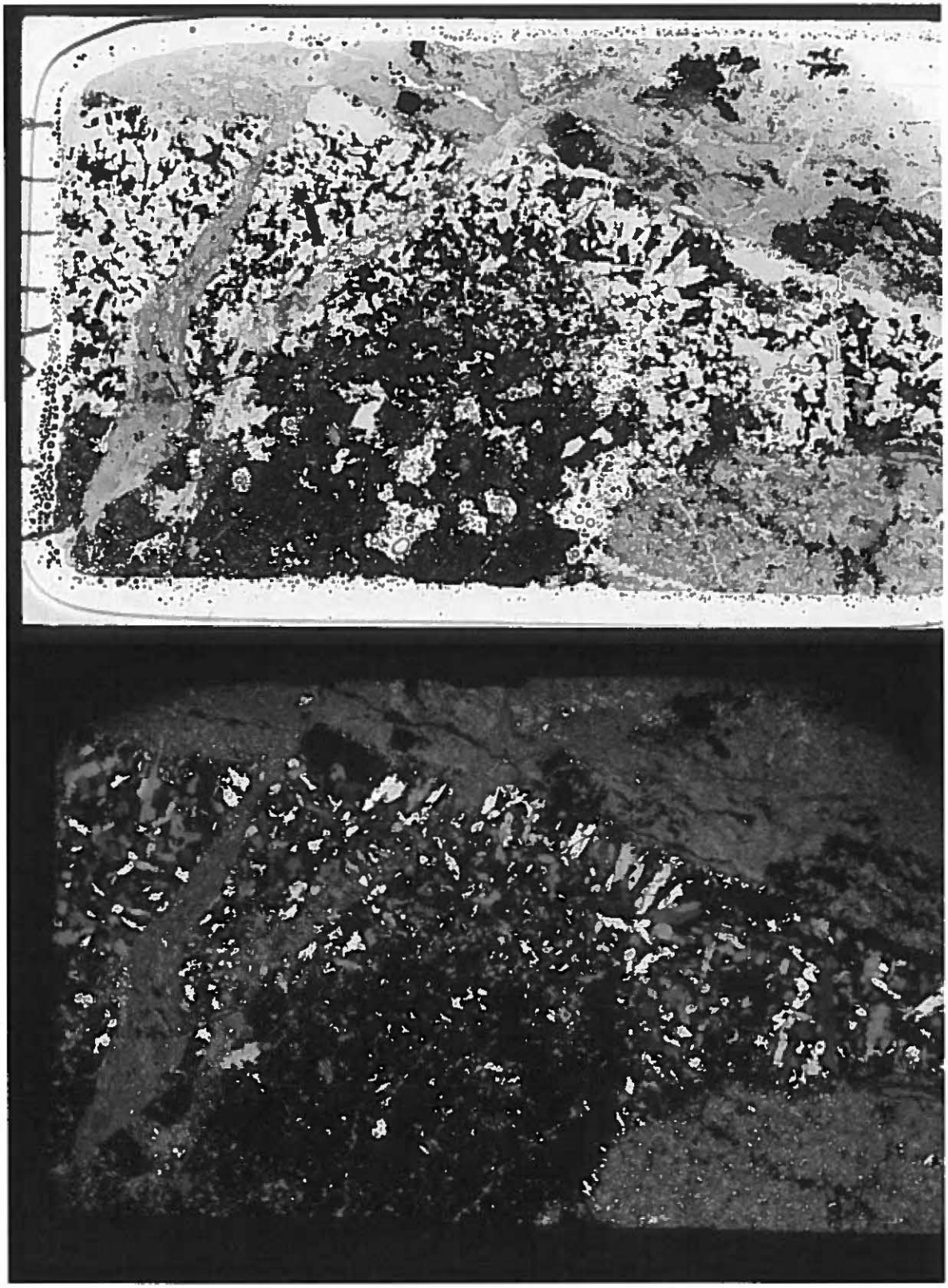


Figure 139. Polished section scan of MIN-17.



Figure 140. Polished section scan of MIN-18.



Figure 141. Polished section scan of MIN-19.



Figure 142. Polished section scan of MIN-20.

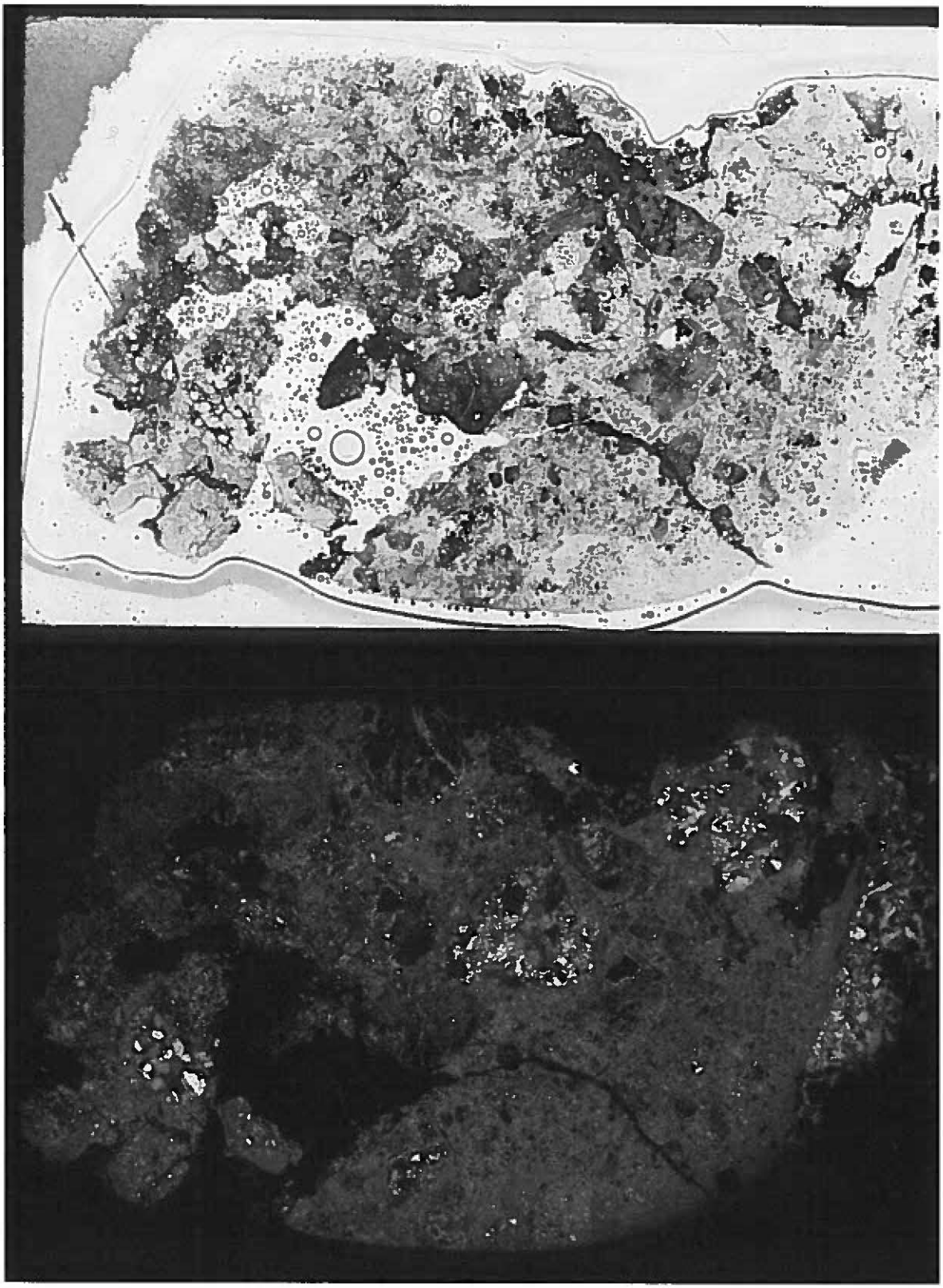


Figure 143. Polished section scan of MIN-21.

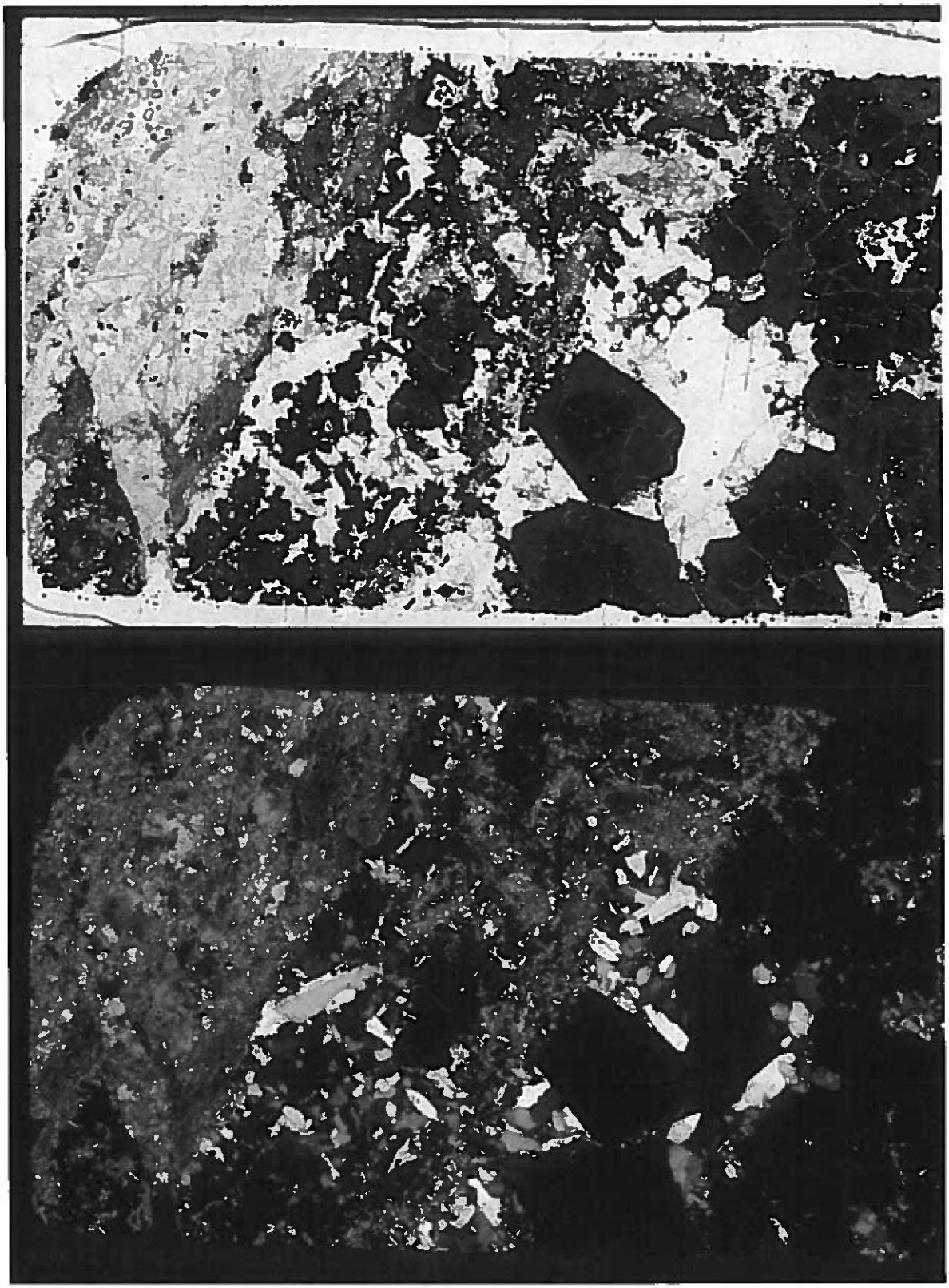


Figure 144. Polished section scan of MIN-22.



Figure 145. Polished section scan of MIN-23.

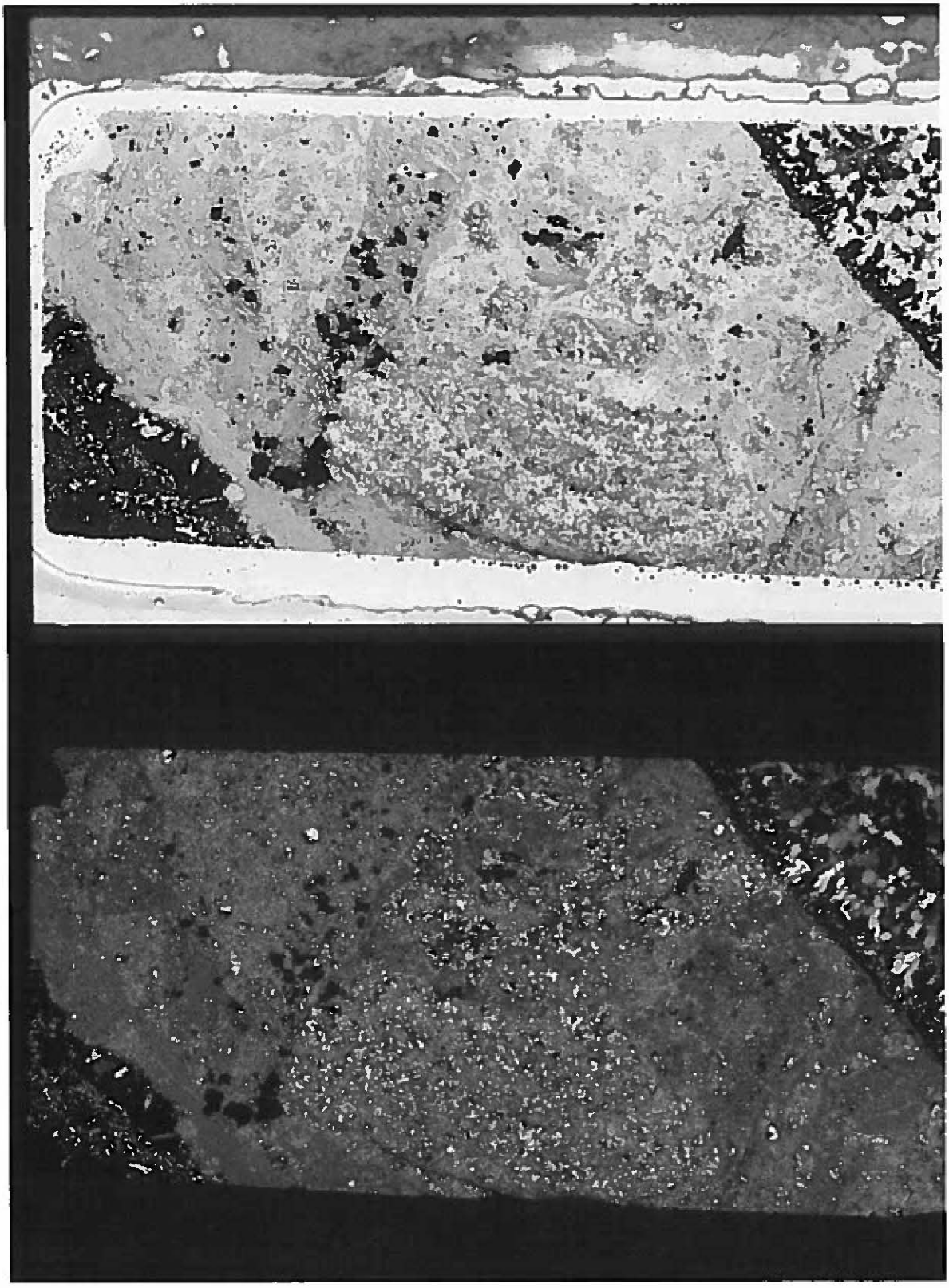


Figure 146. Polished section scan of MIN-24A.

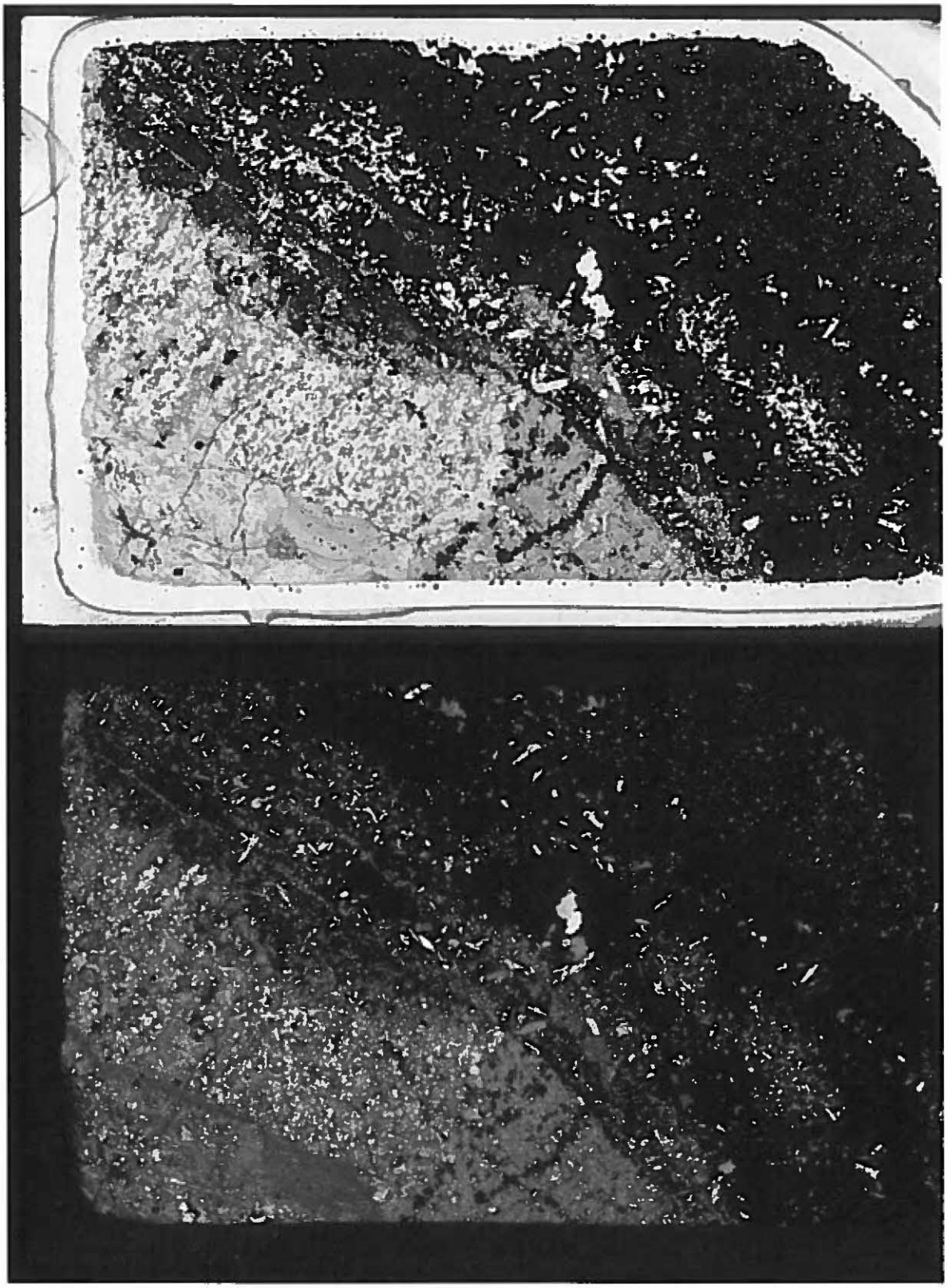


Figure 147. Polished section scan of MIN-24B.

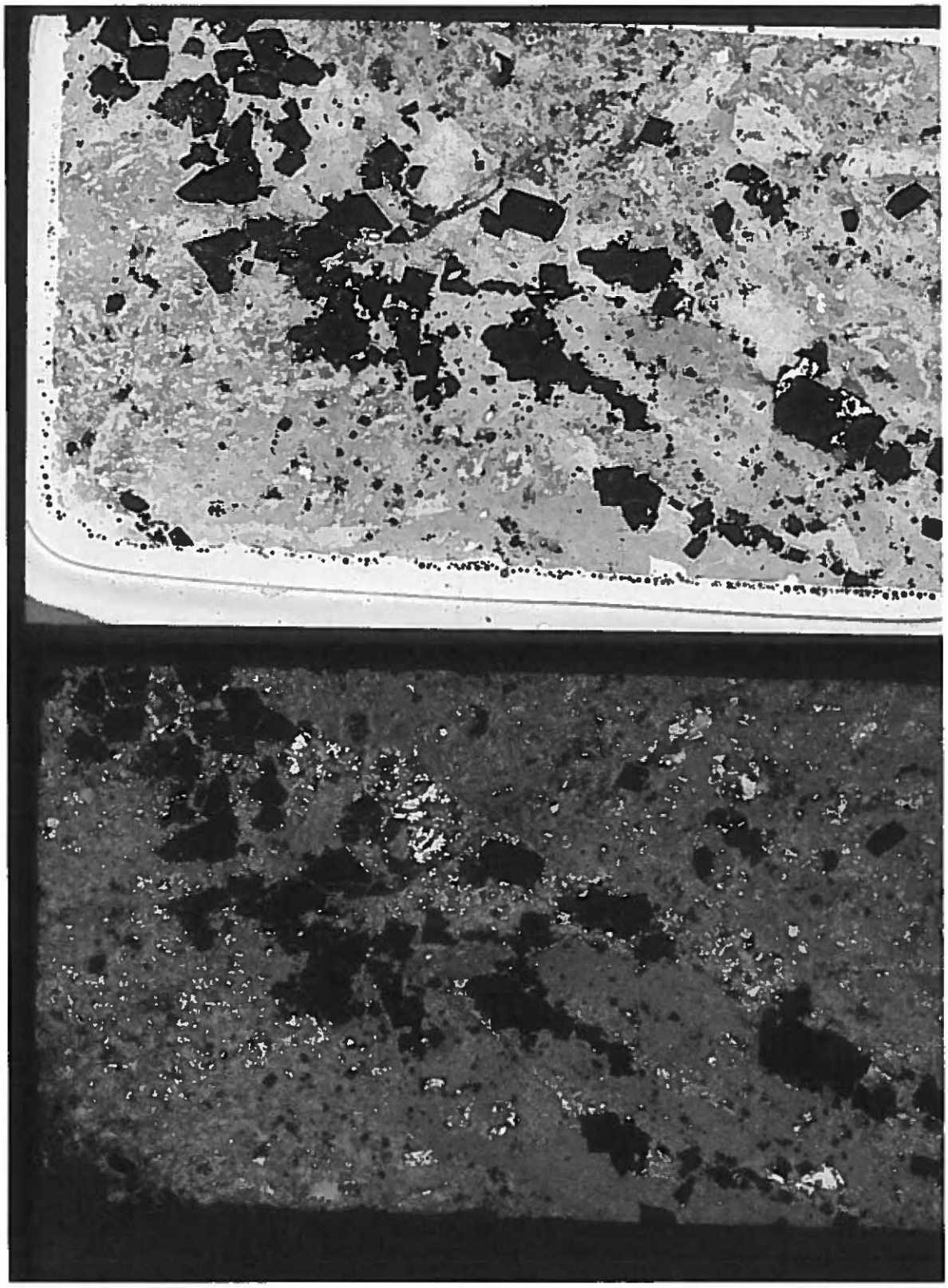


Figure 148. Polished section scan of MIN-25.

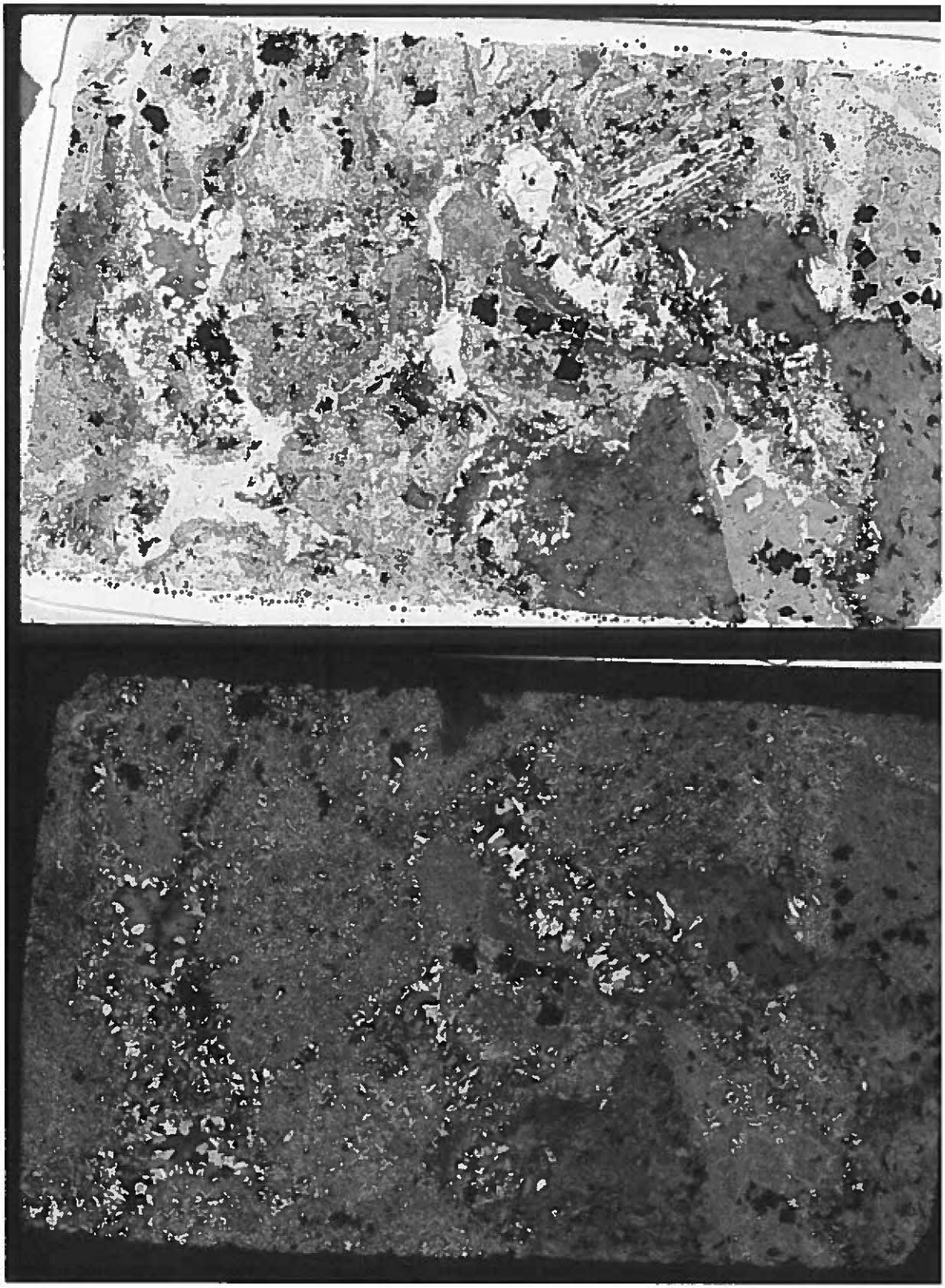


Figure 149. Polished section scan of MIN-26.

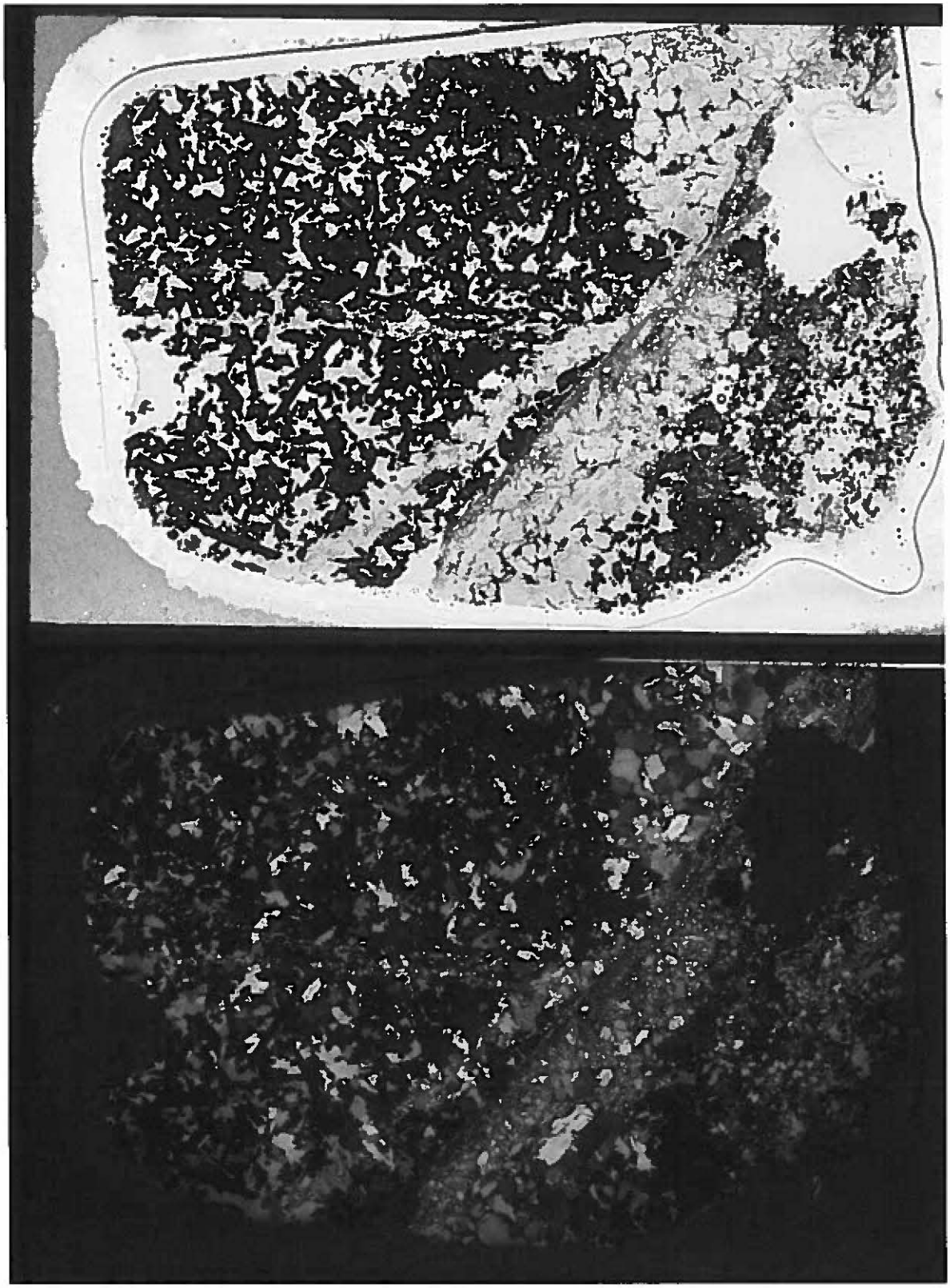


Figure 150. Polished section scan of MIN-27.

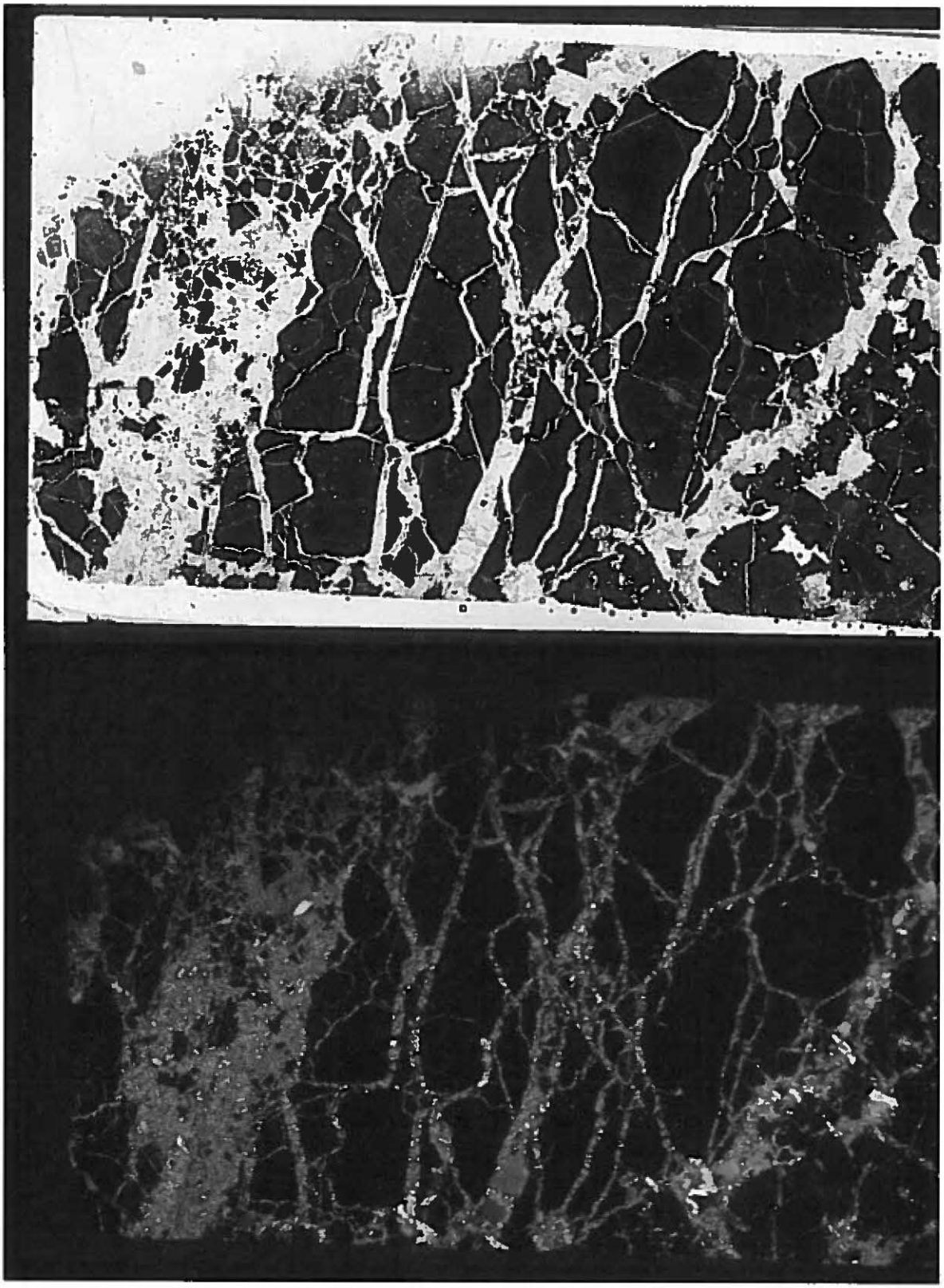


Figure 151. Polished section scan of MIN-28.

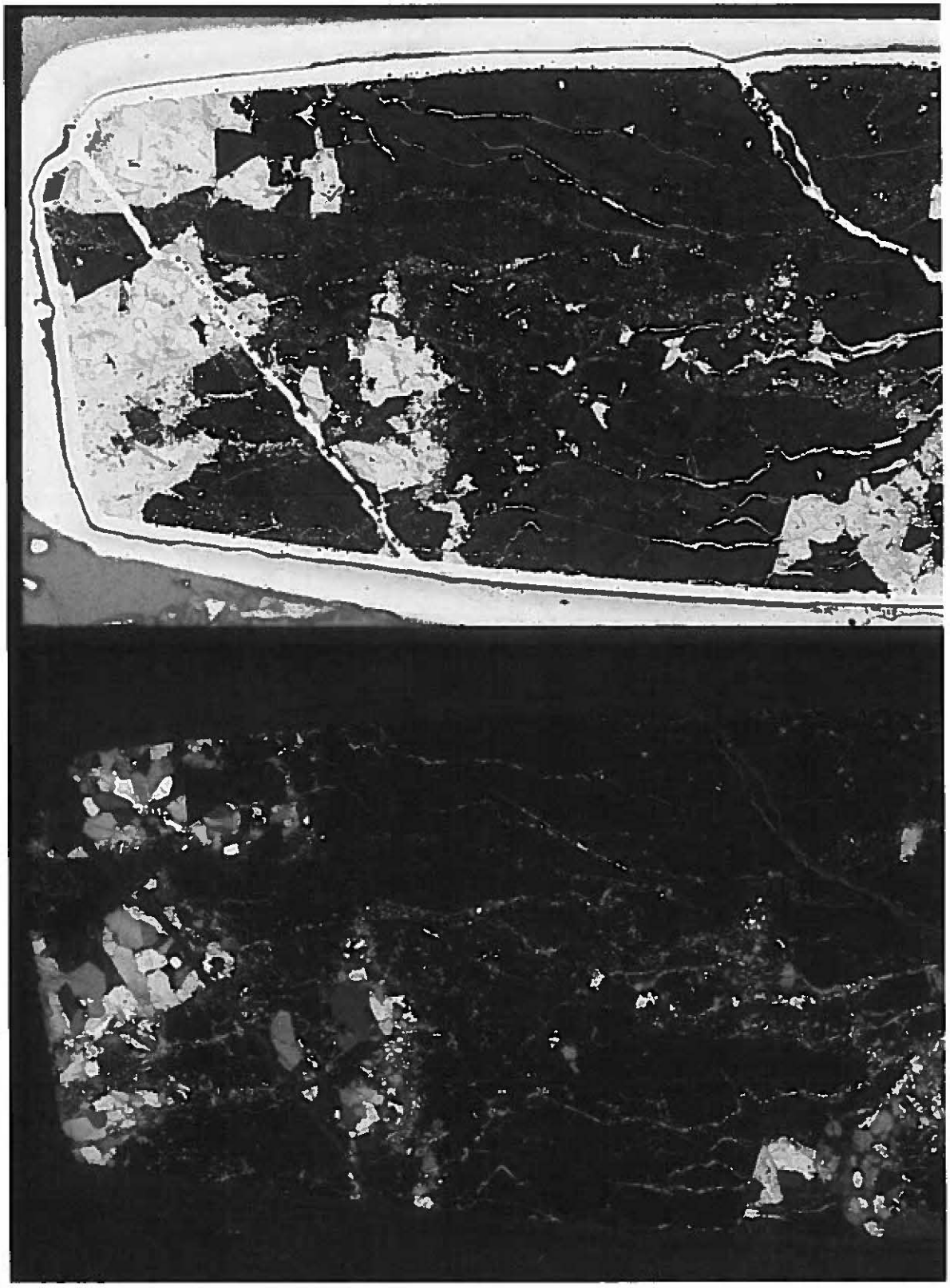


Figure 152. Polished section scan of MIN-29.

Appendix B: EDX spectra of minerals observed in polished section

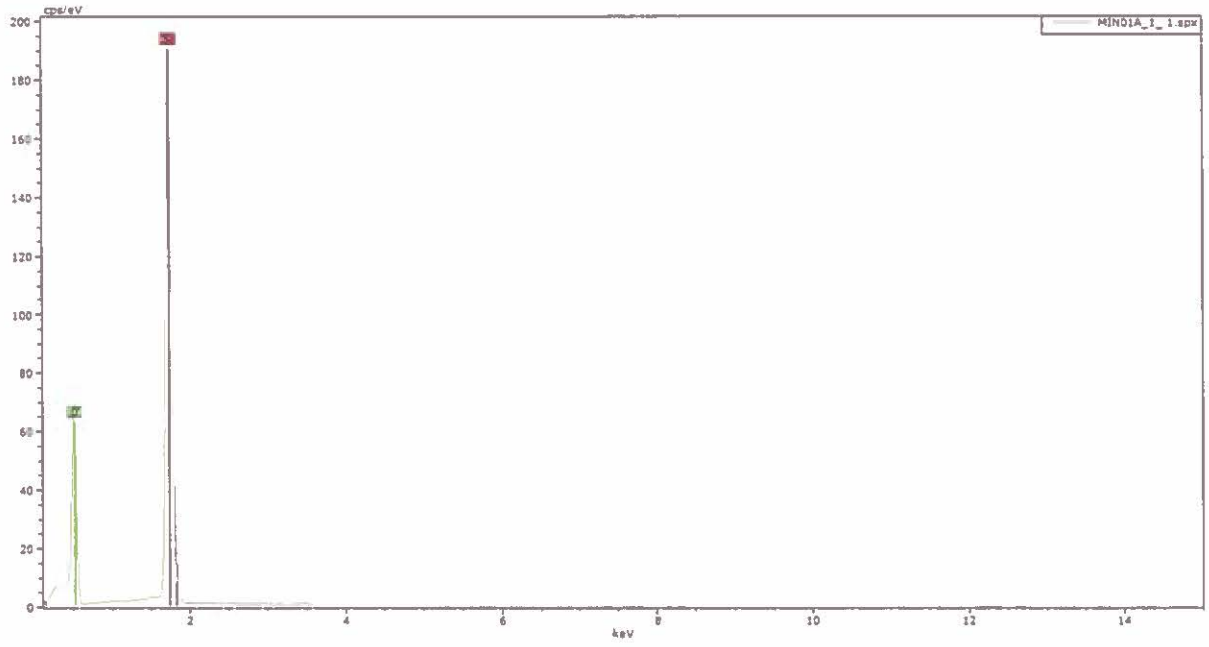


Figure 153. EDX spectrum of quartz.

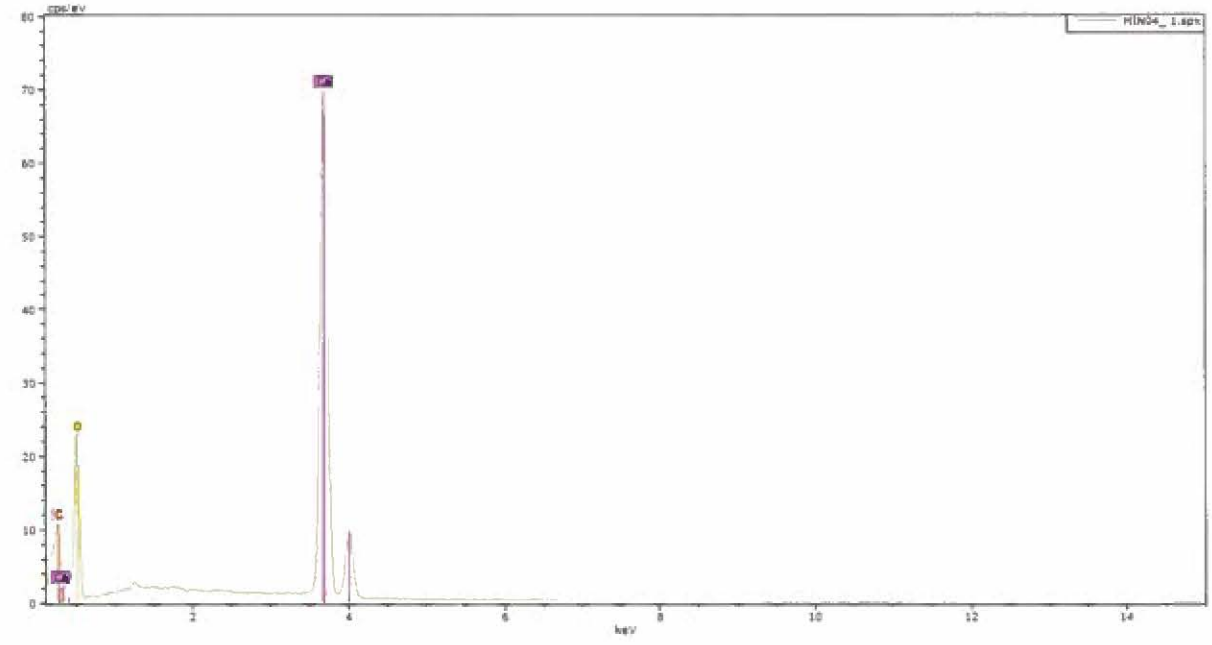


Figure 154. EDX spectrum of calcite.

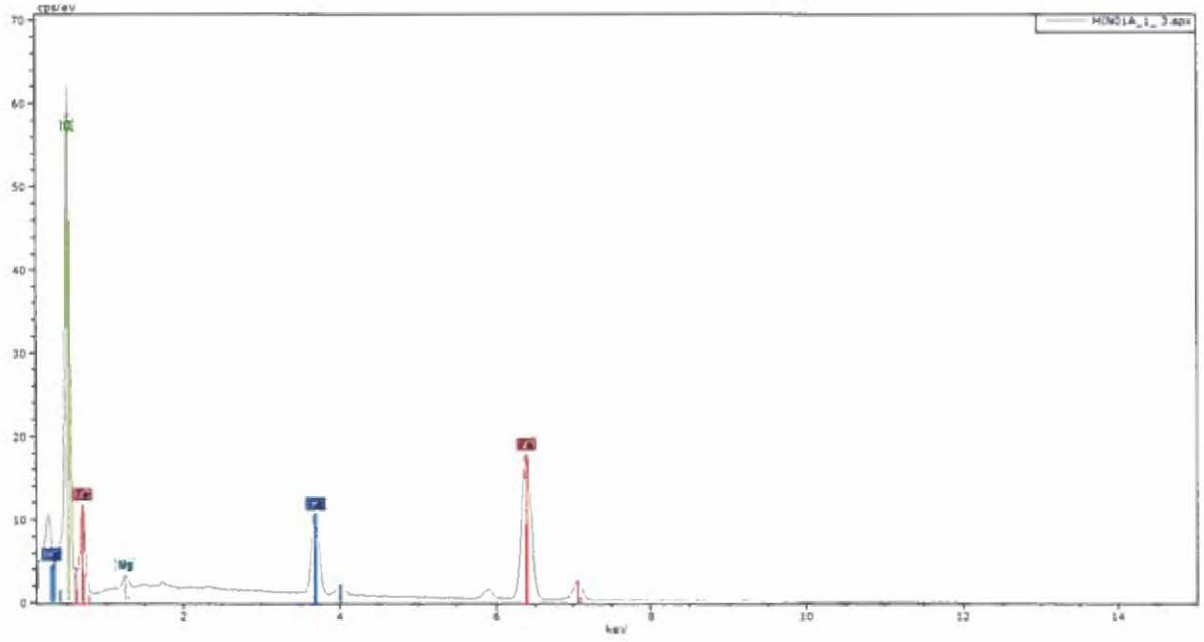


Figure 155. EDX spectrum of ankerite.

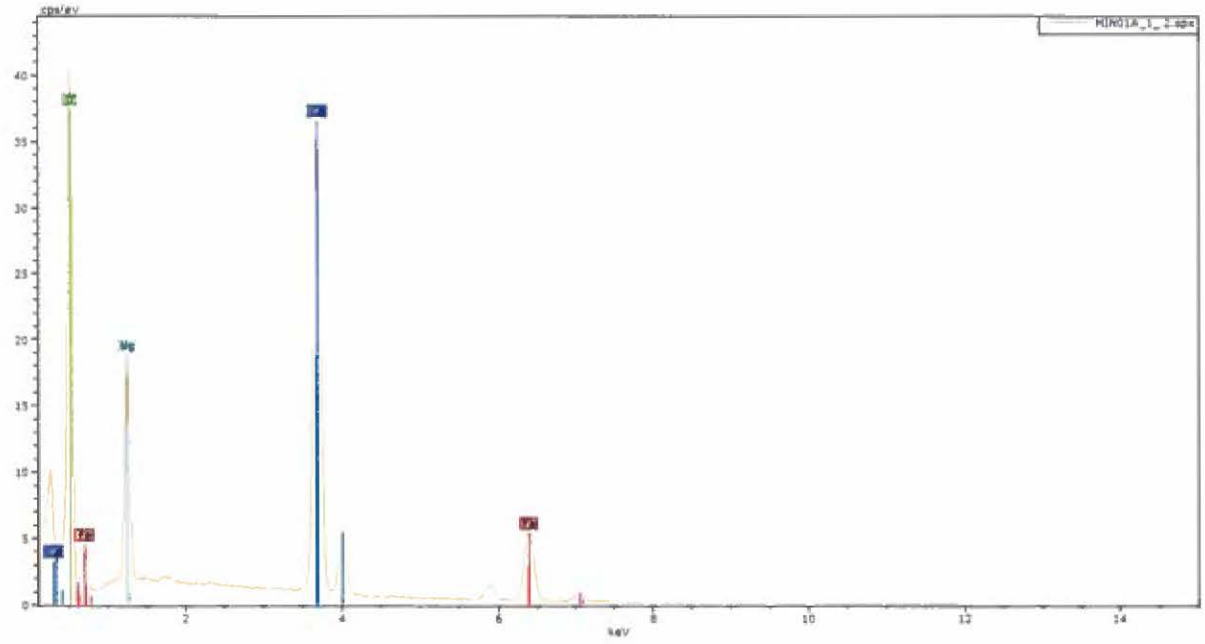


Figure 156. EDX spectrum of dolomite with a small Fe peak.

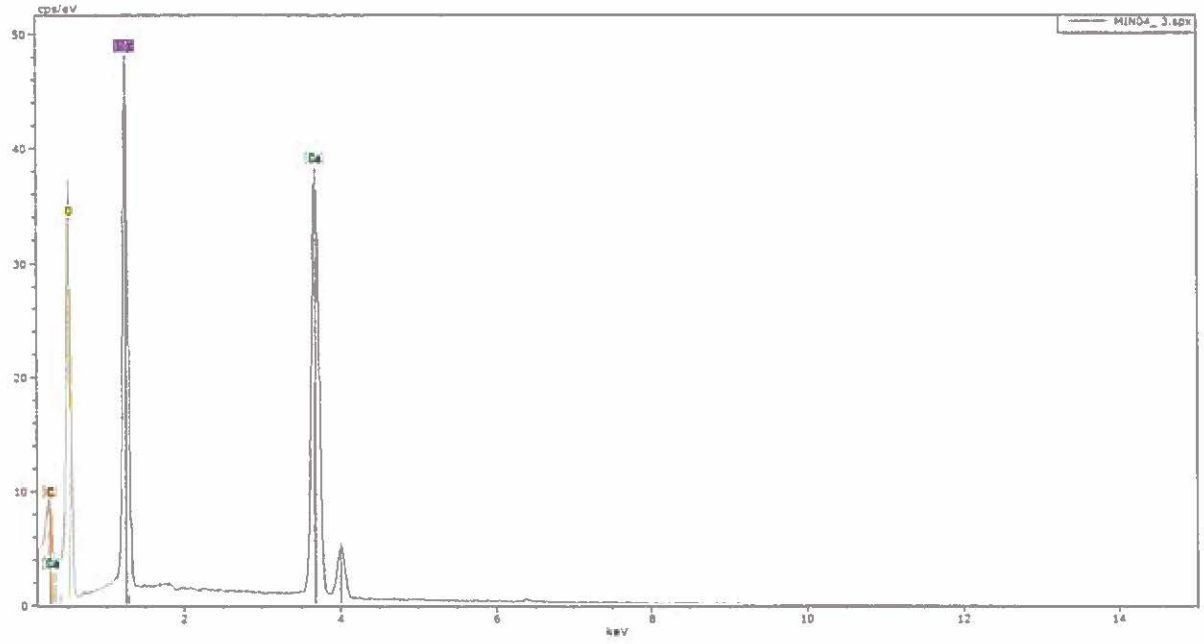


Figure 157. EDX spectrum of dolomite with no Fe peak.

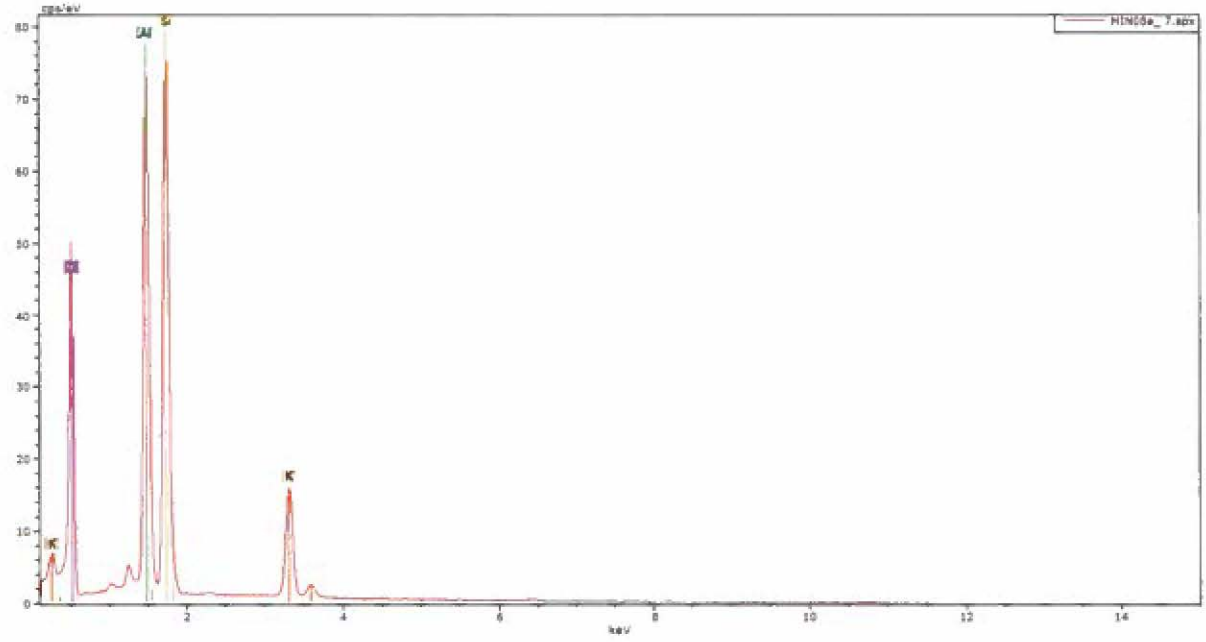


Figure 158. EDX spectrum of muscovite.

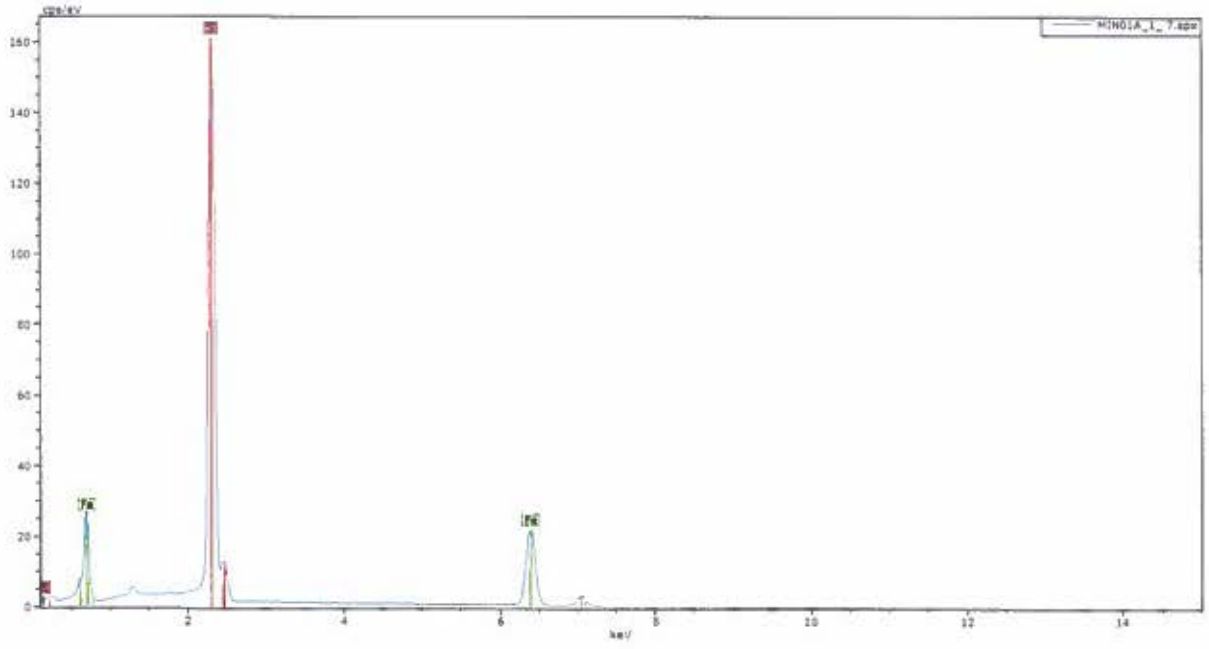


Figure 159. EDX spectrum of pyrite.

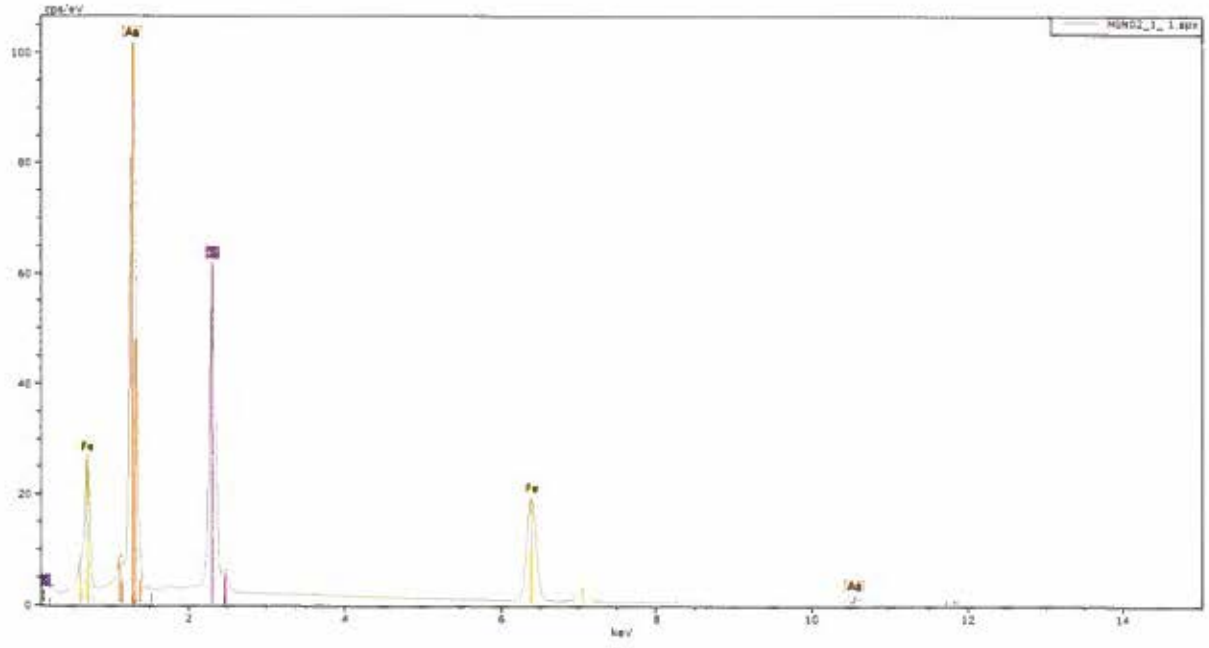


Figure 160. EDX spectrum of arsenopyrite.

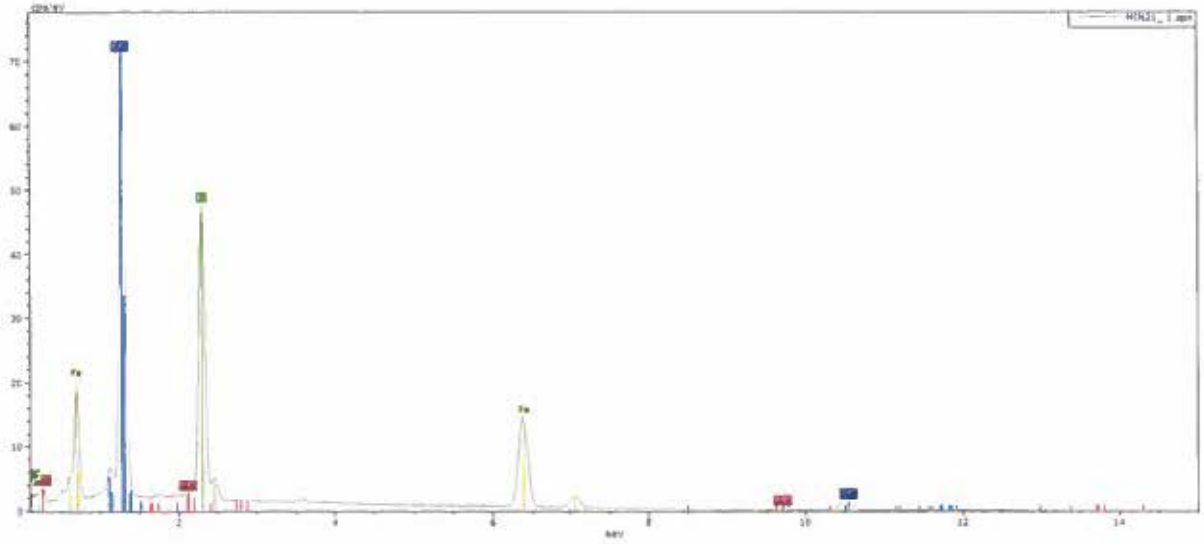


Figure 161. EDX spectrum of arsenopyrite with a possible, very small, Au peak.

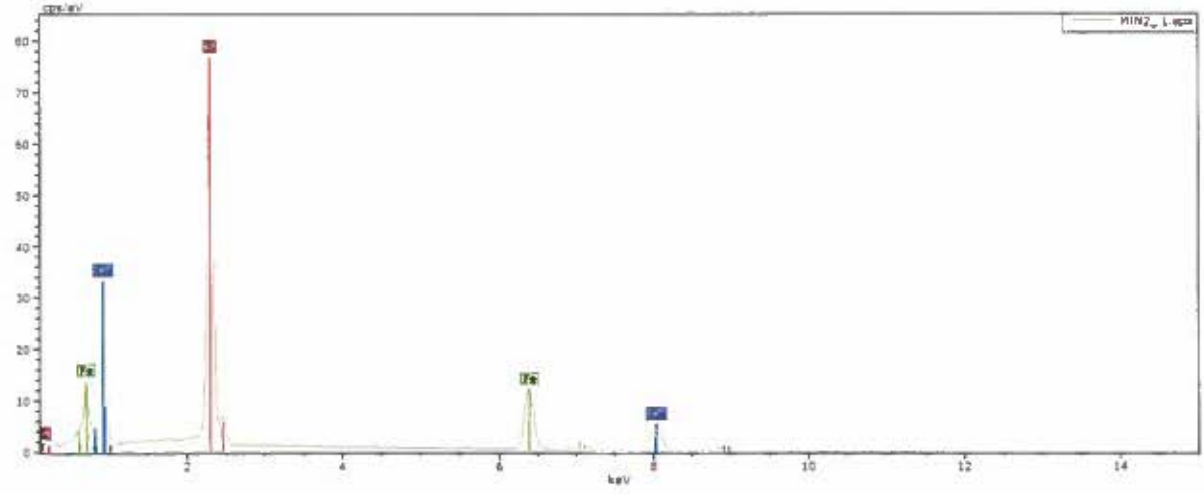


Figure 162. EDX spectrum of chalcopyrite.

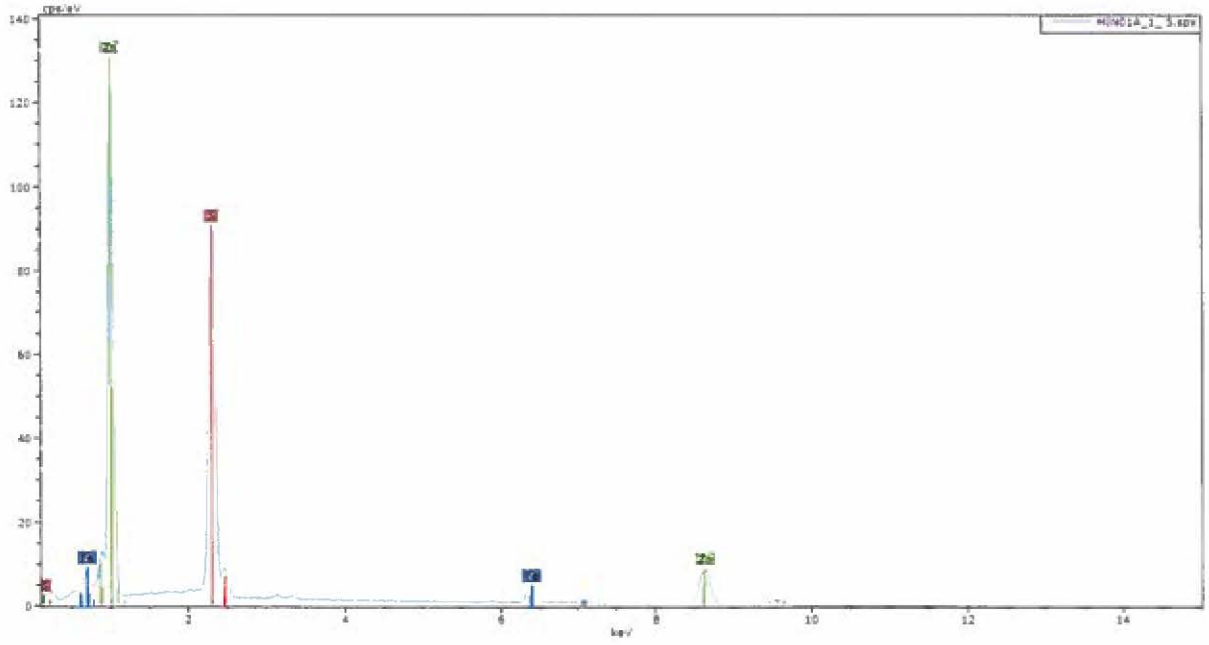


Figure 163. EDX spectrum of sphalerite.

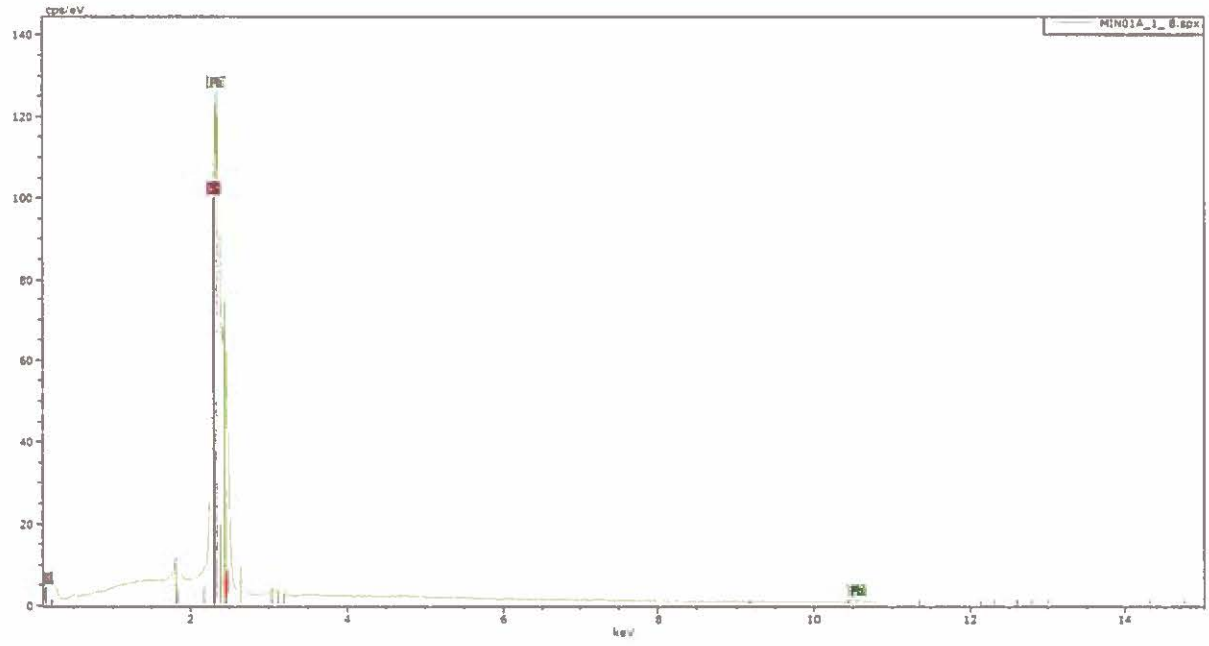


Figure 164. EDX spectrum of galena.

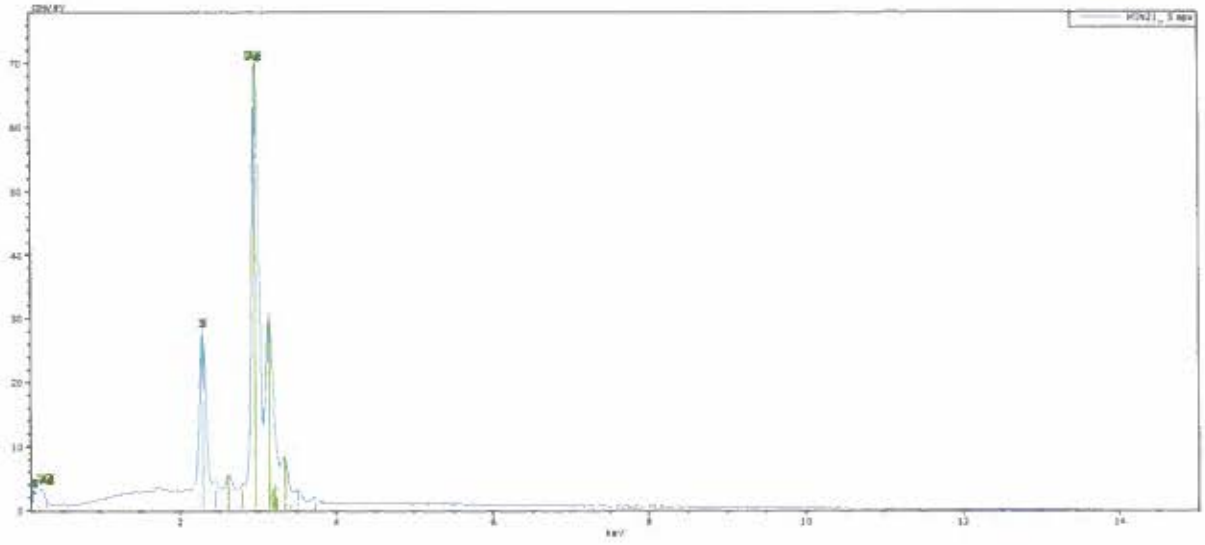


Figure 165. EDX spectrum of stibnite.

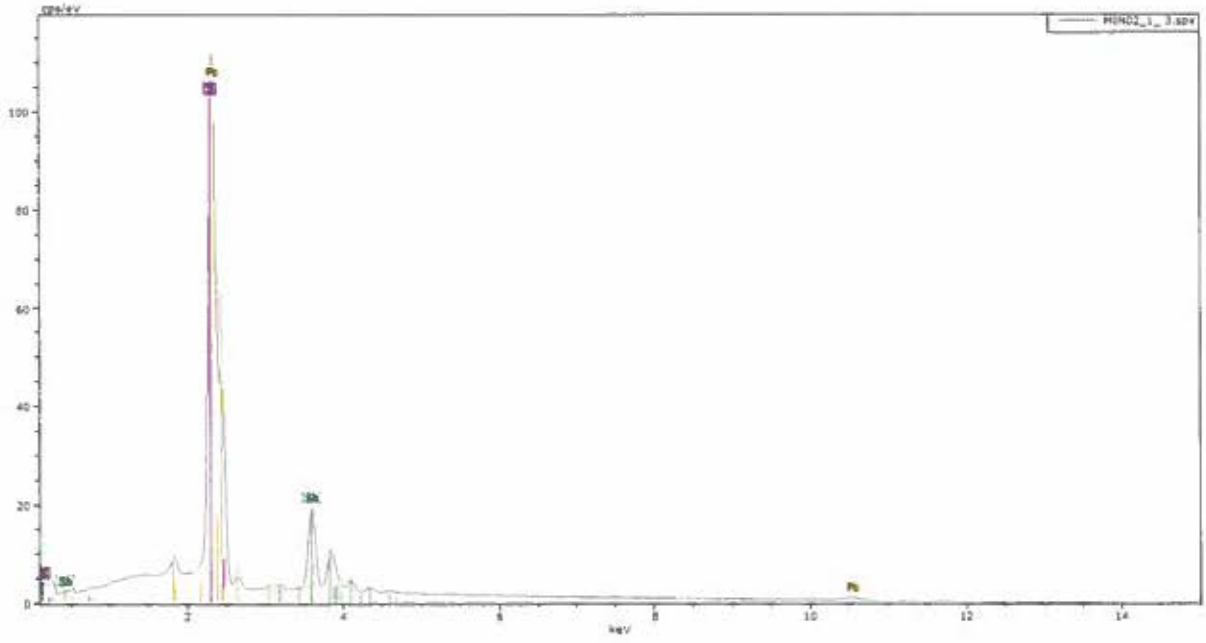


Figure 166. EDX spectrum of boulangerite.

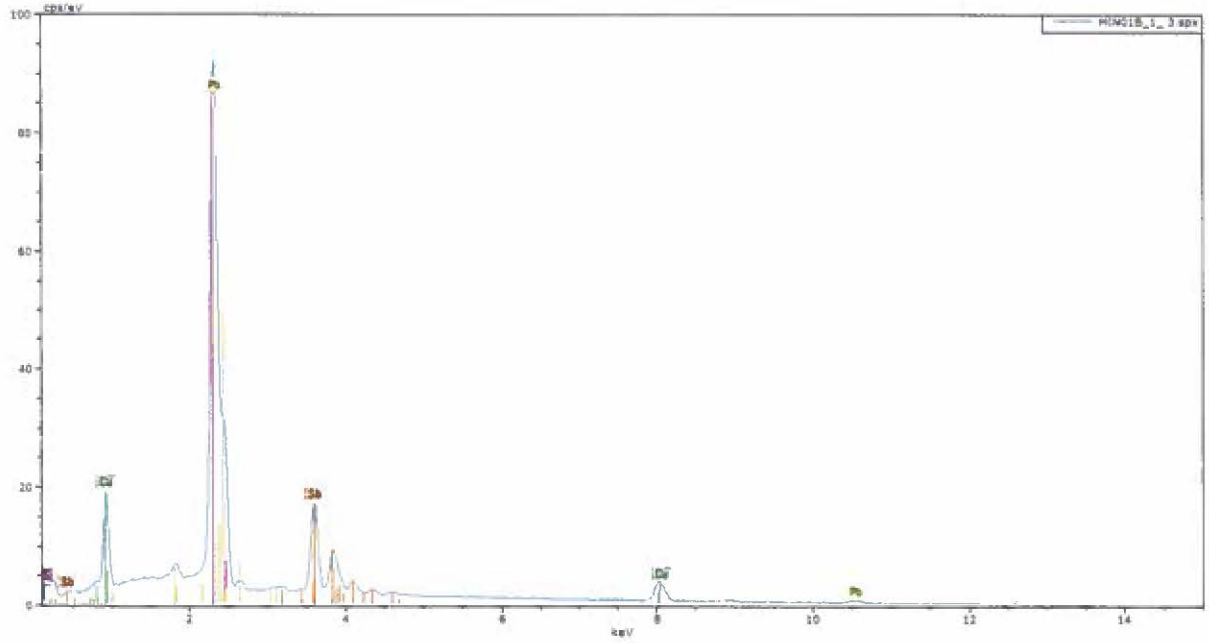


Figure 167. EDX spectrum of bournonite.

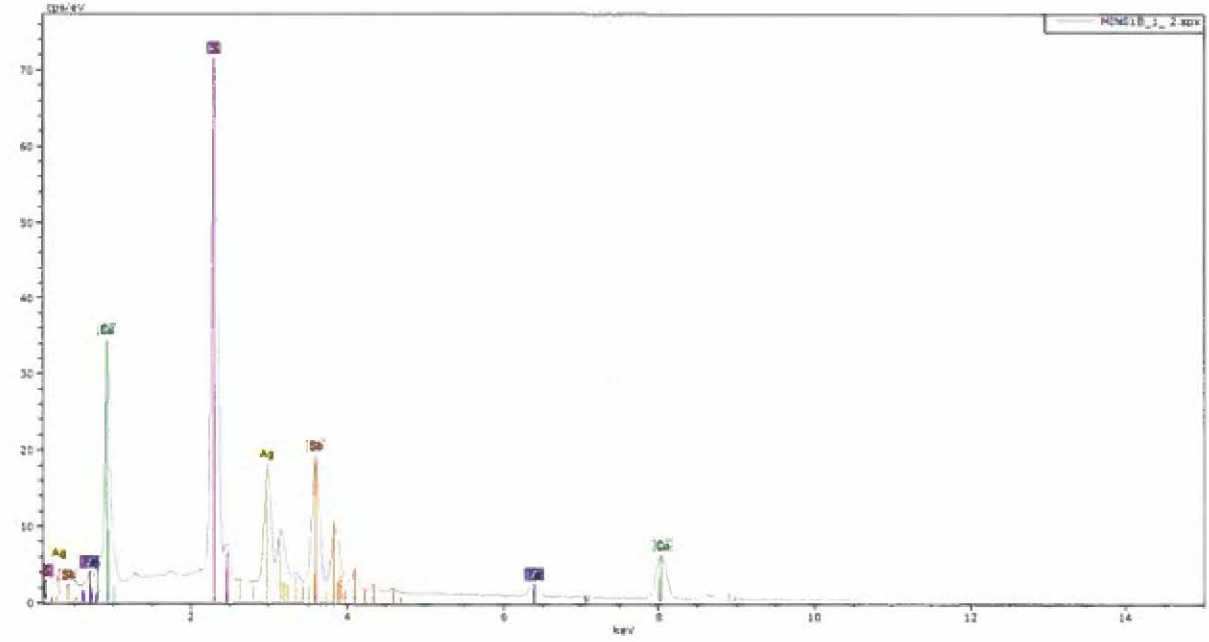


Figure 168. EDX spectrum of freibergite.

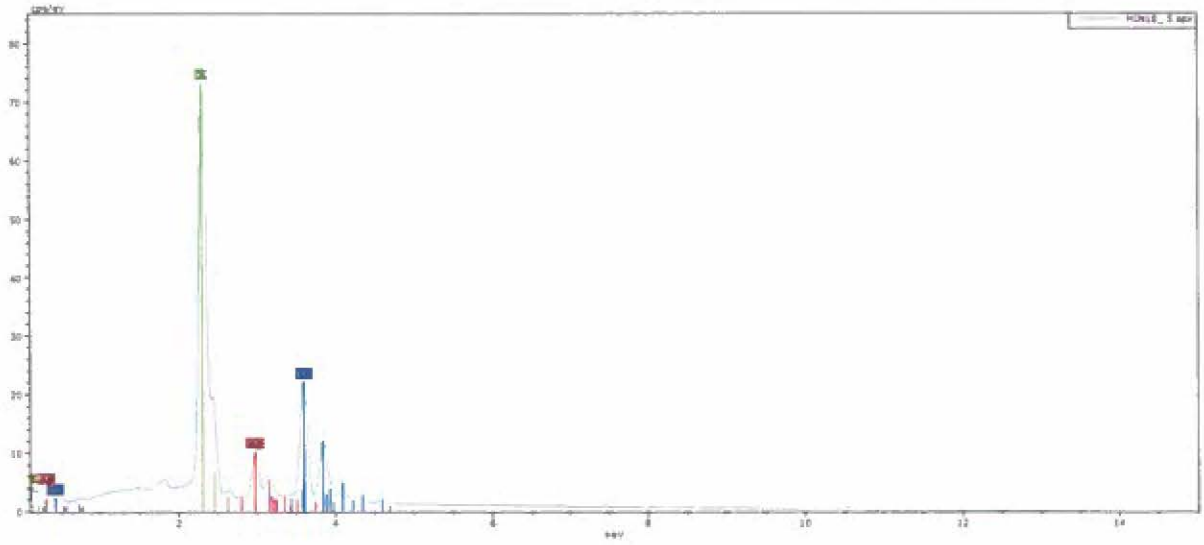


Figure 169. EDX spectrum of pyrargrite with small Pb peak.

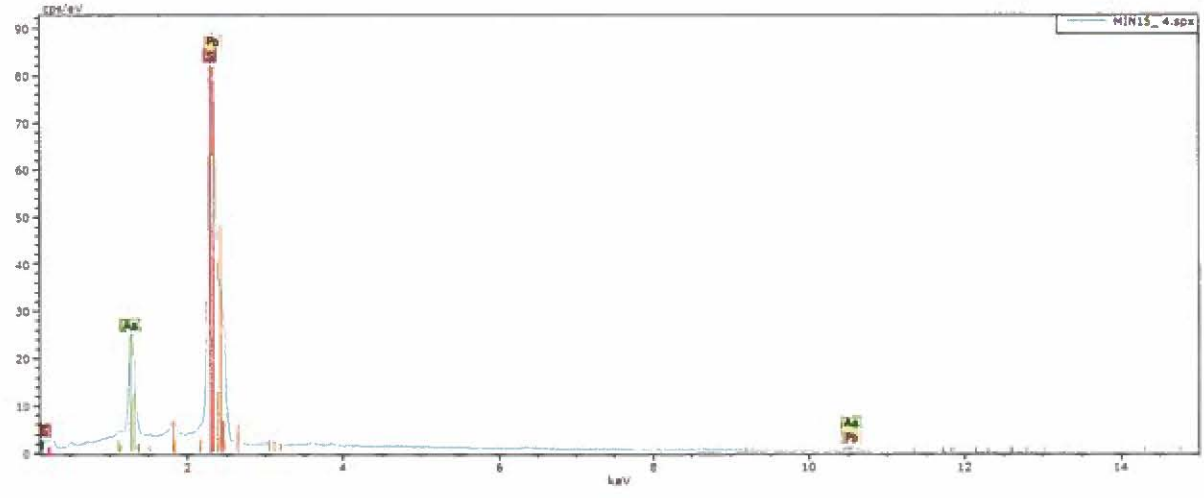


Figure 170. Spectrum of an As-Pb-sulphide.

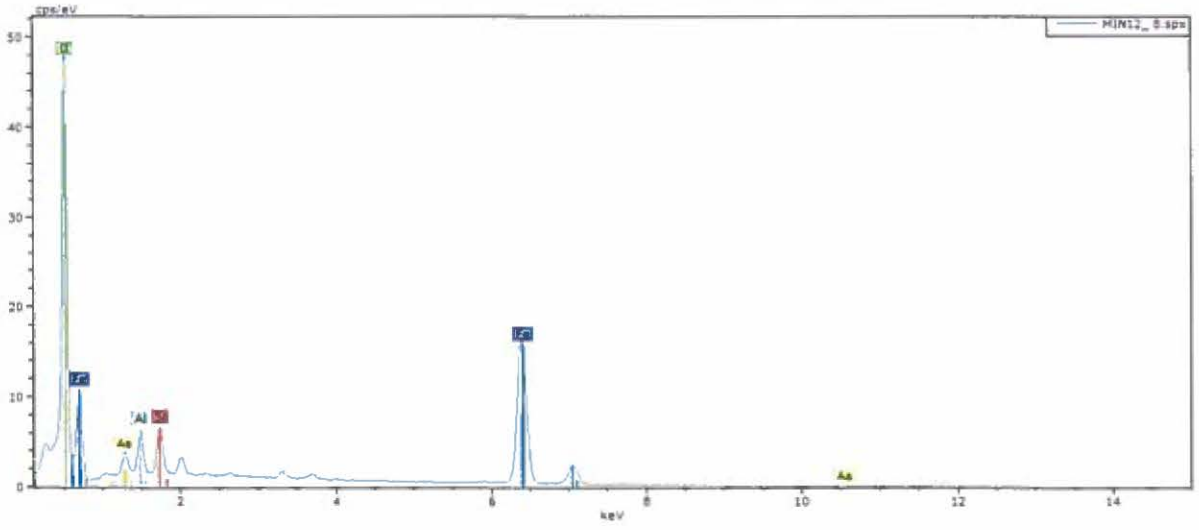


Figure 171. Spectrum of a Fe-oxide.

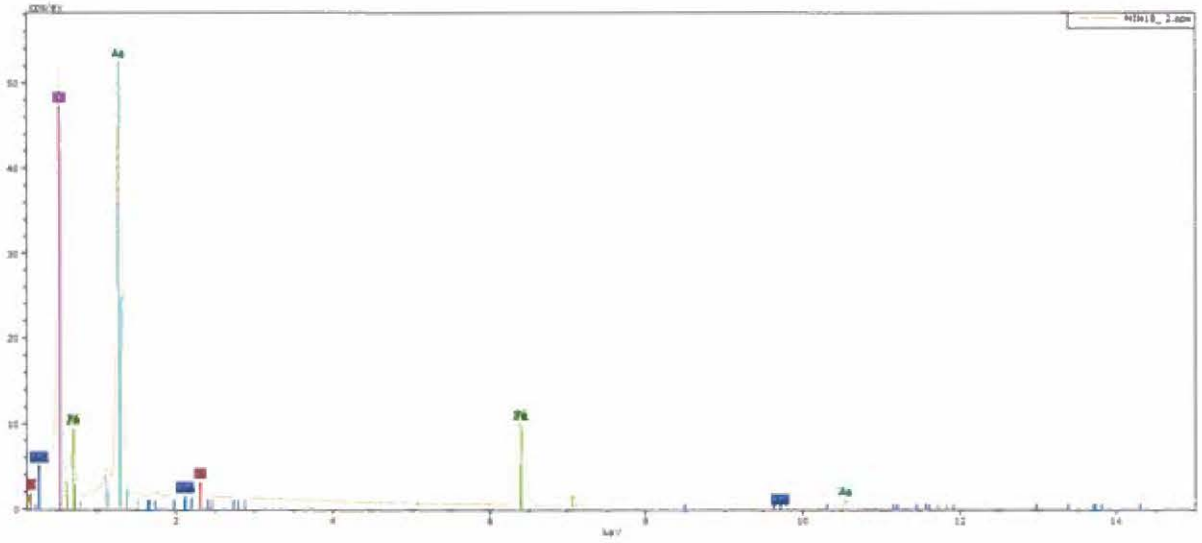


Figure 172. Spectrum of a Fe-As-oxide with a potential small Au peak.

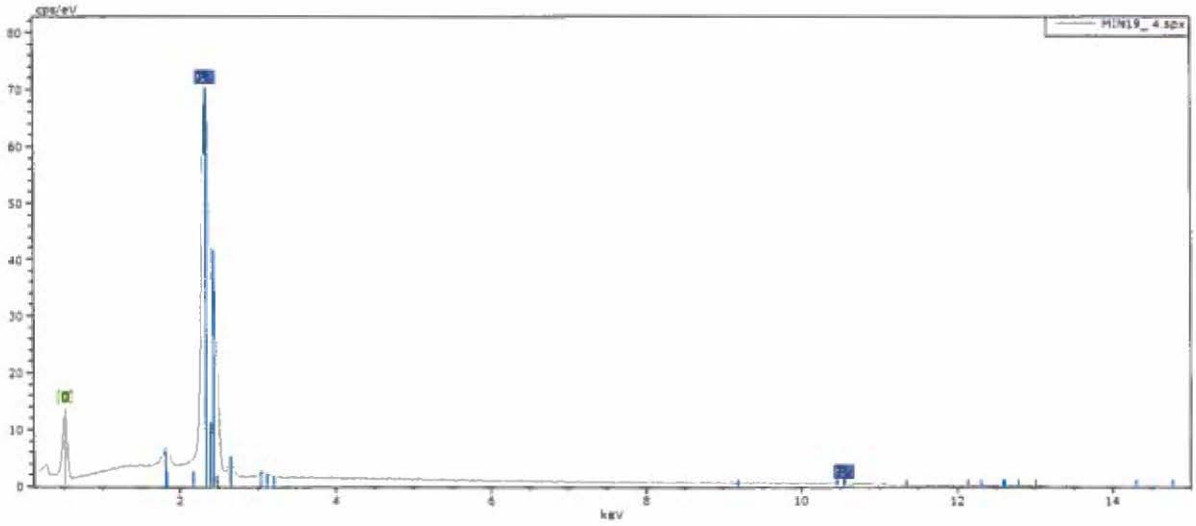


Figure 173. Spectrum of a Pb-oxide.

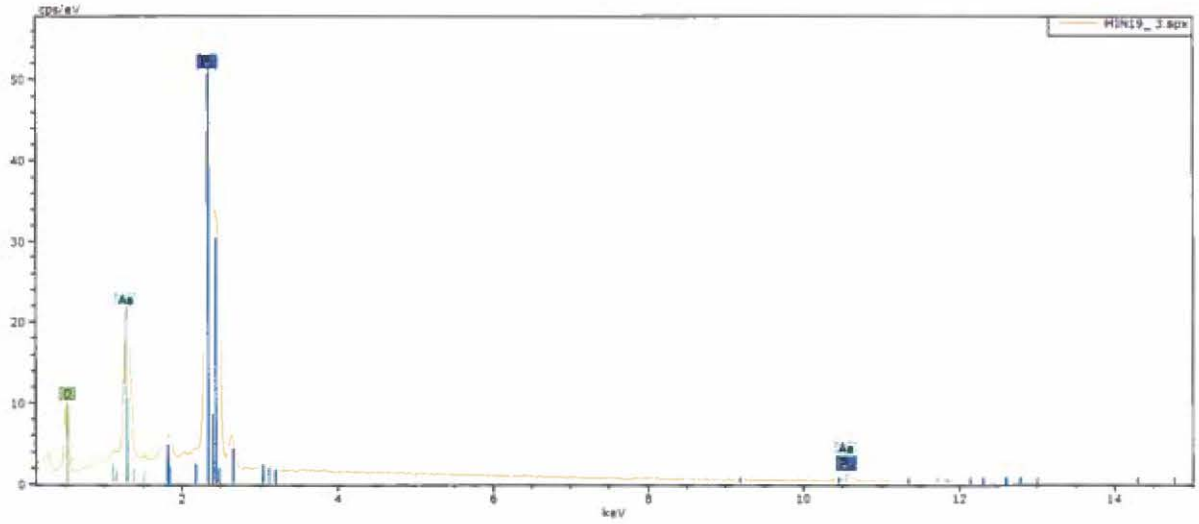


Figure 174. Spectrum of an As-Pb-oxide.

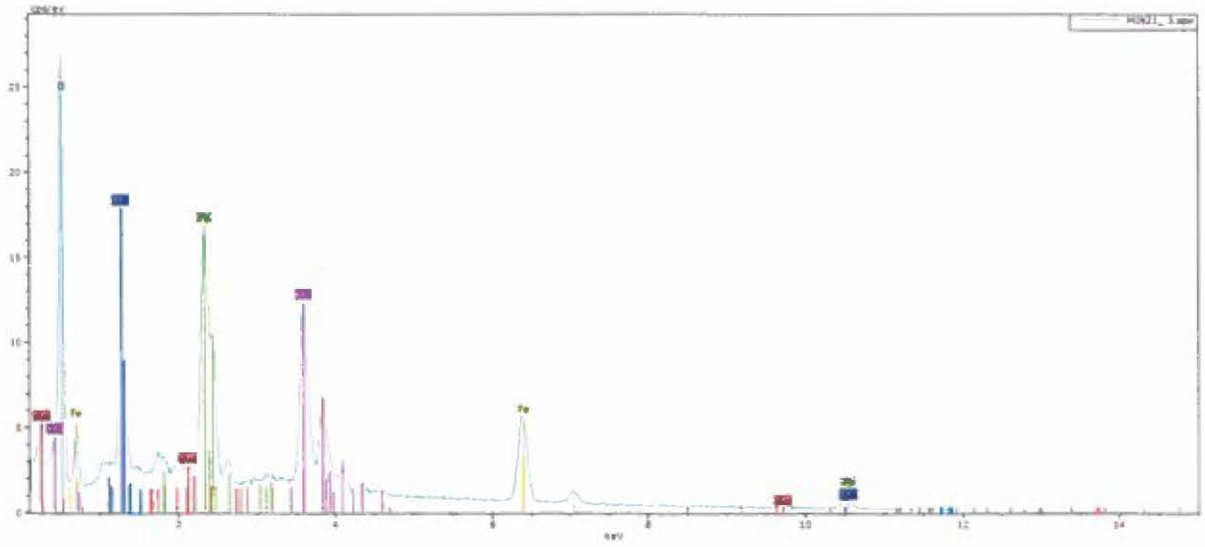


Figure 175. Spectrum of a Fe-As-Sb-Au-Pb-oxide.

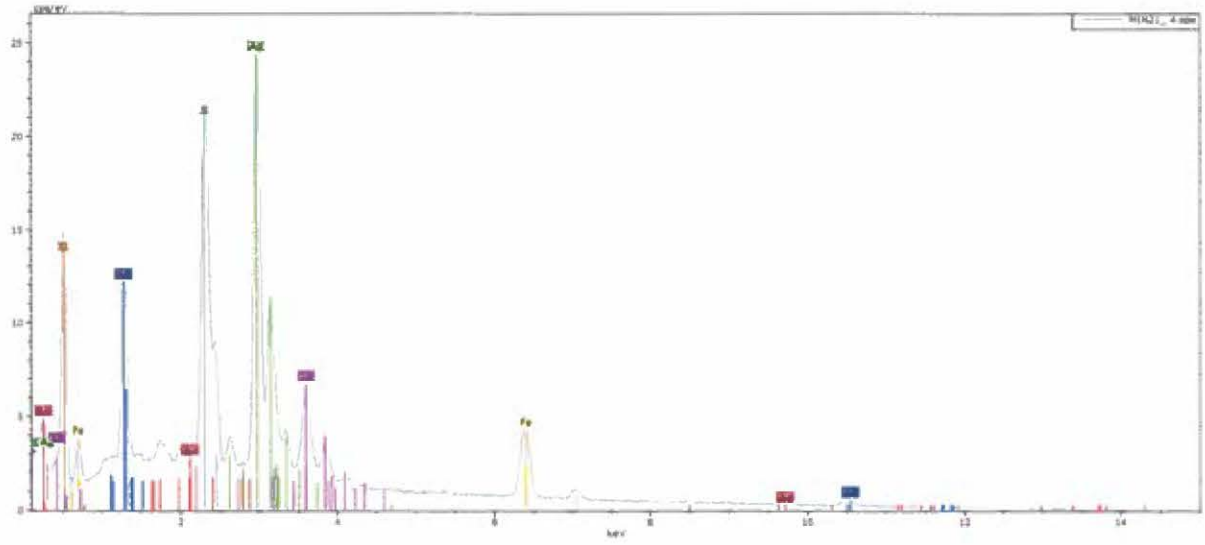


Figure 176. Spectrum of a Fe-As-Ag-Sb-Au-Pb-oxide.

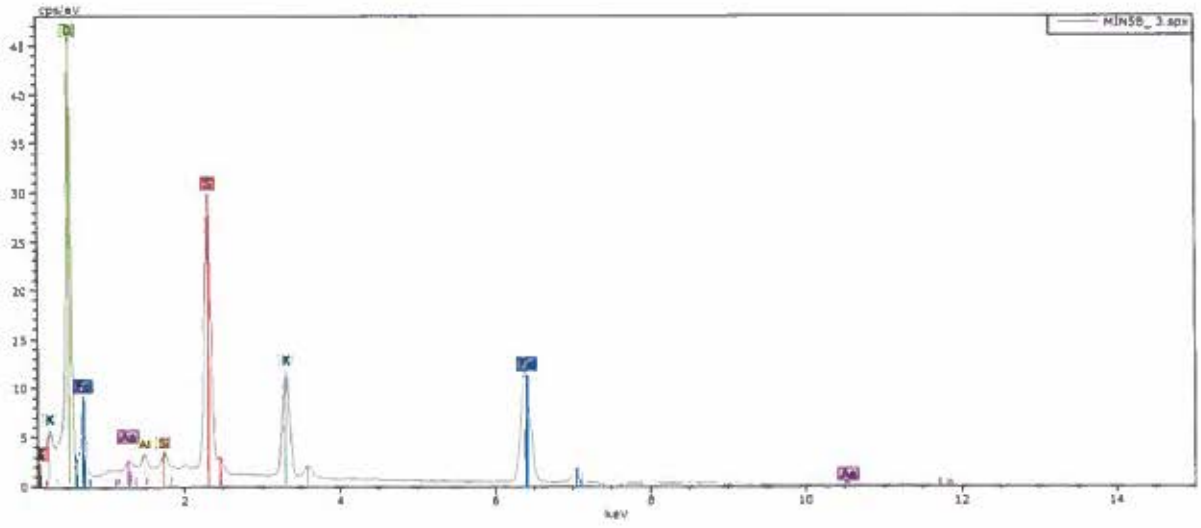


Figure 177. Spectrum of a K-Fe-sulphate.

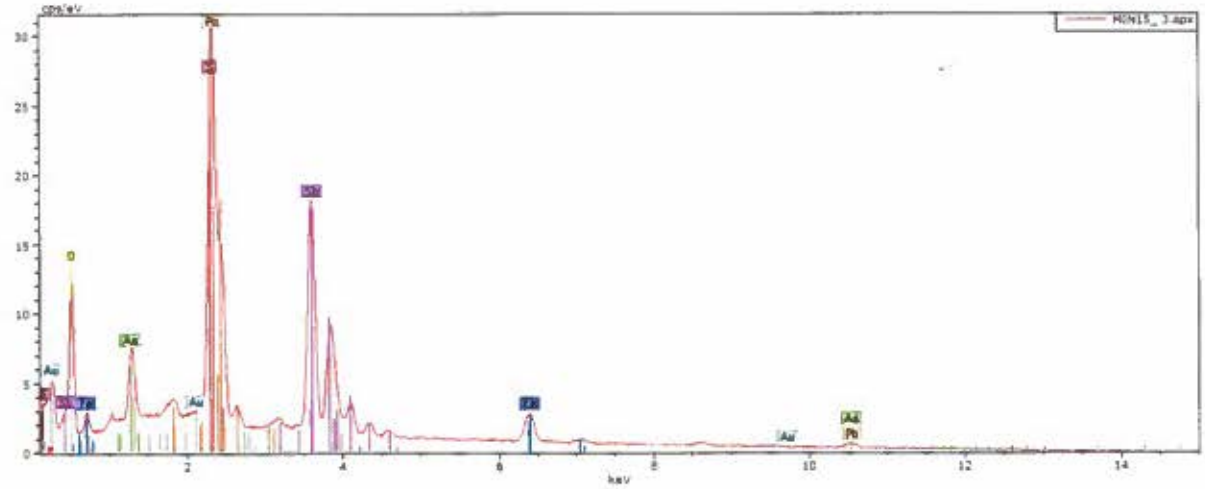


Figure 178. Spectrum of a Fe-As-Sb-Au-Pb-sulphate.

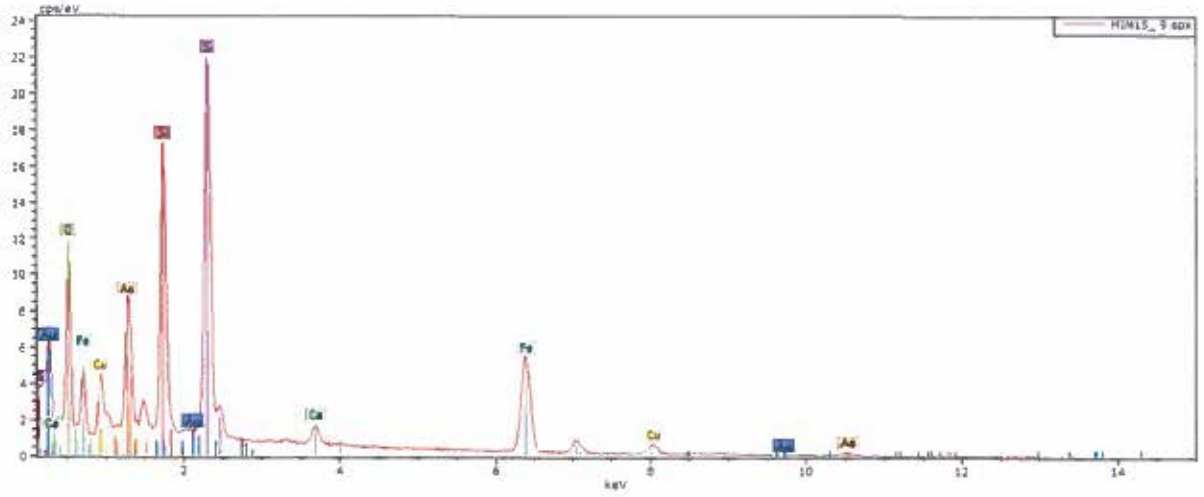


Figure 179. Spectrum of a Ca-Fe-Cu-As-Au-S-silicate.

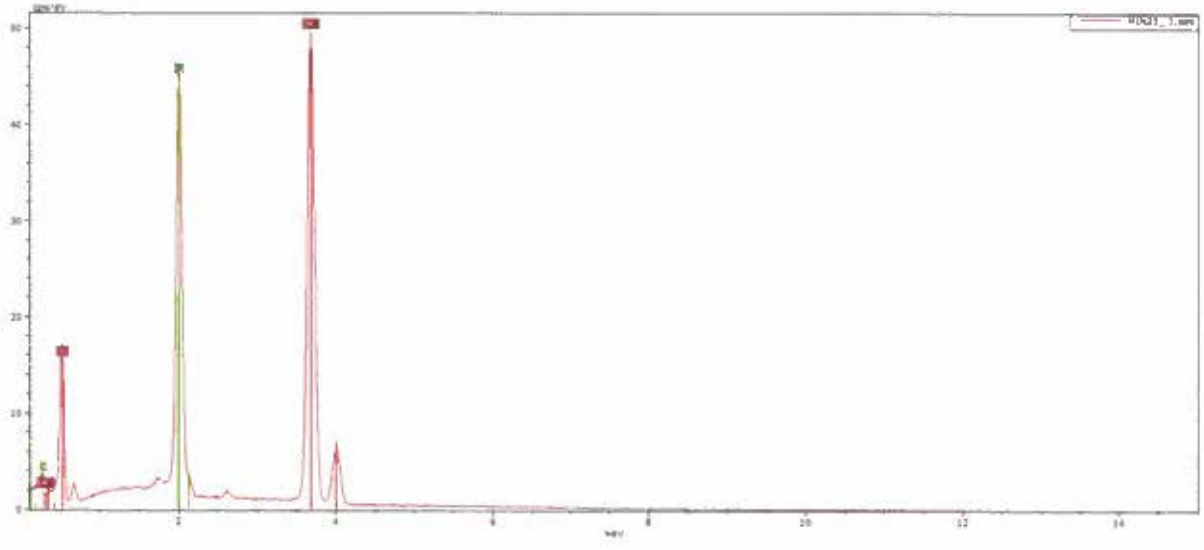


Figure 180. Spectrum of apatite.

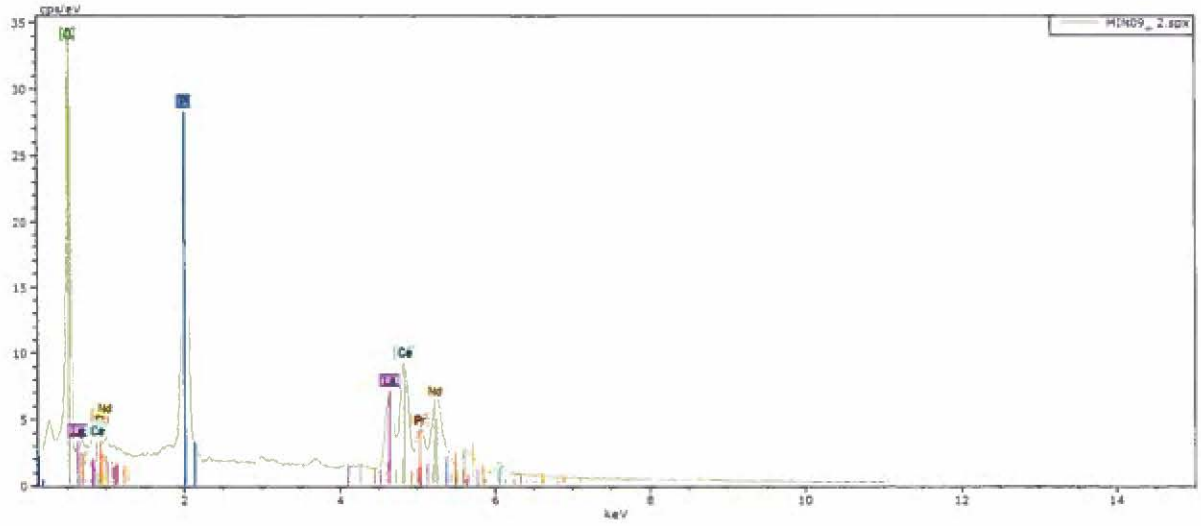


Figure 181. Spectrum of monazite-(Ce)